Proceedings
Nonlinear Water Waves
Workshop

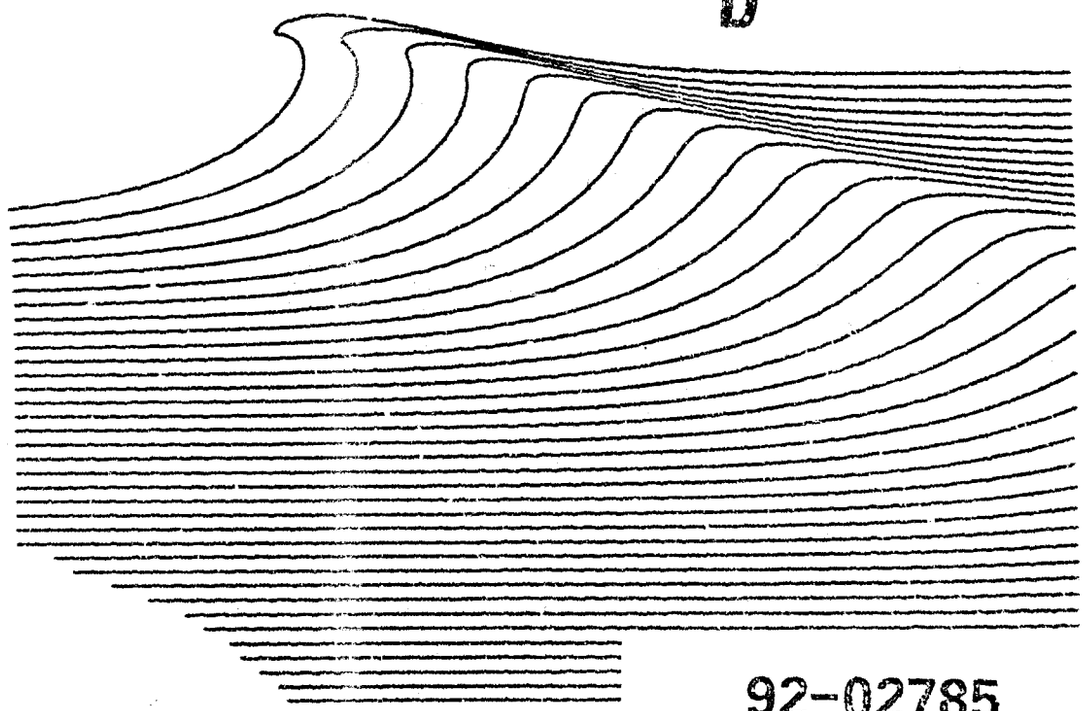

University of Bristol, 1991

This work relates to Department of the Navy Grant N00014-91-J-9038 issued by the Office of Naval Research European Office. The United States has a royalty-free license throughout the world in all copyrightable material contained herein.

Nonlinear Water Waves Workshop

University of Bristol, 22-25 October 1991

PROCEEDINGS

The aim of this workshop was to take advantage of the recent freedom available to scientists in the Soviet Union (now Commonwealth of Independent States) to travel to the West in order to develop both contacts and an awareness of current research between research workers from East and West, most of whom have formerly had little contact. We consider this aim was achieved and are grateful for the substantial financial support from the European Office of the U.S. Office of Naval Research and the European Research Office of the U.S. Army. In addition we thank the home instiutions or other fund providers which supported the travel costs of participants and the subsistence of western participants. The support of Bristol University's Department of Mathematics in holding the meeting is greatly appreciated.

Editor:
D.H. Peregrine

ISBN 0-86292-390-5
University of Bristol, Department of Mathematics

CONTENTS

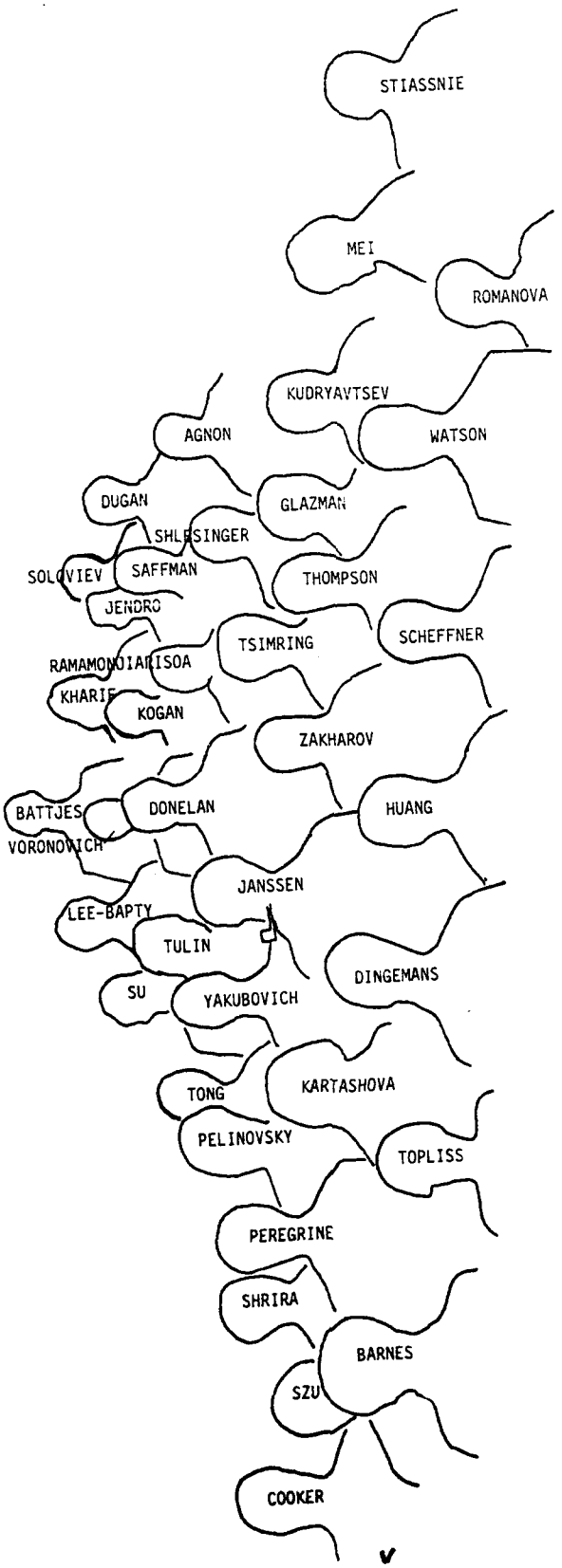

Guide to photogtaph of participants in the Nonlinear Water Waves Workshop taken on 24 October 1991

PARTICIPANTS

Prof Y. Agnon
Dept. of Civil Engng.
Technion
Haifa 32000, Israel

Mr B.C. Barber
Space Dept, Defence Res. Agency
RAE Farnborough
Hants GU14 6TD
ENGLAND

Mr T. Barnes
Dept. of Mathematics
University of Bristol
Bristol BS8 1TW
ENGLAND

Prof J.A. Battjes
Civil Engineering Dept
Delft University of Technology
P O Box 5048, 2600 GA Delft
THE NETHERLANDS

Prof M. Berry
Physics Laboratory
Tyndall Avenue
Bristol BS8 1TL
ENGLAND

Dr M.J. Cooker
School of Mathematics
University Walk
Bristol BS8 1TW
ENGLAND

Dr M.W. Dingemans
Delft Hydraulics
P O Box 152 8300 AS Emmeloord
THE NETHERLANDS

Dr J.W. Dold
School of Mathematics
University Walk
Bristol BS8 1TW
ENGLAND

Dr M.A. Donelan
Research Applics. Branch
National Water Resource Inst.
POBox 5050 Burlington
Ontario L7R 4A6
CANADA

Prof. P.G. Drazin
School of Mathematics
University Walk
Bristol BS8 1TW
ENGLAND

Dr J.P. Dugan
ONR European Ofrice
223 Old Marylebone Road
London NW1 5TH
ENGLAND

Prof. D.V. Evans
School of Mathematics
University Walk
Bristol BS8 1TW
ENGLAND

Dr V. Galaktionov
Keldysh Inst.of Appl.
Mathematics
Miusskaya Sq . 4
125047 Moscow
RUSSIA

Dr R. Glazman
Jet Propulsion Lab.
Mailstop 300-323
4800 Oak Grove Drive
Pasadena. CA 91109
USA

Mr R. Gwynllyw
School of Mathematics
University Walk
Bristol BS8 1TW
ENGLAND

Dr N.E. Huang
Lab. for Oceans, Code 971
Goddard Space Flight Center
Greenbelt, MD 20771
USA

Dr P.A.E.M Janssen
KNMI, Postbus 201
3730 Ae de Bilt
THE NETHERLANDS

L.Cdr L Jeadro
ONR Europe
223 Old Marylebone Road
London NW1 5TH

Dr E. Kartashova
P.P.Shirshov Inst of Oceanology
USSR Acad. of Sciences
Krasikova 23
Moscow 177218
RUSSIA

Dr C. Kharif
Inst.de Mech.Stat.d'la
Turbulence
Lab.de Luminy, Campus Univ.903
13288 Marseille Cedex 9
FRANCE

Dr V. Krasitskii
P.P.Shirshov Inst of Oceanology
USSR Acad. of Sciences
Krasikova 23
Moscow 177218
RUSSIA

Dr V. Kogan
Inst of Appl.Phys.
USSR Acad. of Sciences
46 Uljanov Street
603600 Nizhny Novgorod
RUSSIA

Dr V. Kudryavtsev
Marine Hydrophys. Inst
UKR Acad. of Science
26 Lenin Str.
Sebastopol 335000
UKRAINE

Dr I.P. Lee-Bapty
Space Dept., Q134 Bldg.
RAE Farnborough
Hants GU14 6LN
ENGLAND

Dr R.S.Mackay
Inst. of Mathematics
Univ. of Warwick
Coventry CV4 7AL
ENGLAND

Prof.C.C. Mei
Dept.Civil.Engng.,48-413
M.I.T.
Cambridge, Mass 02139
USA

Dr E. Pelinovsky
Inst of Appl.Phys.
USSR Acad. of Sciences
46 Uljanov Street
603600 Nizhny Novgorod
RUSSIA

Prof. D.H. Peregrine
School of Mathematics
University Walk
Bristol BS8 1TW
ENGLAND

Dr A. Ramamonjiarisoa
Inst.de Mech.Stat.d'la Turbulence
Lab. de Luminy
Campus Univ. 903
13288 Marseille Cedex 9
FRANCE

Dr N. Romanova
Inst. for Atmos. Phys.
Academy of Sciences
Pyzhevsky 3
Moscow 109017
RUSSIA

Prof. P.G. Saffman
217-50 Appl.Math.
California Inst. Technology
Pasadena, CA 91125
USA

Dr N. Scheffner
US Army, Engng.Wat.Exp.Station
Coastal Engng.Res.Center
3909 Halls Ferry Road
Vicksburg, Miss.39180-6199
USA

Dr M. Shlesinger
Director, Physics
Office Naval Research
800 N Quincy St
Arlington, VA 22217
USA

Dr V.I. Shrira
Shirshov Inst.Oceanology
Krasikova 23
Moscow 117218
RUSSIA

Dr Y. Soloviev
Marine Hydrophys. Inst
UKR Acad. of Science
26 Lenin Str.
Sebastopol 335000
UKRAINE

Dr. M. Stiassnie
Civil Engineering Dept
The Technion
Haifa 32000
ISRAEL

Dr M.-Y. Su
Code 331, Naval Ocean R&D Act.
Stennis Space Center
Mississippi 39529-5005
USA

Dr H.H. Szu
Information Sci. Group Leader
Code R44
Naval Surface Warfare Center
Silver Spring, MD 20903-5000
USA

Dr E.F. Thompson
Coastal Engng.Res.Center
US Army, Engng.Wat.Exp.Station
3909 Halls Ferry Road
Vicksburg, Miss. 39180-6199
USA

Mr R. Tong
School of Mathematics
University Walk
Bristol BS8 1TW
ENGLAND

Ms M. Topliss
School of Mathematics
University Walk
Bristol BS8 1TW
ENGLAND

Dr L.Ch. Tsimring
Inst of Appl.Phys.
USSR Acad. of Sciences
46 Ulyanov Str
603600 Nizhny Novgorod
RUSSIA

Prof M.P. Tulin
Ocean Engng. Lab.
University of California
Santa Barbara, CA 93106
USA

Dr A.G. Voronovich
P.P.Shirshov Inst of Oceanology
USSR Acad. of Sciences
Krasikova 23
Moscow 177218
RUSSIA

Dr G. Watson
School of Mathematics
University Walk
Bristol BS8 1TW
ENGLAND

Dr E.I. Yakubovich
Inst of Appl.Phys.
USSR Acad. of Sciences
46 Ulyanov Str
603600 Nizhny Novgorod
RUSSIA

Prof V.I. Zakharov
Landau Inst.of Theoret. Physics
GSP-1 117940 Kosygina St.2
Moscow V-334
RUSSIA

NONLINEAR SHOALING OF WIDE-BANDED SEAS

by

Yehuda Agnon and Alexandru Sheremet*

ABSTRACT

The interaction of surface waves is simplified when the dispersion is weak. This can happen due to the spectrum being narrow-banded, leading to a nonlinear Schrodinger Equation. Alternatively, when the wavelength is large compared to the water depth, dispersion is again weak, leading to Boussinesq Equations.

On an even bottom, Zakharov Equation describes the time evolution of an initial wave spectrum in the wave number domain.

The present work introduces a variant of the Zakharov Equation in the frequency domain, which is valid for bottom slopes smaller, or of the order of the wave steepness (ε).

The evolution equation has terms due to triad interaction, which occurs at characteristic time and spatial scales which are 0 (ε^{-1}L) and (ε^{-1}T), where L and T are the wavelength and its period. In the limit of shallow water, the triad interaction model tends to the Boussinesq model.

By discretizing the wave spectrum, mixed initial and boundary value problems can be computed. As an illustration, the steady state solution for shoaling of a sinusoidal envelope and the associated set down wave was computed as well as shoaling of two wider spectra. The combined effect of shoaling and energy transfer between the wave components is clearly evident. Dispersion is fully accounted for.

* *Coastal and Marine Engineering Research Institute (CAMERI)*
Department of Civil Engineering, Technion-Israel Institute of Technology, Haifa 32000, Israel

INTRODUCTION

As ocean surface gravity waves shoal, the wave field undergoes substantial evolution from its deep-water state. Narrow band spectra develop secondary peaks at harmonics of the peak frequency; broadband spectra show an increase of energy over a wide range of frequencies higher than most of the energetic part of the spectrum. Phase velocities depart substantially from those predicted by the linear dispersion relation and the shape of individual waves changes from almost symmetrical in deep water to one with sharp crests and flat, broad troughs in shallow water (see Elgar & Guza, 1985).

Linear theory, often used as a basis for shoaling models, does not predict most of these changes. Superposition of motions with different frequencies is used to satisfy arbitrary conditions at a given point. This way, exact solutions have been found in the case of bottom slope given by $h_x=\pi M/2N$, M, N integers (see Whitham, 1979 for a review). For the case of small bottom slope, WKB expansions have also been used (Chu & Mei, 1970). The solutions found satisfy locally the flat bottom equations, and the amplitude of each component mode varies slowly according to the equation for the conservation of the energy flux at the lowest order. Separate components evolve separately, without interaction. The linear theory is roughly consistent (up to 20%) with measurements of shoaling wave heights, but is is intuitively clear that the processes preceding the breaking of the waves are essentially nonlinear.

The extensive work devoted recently to the study of the limits and applicability of special wave evolution equations, like nonlinear Schrodinger, KdV, Boussinesq'-type systems, has offered a ready background for the incorporation of nonlinear effects in shoaling models. Starting from previous work in similar nonlinear problems for the flat bottom case (Davey & Stewartson, 1976, Djordjevic & Redekopp, 1977), Djordjevic' to derive a cubic nonlinear Schrodinger equation describing the evolution of the envelope of a gravity wave-train over uneven bottom. Using more explicit conditions of narrow spectrum and weak dispersion, Stiassnie (1983) derived a similar equation starting from Whitham's set of modulation equations (Whitham, 1974). In a recent more extensive work, Suh, Darlymple & Kirby (1990) obtained an evolution equation for Stokes waves over mildly varying topography, including refraction, diffraction and nonlinear cubic interactions. All these works assume slowly varying bottom ($h_x = O(\varepsilon^2)$, $\varepsilon = ka$, steepness of wave parameter), a narrow spectrum and mild dispersion of the waves. The nonlinear interaction is relegated to the third order, cubic type, and the implicit assumption is that for the envisaged spectrum, the water is deep (assumption consistent with the Stokes-type expansion used). However, earlier work of Benney & Saffmann (1966), Newell (1968), Longuet-Higgins (1976) and Herterich & Hasselmann (1980) has shown that the cubic interactions mechanisms can cause significant changes in the spectrum of a wave field over distances of several hundreds of kilometers or more. They cannot account for the much faster exchange of energy during the shoaling process (length scale: a few hundred meters),

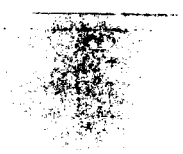

where the water becomes eventually shallow, (Freilich & Guza, 1984, Elgar & Guza, 1985). The stronger mechanism of quadratic interactions should be taken into account. Attention turns to modelling of the shoaling processes at the other end of the shoaling region, the shallow one.

Generalization of Boussinesq and KdV equations to include the effects of sloping bottom were obtained by Peregrine (1967), Ostrowski & Pelinovski (1970) and Grimshaw (1970). Using as a starting point the equations derived by Peregrine, Freilich & Guza (1984) obtained two nonlinear shoaling models, describing the evolution of the amplitudes and phases of the Fourier modes of the spectrum. Their mechanism of energy exchange is near or exact resonance interactions of second order (quadratic), mild or no dispersion at all is assumed, and the bottom slope $h_x = O(\varepsilon)$, $\varepsilon = \frac{h^2}{\lambda^2}$ being the (small) dispersion parameter.

A picture of the alternate energy exchange mechanism may be obtained from the cited works invoking as a guiding model the equation for the evolution of a gravity-capillary wave spectrum over flat bottom of arbitrary depth due to Stiassnie & Shemer (1984), who extended the previous fundamental work on interactions of deep-water gravity waves by Zakharov (1968) and Crawford, Saffmann & Yuen (1980).

The shoaling wave field propagates from deep-water into intermmediate-depth and then eventually shallow water. At the deep-water end of the shoaling region, the Stokes-expansion models work; the wave field is best described by free waves and sub/super-harmonic locked waves, completely determined by the free ones; quartet near-resonance is dominant, and as the water becomes shallow, exact triad resonance is approached; the locked waves become free waves, energy exchange between modes is faster as interactions grow stronger, and the spectrum widens. All mentioned works offer a description restricted to a single mechanism (cubic interaction or quartet near/exact resonance interactions). In either case, the dispersion is taken to be weak. To our knowledge, no attempt has been made to the present to model the transition between these limits of the shoaling phenomenon.

The issue of transition from forced waves to free waves as triad resonance which is approached for quasi-steady waves on an even bottom has been addressed by Agnon (1991). In the present work , we follow Crawford et al's (1980) derivation of the Zakharov equation to obtain an evolution equation for the shoaling of wide-spectrum waves all the way from deep water to shallow water. The equation, in the frequency domain, is valid for bottom slopes as steep as O (ε), the order of the wave steepness.

In this presentation only triad interaction terms are included. The waves are assumed undirectional for simplicity of presentation. Some results for the evolution of a sinosoidal envelope and the associated set down waves, as well as results for a Pierson-Moskowitz type spectrum are presented.

Extensions that include quartet interaction and directional spectra were also performed. They are beyond the present scope.

In accordance with the above setting of the problem, a small parameter ε may be defined:

$$\varepsilon = 0\,(h_x) \approx 0\,(ka) << 1 \tag{1}$$

h_x, k, a being the local slope of the bottom, the wave number and the amplitude of the waves. The equations governing the irrotational flow of an inviscid fluid with a free surface are scaled and terms to order O (ε) retained.

The fast time variation is separated from the slower time scale of the modulation by means of a multiple scale approach and the fast-time Fourier Transform of the equations are taken with the slow time t_1 defined as:

$$t_1 = \varepsilon t \;;\; \frac{\partial}{\partial t} = \frac{\partial}{\partial t} + \varepsilon \frac{\partial}{\partial t_1} \tag{2}$$

The resulting system is:

$$\widehat{\Phi}_{xx}\,(x,y,\omega,t_1) + \widehat{\Phi}_{yy}\,(x,y,\omega,t_1) = 0 \qquad -h\,(x) \le y \le \varepsilon\eta\,(x,t,t_1)$$

$$h_x\,\widehat{\Phi}_x\,(x,y,\omega,t_1) + \widehat{\Phi}_y\,(x,y,w,t_1) = 0 \qquad \text{on} \qquad y = -h\,(x) \tag{3a}$$

$$i\omega\widehat{\psi}\,(x,\omega,t_1) + \varepsilon\widehat{\psi}_{t_1}\,(x,\omega,t_1) + \widehat{\eta}\;(x,\omega,t_1) +$$

$$+ \frac{\varepsilon}{4\pi}\int\!\!\int_{-\infty}^{\infty} \widehat{\psi}_x\,(x,\omega_1,t_1)\cdot\widehat{\psi}_x\,(x,\omega_2,t_1)\,\delta\,(\omega-\omega_1-\omega_2)d\omega_1\,d\omega_2$$

$$- \frac{\varepsilon}{4\pi}\int\!\!\int_{-\infty}^{\infty} \widehat{W}^s\,(x,\omega_1,t_1)\cdot\widehat{W}^s\,(x,\omega_2,t_1)\,\delta\,(\omega-\omega_1-\omega_2)d\omega_1\,d\omega_2 = O\,(\varepsilon)^2$$

$$i\omega\widehat{\eta}\,(x,\omega,t_1) + \varepsilon\widehat{\eta}_{t_1}\,(x,\omega,t_1) - \widehat{W}^s\,(x,\omega,t_1) +$$

$$+ \frac{\varepsilon}{2\pi}\int\!\!\int_{-\infty}^{\infty} \widehat{\psi}_x\,(x,\omega_1,t_1)\cdot\widehat{\eta}_x\,(x,\omega_2,t_1)\,\delta\,(\omega-\omega_1-\omega_2)d\omega_1\,d\omega_2 = O\,(\varepsilon^2)$$

$$\text{on } y = \varepsilon\eta\,(x,t,t_1)$$

where the Fourier Transforms are:

$$\widehat{\Phi}\,(x,y,\omega,t_1) \;-\; \text{velocity potential}$$

$$\widehat{\eta}\,(x,\omega,t_1) \;-\; \text{surface elevation} \tag{3b}$$

$$\widehat{\psi}\,(x,\omega,t_1) \;=\; \widehat{\Phi}\,(x,y=\varepsilon\eta\,(x,t,t_1),\,\omega,t_1)$$

$$\widehat{W}^S(x,w,t_1) = \widehat{\Phi}_y(x,y=\varepsilon\eta(x,t,t_1),\omega,t_1)$$

Following Crawford et al's work, we proceed to solve as a first problem the Laplace equation together with the bottom boundary condition, expressing the velocity potential as:

$$\widehat{\Phi}(x,y,\omega,t_1) = \left[\widehat{\phi}_F(x,y,\omega,t_1) + \widehat{\phi}_L(x,y,\omega,t_1)\right] e^{-i\theta} \qquad (4)$$

$$\theta = \int k(x,\omega)\,dx \;;\; \omega^2 = k\ \text{th}\ kh$$

The indices F and L stand for free and locked waves. The individual characteristics of the two types of waves are taken into account by the use of the following orderings:

$$\widehat{\phi_F} = \phi_F(\varepsilon x,y,\omega,t_1) \;;\; \widehat{\phi_{Fx}} = (\varepsilon) \qquad (5)$$

$$\widehat{\phi_L} = \phi_L(x,y,\omega,t_1) \;;\; \widehat{\phi_{Lx}} = (\varepsilon)$$

The surface velocity potential $\widehat{\psi}$ and surface vertical $\widehat{W}^S$ are then expressed in terms of the velocity potential $\widehat{\Phi}$, the hyperbolic functions that appear in $\widehat{\Phi}$ are expanded in series of powers of ε and finally, the unknown function due to the incompleteness of the first problem is eliminated between $\widehat{\psi}$ and $\widehat{W}^S$ to express $\widehat{W}^S$ only in terms of the surface velocity potential and surface elevation. With the new found $\widehat{W}^S$ we return to the surface boundary conditions in (3) and, after eliminating $\widehat{\eta}$, obtain the evolution equation:

$$\widehat{\psi}_{t_1} + \frac{1}{2} C_{gx} \widehat{\psi} + C_g \widehat{A}_x e^{-i\theta} = \qquad (6a)$$

$$= \int_{-\infty}^{\infty} V(\omega,\omega_1,\omega_2)\,\widehat{\psi}_1\,\widehat{\psi}_2\,\delta(\omega-\omega_1-\omega_2)\,d\omega_1\,d\omega_2 + O(\varepsilon^2)$$

where the kernel is given by:

$$V(\omega,\omega_1,\omega_2) + \frac{1}{8\pi}\left[\,2k_1k_2 + (\omega_1\omega_2)^2 + k_1^2\frac{\omega_2}{\omega} + k_2^2\frac{\omega_1}{\omega} - \omega^2\omega_1\omega_2\,\right] \qquad (6b)$$

and:

$$\widehat{\psi}(x,\omega,t_1) = \widehat{A}(x_1,\omega,t_1)e^{-i\theta}$$

C_g is the group velocity and $\widehat{\psi}_{1,2}$, $k_{1,2}$ are shorthand for $\widehat{\psi}(x,\omega_{1,2},t_1)$, $k(x,\omega_{1,2})$.

The induced mean flow of the wave field may be described in the limit $\omega \to o$. The group velocity becomes:

$$Cg \rightarrow \sqrt{h(x)}$$

assuming a flat bottom the equation for the 'zero' frequency mode will be:

$$\hat{A}_{t_1}(x,0,t_1) + \sqrt{h(x)} \quad \hat{A}_x(x,0,t_1) \; = \; \int_{-\infty}^{\infty} V(0,\omega,-\omega) \; \hat{A}(x,\omega,t_1) \, \hat{A}(x,-\omega,t_1) \, d\omega \qquad (7)$$

with the kernel given by:

$$V(0,\omega,-\omega) = \frac{1}{8\pi} \; (\omega^4 - k^2)$$

In Fig. 1a we show the evolution of the amplitudes of two short and the associated long wave using linear theory and computing the locked waves, Fig. 1b shows results of Frielich's model, Fig. 1c shows results of the present analysis. Fig. 2a shows the transformation of a Pierson-Moskowitz model from 14m to 4m depth and Fig. 2b shows the corresponding transformation of a modified JONSWAP spectrum. These are averages over 14 sets of initial conditions with random phases.

REFERENCES

Y. Agnon, 1991. On a uniformly valid model for surface wave interaction, submitted for publication.

D.J. Benney and P.G. Saffmann, 1966. Nonlinear interactions of random waves in a dispersive medium. *Proc. Roy. Soc. Lond.* A **289**, pp 301-320.

V.H. Chu and C.C. Mei, 1970. On slowly-varying Stokes waves. J. *Fluid Mech.* **41**, pp 873-887.

D.R. Crawford, B.M. Lake, P.G. Saffmann and H.C. Yuen, 1981. Stability of weakly nonlinear deep-water waves in two and three dimensions. *J. Fluid Mech.* **105**, pp 177-191.

A. Davey and K. Stewartson, 1974. On three-dimensional packets of surface waves. *Proc. Roy. Soc. London.* A**388**, pp 101-110.

V.D. Djordjevic and L.G. Redekopp, 1978. On the development of packets of surface gravity moving over an uneven bottom. *J. App. Math. Phys.* (ZAMP) **29**, pp 950-962.

S.Elgar and R.T. Guza, 1985. Shoaling gravity waves: Comparison between field observations, linear theory, and a nonlinear model. *J. Fluid Mech.* **158**, pp 47-70.

H. Freilich and Guza, 1984. Nonlinear effects on shoaling surface gravity moves. *Philos. Trans. Roy. Soc.* A **311**, pp 1-41.

R. Grimshaw, 1970. The solitary wave in water of variable depth. *J. Fluid Mech.* **42**, pp 639-656.

K. Herterich and K. Hasselmann, 1980.A similarity relation for the nonlinear energy transfer in a finite-depth gravity-wave spectrum. *J. Fluid Mech.* **97**, pp 215-224.

M. S. Longuet-Higgins, 1976. On the nonlinear transfer of energy in the peak of a gravity wave spectrum: a simplified model. *Proc. Roy. Soc. London.* A **347** pp 311-328.

A.C.Newell, 1968. The closure problem in a system of random gravity waves. *Rev. Geophys.* **6**, pp 1-31.

L.A. Ostrovski and E.L. Pelinovski, 1970. Wave transformation on the surface of a fluid of variable depth. *Izv. Atmos. Ocean. Phys.* **6**, pp. 552-555.

D.H. Peregrine, 1967. Long waves on a beach. *J. Fluid Mech.* **27**, pp 815-827.

M. Stiassnie, 1983. Derivation of the nonlinear Schrodinger Equation for shoaling wave-groups. *J. App. Math. Phys. (ZAMP),* **34**, pp 534-544.

M. Stiassnie and L. Shemer, 1984. On modifications of the Zakharov equation for surface gravity waves. *J. Fluid Mech.* **43**, pp 47-67.

K.D. Suh, R.A. Darlymyle and J.T. Kirby, 1990. An angular spectrum model for the profogation of Stokes waves. *J. Fluid Mech.* 221, pp. 205-232.

G.B. Whitham, 1974. Linear and nonlinear waves. Wiley, New York.

G.B. Whitham, 1979. Lectures on wave propogation. Bombay: Tata Institute of Fundamental Research.

V.E. Zakharov, 1968. Stability of periodic waves of finite amplitude on the surface of a deep fluid. *J. App. Mech. Tech. Phys.* (Engl. transl.) **9**, pp. 190-194.

(a)

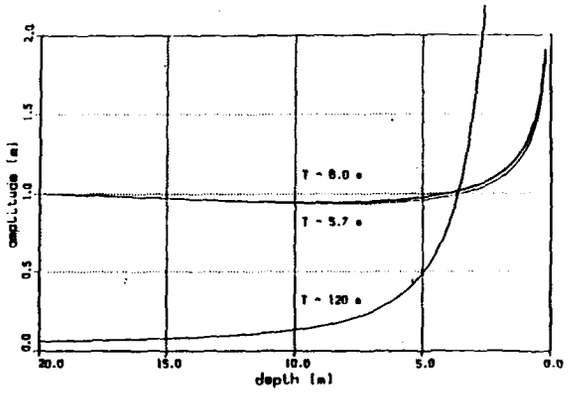

(b)

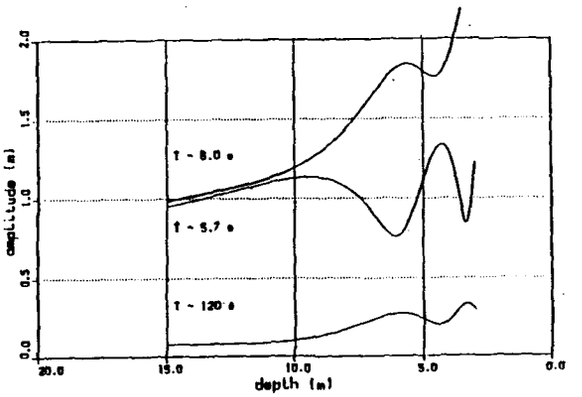

(c)

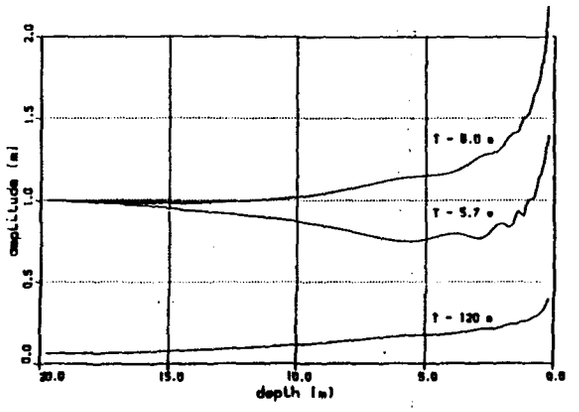

Fig. 1 (a) The evolution of the amplitudes of two short and the associated long wave using linear theory and computing the locked waves. (b) Results of Frielich's model. (c) Results of the present analysis.

(a)

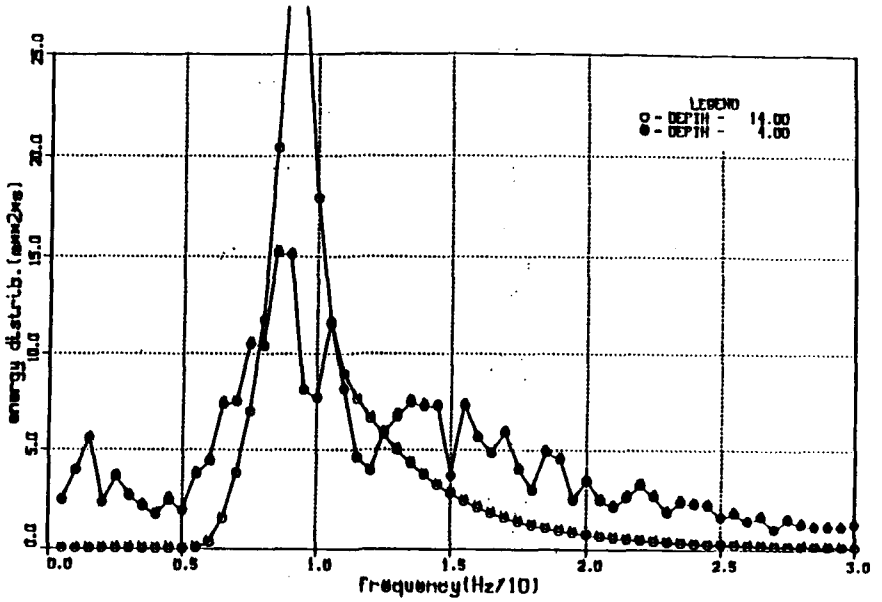

(b)

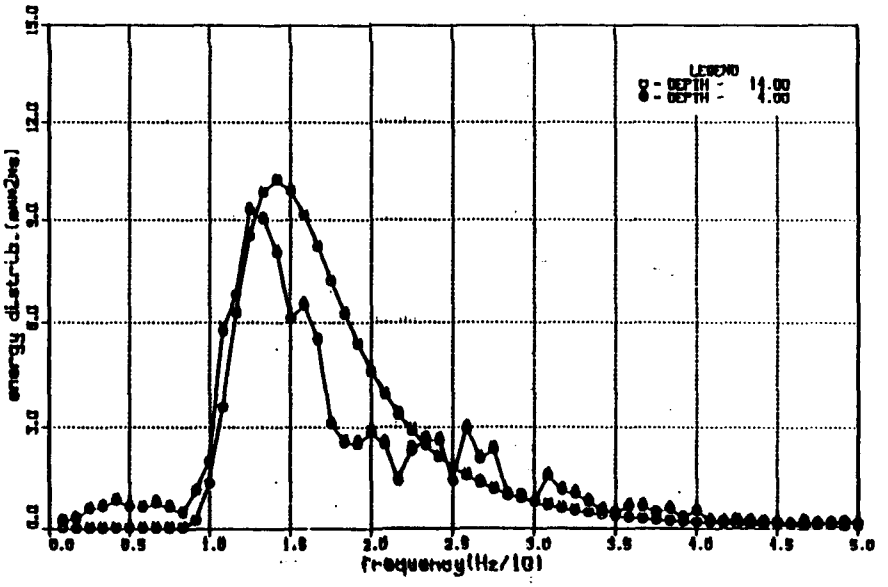

Fig. 2 (a) The transformation of a Pierson-Moskowitz model from 14m to 4m depth . (b) The corresponding transformation of a modified JONSWAP spectrum.

Discussion of Agnon and Shermat's paper

M.W. Dingemans

In your evolution equation for the complex envelope A I miss interaction with the mean motion (zeroth-harmonic). Because of the restricted depth there should be also a mean motion equation.

Furthermore, you neglected the reflection and this means that no reflection of free long waves is possible any more.

Author's reply

The 'mean motion' is included in the evolution equation as the zeroth harmonic, since the spectrum encompasses the whole frequency range. The reflection and the mean motion are not included in the specific truncated 3 wave interaction. You are right that at high order and steep bottom we need to include additional linear terms that include the bottom slope.

P. Janssen

You referred to Freibel results as being too erratic. I have two comments on this. a) Did you compare with what is happening in nature and b) did you include effects of bottom friction in the two models as this might smooth the results significantly, e.g. it might reduce the overshoot behaviour.

Author's reply

We did not compare with measurements. This is still planned. We have examined measurements that we have carried out in another setting in a wave tank, and they, too, exhibit extensive spectral modifications. At present we have not included bottom friction effects so we do not know how significant a modification they will induce.

E. Pelinovsky

For interpretation of non-monotonical behavior of spectral components it's interesting to know the relation between depth scale and nonlinearity length. I think that such a situation is typical if the depth scale is smaller than nonlinearity length. It's interesting to investigate the cnoidal wave stability when the depth decreases (if wave is equal to two harmonics only).

Author's reply

Thank you for the suggestion. In fact the model is more general than Boussinesq theory and can treat arbitrary depth to wavelength ratio, so the whole range from Stokes to cnoidal waves can be studied.

D.H. Peregrine

Please clarify the role of the WKB approximation in your modelling.

Author's reply

In the general part of the model WKB comes in for separating fast and slow variables in the time dependence only. This stage does not address the issue of propagation direction and places no limitation regarding the presence of reflected waves.

In the truncated model computations were made for three waves climbing a slope, picturing a situation with negligible reflection.

L. Tsimring

As far as I understand, you have studied the case of one-dimensional spectrum of waves. I think that taking into account non-one-dimensional triplets and quadruplets can amplify greatly the effectiveness of wave-wave interactions over the even bottom.

Author's reply

The approach is designed for 2-D spectra. In the presentation we have shown the 1-D case for simplicity of writing and computation.

Spectral evolution in waves traveling over a shoal

J.A. Battjes[†] *and S. Beji*[††]

Abstract

Nonlinear aspects of breaking and non-breaking waves propagating over a submerged trapezoidal bar have been investigated by laboratory experiments, with special emphasis on the generation of high-frequency energy. Data collected from the measurements are used for computing spectral and bispectral estimates in order to assess the contribution of wave breaking to the spectral evolution, as distinguished from that of the conservative nonlinear interactions. It is found that wave breaking itself, even in the case of plunging breakers, does not play a decisive role in the evolution of the spectral shape, but contributes by simply extracting energy in almost averaged manner. An approach is described to utilize this observation by using a semi-empirical formulation for dissipation due to breaking in conjunction with a weakly nonlinear numerical model.

1.Introduction

Harmonic generation in waves passing over submerged obstacles has long been known both experimentally and theoretically. Jolas (1960) carried out experiments with a submerged shelf of rectangular cross section and observed harmonics of a simple incident wave on the transmission side [1]. A few years later, in nonlinear optics, an analogous phenomenon concerning the transmission of a laser beam through a quartz crystal was explained theoretically by Armstrong *et al.* (1962). At about the same time, Phillips [2] gave the theoretical foundations of *nonlinear resonant interactions* between discrete wave components for deep water waves. Hasselmann (1962-63) extended the theory to the case of a continuous spectrum [3]. Mei and Ünlüata (1971), Tappert and Zabusky (1971), Johnson (1972), and Bryant (1973) made important contributions which further clarified the nonlinear interactions in shallow water waves [1, 4, 5].

Despite these achievements, the incorporation of wave breaking into these models remains basically unsolved. This deficiency severely limits their range of applicability, especially in coastal waters. While for non-breaking waves the generation of high frequency wave energy may entirely be attributed to conservative nonlinear effects, there have been doubts about the role of breaking. Some researchers hypothesized it was the wave breaking that controlled the phenomenon rather than conservative nonlinear interactions [6, 7]. The aim of the ongoing work reported here is to help resolve these questions and to contribute to the development of capabilities for numerical modeling of the most important processes observed.

The organization of the paper is as follows. The next section gives a brief description of the experimental arrangements, the bottom profile, and the wave conditions for the measurements. Section 3 begins with some descriptive features of the experiments. Measured power spectra at selected locations and the corresponding spatial variations of potential energy over the submerged bar are given next. The numerical model is introduced in Section 4 and numerical simulations of nonlinear (non-breaking) random waves are compared with the measurements both in time and in spectral domain. Also, an approach is sketched for predicting the spectral evolution of breaking waves.

[†] *Professor, Dept. of Civil Eng., Delft University of Technology, P.O. Box 5048, 2600 GA, Delft, The Netherlands.*

[††] *Post-doctorate fellow, Dept. of Civil Eng., Delft University of Technology, The Netherlands.*

2.Experiments

In order to assess the contribution of wave breaking to the generation, transfer, and dissipation of high frequency energy observed in the power spectra of waves traveling over submerged bars, tests were performed both for non-breaking and breaking (spilling and plunging) waves.

The experiments were carried out in the wave-flume of the Department of Civil Engineering, Delft University of Technology. The flume is 37.7 m long and 0.8 m wide. In its midsection, a trapezoidal submerged bar was built (see Figure 1.) At the downwave end a gently sloping spending beach was present (from previous experiments). The still-water depth was 0.4 m over the original, horizontal flume bottom and had a minimum of 0.10 m above the bar crest. Periodic and irregular input waves were used, the latter with a JONSWAP-type spectrum and a custom-made, very narrow band spectrum which eliminated effects of high-frequency tail in the input spectrum. Peak frequencies were f_p=0.4 Hz and f_p=1.0 Hz. Measurements of the free surface elevations were made with parallel-wire resistance gages at 8 different locations as sketched in Figure 1.

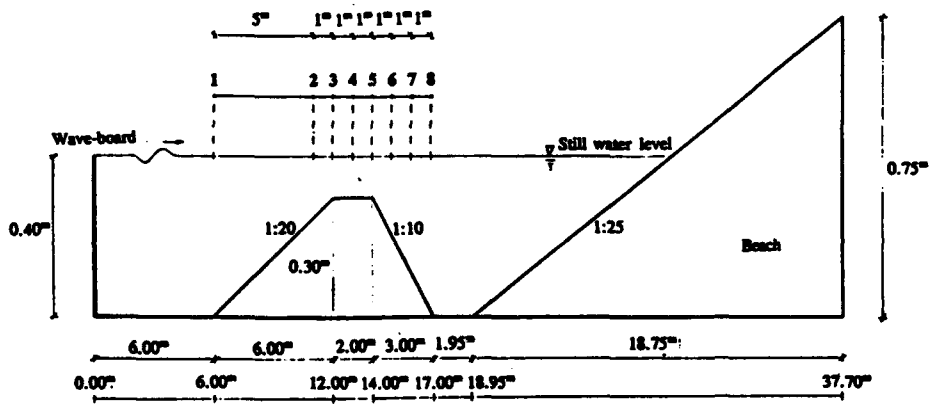

Figure 1 Longitudinal cross-section of wave flume and locations of wave gages.

3.Experimental Results

3.1 Descriptive features

Figures 2a and 2b exhibit the evolutions of the "long" (f=0.4 Hz) and "short" (f=1.0 Hz) waves over topography for monochromatic waves. The records were taken at the stations shown in Figure 1.

The long waves (f=0.4 Hz), once having gained in amplitude, gradually gave rise to one or more waves traveling at nearly the same speed with them in their tails. The evolution continued as the waves propagate over the upslope and horizontal part of the shoal. This phenomenon is reminiscent of the soliton formation behind a solitary wave, a subject which has been studied extensively [8,9]. As these finite amplitude long waves with their accompanying tails moved into the deeper water -downslope- they *decomposed* into several smaller amplitude waves of nearly harmonic frequencies. These released harmonic components then moved at different phase speeds but continued to exchange energy for several wave-lengths; the amplitudes of some of the higher frequency

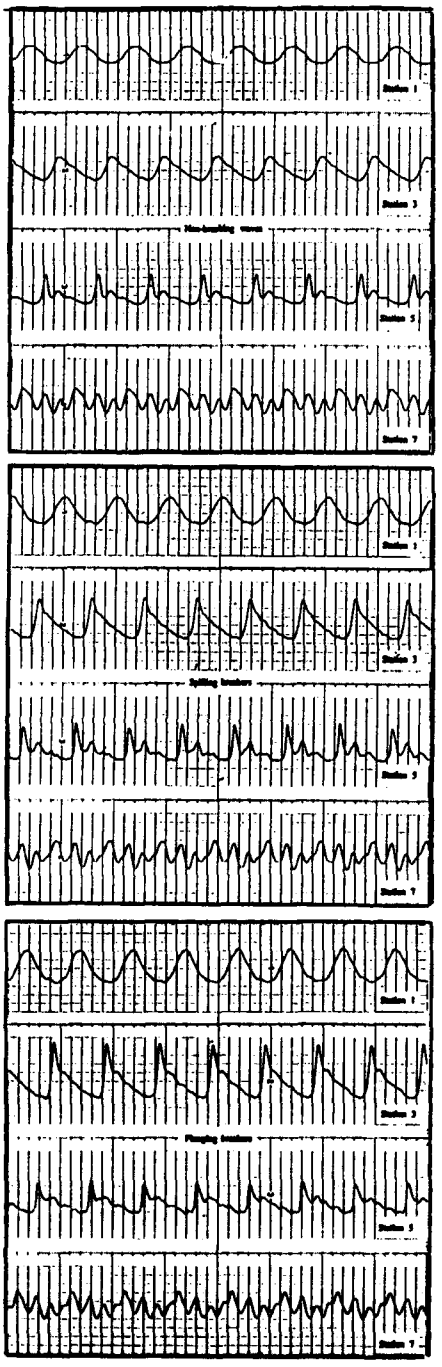

Figure 2a Evolving long waves (T=2.5 s).

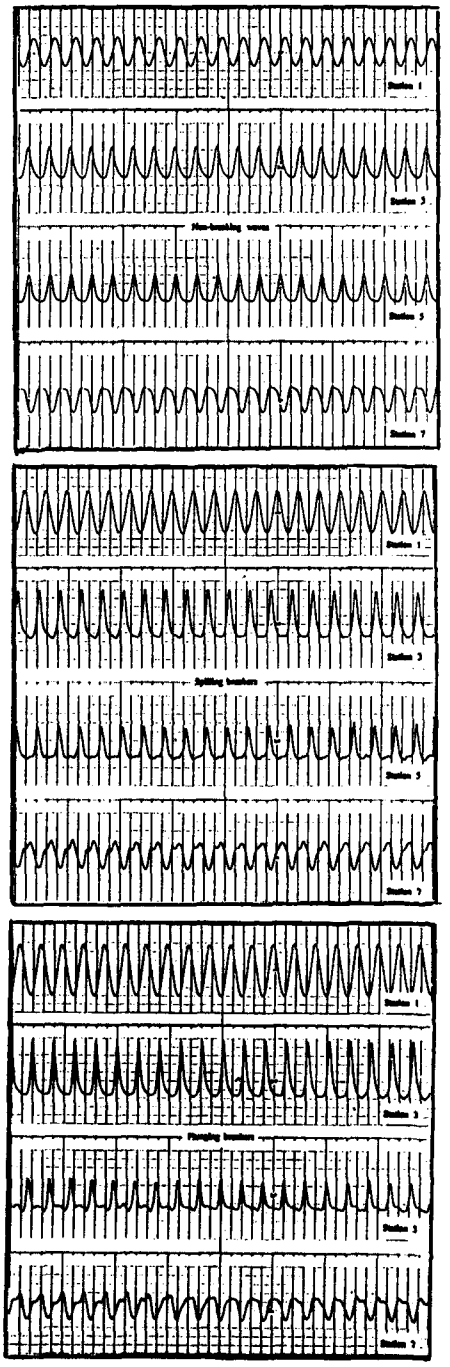

Figure 2b Evolving short waves (T=1.0 s).

components even became larger than that of the primary wave itself.

The short waves (f=1.0 Hz), on the contrary, did not develop any tail waves as they grew in amplitude but kept their vertical symmetry and appeared as higher-order Stokes waves. Decomposition in the deeper region was not nearly drastic as that of the longer waves and only relatively smaller amplitude second order harmonics were released.

It is readily seen in the records in Figure 2 that wave breaking does not alter the evolution of the wave forms drastically. From a practical point of view this is encouraging because it implies the possibility of combining a conservative (weakly) nonlinear model, such as a Boussinesq model, with a semi-empirical formulation of the dissipated energy in averaged form. This line of development is pursued presently; preliminary results are given below.

3.2 Spectral evolution

As indicated in Section 2, irregular waves were generated with two different types of spectra. Figure 3 shows the spectral evolutions for the breaking, spilling, and plunging waves (f_p=0.4 Hz) at three selected stations for the case of the custom-made narrow band spectrum, for nonbreaking waves, spilling breakers and plunging breakers. It can be observed that the primary wave energy at any given station remains clearly separated from that of the higher frequency part generated by nonlinear interactions. It is important to notice that the overall features of the spectral shape evolution for different wave conditions (nonbreaking or breaking) do not differ appreciably. Further clarification is offered in Figure 4 where the spatial variations of normalized potential energy of the total, the primary, and the higher frequency components are plotted. In computing the primary wave energy the range of integration is taken between 0.0 Hz and 0.6 Hz while for higher frequency energy it is between 0.6 Hz (= 1½ f_p) and 2.5 Hz. The total energy is obtained simply by adding the two. In each case the variations are normalized with respect to the total measured at station 1.

3.3 Bispectral Evolution

Bispectral estimates for a JONSWAP-type incident wave spectrum for non-breaking and plunging waves at selected stations were computed. The results of these computations are outlined below.

In the case of non-breaking waves, at station 3, where the waves enter the shallowest region, primary frequency components interact strongly with themselves, f_p-f_p, and provide a driving mechanism for the generation of the second harmonic components, $2f_p$. At station 5, the second and third harmonic components, $2f_p$ and $3f_p$, grow strong enough to engage in appreciable interactions with the primary waves components, f_p-$2f_p$ and f_p-$3f_p$. Although not as strong, the interactions of the second harmonics with themselves, $2f_p$-$2f_p$, are also visible. At station 7, in the deeper region behind the bar, the strength of the interactions is diminished, and the primary wave component interactions, f_p-f_p, are no longer dominant because the amplitudes of higher frequency waves are now comparable with those of the peak frequency components.

In the case of plunging breakers, at station 3, the nonlinear interactions are already spread to encompass the higher frequencies. This is not surprising because the significant wave height is now 1.7 times greater than its counterpart in the non-breaking case. However, as we move to station 4 we see a sharp decrease -nearly 50%- in the strength of nonlinear interactions. This is a direct consequence of wave breaking: *clipping* wave heights by breaking reduces the degree of nonlinearity. At station 7 the strength of interactions is only a fraction of those in the previous cases but not expended completely. Indeed the significant wave height in this case at this particular station is still

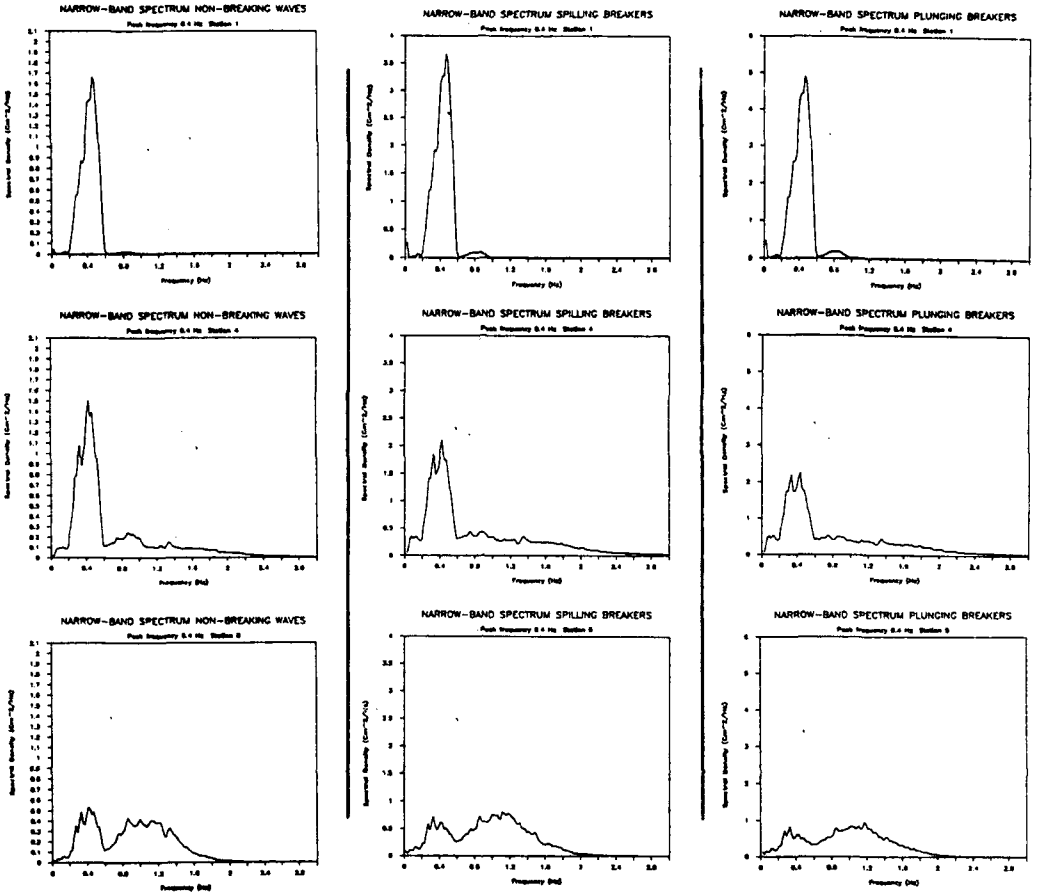

Figure 3 Spectral evolutions for non-breaking, spilling, and plunging waves.

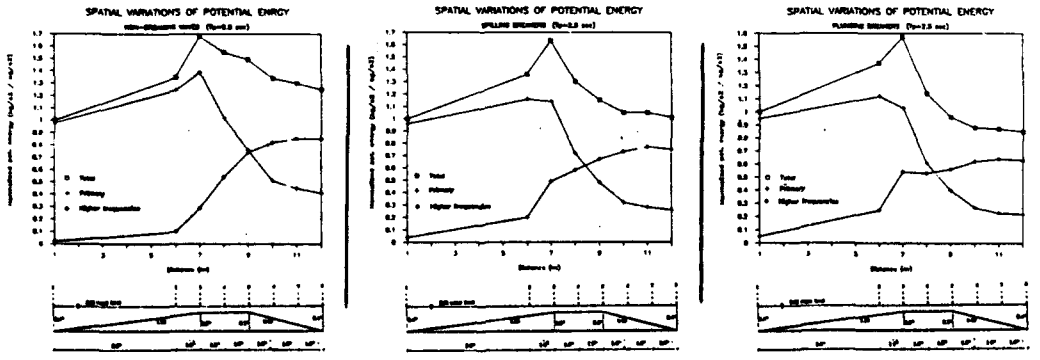

Figure 4 Spatial variations of total potential energy of the primary wave field and of higher frequencies.

1.4 times greater than the one measured for non-breaking waves. The strength of the nonlinear interactions is likewise greater.

4.Numerical modeling

4.1 Introduction

The observation that in our experiments the evolution of the spectral shape is not significantly affected by wave breaking suggests the possibility of using a (non-spectral) model for the dissipation of total wave energy by breaking, in conjunction with a conservative (potential-flow) model incorporating nonlinear wave-wave interactions. This development is in progress.

4.2 Numerical model

As a first step, a conservative nonlinear wave propagation model has to be chosen. "Exact" nonlinear models solving the full governing equations [10] are considered to be too demanding in computational effort in view of the intended operational use (ultimately). Instead, a Boussinesq type model was chosen because it does contain nonlinearity and it is suited for shallow-water conditions. We used it in the following form:

$$u_t + uu_x + g\zeta_x = \frac{1}{3}h^2 u_{xxt} + hh_x u_{xt} + bh^2 (u_t + g\zeta_x)_{xx}$$

$$\zeta_t + [(h+\zeta)u]_x = 0$$

where ζ denotes the surface displacement and u the vertically averaged horizontal velocity. For $b=0$ the momentum equation reduces to its standard form as it was derived by Peregrine [11] for a gently sloping bottom. For $b=1/15$ a major improvement for the dispersion characteristics is achieved. This extension to the original Boussinesq equations was first suggested by Witting [12] and then recapitulated by Madsen *et al.*[13]. A mathematical model with good dispersion characteristics is essential in this study because the waves decomposing behind the submerged obstacle generate free high frequency components which in essence may be regarded as relatively deep water waves.

In the numerical treatment of the governing equations, except for some minor but crucial adjustments, we basically followed the guidelines given in Peregrine (1967). Details of the numerical scheme will be reported elsewhere.

In figure 5a measured surface elevations are compared with the computational results for non-breaking but nonlinear random waves at selected stations. Figure 5b shows the comparisons for the measured and computed spectra at the same stations. The agreement is remarkable and justifies our choice of the governing equations.

4.3 Breaking waves

In the previous part we emphasized the overall similarity observed in the spectral evolution of breaking and non-breaking waves and substantiated it with laboratory measurements. The results clearly suggested the crucial point that for sufficiently high nonlinearity the spectral evolution for different wave conditions differed only by a scaling factor. This in turn implies that in this definite range it is possible to predict the spectral evolution of a certain wave field from the knowledge of another wave field provided that appropriate scaling is used and that the *overall* energy loss due to breaking is accounted for. This line of attack is presently in progress.

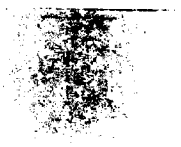

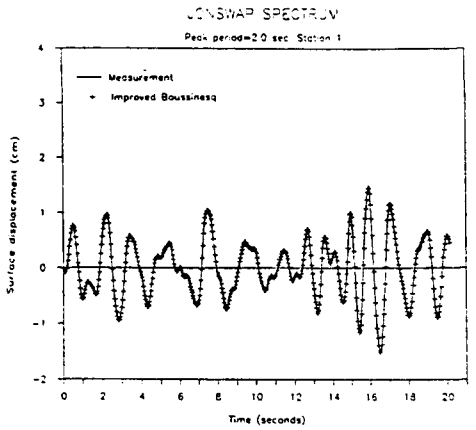

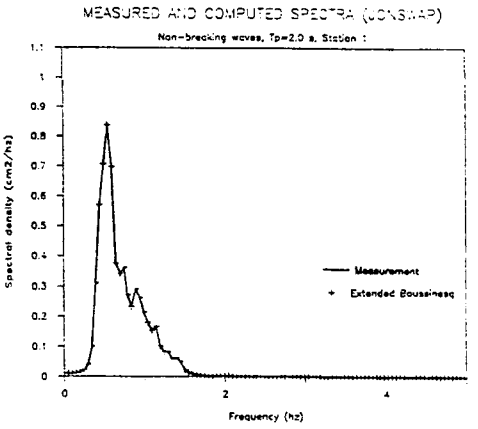

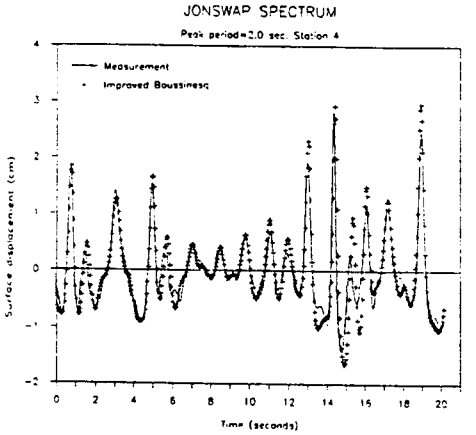

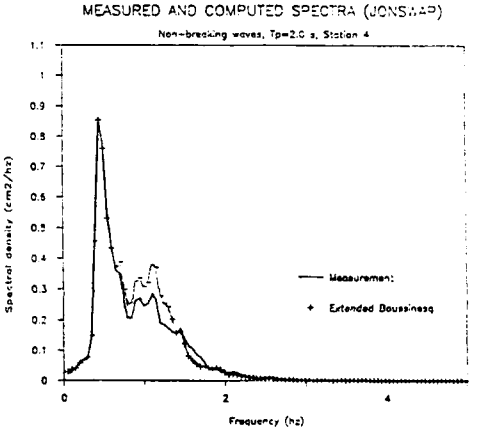

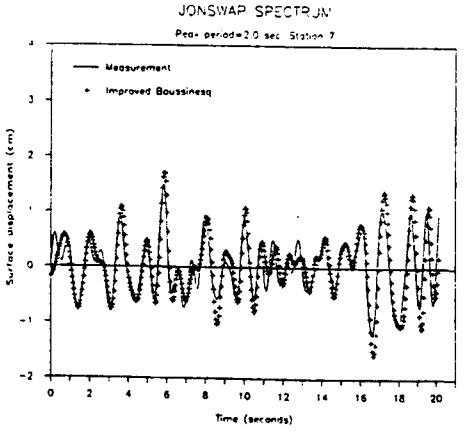

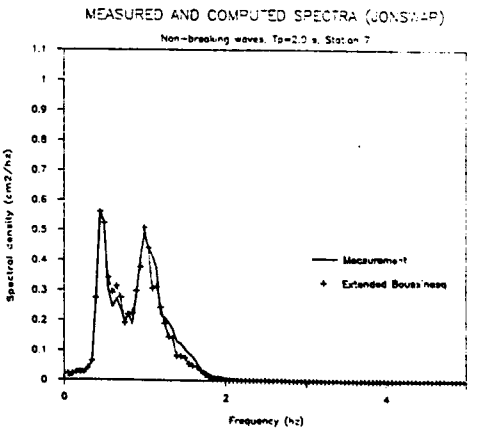

Figure 5a Time domain comparisons of measurements with numerical simulations. (f_p=0.5 Hz.)

Figure 5b Spectral domain comparisons of measurements with numerical simulations. (f_p=0.5 Hz.)

5.Conclusions

Spectral and bispectral estimates computed from laboratory measurements are analyzed to clarify the effects of wave breaking on the inherently nonlinear phenomenon of high frequency energy generation and transfer in the power spectra of waves traveling over submerged profiles. It is found that wave breaking merely dissipates energy in averaged manner and does not introduce drastic alterations to the spectral shape. However it does reduce the strength of nonlinear interactions severely by *clipping* the wave heights. In this respect breaking works, as in the classical sense, as a limiting mechanism.

A practical implication of these findings is the apparent possibility of combining a weakly nonlinear non-dissipative model with a semi-empirical dissipation formulation for the total energy. This is the subject matter of ongoing research.

Acknowledgements

The software used for bispectral computations was developed by Dr. J.R.C. Doering in the course of his doctoral studies at Dalhousie University and was obtained through a personal communication. The financial support for this project was provided in part by the EC-MAST program within the framework of WASP-project.

References

[1] Mei, Chiang C., *The Applied Dynamics of Ocean Surface Waves*, World Scientific, Singapore, 1989.

[2] Phillips, O.M., On the dynamics of unsteady gravity waves of finite amplitude, Part 1. The elementary interactions, J. Fluid Mech., **9**, pp.193-217, 1960.

[3] Hasselmann, K., On the non-linear energy transfer in a gravity-wave spectrum, Part 1. General theory, J. Fluid Mech., **12**, pp.481-500, 1962.

[4] Johnson, R.S., Some numerical solutions of a variable-coefficient Korteweg-de Vries equation (with applications to solitary wave development on the shelf), J. Fluid Mech., **54**, pp.81-91, 1972.

[5] Bryant, P.J., Periodic waves in shallow water, J. Fluid Mech., **59**, pp.625-644, 1973.

[6] Sawaragi, T. and K. Iwata, On wave deformation after breaking, *Proc. of the 14th Conf. on Coastal Eng.*, ASCE, pp.481-498, 1974.

[7] Dingemans, M.W., Investigations in the undular-bore formulation, *Tech. rep.*, Part I, 68 pp., Delft Hydraulics, Delft, The Netherlands, May 1989.

[8] Ono, H., Wave propagation in an inhomogeneous inharmonic lattice, J. Phys. Soc. Jap., **32**, pp.332-336, 1972.

[9] Johnson, R.S., On the development of a solitary wave over an uneven bottom, Proc. Cambridge Philos. Soc., **73**, pp.183-203, 1973.

[10] Ohyama, T. and K. Nadaoka, Development of a numerical wave tank for analysis of nonlinear and irregular wave field, (to appear in Fluid Dynamics Res.,) 1991.

[11] Peregrine, D.H., Long waves on a beach, J. Fluid Mech., **27**, pp.815-827, 1967.

[12] Witting, J.M., A unified model for the evolution of nonlinear water waves, J. Comp. Phys., **56**, pp.203-236, 1984.

[13] Madsen, P.A., R. Murray, and O.R. Sørensen, A new form of the Boussinesq equations with improved linear dispersion characteristics, Coastal Eng., **15-4**, pp.371-388, 1991.

Discussion of Battjes and Beji's paper

N. Huang

Have you measured reflection caused by the bottom topography? In a similar set-up, I have measured reflection of the shoulder of a false bottom, which caused the local energy density to bias high.

Author's reply

Previous experiments with comparable bottom topography has indicated a reflection coefficient less than about 5% in the frequency range of the incident waves ($f > 0.3$ Hz, say).

D.H. Peregrine (comment)

The figure showing variation of potential energy density with distance in the non-breaking case may be interpreted as indicating the rate of flow of energy, if we assume there is no significant deviations from equi-partition of energy. This implies a progressive increase in the rate of wave energy flow on the top of the bar where nonlinear effects are strongest.

One phenomenon which may be related is the forward transfer of energy that occurs between solitary waves when one wave overtakes a slightly smaller one. There is a change of identities of individual crests implying a "local group velocity" greater than the phase velocity of each wave as energy is transferred to the leading crest.

Numerical Solutions of Violent Water-Wave Impact Against a Vertical Wall

M.J. Cooker & D.H. Peregrine,
Department of Mathematics, University of Bristol, Bristol BS8 1TW, U.K.

This paper is concerned with the very large and short-lived fluid pressures exerted by water waves when they impact a structure. Further details are reported by Cooker and Peregrine (1990 a,b). Numerical solutions of two-dimensional potential flow, with a free surface, carried out using a boundary-integral method, are presented. The method is that due to Dold and Peregrine (1986), and as extended by Tanaka et al (1987) and Cooker (1990). The pressure is constant (zero) on the free surface, and the exact equations of motion are used to track the unsteady free-surface motion. The results show that when a wave is made to break against a wall the waterline can experience an acceleration of thousands of g, and that this accompanies pressures which are more than ten times the hydrostatic pressure (due to the height of fluid in the wave).

We limit ourselves to reporting results for a simple wave travelling over a flat bed at $y = -h$, but we have computed similar effects with other types of wave. The wave surface is a transition in water level between $y = 0$ at $x = -\infty$, and $y = \Delta h$ at $x = +\infty$. This free surface level is accompained by a flow which, at $x = +\infty$ is uniform and directed to the left, and there is zero flow at $x = -\infty$. The initial data (connecting water height with velocity potential) is specified by shallow water theory, and specifies the initial disturbance to be left-propagating at all points, within the context of that theory. Figure 1 shows the subsequent, fully nonlinear motion for a wave of height $\Delta h = 1.5\ h$, and initial maximum slope 16°. The wave breaks and the horizontally projected jet has a speed of $2.6\ \sqrt{(gh)}$ and the surface particle acceleration under the arch of the wave is approximately 4 g.

We simulate wall-wave impact by colliding two identical waves which are symmetically arranged about $x = 0$ (the position of the wall). Experimenters have long-known that the greatest peak pressures on a vertical wall are exerted when the wave face is parallel to the wall at the moment of impact. Figure 2 shows the result when we arrange the initial wall-wave distance so that the wave face just becomes vertical before meeting the wall. The subsequent motion in the region shown in figure 2 is presented in figure 3. The free surface motion occurs in two successive stages: first, the surface near the waterline contracts with a remarkably self-similar motion. Secondly, a very narrow vertical jet forms at the wall. The waterline acceleration is very high at the instant the

jet forms: 1136 g. The acceleration is even greater at later times, at points near the jet base, and reaches 8500 g. The speed of the jet tip increases to 19.5 $(gh)^{1/2}$ at the last computed time.

The remarkably high fluid accelerations are associated with very high fluid pressure gradients, and pressures, in the fluid. There is a pressure maximum of 46 ρgh at the wall, and it lies a distance of only 0.05 h beneath the surface. The pressure rises to this maximum in a time of only $0.01(h/g)^{1/2}$ (for a 15cm wave in a depth h = 10cm , this pressure rise-time is 1 millisecond). However, in the vertical jet the pressure gradients are much smaller and we might expect the subsequent motion of the fluid in the jet to be effectively under free-fall. On this basis the fluid in the jet tip will be thrown to a height of nearly 200 h (in the absence of air resistance). Judging from photographs of storm waves this is not an unreasonable figure for the height to which spray might be projected.

Further work is being carried out to characterise the types of wave face motion, and to compare with experiments and other simpler models of wave impact, such as pressure impulse theory (see Cooker and Peregrine, 1990 a). In this way we hope to shed light on the open problem of how to scale peak pressure data measured in small laboratory tanks up to full-scale waves on the seashore.

Acknowledgement: *Financial support from U.K. Science and Engineering Research Council grants GR/F 28298 and GR/G 21032 , is gratefully acknowledged.*

REFERENCES

COOKER M.J. (1990) "The interaction between steep water waves and coastal structures" Ph.D. Thesis, Faculty of Science, University of Bristol, 209pp.

COOKER M.J., D.H. Peregrine (1990 a) "A model for breaking wave impact pressures" Proc. 22nd Intl. Conf. on Coastal Engineering, ASCE 1473-1486.

COOKER M.J. , D.H. Peregrine (1990 b) "Computations of violent motion due to waves breaking against a wall" Proc. 22nd Intl. Conf. Coastal Eng. ASCE 164-176.

DOLD J.W., D.H. Peregrine (1986) "An efficient boundary-integral method for steep unsteady water waves" in "Numerical methods in fluid dynamics II" edited by K.W. Morton, M.J. Baines, Oxford University Press 671-679.

TANAKA M., J.W. Dold, M. Lewy, D.H. Peregrine (1987) "Instability and breaking of a solitary wave" Journal of Fluid Mechanics 185, 235-248.

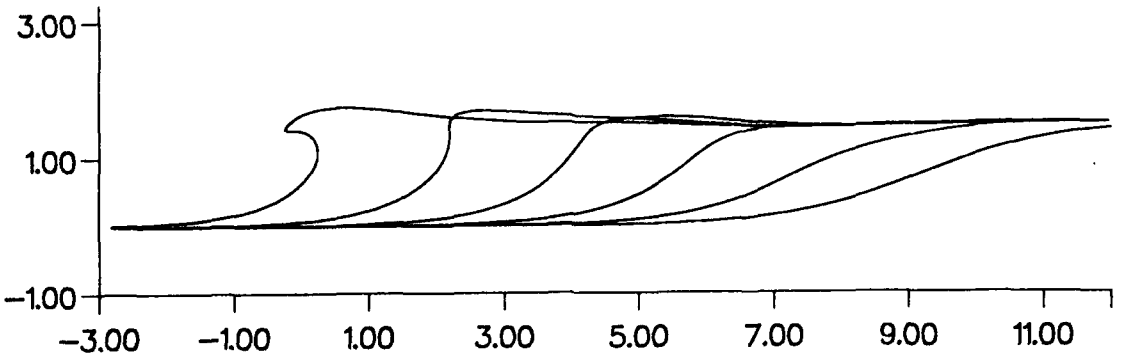

FIGURE 1. The breaking of a long wave into still water with no wall. Initially the wave is a transition between still water and a free surface at y = 0 at x = $-\infty$, and a uniform flow with a free surface of height Δh = 1.5 at x = $+\infty$. The wave travels right to left over a flat bottom at y = - h. Times 0 [1] 5 $\sqrt{(h/g)}$.

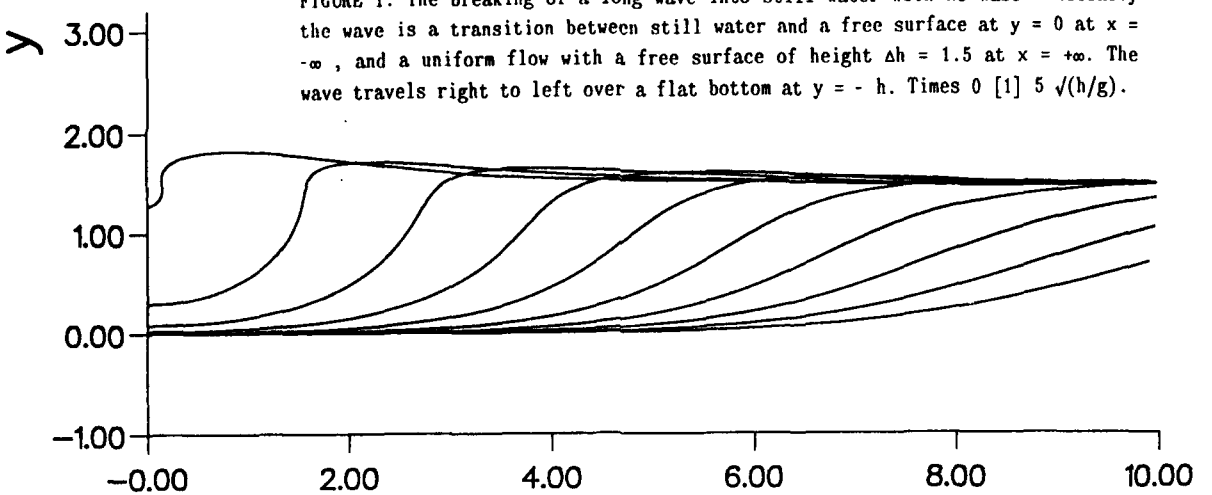

FIGURE 2. Two waves of the type shown in figure 1 collide at x = 0. (Only the right-half of the computation domain is shown.) Times are 0.0 [0.6] 5.4 $\sqrt{(h/g)}$.

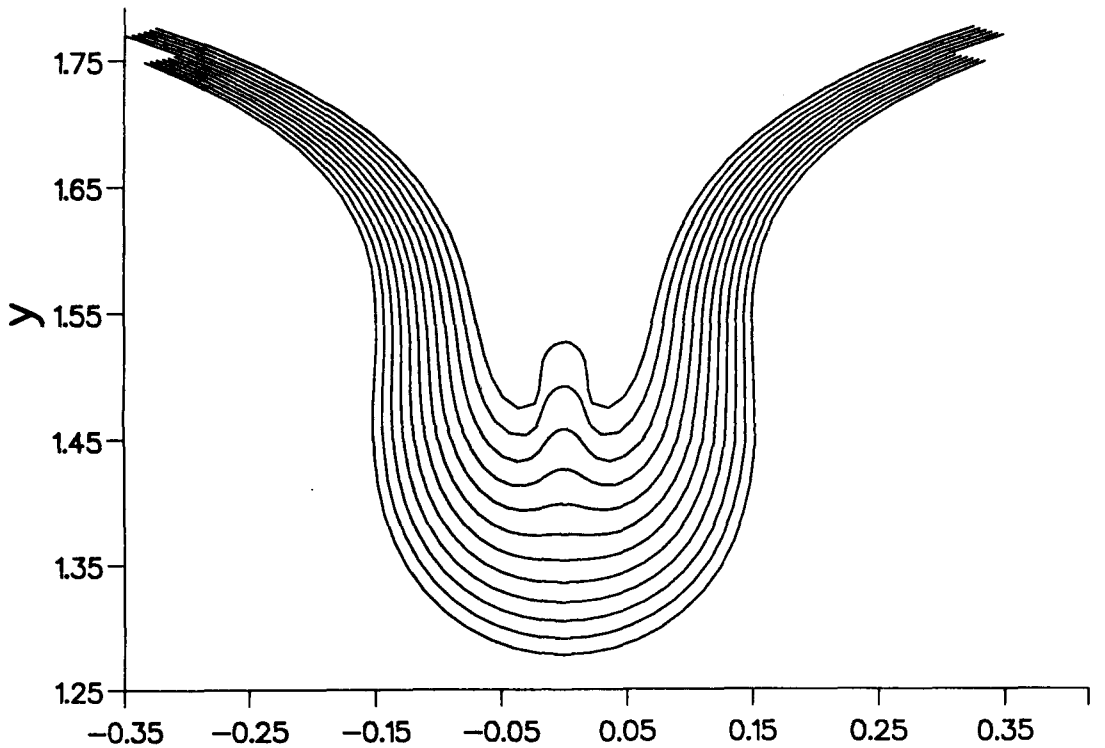

FIGURE 3. Detail of the zone shown in figure 2 at later times: 5.400 [0.002] 5.422 $\sqrt{(h/g)}$. Both halves of the computation domain are shown. Note the vertically rising jet. The jet tip (waterline) acceleration has a maximum of 1135 g when the jet first appears, and its speed is 19.5 $\sqrt{(gh)}$ at t = 5.422 $\sqrt{(h/g)}$.

Use of Hamiltonian techniques in water wave propagation problems

M.W. Dingemans* and A.C. Radder†

1. Introduction.

The governing equations for irrotational wave motion on an incompressible inviscid fluid are given by the Laplace equation and the three boundary conditions:

$$\nabla^2\Phi + \frac{\partial^2\Phi}{\partial z^2} = 0 \quad ; \quad -h(\boldsymbol{x}) \le z \le \zeta(\boldsymbol{x},t) \tag{1}$$

$$\frac{\partial\Phi}{\partial t} + \frac{1}{2}\left\{(\nabla\Phi)^2 + \left(\frac{\partial\Phi}{\partial z}\right)^2\right\} - \mathcal{T}[\zeta] + g\zeta = 0 \quad ; \quad z = \zeta(\boldsymbol{x},t) \tag{2}$$

$$\frac{\partial\zeta}{\partial t} + \nabla\Phi\cdot\nabla\zeta = \frac{\partial\Phi}{\partial z} \quad ; \quad z = \zeta(\boldsymbol{x},t) \tag{3}$$

$$\frac{\partial\Phi}{\partial z} + \nabla\Phi\cdot\nabla h = 0 \quad ; \quad z = -h(\boldsymbol{x}), \tag{4}$$

where

$$\mathcal{T}[\zeta] = \gamma\nabla\cdot\left[\frac{\nabla\zeta}{\left(1+|\nabla\zeta|^2\right)^{1/2}}\right], \tag{5}$$

and γ is the surface tension and two-dimensional vectors have been used, $\boldsymbol{x} = (x,y)^T$. It has been shown that the Hamiltonian constitutes a variational principle when it is expressed in terms of the free surface elevation ζ and the value of the velocity potential at the free surface $\varphi(\boldsymbol{x},t) = \Phi\{(\boldsymbol{x},\zeta(\boldsymbol{x},t),t\}$, see, e.g., Zakharov (1968) and Broer (1974). The total energy of the fluid is given by

$$\begin{aligned}\mathcal{H} &= \iint d\boldsymbol{x}\,dy\,H = \iint dx\,dy\,(V+T) = \\ &= \rho\iint dx\,dy\left\{\frac{1}{2}g\zeta^2 + \gamma\left[\sqrt{1+|\nabla\zeta|^2}-1\right] + \int_{-h}^{\zeta} dz\frac{1}{2}\left[(\nabla\Phi)^2 + \left(\frac{\partial\Phi}{\partial z}\right)^2\right]\right\}.\end{aligned} \tag{6}$$

Notice that the Hamiltonian density is effectively a function of ζ and φ. Variation of $\mathcal{H}$ to ζ and φ gives the two canonical equations:

$$\frac{\delta\mathcal{H}}{\delta\varphi} = \rho\frac{\partial\zeta}{\partial t} \quad \text{and} \quad \frac{\delta\mathcal{H}}{\delta\zeta} = -\rho\frac{\partial\varphi}{\partial t}, \tag{7}$$

* Delft Hydraulics, P.O. Box 152, 8300 AD Emmeloord, The Netherlands
† Rijkswaterstaat, P.O. Box 20907, 2500 EX The Hague, The Netherlands

where δ denotes the variational derivative. Notice that Eqs. (7) are the free surface conditions (2) and (3) while Eqs. (1) and (4) have been used as side conditions.

As a variation of the Hamiltonian is equivalent with the original full set of water wave equations, the same equations are found, but one has the opportunity to find approximate equations from an approximation of the Hamiltonian. When the positive definiteness of the exact Hamiltonian density H is also carried over to the approximate density H_a, then good dynamical behaviour is guaranteed. Every approximation $\mathcal{H}_a$ which maintains the symmetries of $\mathcal{H}$ guarantees automatically the corresponding conservation laws to hold.

The major difficulty in applying the Hamiltonian is that the kinetic energy density should be formulated in terms of the free surface value of the velocity potential and of ζ.

2. Boussinesq-type approximation.

The kinetic energy $\mathcal{T}$ is splitted into a contribution $\mathcal{T}_0$ in the region below $z = 0$ and $\mathcal{T}_s$ above $z = 0$ (Broer, 1974 and Broer et al., 1976). Using Green's identity, $\mathcal{T}_0$ can be written as

$$\mathcal{T}_0 = \frac{1}{2}\rho \int dx \int_{-h}^{0} dz \left[(\nabla\Phi)^2 + \left(\frac{\partial\Phi}{\partial z}\right)^2 \right] = \frac{1}{2}\rho \int dx\, \varphi_0 \left(\frac{\partial\Phi}{\partial z}\right)_{z=0}, \text{ with } \varphi_0 = \Phi(x,0,t). \tag{8}$$

An expression for $(\partial\Phi/\partial z)_{z=0}$ is obtained by solving the Laplace equation for Φ in $[-h,0]$ with the bottom condition and with $\Phi = \varphi_0$ at $z = 0$. For a horizontal bottom this can be done by means of Fourier transforms. One obtains the general solution (Broer, 1974)

$$\left(\frac{\partial\Phi}{\partial z}\right)_{z=0} = -h\mathcal{R}\frac{\partial^2\varphi_0}{\partial x^2} \tag{9}$$

with $\mathcal{R}$ an integral operator with kernel $R(x-x')$

$$R(x-x') = \frac{1}{2\pi}\int dk \frac{\tanh kh}{kh} e^{ik(x-x')} = \frac{1}{2\pi}\int dk \hat{R}(k) e^{ik(x-x')} = -\frac{1}{\pi h}\log\tanh\frac{\pi|x-x'|}{4h},$$

where log is the natural logarithm and $\hat{R}$ is the symbol of $\mathcal{R}$: $\hat{R} = \dfrac{\tanh kh}{kh}$. For $\mathcal{T}_0$ is then obtained

$$\mathcal{T}_0 = \frac{1}{2}\rho \int dx \frac{\partial\varphi_0}{\partial x} h\mathcal{R}\frac{\partial\varphi_0}{\partial x}.$$

The contribution $\mathcal{T}_s$ is expanded in a Taylor series around $z = 0$[1]:

$$\begin{aligned}\mathcal{T}_s &= \frac{1}{2}\rho\int dx \left\{ \zeta \left[\left(\frac{\partial\varphi_0}{\partial x}\right)^2 + \left(\frac{\partial\varphi_0}{\partial z}\Big|_{z=0}\right)^2 \right] + \cdots \right\} = \\ &= \frac{1}{2}\rho\int dx \left\{ \zeta \left(\frac{\partial\varphi_0}{\partial x}\right)^2 + \zeta\left(h\mathcal{R}\frac{\partial^2\varphi_0}{\partial x^2}\right)^2 + \cdots \right\}.\end{aligned}$$

[1] It is here that use is made of the fact that the waves are fairly long.

Still an explicit expression in terms of the free surface velocity potential φ is needed. We need the transformation of φ_0 to φ. This is achieved by performing a Taylor series expansion of $\Phi(x,z,t)$ around $z=0$: $\Phi(x,z,t) = \sum_{n=0}^{\infty} \frac{1}{n!} z^n \left(\frac{\partial^n \Phi}{\partial z^n}\right)_{z=0}$ and for long waves only a few terms are needed. From the Laplace equation a recurrent expression follows:

$$\left(\frac{\partial^n \Phi}{\partial z^n}\right)_{z=0} = -\frac{\partial^2}{\partial x^2}\left(\frac{\partial^{n-2}\Phi}{\partial z^{n-2}}\right)_{z=0} \qquad n = 2,3,\cdots$$

from which we obtain with (9)

$$\left(\frac{\partial^{2n}\Phi}{\partial z^{2n}}\right)_{z=0} = (-1)^n \frac{\partial^{2n}\varphi_0}{\partial x^{2n}} \qquad \text{and} \qquad \left(\frac{\partial^{2n+1}\Phi}{\partial z^{2n+1}}\right)_{z=0} = (-1)^n h\mathcal{R}\frac{\partial^{2n+2}\varphi_0}{\partial x^{2n+2}} .$$

The series expansion of $\varphi = \Phi(x,\zeta,t)$ then is

$$\Phi = \varphi_0 - S\varphi_0 \quad \text{with} \quad S \equiv \sum_{n=0}^{\infty} \frac{(-1)^n \zeta^{2n+1}}{(2n+1)!}\left\{\frac{\zeta}{2n+2} + h\mathcal{R}\right\}\frac{\partial^{2n+2}}{\partial x^{2n+2}} .$$

This series should be inverted so as to obtain φ_0 as function of φ. By iteration we obtain (Timmers, 1976):

$$\begin{aligned}\varphi_0 &= \varphi + S\left[\varphi + S\left\{\varphi + S(\cdots)\right\}\right] = \sum_{n=0}^{\infty} S^n\varphi = \\ &= \varphi + \zeta h\mathcal{R}\varphi_{xx} + \frac{1}{2}\zeta^2\varphi_{xx} + \zeta h\mathcal{R}\partial_x^2\left(\zeta h\mathcal{R}\varphi_{xx}\right) + \cdots\end{aligned}$$

and thus

$$\frac{\partial\varphi_0}{\partial x} = \varphi_x + \partial_x\left(\zeta h\mathcal{R}\varphi_{xx}\right) + \frac{1}{2}\partial_x\left(\zeta^2\varphi_{xx}\right) + \cdots . \tag{10}$$

Then $\mathcal{T}_0 = \frac{1}{2}\rho\int dx \frac{\partial\varphi_0}{\partial x} h\mathcal{R}\frac{\partial\varphi_0}{\partial x}$ can be rewritten in surface variables. The Hamiltonian $\mathcal{H}$ then becomes in lowest order

$$\mathcal{H} = \frac{1}{2}\rho\int dx\left(\varphi_x h\mathcal{R}\varphi_x + \zeta\varphi_x^2 + g\zeta^2\right) . \tag{11}$$

The canonical equations are

$$\frac{\partial\zeta}{\partial t} = -\frac{\partial}{\partial x}\left(h\mathcal{R}\varphi_x\right) - \frac{\partial}{\partial x}\left(\zeta\varphi_x\right) \quad \text{and} \quad \frac{\partial\varphi}{\partial t} = -\frac{1}{2}\varphi_x^2 - g\zeta . \tag{12}$$

Approximations of the non-local integral operator $\mathcal{R}$ then yields specific sets of Boussinesq-like equations. Notice that the density H in (11) is not positive definite. The density can be made positive definite in the following way.

$$\begin{aligned}\mathcal{H} &= \frac{1}{2}\rho\int dx\left(\varphi_x h\mathcal{R}\varphi_x + \zeta\varphi_x^2 + g\zeta^2\right) \cong \frac{1}{2}\rho\int dx\left[\varphi_x\left(h+\zeta\right)\mathcal{R}\varphi_x + g\zeta^2\right] = \\ &= \frac{1}{2}\rho\int dx\left[\left(h+\zeta\right)\left\{\mathcal{G}\left(\varphi_x\right)\right\}^2 + g\zeta^2\right] ,\end{aligned} \tag{13}$$

with $\widehat{\mathcal{G}^2} = \hat{\mathcal{R}}$. Notice that the approximation consists of taking $\varphi_x \zeta \mathcal{R} \varphi_x$ instead of $\zeta \varphi_x^2$ which is permitted because for long waves one has $\mathcal{R} = 1 + \cdots$ where the dots represent higher-order terms.

For the localization of the operator $\mathcal{G}$ we proceed as follows. We consider first the horizontal bottom case. Because $\mathcal{G}^2 = \mathcal{R}$ we have

$$\hat{\mathcal{G}} = \sqrt{\frac{\tanh kh}{kh}} \, .$$

A [1/1] Padé approximation of $\hat{\mathcal{G}}$ for long waves (small kh) is of the following form

$$[1/1]\ \hat{\mathcal{G}} = \hat{G}_a = \frac{1 + \frac{1}{6}\alpha (kh)^2}{1 + \frac{1}{6}\beta (kh)^2}$$

and leads to $\alpha = 9/10$ and $\beta = 19/10$. With operator-correspondence $ik \sim \partial_x$ we then obtain for the localized approximation $\mathcal{G}_a$ of $\mathcal{G}$:

$$\mathcal{G}_a \equiv \frac{1 + \frac{9}{60} h^2 \frac{\partial^2}{\partial x^2}}{1 + \frac{19}{60} h^2 \frac{\partial^2}{\partial x^2}} \, . \tag{14}$$

For the uneven-bottom case the situation is more complicated. In the first place it is not possible to obtain an exact solution for $\mathcal{T}_0$ with Fourier techniques. For one horizontal dimension, an expansion of the stream function from the bottom upwards, in which the long-wave assumption has to be imposed, leads to an Hamiltonian of the form (11) with $\mathcal{R}$ now given by (see Timmers, 1976)

$$\mathcal{R} \equiv 1 + \frac{1}{2} h \frac{\partial^2}{\partial x^2} h - \frac{1}{6} h^2 \frac{\partial^2}{\partial x^2} \, . \tag{15}$$

In the same way as before a positive definite Hamiltonian can be obtained with the approximate operator $\mathcal{G}_a = \mathcal{L}_\alpha^{-1} \mathcal{L}_\beta$ with $\alpha = 0.9$ and $\beta = 1.9$ and with $\mathcal{L}_\gamma$ given by

$$\mathcal{L}_\gamma = 1 - \frac{1}{4} \gamma h \frac{\partial^2}{\partial x^2} h + \frac{1}{12} \gamma \frac{\partial}{\partial x} h^2 \frac{\partial}{\partial x} \, , \ \gamma = \alpha \text{ or } \beta \, . \tag{16}$$

Other forms of $\mathcal{L}_\gamma$ are possible depending on the treatment of the bottom derivatives. The present form of $\mathcal{G}_a$ is a symmetric one which has better numerical properties than non-symmetric forms (Mooiman, 1991).

For two horizontal dimensions one has

$$\mathcal{H} = \frac{1}{2} \rho \iint dx\, dy \, \left\{ (h + \zeta) \, [\mathcal{G}_a (\nabla \varphi)]^2 + g \zeta^2 \right\} \tag{17}$$

with the approximate operator $\mathcal{G}_a$ written as $\mathcal{G}_a = \mathcal{L}_\beta^{-1} \mathcal{L}_\alpha$ and $\alpha = 0.9$ and $\beta = 1.9$. The operator L_γ ($\gamma = \alpha$ or β) is given for uneven bottom as

$$\mathcal{L}_\gamma = 1 - \frac{1}{4} \gamma h \frac{\partial^2}{\partial x_i \partial x_i} h + \frac{1}{12} \gamma \frac{\partial}{\partial x_i} h^2 \frac{\partial}{\partial x_i} \, , \tag{18}$$

where $(x, y) = (x_1, x_2)$ and the summation convention has been used.

3. Comparison with measurements.

The shoal experiment as described by Berkhoff et al. (1982) is used to compare a numerical solution of the Boussinesq-like model with measurements. The Boussinesq-like model is derived from the Hamiltonian (17) with the approximate operator defined with (18). A measuring area of 20 m by 20 m has been taken in a wave basin of 30 m by 35 m. The bottom geometry consists of a sloping bottom and a shoal (parabolic in height and elliptic in circumference) and has been shown in Fig. 1.

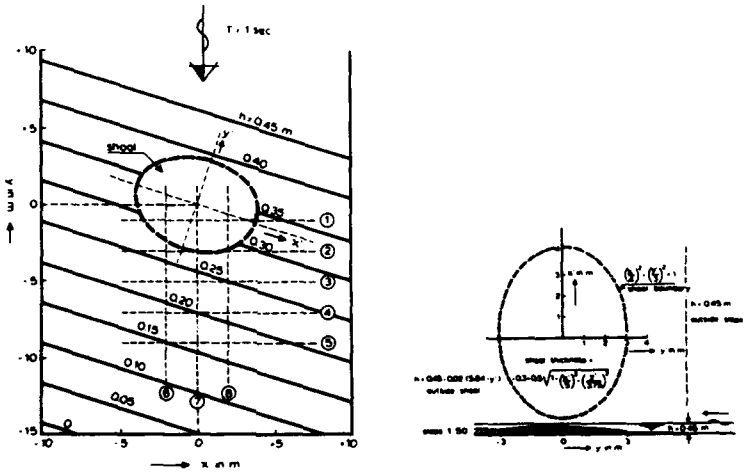

FIG. 1. *The geometry of the measurements*

The grid size for the measurements was .25 m by .25 m or .50 m by .50 m. Here regular waves are considered. The wave period is 1 s and the wave height near the wave board is 4.64 cm. For the numerical computation a region of 25 m by 30 m with grid size of 6.25 by 6.25 cm has been taken, and thus, near the wave board at .45 m depth with a wave length of 1.50 m this means that 24 meshes per wave length in the deeper part have been taken. The time-step chosen was 0.025 s and thus 40 time-steps in one wave period were taken. The computation was carried out for 1200 time steps (30 wave periods). The wave amplitude distribution relative to the incoming wave height is given as a percentage in Fig. 2a, while isolines from the measurements are given in Fig. 2b.

In order to look in more detail, the results of the computation and the measurement is compared along the sections 5 and 6, which are the most informative sections of these measurements, see Fig. 3. For a parabolic model similar results have been shown in Dingemans et al. (1984) and, in more detail, in Dingemans and Radder (1986).

Although the depth/wave length ratio $h/\lambda = 1/3$ is rather large in the deeper part of the basin (much larger than the value of 1/7 which should normally be applied), the resulting amplitudes are remarkably good.

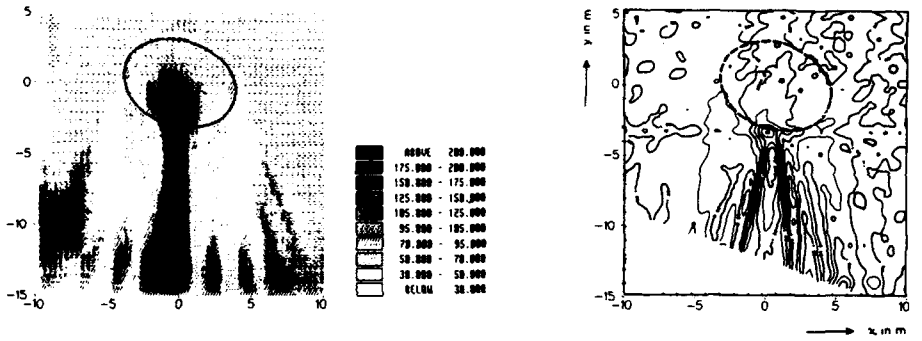

FIG. 2. *The wave height distribution in computation (a) and in measurement (b)*

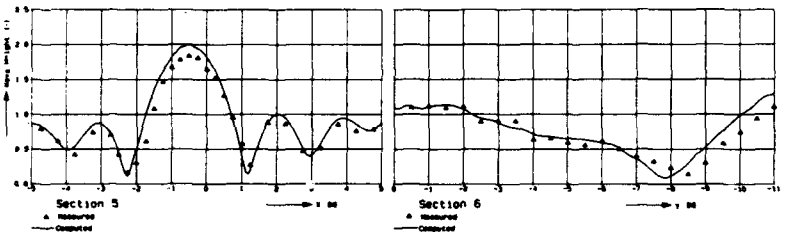

FIG. 3. *The wave height distribution along sections 5 and 6; triangles: measurement, line: computation*

4. Approximation valid for all depths.

For problems with one horizontal dimension an approximate Hamiltonian can be developed which is uniformly valid from deep to shallow water (Radder, 1992). In this case, the kinetic energy density T can be written as

$$T = -\frac{1}{2}\rho\varphi\frac{\partial\psi}{\partial x} \cong \frac{1}{2}\rho\frac{\partial\varphi}{\partial x}\psi\,, \tag{19}$$

where $\psi = \Psi(x, \zeta(x,t), t)$ is the stream function evaluated at the free surface.

To express ψ in terms of the canonical variables φ and ζ, a conformal mapping of the fluid domain $Z = x + iz$ into an infinite strip in the complex $W-$plane $W = \chi + i\xi$ is used (Woods, 1961)

$$Z(W) = \frac{1}{2}\int_{-\infty}^{\infty} d\chi' \left\{ \tanh\left[\frac{\pi}{2}(W-\chi')\right]\zeta(\chi') + \coth\left[\frac{\pi}{2}(W-\chi')\right]h(\chi') \right\}\,. \tag{20}$$

A solution for the stream function $\Psi(x,z,t)$ at the free surface is sought for in two steps:

1. Solve the problem in the $W-$plane
2. Find the inverse transformation $\chi(x)$ along the free surface.

A solution of the linear problem $\frac{\partial^2\Psi}{\partial\chi^2} + \frac{\partial^2\Psi}{\partial\xi^2} = 0$ in $0 \le \xi \le 1$ and the boundary conditions $\Psi = 0$ at $\xi = 0$ and $\Psi = \psi(\chi)$ at $\xi = 1$ by means of Fourier transforms gives at the free

surface $\xi = 1$

$$\psi(\chi) = -\frac{1}{\pi}\int_{-\infty}^{\infty}\frac{d\varphi}{d\chi'}\log\tanh\left(\frac{\pi}{4}\,|\chi-\chi'|\right)d\chi' \,. \tag{21}$$

To express (21) in terms of variables of the physical plane, an expression for the function $\chi(x)$ along the free surface has to be found. This crucial step leads, through a Fourier transform of the imaginary part of (20), to a symbolic operator equation which can be solved by an expansion in partial fractions (for details, see Radder, 1992). The result is, for a horizontal bottom and with the notation $\eta(x) = h + \zeta(x)$

$$\frac{d\chi}{dx} = \frac{1}{(1+\varepsilon)\eta} \,. \tag{22}$$

where the function $\varepsilon(x)$ is here given by the first-order approximation[2]

$$\frac{1}{1+\varepsilon} \cong 1 + \frac{1}{\eta(p)}\int_0^{\infty}\frac{dq}{\exp(\pi q)-1}\frac{d}{dq}\left[\eta(p+q)+\eta(p-q)\right] \,, \tag{23}$$

and $p = \int_0^x dr/\eta$. From (19), (21) and (22) one obtains for the kinetic energy density the expression

$$T = \frac{1}{2}\rho\int_{-\infty}^{\infty}dx'\varphi_x\varphi_{x'}R_\varepsilon(x,x';\eta) \,, \tag{24}$$

where the symmetric function R_ε is given by

$$R_\varepsilon(x,x';\eta) \equiv -\frac{1}{\pi}\log\tanh\left(\frac{\pi}{4}\left|\int_x^{x'}\frac{dr}{(1+\varepsilon)\eta}\right|\right) \,. \tag{25}$$

It is noted that the kinetic energy functional, expressed in the χ-variable, is *positive definite*, and this property is preserved on transforming from χ to x when the Jacobian (22) is positive and bounded.

Linear theory is obtained for $\varepsilon = 0$ and $\eta = h$ (i.e., infinitesimal waves, and thus ζ is neglected); the expression for $R_\varepsilon \equiv R_0$ then coincides with the one given by Broer (1974) for linear waves. For deep water it turns out that $\varepsilon = O(ka)$ and then Stokes' theory is appropriate, $\eta \cong h$, so that

$$R_\varepsilon(x,x';\eta) \equiv -\frac{1}{\pi}\log\tanh\left(\frac{\pi}{4h}\left|\int_x^{x'}\frac{dr}{1+\varepsilon}\right|\right) \,. \tag{26}$$

For shallow water we have $\varepsilon = O(kh\cdot ka)$ and we can put $\varepsilon = 0$ (Boussinesq approximation). Then:

$$R_\varepsilon(x,x';\eta) \equiv -\frac{1}{\pi}\log\tanh\left(\frac{\pi}{4h}\left|\int_x^{x'}\frac{dr}{1+\frac{\zeta}{h}}\right|\right) \,. \tag{27}$$

[2] higher-order expressions have been given by Radder (1992).

The advantage of a Hamiltonian model based on (27) as compared with the Boussinesq model (13) is that in the former model the linear theory is recovered in case of deep water. For practical applications, such as the evolution of a solitary wave over an uneven bottom, numerical solution of the resulting integral equations is needed (see Zwartkruis, 1991).

Finally, from (22) and (23) we may infer an integral criterion for wave breaking in deep and shallow water. By definition, breaking is considered here to occur at points where $d\chi/dx = 0$, and the approximation (23) then leads to the criterion

$$\eta(p) + \int_0^\infty \frac{dq}{\exp(\pi q) - 1} \frac{d}{dq} [\eta(p+q) + \eta(p-q)] = 0 \,. \tag{28}$$

The implication of condition (28) is currently under investigation. As a preliminary result, for the case of a fifth-order Stokes wave in deep water, it is found that according to (28) this wave breaks at the crest when the steepness ka becomes 0.46. This is in good agreement with the exact value of 0.443, for a wave with a stagnation point.

5. References.

Berkhoff, J.C.W., Booij, N. and Radder, A.C. (1982) *Verification of numerical* wave propagation models for simple harmonic linear water waves. *Coastal Engineering* **6** pp. 255-279

Broer, L.J.F., (1974). On the Hamiltonian theory of surface waves. *Appl. Sci. Res.* **29**, pp. 430-446.

Broer, L.J.F., Groesen, E.W.C. van, and Timmers, J.M.W. (1976). Stable model equations for long water waves. *Appl. Sci. Res.* **32(6)**, pp. 619-636.

Dingemans, M.W. and Radder, A.C. (1986). Surface wave propagation over an uneven bottom; wave deformation by a shoal; effect of non-linearity. *Delft Hydraulics*, Report W301 part 6.

Dingemans, M.W., Stive, M.J.F., Kuik, A.J., Radder, A.C. and Booij, N. (1984). Field and laboratory verification of the wave propagation model CREDIZ. *Proc. 19th Conf. on Coastal Engng.*, Houston, pp. 1178-1191

Mooiman, J. (1991). Boussinesq equations based on a positive definite Hamiltonian. *Delft Hydraulics*, Report Z294, Sept.

Radder, A.C. (1992) An explicit Hamiltonian formulation of surface waves in water of finite depth. *J. Fluid Mechanics* , to appear

Timmers, J.M.W. (1976). Equations for long low water waves (*in Dutch*). Masters thesis, Technical University of Eindhoven.

Woods, L.C. (1961). *The theory of subsonic plane flow.* Cambridge University Press.

Zakharov, V.E., (1968). Stability of periodic waves of finite amplitude on the surface of a deep fluid. Zh. Prikl. Mekh. i Techn. Fiz. **9(2)**, pp. 86-94 [*Soviet Physics, J. Appl. Mech. Techn. Phys.* **2**, pp. 190-194.]

Zwartkruis, T.J.G. (1991). Computation of solitary wave profiles described by a Hamiltonian model for surface waves. ECMI-Report, Eindhoven University of Technology, Parts 1 and 2.

MEASUREMENTS AND NUMERICAL CALCULATIONS OF THE EVOLUTION OF NONLINEAR WAVE GROUPS

by

Mark. A. Donelan and William M. Drennan

The dispersive nature of deepwater waves is employed to produce coalescing groups of waves both in a large laboratory tank and a computer simulation. Gaussian envelopes are chosen since the exact solution for the evolution of linear gaussian wave groups is known and provides a test of the numerics. We explore the physical and numerical results in regard to the effects of amplitude dispersion on group propagation and on the spectral redistribution of energy as the groups coalesce and become highly nonlinear.

Discussion of Donelan and Drennan's paper

M. Stiassnie

Why are you trying to compare the time-scales of your experiments with those of the energy transfer equation? In your experiment you choose very specific phases whereas in the energy-transfer equation they are assumed to be uncorrelated, at least to lowest order.

P. Janssen

It is possible to have this fast nonlinear transfer of energy in a random sea (with Gaussian distribution) under the condition that the spectrum is sufficiently narrow. The result is the random version of the Benjamin-Feir instability (cf. Alber & Saffman, Janssen).

Author's reply

The point was not to verify the weak nonlinear interactions, but rather to illustrate that the time scales of these transfers, which occur in very steep groups, are much faster than those of the weak nonlinear interactions.

Wave breaking and other issues in dynamics and statistics of wind waves

Roman E. Glazman
Jet Propulsion Laboratory, California Institute of Technology,
Mail Stop 300-323, 4800 Oak Grove Drive, Pasadena, CA 91109

Abstract

Based on theoretical predictions of stationary wave spectra, various statistical properties of developed seas can be evaluated and related to external factors of air-sea interactions. Of particular importance are the wave slope variance, the rates (temporal and spatial) of steep and breaking wave events, the surface skewness, the mean height of specular facets, etc. The first two quantities are highly important for wave dynamics and air-sea energy and momentum exchanges. Wave field statistics associated with high spectral moments manifest themselves in microwave remote sensing signatures of the ocean surface, and their observed dependence on external factors can be compared with theoretical predictions. Such comparisons are highly desirable in view of the fact that satellite data, in contrast to most conventional wave observations, cover open ocean conditions where the wind fetch attains hundreds of kilometers. A peculiar feature of open ocean waves is the existence of an extended range of wavenumbers within which the energy and action are cascaded from the generation range to lower wavenumbers. The inverse cascade (characterized by the minus-ten-thirds law in terms of the energy spectrum [Zakharov and Zaslavskii, 1981]) results in much greater values of the wave age than that associated with the "fully developed sea." The latter, in our view, remains a poorly defined concept with dubious experimental support. The present paper provides a brief review of sea surface's statistical properties based on the weak turbulence theory as well as a heuristic extension of the theory to account for a greater number of resonantly interacting Fourier harmonics. Also presented is a summary of satellite and in situ observations. The attention is focused on the following two central topics.
1. The intrinsic inner scale:
The surface elevation field described by the Zakharov-Filonenko spectrum is statistically self-affine with the corresponding Hausdorff dimension 9/4. Implications for air-sea interactions emerge when the small-scale roughness becomes independent of the spectral peak range (the "fractal regime" in surface geometry), leading to a universal regime of air-sea interactions. At high energy inputs (wind speed above 7 m/s), the apparent unboundedness of the wave slope variance necessitates the existence of a transitional subrange in the wave spectrum. This subrange, introduced heuristically, is characterized by a locally accelerated decay of the spectral density function as the wavenumber increases. It is matched with the Phillips subrange (k-to-the minus-four) at yet higher wavenumbers approaching the capillary range. Weakly-nonlinear four-wave interactions (which dominate wave dynamics) coexist with highly localized strongly nonlinear events of steep and breaking waves. This allows one to study statistics of breaking waves as rare events of high level excursion by a (three-dimensional) field of the wave slope (or of the vertical acceleration). The intrinsic inner scale for the dissipation subrange is estimated by comparing theoretical predictions with observations of whitecaps.

Mean Gaussian curvature, mean height of specular facets and breaking wave statistics are critically dependent on high spectral moments, hence of the value of the intrinsic inner scale. Therefore, favorable comparisons of these statistics with experimental data provide an indirect confirmation of the theory.
2. The mean number of resonantly interacting Fourier components. The coexistence of the weakly nonlinear inertial cascade described in the framework of the weak turbulence theory (WTT) [a series of papers by Zakharov and his collaborators spanning the period 1966 to the present] with intermittent events of steep and breaking wavelets points to the tentative nature of the four-wave approximation employed in WTT. Apparently, the actual number of resonantly interacting wave components represents the statistical average over a surface area and time interval. Extending Kolmogorov's hypothesis of localness of wave-wave interactions (in the wavenumber-frequency space) to the case of wind generated surface gravity waves, the stationary spectrum for an arbitrary number of resonantly interacting components is derived. The actual number is determined as a function of the energy input from wind using the Miles mechanism for the wind energy input. The derivation is based on the notion of the interaction time for the energy transfer from the nth step in the energy cascade to the (n+1)th step.

REFERENCES:
Glazman, R.E., and P. Weichman, 1989. Statistical geometry of a small surface patch in a developed sea. J. Geophys. Res., 94(C4), 4998-5010.
Glazman, R.E., and P. Weichman, 1990. Reply. J. Geophys. Res., 95(C2), 1771-1773.
Glazman, R.E., 1991a. Statistical problems of wind-generated gravity waves arising in microwave remote sensing of surface winds. IEEE Trans. Geosci. Rem. Sensing. 29(1), 135-142.
Glazman, R.E., 1991b. Reply. J. Geophys. Res., 96(C3), 4979-4983.
Glazman, R.E., 1991c. Multiwave interaction theory for wind-generated surface gravity waves. Journal of Fluid Mech. To appear.
Zakharov, V.E., 1984. Kolmogorov spectra in weak turbulence problems. Handbook of Plasma Physics, Eds. M.N.Rosenbluth and R.Z. Sagdeev. Vol.2: Basic Plasma Physics II. Chapter 5.1. pp.3-36, Elsevier Science Publishers.
Zakharov, V.E. and N.N. Filonenko, 1966, The energy spectrum for stochastic oscillation of a fluid's surface. Doklady Academii Nauk S.S.S.R., 170(6), 1292-1295, (in Russian)
Zakharov, V.E. and M.M. Zaslavskii, 1982. The kinetic equation and Kolmogorov spectra in the weak turbulence theory of wind waves. Izvestiya, Atmospheric and Oceanic Physics (English Translation), 18(9), 747-753

Discussion of Glazman's paper

M.A. Donelan (comment)

Regarding the use of -7/2 power for the description of high wavenumber spectra of wind waves, the evidence from a variety of observations is that a slice through the wavenumber spectrum $\psi(k,\theta)$ in the downwind direction is proportional to k^{-4} in the gravity-range of the spectrum. However, at wavenumbers from twice the peak (of the spectrum) to ten times the peak, the spectrum broadens in direction so that the frequency spectrum looks more like ω^{-4} (corresponding to $|k|^{-7/2}$) rather than ω^{-5}.

THE LOCAL PROPERTIES OF OCEAN SURFACE WAVES BY THE PHASE-TIME METHOD

Norden E. Huang
NASA Goddard Space Flight Center
Greenbelt, Maryland 20771 USA

The traditional methods for analysis ocean wave data are limited to the Fourier Transform for power spectrum, and standard statistical procedures for various probability density functions. But these methods address only the universal rather than the local properties of the ocean wave field. From the dynamic point of view, association of the local wave properties with real time is crucial for many important problems of wave studies: the groupiness, the interactions of small waves with the underlying long waves, and the local deformation of the wave profile to breaking. Yet, none of the traditional methods can resolve them. The local properties, however, can be associated with real time readily through the phase function of the wave data. Although phase function has been examined by Rice (1954), Bitner-Gregersen and Gran(1983), Meville (1983) and Read and Sobey (1987), none of them has explored the importance of using phase function to associate the events to real time and to study the local properties of the wave field. In fact, the importance of the phase function has been grossly overlooked. In the past, the typical treatment of the phase is to wrap the phase result around $\pm\pi$ or 0 and 2π. The wrapped phase will give an uninformative uniformly distributed phase statistics (Melville, 1983 and Tayfun and Lo, 1989, 1990). In this short note, we will examine the phase function without wrapping around the fixed 2π interval. The unwrapped phase reveals new properties of the wave field in the group structures as well as the possible fractal properties of the wave field.

The essence of the phase-time method can be summarized as follows: First, we make the real time series, $\zeta(t)$, an analytic function, $Z(t)$, with

$$Z(t) = \zeta(t) + i\,\xi(t), \tag{1}$$

in which $\xi(t)$ is the Hilbert transformation of $\zeta(t)$, defined as

$$\xi(t) = \frac{1}{\pi} P \int_{-\infty}^{\infty} \frac{\zeta(t')}{t'-t}\, dt', \tag{2}$$

with P indicating the Cauchy principal values. Secondly, from the analytic data, we can obtain the phase function, $\phi(t)$, as

$$\phi(t) = \arctan\left(\frac{\xi(t)}{\zeta(t)}\right). \tag{3}$$

The phase function is the key for the phase-time analysis. It can be further decomposed into the mean frequency, n_0 , and a deviation part, $\Theta(t)$, as

$$\phi(t) = n_0\, t + \Theta(t). \tag{4}$$

In the past, this phase function is wrapped around the fixed modulus of 2π. By unwrapping and detrending the phase data, we obtain the detailed information on the variable part of the phase, $\Theta(t)$. By definition, the time derivative of the phase function is the local frequency of the time series; i. e.

$$\frac{\partial \phi}{\partial t} = n_0 + \frac{\partial \theta}{\partial t}. \tag{5}$$

Thus derivative of $\Theta(t)$ actually gives the frequency deviations from the mean. Positive values represent a higher frequency than the mean, or a faster rate of change; negative values represent lower frequency than the mean, or a slower rate of change.

Now we will apply the phase-time method to a typical data set of wave data measured by a 3 meter buoy off the east coast of the US. The data given in Figure 1a is digitized at 1 Hz, for a total of 90 minutes. The unwrapped phase function is given in Figure 1b. Presented in this format, the phase function looked rather smooth. The mean slope of the data is 0.7 rad/sec, which is equivalent to a mean frequency of 0.1 Hz or a mean period of ten seconds. After detrending the phase, the residual is the deviation from the mean, or the $\Theta(t)$ function as given in Equation (4). The result is shown in Figure 1c. The $\Theta(t)$ function is very jagged; in fact, it looks similar to the Weierstrass-Mandelbrot function discussed by Berry and Lewis (1980). A spectrum of the $\Theta(t)$ is given in Figure 2. This spectrum cover a frequency range of three decades, yet it shows no scale at all, which suggests that the phase function is a self-similar process or fractal. According to the relationship between spectral slope and the fractal dimension established by Berry (1979)

$$D = (5 - \alpha) / 2, \qquad (6)$$

where $-\alpha$ is the slope of the power spectrum of the time series, and D is the fractal dimension. From Figure 2, the slope of the spectrum of our data is at -2.2, which gives a fractal dimension of 1.4 according to equation (6).

Next, we will examine the phase function along the time axis. The positive slope of the phase function suggests higher local frequency, and negative slope of the phase function suggests lower frequency. Figure 1c shows that the phase function, though random, exhibit long persistent runs.

In addition to this frequency modulations, there are also two visibly different types of wave groups: The first type consists of a number of waves propagate at a similar group velocity. This event is indicated by the near straight lines sections in the $\Theta(t)$ function. These are the groups that fit the traditional definition of the group. The second type consists of a single large wave amidst of the small waves. The single large waves have a much lower frequency than the neighboring waves. It can propagate much faster than the ambient waves as sweep up energy as it moves. The existence of this second type of group has never been clearly documented; yet report of the freak wave coming out of nowhere attests to their existence. Surprisingly, this new type of groups is also very common in our data. The existence of this new type of group can be easily identified by a local break in the phase function.

Refferences:

Berry, M. V. and Z. V. Lewis 1980 Proc. Roy. Soc. Lond., A 370, 459-484.

Bitner-Gregersen, E. M. and S Gran, 1983 Applied Ocean Res., 5, 210-214.

Meville, W. K. 1983 J. Fluid Mech., 128, 489-506

Read, W. W. and R. J. Sobey 1988 J. Waterway, Port, Coastal, and Ocean Engineering, 113, 507-522

Rice, S. O. 1954 Selected Papers on Noise and Stochastic Processes, Dover, New York.

Tayfun, M. A. and J. M. Lo 1989 J. Waterway, Port, Coastal, and Ocean Engineering, 115, 594-613.

Tayfun, M. A. and J. M. Lo 1990 J. Waterway, Port, Coastal, and Ocean Engineering, 116, 79-100.

FIG 1a

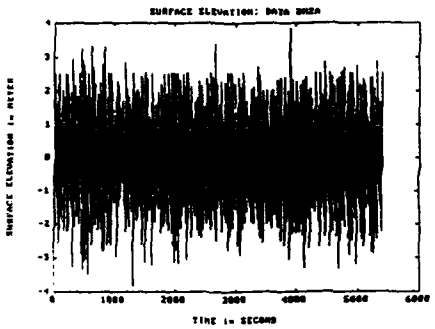

FIG 1b

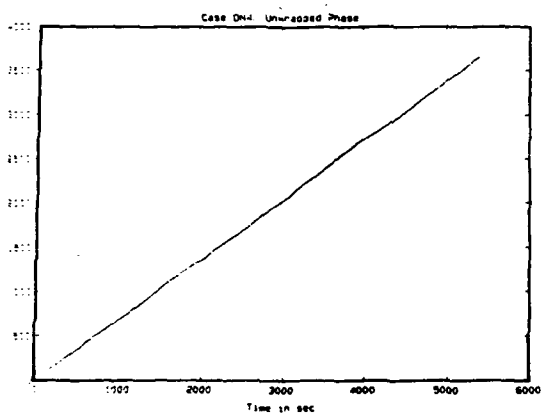

FIG 1c

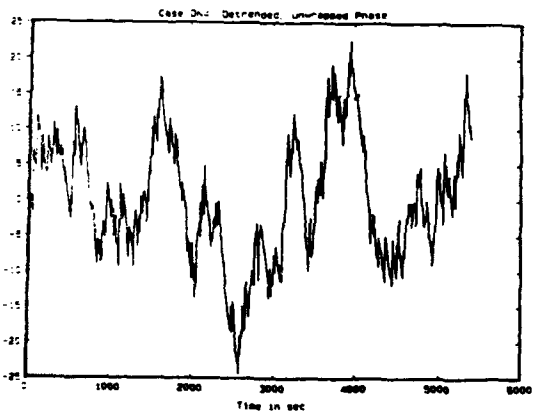

Figure 1 (a), (b), (c)

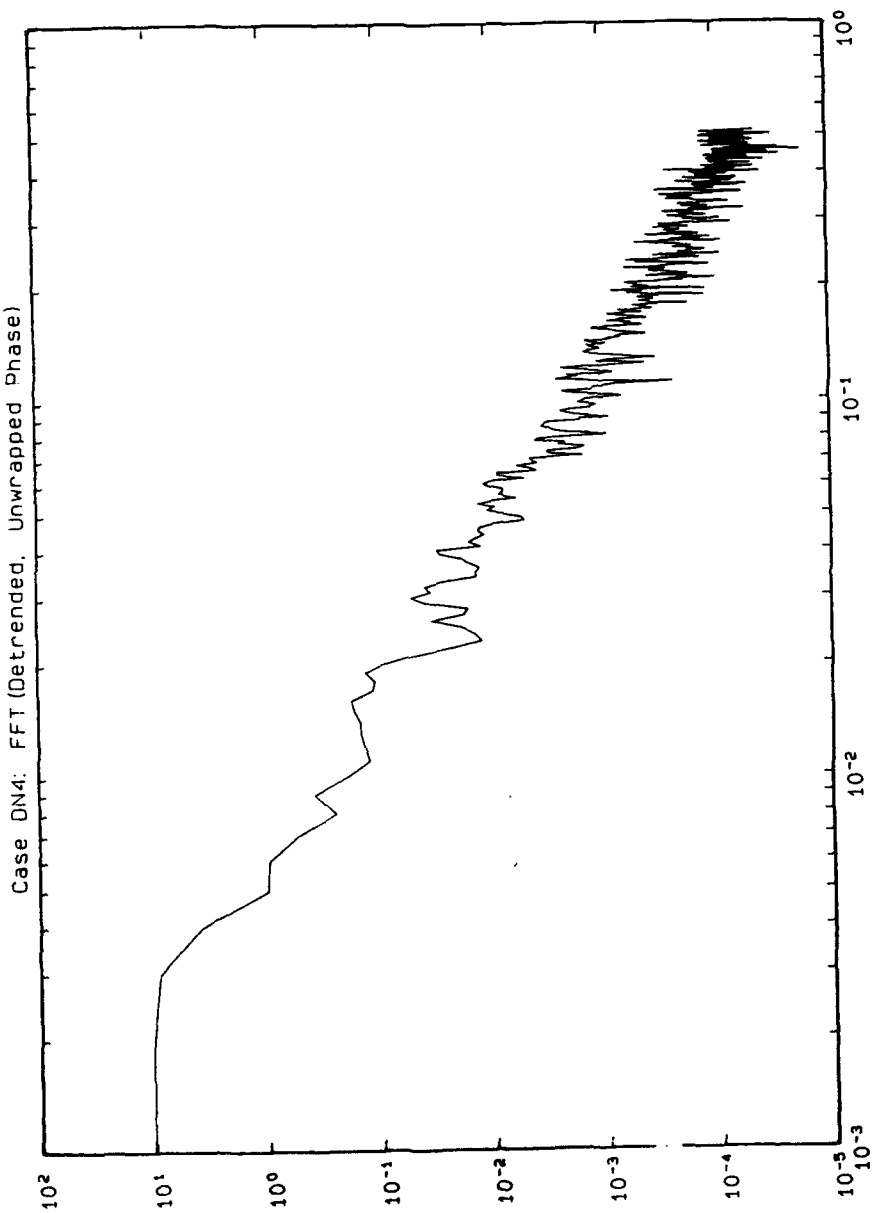
Case DN4: FFT (Detrended, Unwrapped Phase)
10^{2}
10^{1}
10^{0}
10^{-1}
10^{-2}
10^{-3}
10^{-4}
10^{-5}
10^{-3}
10^{-2}
10^{-1}
10^{0}
Freq in Hz

Figure 2

Discussion of Huang's paper

Y. Agnon

It may be worthwhile to compute the fractal dimension of the phase record directly, as there may not be a unique relation between power law behaviour and a specific fractal dimension (e.g. it may be multi-fractal).

Author's reply

We are planning to do that soon on more detailed data measured by wave probes mounted on a SWATH ship. The data rate from the probe is 20 Hz. We can trust that data to, at least, a few Hz.

M. Cooker

Please could you clarify the size of the vertical accelerations you obtained in your lab. data, in relation to gravitational acceleration.

Author's reply

The vertical acceleration is given in units of cm/sec^2 on the figure. The maximum value reaches $1500cm/sec^2$ in the case I presented.

Stability of steep gravity waves and the average Lagrangian

by
Peter.A.E.M. Janssen
Department of Oceanography
Royal Netherlands Meteorological Institute (KNMI)
De Bilt, The Netherlands

Abstract

Some time ago it was discovered that steep gravity waves are subject to exchange of stability at the steepness which corresponds to a maximum of the total energy. This was found numerically by Tanaka (1983, 1985), following the work of Longuet-Higgins (1978) on superharmonic instability and by Saffman (1985) using the Hamiltonian of water waves. The instability occurs because of the coalescence of the pure shift mode ($m = 1$) and the $m = 2$ mode, where m denotes the number of zeroes in one wave length of the basic wave.

In this talk we discuss the application of Whitham's averaged Lagrangian method to the exchange of stability of steep gravity waves at the extremum of the energy. The usual approach, where the average Lagrangian is regarded as a function of angular frequency ω, wave number k and wave steepness a only, fails just at the point where the energy becomes extremal. This was already noted by Peregrine and Thomas (1979), and by Whitham (1981). The principle reason for this is that in the dispersion relation for the frequency σ of the perturbation of the basic wave, the coefficient in front of the highest power vanishes just at the extremum, thereby resulting in a perturbation with infinite frequency σ and group speed.

This suggest that in the average Lagrangian also effects of the time derivatives of amplitude and frequency should be taken into account. We therefore investigated the properties of the Lagrangian

$$(*) \qquad L = L(\omega, k, a, a_T, \omega_T)$$

where T refers to the long modulation time scale. Application of this Lagrangian to the stability problem of a steep gravity wave shows that all frequencies of the perturbation remain finite, but that there is exchange of stability at the extremum of the energy.

In the usual approach (see e.g. Peregrine and Thomas (1979) or Lighthill (1967) the modulation frequency may be determined explicitely if the dependence

of frequency and energy of the basic wave on steepness is known. Unfortunately, such an elegant property has not yet been found for the Lagrangian (*). In its stead, it can be shown that if the Fourier amplitudes of the surface elevation of the basic wave are known, the frequency σ of the perturbation may be determined.

References

[1] Tanaka, M. 1983. The stability of steep gravity waves. *J. Phys. Soc. Japan* 52, 2047-3055.

[2] Tanaka, M. 1985. The stability of steep gravity waves. Part 2. *J. Fluid Mech.* 156, 281-289.

[3] Longuet-Higgins, M.S. 1978. The instabilities of gravity waves of finite amplitude in deep water. I. Superharmonics. *Proc. R. Soc. Lond.* A360, 471-488.

[4] Saffman, P.G. 1985. The superharmonic instability of finite-amplitude water waves. *J. Fluid Mech.* 159, 169-174.

[5] Peregrine, D.H. and Thomas, G.P. 1979. Finite-amplitude deep- water waves on currents. *Phil. Trans. R. Soc. Lond.* A292, 371-390.

[6] Whitham, G.B. 1981. On finite amplitude water waves. *Proc. Indian Acad. Sci. (Eng. Sci.)* 4, Part 3, 259-268.

[7] Lighthill, M.J. 1967. Some special cases treated by the Whitham theory. *Proc. R. Soc. Lond.* A299, 28-53.

Discussion of Janssen's paper

M. Cooker

You made reference to the work of Whitham (1981) in your talk. Please can you give the complete reference.

Author's reply

G.B. Whitham (1981) Proc. Indian Acad. Sci. (Engg.Sci.) Vol. 4, Pt.3, p 259-268.

M.W. Dingemans (remark)

The fact that you got good convergence with only 20 modes, whereas Longuet-Higgins (1978) needed more than 300 nodes is, in my opinion, due to the fact that your B_{mn} coefficients are determined using $e^{k\eta}.\cos(..)$ with η the full expansion. This is the same as occurs in widely separated scales of wave interaction (i.e. gravity waves and capillary waves). Usually all expansions are from the mean free surface. When the shortest-wave expansions are from the surface of the longer waves, much improved convergence characteristics are found, see a paper of B.Y. West in 1988 or 1989.

Author's reply

This agrees with the conjecture I made during the talk.

E. Pelinovsky (comment)

Physical explanation of non-monotonical behavior of adiabatic invariant. $\partial\mathcal{L}/\partial\omega$ is connected with the bifurcation in dynamical system which consists from amplitudes of spectral components of nonlinear travelling wave. (See my papers in Physics, ser.D, N1 and 3 for 1981).

D.H. Peregrine

You spared us the details of the X derivatives. What do they tell us about the group velocity of these perturbations?

Author's reply

Including modulations in space one obtains the following stability diagram. (Here ℓ is the modulation wave number)

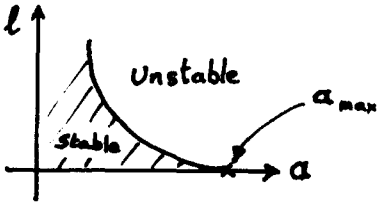

The group speed of the perturbation $(\partial\sigma/\partial\ell)$ is regular up to the extremum in the energy, but becomes (of course) complex in the unstable region.

RESONANT INTERACTIONS OF THE WATER WAVES WITH DISCRETE SPECTRA

Elena A. Kartashova

P.P.Shirshov Institute of Oceanology
USSR Acad. of Sciences
Krasikova 23
Moscow 117218
USSR

1. Introduction

In linear setting, wave motions in dispersive media can be adequately described with the help of Fourier analysis, when solution is represented as a set of Fourier components of the form

$$C \exp i(\vec{k}\vec{x} - \omega t),$$

where ω is a frequency and $\vec{k}$ is a wave vector. Under assumption of weak nonlinearity, interaction of wave components occurs on the resonance surfaces, given by the synchronism conditions

$$(1) \qquad \begin{cases} \pm\, \omega(\vec{k}_1) \pm \ldots \pm \omega(\vec{k}_s) = 0 \\ \pm\, \vec{k}_1 \pm \ldots \pm \vec{k}_s = 0 \end{cases}$$

for s interacting waves. As a rule, weakly nonlinear resonant interactions are considered in infinite domains and in this case ω is a function of real variables. These wave interactions have some common properties: each wave takes part in the interactions, any wave has infinite number of interacting partners, evolution of a stochastic wave field due to these interactions adequately described in terms of kinetic equations.

We show that all these properties are not conserved for the resonant

interactions considered in bounded domains (so called resonators) and for the problems with periodical boundary conditions. The specific properties of this class of problems are the consequence of the fact that for every dispersion relation considered solutions are to be sought among vectors with integer components only. The lecture is concerned with the implications of the general properties of resonantly interacting waves with discrete spectrum for the case of water waves.

2. General results

We have shown that if ω, as a function of integer variable, satisfies certain conditions, then the system (1) has *some unexpected properties*. We have found that:

(1) Waves can be partitioned into disjoint classes which do not cross-interact; there is *no energy flux* among *these classes*, so it is possible to study each class independently; the number of elements of some class is not large (as a rule, class contains 3 to 5 waves).

(2) Most of the waves *do not take part in any interactions at all* (for instance, in case of planetary waves on a sphere it amounts to 60% of all waves; for Rossby waves in a square basin on the beta-plane the number of "passive" waves exceeds more than 80% of all waves).

(3) *The number of resonantly interacting waves does strongly depend on the basin form* (for example, on the ratio of the basin sides); there exist many basins where interactions are prohibited at all; for some fixed $\omega(\vec{k})$ we can described the set of such basins.

(4) *Interactions are local* in the sense that for any given wave its interaction domain (i.e. one in which the waves which could interact with this one, lie) is bounded in $\vec{k}$ - space and can be written out effectively.

Below we give graphic interpretation of the results obtained. Consider a two-dimensional integer lattice whose node (m,n) represents a two-dimensional wave vector. Draw arcs between those lattice nodes which

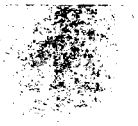

belong to one and the same solution. Then (1) describes the structure of emergent graph (see fig. below).

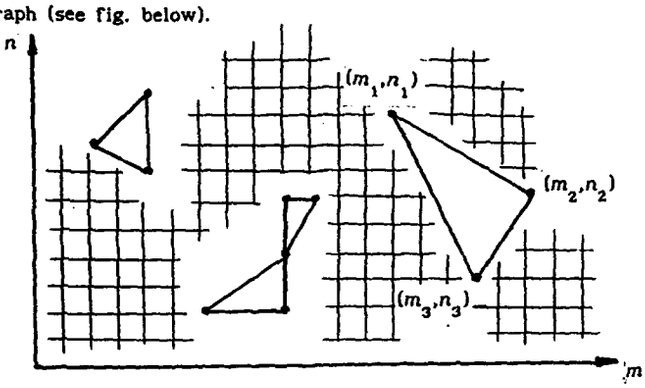

Property (2) means here that the most nodes of the lattice do not belong to the graph.Property (3) states that a node does or not does belong to the graph depending on which lattice domain we are studying. And, finally, (4) means that there no arcs between the nodes widely separated.

We have verified that for some particular wave types (e.g. planetary waves on a sphere and in a rectangular basin on the beta-plane, internal waves etc) the properties mentioned above hold (see ref. [1] ~ [4]).

At the same time it turned out that the water waves have their own peculiarities. Below we consider two examples of water waves: capillary waves and gravity waves in deep water.

3. Capillary waves, $\omega^2 = \gamma k^3$

For three-wave interactions, the first equation of sys.(1) takes the form

$$k_1^{3/2} + k_2^{3/2} = k_3^{3/2} \tag{2}$$

To construct partitioning of the solution set of eq. (2) we need the following definitions.

DEF. 1. Let (m,n) be a vector with positive coordinates, $m,n \in \mathbb{N}$. Let us consider the norm of this vector

$$||(m,n)|| = (m^2 + n^2)^{1/2}$$

and represent it in the form

$$(m^2 + n^2)^{1/2} = gq^{1/2}, \quad g, q \in \mathbb{N}$$

where q is square-free, i.e. $q = p_1 p_2 \cdots p_l$, all p_j are different primes, $j = 1,\ldots,l$. We call q the index of the vector (m,n).

DEF. 2. Let us call the class of index q the set of vectors with integer coordinates shearing the same index. Notation: Cl_q.

It is not difficult to prove (similarly to how it has been done in [2]) that if three vectors (m_1,n_1), (m_2,n_2), (m_3,n_3) fulfill eq. (2), then they belong to the same class, i.e.

$$\exists\, q \in \mathbb{N} : (m_l,n_l) \in Cl_q, \; l = 1, 2, 3.$$

Let us fix some index q and consider solutions of eq. (2) in the class Cl_q. Then $k_l = p_l^2 q$, $l = 1, 2, 3$, $p_l \in \mathbb{N}$ and the eq. (2) can be written in the form

(3) $$p_1^3 + p_2^3 = p_3^3$$

It is a particular case of Fermat's Great theorem, for exponent $n = 3$, and for this exponent the theorem had been proved in the last century, i.e. eq. (3) has no solutions. As index we have fixed is arbitrary, this means that all the classes are empty, $Cl_q = \varnothing$, $\forall\, q$. Notice that in this case we did not even investigate both equations of the sys. (1) as all information about the solutions has already been obtained from consideration of the first equation. We did not write out the norms of the vectors $\vec{k}_l$ in terms of its coordinates on purpose, just to show that in this case the result does not depend on dimension of wave vector. It is not always so, and partition into classes, found for the wave vectors of dimension two may, for the same dispersion relation, disappear for one-dimensional wave vectors (as it does actually happen in the case of Rossby waves).

Thus we obtained that there are no exact resonant interactions among capillary waves, and this result does not depend on dimension of wave

vector. As a rule, partitioning into classes and properties of classes are strongly depending on the dimension of wave vector. It can be seen extremely well in the case of gravity waves in deep water - this is our next example.

4. Gravity waves in deep water, $\omega^2 = gk$

For these waves a few distinct cases must be considered.

First of all, here we study the sys.(1) here in the form

$$\begin{cases} k_1^{1/2} + k_2^{1/2} = k_3^{1/2} + k_4^{1/2} \\ \vec{k}_1 + \vec{k}_2 = \vec{k}_3 + \vec{k}_4 \end{cases}$$

If dim $\vec{k}_i = 1 \quad \forall\, i = 1, 2, 3, 4$, then solutions of this system have pair-wise coinciding components. It means that there are no other possibilities but

$$\vec{k}_1 = \vec{k}_4 \quad \& \quad \vec{k}_2 = \vec{k}_3 \quad \text{or} \quad \vec{k}_1 = \vec{k}_3 \ \& \ \vec{k}_2 = \vec{k}_4 \ .$$

Those solutions are trivial as no new waves emerge due to these interactions.

If dim $\vec{k}_i = 2 \quad \forall\, i = 1, 2, 3, 4$, then it is not hard to construct an infinite number of solutions. But all of them will also have a very specific form: wave vectors must have pair-wise equal lengths, what we have called "the mirrored interactions".

Notice that in both those occasions the structure of the solution set becomes more complicated compared to the cases considered in the sec.3 and in the [2]. Theoretically here there can exist solutions containing components from different classes. We have called this situation "*gluing of the classes*". Occurrence of gluing is constrained by the set of additional conditions, which can be demonstrated with help of the following statement.

Proposition 1. Let vectors $\vec{k}_1, \vec{k}_2, \vec{k}_3, \vec{k}_4$ are solutions of the sys.(4) and dim $\vec{k}_i = 1$ or 2, $\forall\, i = 1, 2, 3, 4$. Then two possibilities exist:

a) $\exists\, q : \vec{k}_i \in Cl_q \quad \forall\, i = 1,2,3,4$

or

b) $\exists\, q_1, q_2 : \vec{k}_1, \vec{k}_3 \in Cl_{q_1}$ & $\vec{k}_2, \vec{k}_4 \in Cl_{q_2}$

or

$\exists\, q_1, q_2 : \vec{k}_1, \vec{k}_4 \in Cl_{q_1}$ & $\vec{k}_2, \vec{k}_3 \in Cl_{q_2}$

The proof follows immediately from elementary properties of integers. The only point we have to stress here is that construction of classes' set depends on the dimension of wave vector. If dim $k_i = 1$, the partitioning into classes coincides with that constructed in sec.3. If dim k_i=2, then we call class index q such number that

$$(m^2 + n^2)^{1/4} = rq^{1/4}, \qquad r, q \in \mathbf{N},$$

where q is free of fourth degrees, i.e.

$$q = p_1^{\alpha_1} p_2^{\alpha_2} \dots p_s^{\alpha_s}, \quad \alpha_i \in \{1, 2, 3,\},$$

where all p_i are different primes, $i = 1,..,s$.

4.2. Special case of $s \geq 4$ waves

It is not difficult to prove the following fact.

Proposition 2. For arbitrary dimension of wave vectors, the system of equation

$$\begin{cases} k_1^{1/2} = k_2^{1/2} + \dots + k_s^{1/2} \\ \vec{k}_1 = \vec{k}_2 + \dots + \vec{k}_s \end{cases}$$

does not have integer solutions for $\forall\, s \in \mathbf{N}$, $s < \infty$ (i.e. s may be an arbitrary large number but finite).

4.3. The case of 5 waves

In this case we have the following system of equations:

$$(4)\qquad \begin{cases} k_1^{1/2} + k_2^{1/2} = k_3^{1/2} + k_4^{1/2} + k_5^{1/2} \\ \vec{k}_1 + \vec{k}_2 = \vec{k}_3 + \vec{k}_4 + \vec{k}_5 \end{cases}$$

This system has infinite set of nontrivial solutions and they could be found in every dimension. There exist the partitioning into classes for wave vectors in this case too, and it is not very difficult to see that for 5-waves interactions there occurs no gluing of classes. Really, let us consider a system (4) (for simplicity, dim $\vec{k}_i = 1$). It is evident that $\vec{k}_3$, $\vec{k}_4$, $\vec{k}_5$ can not belong to the different classes. Therefore, let us transform this system into

$$(5)\qquad \begin{cases} (k_1 k_2)^{1/2} = (k_3 k_4)^{1/2} + (k_3 k_5)^{1/2} + (k_4 k_5)^{1/2} \\ k_1 + k_2 = k_3 + k_4 + k_5 \end{cases}$$

and suppose, for example, that k_4, k_5 lie in the same class, i.e.

$$k_4^{1/2} = d_4 q^{1/2}, \quad k_5^{1/2} = d_5 q^{1/2}$$

then

$$(k_4 k_5)^{1/2} = d_4 d_5 q \in \mathbb{N}$$

and therefore

$$\vec{k}_1, \vec{k}_2, \vec{k}_3 \in Cl_q \text{ , QED.}$$

5. Conclusion

We have shown that the character of interactions for systems with discrete spectrum does qualitatively differ from the continuous case for water waves as well. It has been demonstrated that peculiarities of the interactions are preserved even for the multiple waves interactions. The very specific form of solutions in sec. 4.1 and in sec. 4.3, the existence of classes can be considered, for instance, as a basis for developing specific "local" computational models. Moreover, there appears a possibility to "cut off" (i.e. not to take into account in calculations) exactly those modes which do not take part in interactions.

All these results are obtained for the exact resonances, but particularly interesting is the question concerning the existence of so-called approximate interactions, for which equation

$$\pm\, \omega(\vec{k}_1) \pm \ldots \pm \omega(\vec{k}_s) = o$$

is slightly violated, but frequency deviation is much smaller than $\omega(\vec{k}_i)$ $\forall$ i. It means that resonance has some non-zero width. There are some strong indications that peculiarities of the interactions obtained above will be conserved for some resonant width, it should be done similar to what we have done in [1] and [3].

Summing it all up, we come to conclusion that all these qualitative peculiarities of water wave interactions have the only source: discreteness of spectra of these systems. Therefore we obtain a possibility to study directly those systems which are innately discrete and must be careful while applying to them results obtained for the continuous case. Moreover, it is quite evident that the discretization of arbitrary systems which is necessary for numerical calculation, may generate artefactuous properties.

References

[1] E.A.Kartashova, L.I.Piterbarg, G.M.Reznik. Weak nonlinear interactions of Rossby waves on a sphere. Oceanology (J. USSR Acad. Sci. Proc.) 29 (1989) 533-542 (in Russian)

[2] E.A.Kartashova. Partitioning of ensembles of weakly interacting dispersive waves in resonators into disjoint classes. Physica D, 46 (1990) 43-56

[3] E.A.Kartashova. Planetary waves: some properties of interactions in rectangular basins. Preprint IINS, N 2 (Moscow, 1990)

[4] E.A.Kartashova. On properties of weakly nonlinear wave interactions in resonators. Physica D (1991), to be published

Discussion of Kartashova's paper

M. Berry

What happens to the resonance equations when the domain boundary is perturbed away from the square that you have assumed? Are there any exact solutions? (In general the waves will not be finite combinations of travelling sine waves.)

Author's reply

In ref.[3] we have first found that the number of noninteracting waves does strongly depend on the form of the basins. We have explicitly written out ratios of rectangular basin sides for which no more than 5% of all waves can (but not must!) take part in interactions. In ref.[4] we have found stronger results; i.e. that there exist infinitely many basins in which resonant interactions are altogether impossible. To do that we first evaluate the number of solutions of system (1.1) in $\mathbb{Z}$ from above by the number of some analogous system in $\mathbb{Z}/p\mathbb{Z}$ for prime p's. There we define the part of those p's for which this syst. will have no solutions at all. All definitions and main statements are given for the case of planetary waves for clarity; it is shown how the results can be naturally generalized to a wide class of other wave types (i.e. with another ω function). As a result, we know that *there are* some exact solutions in the case when the domain boundary is perturbed away from the square, but these solutions are very rare. Moreover, there are many domains where there are no solutions at all.

M.W. Dingemans

Is it possible to use the present method of a square domain as a sort of "canonical problem" for domains which can be viewed as some perturbation of a square domain? It is expected that the exact resonance then is not valid any more, but the case of "near-resonance" occurs. This can give recurrent behaviour as is present for fairly long waves with three-wave interaction.

Author's reply

As I have answered to Prof. Berry, it is possible to use the present method for some (but very simple) perturbations of a square basin and there exist some rare resonances in these new domains. Of course, we have no possibility to say exactly, what would happen after an *arbitrary* perturbation of the domain boundaries. The idea that "near-resonant" interactions will play a main part in such "perturbed" domains seems to me very reasonable. The problem is how to define these "near-resonant" interactions because there are many different possibilities to do this to disturb the coordinates of wave vectors (and here we have to choose the number of changing coordinates) or to disturb the meaning of frequency (and here we have to estimate what wave vector corresponds to a new, "disturbed" meaning of frequency) or something else. So, we need the confidence that all the ways give us the same results or, in the case of different results, we have to find the physical background to choose one definition. All the results obtained would strongly depend on that definition.

M. Stiassnie

Please tell us more about the finite depth (gravity-waves) case. What about the 1D case for the above?

Author's reply

This case is very interesting from a mathematical point of view. The reason is that it was the first case where we have seen not Diophantine equation but equation for the values of the transcendental function. It is not very difficult to show how to transform an equation

$$\sqrt{\kappa_1 th(gk_1)} + \sqrt{\kappa_2 th(gk_2)} = \sqrt{\kappa_3 th(gk_3)} + \sqrt{\kappa_4 th(gk_4)}$$

to the form

$$(*) \qquad \sum_{i=1}^{s} P_i(\kappa_1,\kappa_2,\kappa_3,\kappa_4) e^{R_i(\kappa_1,\kappa_2,\kappa_3,\kappa_4)} = 0,$$

where P_i and R_i are polynomials of the integer variables $\kappa_1,\ldots,\kappa_4$, deg $P_i \leq 16$ $\forall i = 1,\ldots,s$ (I mean the cumulative degree of the arbitrary polynomial P_i over all variables $\kappa_1,\ldots,\kappa_4$). All polynomials R_i are linear and have one of the forms

$$\pm\kappa_1 \pm \kappa_2 \pm \kappa_3 \pm \kappa_4 \text{ or } \pm 2\kappa_1 \pm \kappa_2 \pm \kappa_3 \text{ or } \pm\kappa_1 \pm 2\kappa_2 \pm \kappa_4 \text{ or } \ldots. \text{ or } \pm 4\kappa_4.$$

Let us suppose that we have obtained (*), then we would have the possibility to use a theorem of Weirstrass-Lindemann about algebraic independence of the values of e^x. For us it means that if $R_i \neq 0$ $\forall$ i, then (*) is equivalent to the following

$$(**) \quad \begin{cases} P_1(\kappa_1,\ldots,\kappa_4) = 0 \\ \ldots\ldots\ldots\ldots\ldots \\ P_s(\kappa_1,\ldots,\kappa_4) = 0 \end{cases}$$

and we have to find the solutions of (**) in integers. We must *be very careful* in the cases when there exist a few $R_{i_1}, R_{i_2},\ldots,R_{i_r}$ with the different graphic form but having the coinciding numerical values. For instance,

$$R_{i_1} = \kappa_1 + 2\kappa_2 = \kappa_3; \quad R_{i_2} = 2\kappa_4 + \kappa_1 - \kappa_3;$$

it's clear that $R_{i_1} \neq R_{i_2}$, but for $\kappa_2 = \kappa_4$ we have to make some changes in the system(**): instead of two equations $P_{i_1} = 0$, $P_{i_2} = 0$; it's necessary to put into the system(**) the following equation;

$$P_{i_1} + P_{i_2} = 0.$$

Therefore we have a few hundred different forms of the system(**) and there is only one possibility of finding solutions to them - to use computer and "mathematica". We have not managed this problem, we have only found the way to deal with it.

J.W. Dold (comment)

The question of M. Stiassnie has an important generalisation where for any mode $\vec{\kappa_i}$ the frequency is

$$\omega_i = F(\vec{\kappa_i}, h, a_i)$$

where h is a parameter (like depth) and a_i is the amplitude of the mode. (The value of ω_i may even depend on "tied" higher harmonics such as $2\vec{\kappa_i}, 3\vec{\kappa_i}$ etc.) With this kind of frequency dependence, resonant interactions, may arise on manifolds in amplitude and depth space for any given group of wavenumbers which sum to zero.

Author's reply

As I have said to Dr Stiassnie, we can't use the results obtained for gravity waves on deep water to gravity waves of finite depth but we can, of course, use developed methods to obtain results for this new case. So, a situation you have described is very similar to the former. There is no problem to include in our considerations any given *(finite!)* number of waves and we have managed this problem for several different frequencies, for example, for $\omega = \sqrt{g\kappa}$ as you could see in my report. It is not very difficult too to take into account dependence of the value of ω_i on "tied" higher harmonics such as $2\bar{\kappa}_i$, $3\bar{\kappa}_i$ etc., though we have never done it before but now we can be sure that these two types of changes, i.e. changing the number of interacting waves or addition of tied harmonics to frequency, will not give us a qualitatively new picture it means that these generalizations conserve the existence of non-intersecting wave classes; only the structure of the class set may change (it means, the number of classes, the number of elements in some fixed class etc.) Dependence of the results on the domain boundaries would conserve too. A more complicated problem is to include dependence of the frequency on the amplitude of the mode. This demands a special consideration.

L. Tsimring

My comments also concern the sensitivity of the results presented in the shape of the basin's boundaries. It seems to me that, for instance, weak concavity of boundaries would change drastically the situation, because of the strong stochasticity of wave rays in such a Sinay billiard. This stochastic behaviour of wave rays must lead to a very complicated spectrum for which the analytical theory can hardly be constructed. My opinion is that the lack of resonantly interacting waves is rather an exception than a rule.

Author's reply

It is not my opinion that the lack of resonantly interacting waves is rather an exception than a rule. As I've shown before, weak perturbation of the basin's boundaries conserve the qualitative picture. Moreover, these results keep true for some small non-zero resonance width (and this fact can be reformulated in the terms of basin's boundaries perturbations, it would be the other type of perturbations). So we have some strong indications that it would be impossible to change the situation drastically by means of weak concavity of the basin boundaries. In any case we need some very special changes to obtain a Sinay billiard.

Subharmonic transition of a nonlinear short gravity wave train on deep water.

Joël Poitevin Météo-France/SCEM 75340 Paris France
Christian Kharif I.M.S.T. 13288 Marseille France

1. Introduction

Evolution of trains of surface gravity waves has been extensively studied for the last years. One of the first detailed investigations of the time evolution of nonlinear deep water waves was performed by Lighthill [1]. Two years latter Benjamin and Feir [2], using a perturbation approach, demonstrated that an uniform continuous wave train is unstable to modulational perturbations of its envelope. Experimentally the frequency down-shifting phenomenon has been first reported by Lake et all [3]. Their experiments were performed using initially uniform, or nearly uniform, wave trains. At some distance from the source the modulational instability appears as the growth of two dominant sidebands. Approximate recurrence cycles were observed in which the wave trains became strongly modulated until they were again nearly uniform. A more careful inspection, however, reveals that the dominant component is the component at the lower frequency of the lower sideband of the original carrier : this is the frequency down-shifting phenomenon.

Trulsen and Dysthe [4] have shown using a modified *Schrödinger* equation correct to fourth order in the wave steepness that breaking is an essential ingredient in the process of the frequency down-shifting. Poitevin and Kharif [5] using exact boundary conditions with surface tension and viscosity taken into account founded also that the selective damping of the upper sidebands and fundamental of short gravity wave trains tends to favour the survival of the lower modes. Very recently Hara and Mei [6], considering the effect of moderate wind on the nonlinear evolution of unstable sidebands in narrow-banded waves with turbulent dissipation in water taken into account, observed the frequency down-shift.

In this paper we examine how dissipation and surface tension effect promote growth of the lower sideband of short gravity waves. We ignore the influence of wind on the surface and assume that the waves do not break.

2. Mathematical formulation

The nonlinear evolution of an uniform wave train subject initially to modulational instabilities with the effects of viscosity and surface tension taken into account is studied using a high order spectral method developed by Dommermuth and Yue [7].

We assign (x,z) to be the usual spatial coordinates with z pointing vertically upward and the origin is located at the mean water level. We consider the flow of an incompressible fluid with a free surface on deep water. We describe the fluid velocity $v(x,z,t)$ by means of a velocity potential $\Phi(x,z,t)$. For a fluid with a pressure distribution $p(x,z,t)$ acting on the free surface $z=\eta(x,t)$ the equations of the motion are given by (see e.g West [8]).

$$\Phi_t+1/2\nabla\Phi.\nabla\Phi+g\eta-\alpha\nabla_x[\nabla_x\eta/(1+\nabla_x\eta.\nabla_x\eta)^{1/2}] = 2\nu\nabla_x{}^2\,\Phi-p/\rho_w \qquad \text{on } z=\eta(x,t)$$

$$\eta_t + \nabla_x\Phi.\nabla_x\eta = \Phi_z$$

Where α is the kinematic surface tension, ν is the coefficient of kinematic viscosity, ∇ and ∇_x are respectively the gradient operation ($\partial/\partial x$, $\partial/\partial z$) and the horizontal gradient operation, and the constant fluid density is ρ_w.

In this model the vorticity generated by the viscous damping is neglected, i.e the rotational component of the fluid velocity. So we assume that the dominant characteristics of the surface motion can be described by irrotational flow alone.

The velocity potential $\Phi(x,z,t)$ satisfies the classical Laplace's equation and vanishes at infinite depth. We define the potential velocity at the free surface

$$\Phi^s(x,t) = \Phi(x,\eta(x,t),t)$$

We choose the speed of a small amplitude gravity wave in deep water $(g\lambda_o/2\pi)^{1/2}$ as reference velocity and $\lambda_o/2\pi$ as reference length where λ_o and g are respectively the length of an initial uniform wave train and gravitational acceleration, in order to introduce into the equations dimensionless variables. The pressure on the surface wave is assumed to be constant and, without loss of generality, is taken as zero. The free surface boundary conditions are then written in term of Φ^s

$$\Phi_t^s = -\eta - 1/2(\nabla_x\Phi^s)^2 + 1/2w^2[1+(\nabla_x\eta)^2] + \kappa\nabla_x[\nabla_x\eta/(1+(\nabla_x\eta)^2)^{1/2}]$$

$$+2R_e^{-1}(\nabla_x^2\Phi^s - w\nabla_x^2\eta)/(1+(\nabla_x\eta)^2)$$

$$\eta_t = -\nabla_x\Phi^s.\nabla_x\eta + w[1+(\nabla_x\eta)^2]$$

where $w = (\partial\Phi/\partial z)(x,\eta(x,t),t)$, $\kappa = k_o^2\alpha/\rho_w g$, $R_e = g^{1/2}k_o^{-3/2}/\nu$, $k_o = 2\pi/\lambda_o$

The parameters κ and R_e are dimensionless numbers arising naturally in the problem.

In order to calculate W, the potential Φ is written in a finite perturbation serie up to a given order M.

$$\Phi(x,z,t) = \sum_{m=1}^{M} \Phi^{(m)}(x,z,t)$$

The quantity $\Phi^{(m)}$ is of order ε^m, where ε is the wave steepness. Then expanding each $\Phi^{(m)}$ evaluated on $z = \eta$ in a Taylor serie about $z = 0$ we obtain a sequence of boundary conditions for the unknown $\Phi^{(m)}$'s on $z = 0$.

$$\sum_{m=1}^{M}\sum_{l=0}^{M-m} (\eta^l/l!)(\partial^l\Phi^{(m)}/\partial z^l)(x,0,t) = \Phi^s(x,t)$$

The potential at the free surface Φ^s and the surface elevation η are considered to be known. As in typical mode coupling approach each term $\Phi^{(m)}$ is represented as an eigenfunction expansion of free modes

$$\Phi^{(m)}(x,z,t) = \sum_{n=1}^{N} \Phi_n^{(m)}(t)\, e^{inx}\, e^{|n|z}$$

Substituting these expressions into the development of the potential Φ^s we determine $\Phi_n^{(m)}(t)$. The vertical surface velocity w is then :

$$w = \sum_{m=1}^{M}\sum_{l=0}^{M-m} (\eta^l/l!) \sum_{n=1}^{N} \Phi_n^{(m)}(t)\, e^{inx}\, (\partial^{l+1} e^{|n|z}/\partial z^{l+1})$$

where the deratives $\partial^{l+1} e^{|n|z}/\partial z^{l+1}$ are evaluated at z = 0.

3. Numerical method

The numerical method used to solve the free surface boundary conditions is similar to that developed by Dommermuth and Yue [7]. The temporal evolution of the N wave modes is solved through a pseudo-spectral method and the nonlinear terms are retained up to a fixed order M.

3.1. Pseudo spectral treatment

Once known the surface elevation $\eta(x,t)$ and the potential $\Phi^s(x,t)$ on the free surface at some instant of time t, the modal amplitude $\Phi_n^{(m)}(t)$ are determined using a pseudo spectral method. The spatial derivatives of $\Phi^{(m)}$, Φ^s and η are evaluated in the spectral space while nonlinear product are calculated in the physical space at equidistant points x_j.

3.2. Time integration

The evolution equations for Φ^s and η are integrated in time using a fourth order Runge Kutta integrator with constant time step Δt.

The two step procedure 3.1 and 3.2 is repeated starting from initial conditions.

3.3. Validity of the model

The accuracy and convergence of the model are tested using exact Stokes waves in deep water. The iterative scheme as developed by Longuet-Higgins [9] is used to compute the permanent forms given by the usual parametric representation in a frame of reference moving with constant speed (which will be taken as the phase velocity of the Stokes waves). For a wave steepness $\varepsilon = 0.24$ we obtain relevant results to three significant figures with M = 6, N= 45 and $\Delta t = T/100$ where T is the fundamental period of the Stokes wave. Figure 1 displays that the form of the profile of a Stokes wave of wave steepness ε=0.24 remains permanent. For this numerical experiment we have chosen $\kappa = 0$ and R_e=∞. In figure 2, we compare how well the numerical method conserve energy and volume as the wave evolves with time.

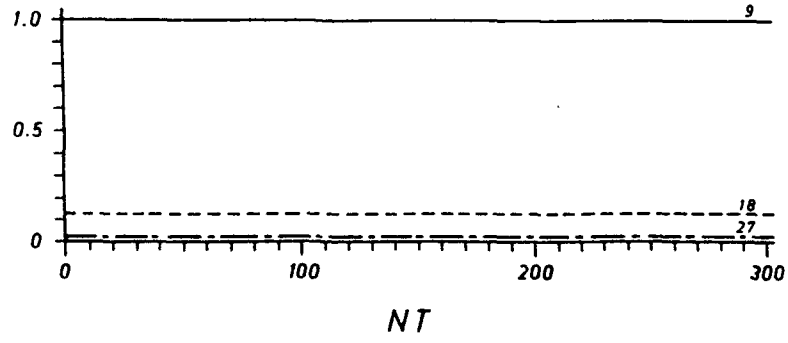

Figure 1. Time histories of the amplitude of the fundamental (k=9), second harmonic (k=18) and third harmonic (k=27) relative to the initial amplitude of the fundamental for an evolving Stokes wave (ak=0.24, k=9). NT is the number of fundamental periods.

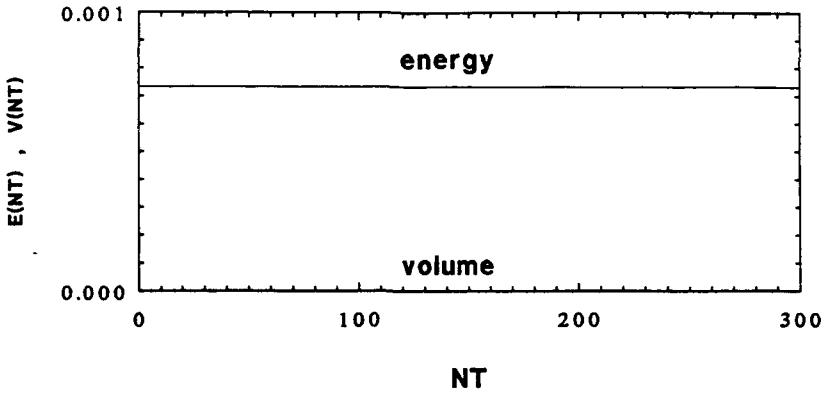

Figure 2. Total energy E and volume V of an evolving Stokes wave (ak=0.24, k=9) as a function of time. NT is the number of fundamental periods.

4. Frequency downshifting

In this section we shall consider the long time evolution of Stokes waves modulated by their most unstable sideband disturbances.

4.1. Instability of a Stokes wave

The procedure used to calculate the instabilities of a Stokes wave for $\kappa = 0$ and $R_e=\infty$, is similar to the method described by Kharif and Ramamonjiarisoa [10].

$$\eta = \bar{\eta} + \eta'$$

$$\Phi^s = \bar{\Phi}^s + \Phi'$$

where $(\bar{\eta}, \bar{\Phi}^s)$ and (η', Φ') correspond respectively to the unperturbed wave (Stokes wave) and infinitesimal perturbative motions ($\eta' << \eta$, $\Phi' << \Phi^s$). Substituting these decompositions in the boundary conditions and using the following forms.

$$\eta' = \exp[(-i\sigma t) + i(px+qy)] \sum_{-M}^{+M} a_j \exp(ijx)$$

$$\Phi' = \exp[(-i\sigma t) + i(px+qy)] \sum_{-M}^{+M} b_j \exp(ijx+\gamma_j z)$$

where $\gamma_j = [(p+j)^2 + q^2]^{1/2}$

An eigenvalue problem for σ with eigenvector $\underline{u} = (a_j, b_j)^t$ is obtained

$$(A_M - i\sigma B_M)\underline{u} = 0$$

where A_M and B_M are $(4M + 2)x(4M + 2)$ complex matrices depending on the unperturbed wave steepness ε and the arbitrary real numbers p and q. The eigenvalue σ satisfies

$$\det(i\sigma B_M - A_M) = 0$$

For $\varepsilon = 0.13$ and 0.24 the most unstable perturbations are resonances of class I (Benjamin-Feir type) with respectively $p = 2/9$, $q = 0$ and $p = 3/9$, $q = 0$. The wavenumber $k=9$ is chosen so that integral numbers of the sideband modes can be fitted into the computational domain. The physical disturbances correspond to the real parts of the expressions η' and Φ'.

4.2. Recurrence

A successful approach to study slowly modulated waves is the nonlinear Schrödinger equation (NLS). Lake et all [3] and Yuen and Ferguson [11] used this approximate equation to describe the long-time evolution of a system composed of a Stokes wave subject to modulational instabilities. Stiassnie and Shemer [12,13] extended to a higher order the so-called Zakharov's equation and then studied the nonlinear interaction of different classes of instability. These investigations showed that, in the absence of viscosity and surface tension, the evolution may be recurring (Fermi-Pasta-Ulam recurrence).

In order to exhibit this phenomenon with $\kappa = 0$ and $R_e = \infty$ we consider as initial condition the superposition of a Stokes wave of amplitude $\varepsilon = 0.13$ and its most unstable perturbation corresponding to $p = 2/9$. For this numerical experiment the results are obtained up to four significant figures with $M=6$, $N=45$ and $\Delta t=T/100$. The normalized amplitudes of the perturbations relative to the fundamental amplitude is initially taken equal to 0.025 but in order to compare our results to those of previous studies we plot in figure 3 the time histories of the fundamental(k=9),dominant subharmonic(k=6) and dominant superharmonic(k=12) with t=0 corresponding to initial normalized disturbance amplitudes fixed at 0.1. The computations predict a first minimum of the fundamental near t=60T which closely corresponds to the timescale for class I interactions. The linear stability gives the initial growth rate $Im(\sigma)=0.0065$ for the most unstable disturbance. Using an exponential extrapolation it is found that the amplitudes of the corresponding modes have values of the same order that the fundamental after T=57T. Then the amplitude of the fundamental increases while those of the subharmonic and superharmonic modes decrease: the initial condition is reconstructed or almost reconstructed. The evolution consists of modulation-demodulation cycles.

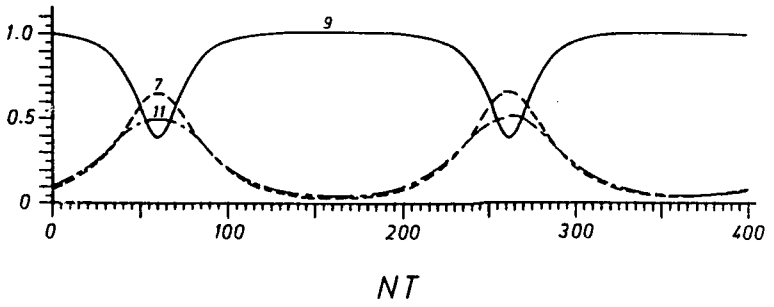

Figure 3. Time histories of the normalized amplitude of the fundamental (k=9), subharmonic (k=6) and superharmonic (k=12) modes for an evolving perturbed Stokes wave ($ak=0.13$, $k=9$). $\kappa=0$ and $R_e=\infty$. NT is the number of fundamental periods.

4.3. Subharmonic transition

In order to better understand the frequency downshifting phenomenon we consider the effects of viscosity and surface tension. As we shall show these two ingredients are responsible for the asymmetrical behaviours of the subharmonic and superharmonic modes of the Benjamin-Feir instability. The evolution equations are integrated with $\kappa = 6.02 \times 10^{-4}$

and $R_e = 1.16 \times 10^5$ corresponding to a train of nine waves with wavelength $\lambda_0/9$ close to eight centimeters. We consider as initial condition a train of Stokes waves of wave steepness $\varepsilon = 0.24$ perturbed by its most unstable disturbance ($p = 3/9$). The growth rate given by the stability calculation is $Im(\sigma) = 0.017$. Viscous damping and capillary effects are only ignored for the computation of the initial conditions.

The long time evolutions of the normalized amplitude of the fundamental (k=9), subharmonic (k=6) and superharmonic (k=12) are shown in figure 4.

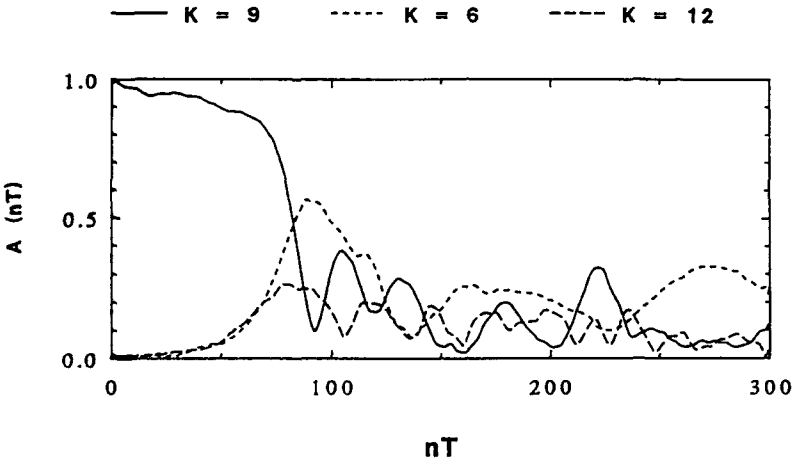

Figure 4. Same as for figure 3 exept ak=0.24, $\kappa = 6.02 \times 10^{-4}$ and $R_e = 1.16 \times 10^5$

Numerical simulations with (i) $\kappa=0$, $R_e=\infty$ (ii) $\kappa = 6.02 \times 10^{-4}$, $R_e=\infty$ and iii) $\kappa=0$, $R_e = 1.16 \times 10^5$ fail respectively at t=80T, 90T and 120T. Some waves steepen and reach the maximum wave steepness corresponding to the first singularity. The combined effect of surface tension and viscous dissipation is to reduce strongly the fast growing local instabilities which quickly lead to breaking and favour the asymmetry of the amplitude evolutions of the lower sideband and the upper sideband. The attenuation rate of the mode corresponding to the wave number k is equal to : $\sigma_v(k) = -2k^2/R_e$. For k=6 and k=12 we obtain the values $\sigma_v(6) = -6.26 \times 10^{-4}$ and $\sigma_v(12) = -2.5 \times 10^{-3}$. The viscosity effect is to attenuate selectively the amplitude of the sidebands.

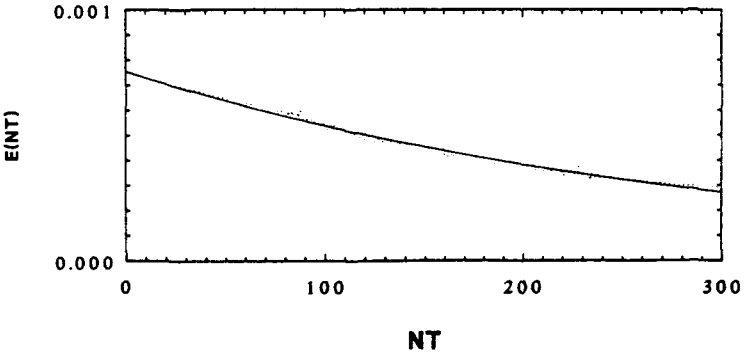

Figure 5. Total energy E of an evolving perturbed Stokes wave train (ak=0.24, k=9) with $R_e = 1.16 \times 10^5$ and $\kappa = 6.02 \times 10^{-4}$. The solid line corresponds to exponential interpolated values. NT is the number of fundamental periods

The dashed line in figure 5 shows the dissipation of total energy due to viscosity of an evolving perturbed Stokes wave of wave steepness ϵ=0.24 and wavelength of 8cm. The solid line corresponds to exponential interpolated values with a rate of attenuation close to -3.41×10^{-3} which is slightly greater than the theoretical value -2.8×10^{-3} given by the expression $-4k^2/Re$ for $R_e=1.16\times10^5$ and k=9. The viscous damping is weakly nonlinear.

Hogan[14] using a fourth order evolution equation for deep water gravity-capillary waves showed for small κ that the growth rate of modulational instability is modified when surface tension is taken into account. The growth rate shift is given by

$$\Delta\sigma = (9-73A)\kappa A^2/16$$

where A is wave steepness . For A>9/73 the rates growth are diminished. Trulsen and Dysthe[4] demonstrated that the upper sideband concentrates around the steepest portions of the wave train where the attenuation of the growth rates due to surface tension has to be considered. This mechanism is to more reduce the rate of growth of the upper sideband and to increase the asymmetry between the two sidebands. The selective damping due to viscosity and the mechanism of localization of the upper sideband on the steepest crests of the wave train produce during the modulation a large difference between the amplitudes of the subharmonic and superharmonic modes as shown in figure 4. Amplitude time histories exhibit the dominance of the subharmonic mode k=6. Figure 6 displays the free surface profile of the wave train at time t=280T. The wave group has lost three waves.

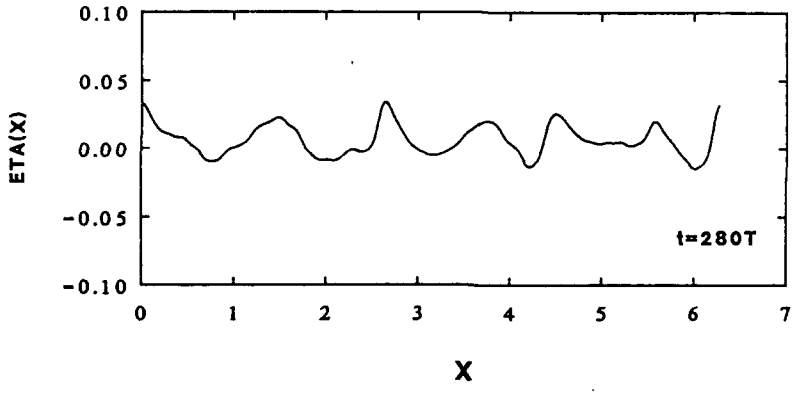

Figure 6. Instantaneous free-surface elevation.

In conclusion it seems that the shift to lower carrier frequencies observed numerically may be explained by the phenomenon of spatial localization combined with a damping process.

REFERENCES

[1] LIGHTHILL M.J.(1965), Contributions to the theory of waves in nonlinear dispersive system, J. Inst. Math. Appl.,1 , pp. 269-306.

[2] BENJAMIN T.B. and FEIR J.E.(1967), The disintegration of wave trains in deep water, J. Fluid Mech., 27, pp. 417-430.

[3] LAKE B.M., YUEN H.C., RUNGALDIER H. and FERGUSON W.E. (1977), Nonlinear deep-water waves; theory and experiments. Part 2. Evolution of a continuous wave train, J. Fluid Mech., 83, pp. 49-74.

[4] TRULSEN K. and DYSTHE K.B.(1990), Frequency down-shift through self modulation and breaking, in the Water Wave Kinematics, ed., A. Torum and O.T. Gudmestad, the Netherlands, pp. 561-572.

[5] POITEVIN J. and KHARIF C.(1991), Subharmonic transition of a nonlinear wave train on deep water, In "Mathematical and numerical aspects of wave propagation phenomena", SIAM Philadelphia.

[6] HARA T. and MEI C.C.(1991), Frequency downshift in narrowbanded surface waves under the influence of wind, J. Fluid Mech., 230, pp. 429-477.

[7] DOMMERMUTH D.G. and YUE D.K.P.(1987), A high order method for the study of nonlinear gravity waves, J. Fluid Mech., 187, pp. 267-288.

[8] WEST B.J. (1982), Statistical properties of water waves. Part 1. Steady-state distribution of wind-driven gravity-capillary waves, J. Fluid Mech., 117, pp. 187-210.

[9] LONGUET-HIGGINS M.S. (1985), Bifurcation in gravity waves, J. Fluid Mech., 151, pp. 457-475.

10] KHARIF C. and RAMAMONJIARISOA A.(1988), Deep-water gravity wave instabilities at large steepness, Phys. Fluid., 31, pp. 1286-1288.

[11] YUEN H.C. and FERGUSON W.E.(1978), Fermi Pasta Ulam recurrence in the two dimensional nonlinear Schrödinger equation, Phys. Fluids., 21, pp. 2116-2118.

[12] STIASSNIE M. and SHEMER L.(1984), On modifications of the Zakharov equation for surface gravity waves, J. Fluid. Mech., 143, pp. 47-67.

[13] STIASSNIE M. and SHEMER L.(1987), Energy computations for evolution of class I and II instabilities of Stokes waves, J. Fluid. Mech., 174, pp. 299-312.

[14] HOGAN S.J. (1985), The fourth-order evolution equation for deep-water gravity-capillary waves, Proc. R. Soc. Lond., A 402, 359-372.

Discussion of Kharif's paper

J.W. Dold

We have found breaking in our surface-integral calculations for ak as small as 0.09 (and a little lower). So it must certainly happen with ak $\approx \frac{1}{4}$ as you calculate.

You argued that breaking is responsible for dissipation of some modes. One would expect it also to create some rotation which is not included in your approach. How important do you do you think rotational effects might be?

Author's reply

Rotational effects on the Benjamin-Feir instability are very important especially for wind waves. Several authors showed that the growth rate of this instability is very sensitive to the current profiles in water. Concerning waves generated by wavemakers Trulsen and Dysthe [4] demonstrated that local breaking waves tend to suppress the superharmonic component of the modulational instability. At present the simulation of two phase flow generated by breaking waves is a challenge. So, at first, we have to consider rotational component induced by viscosity and currents.

C.C. Mei (Comment)

Results without surface tension and dissipation are similar to earlier work by Lo & Mei (1985 J.F.M.) based on Dysthe's equation. For joint effects of dissipation and wind on gravity waves, Hara & Mei (1991 Sept., J.F.M.) is relevant.

D.H. Peregrine

To fully describe the dynamics of your system with surface tension it is necessary to include enough modes to include the capillary waves with the same phase velocity as the primary wave. Please comment on this aspect of your computations.

Author's reply

Our first purpose was to take into account the capillary waves phase locked with the primary waves in order to enhance the damping of the wave train due to viscosity. To describe the ripples on the free surface and if we wish that the fundamental wave belongs to the field of gravity waves, we have to introduce, in the model, modes with high wavenumber. The effects of these high wavenumber modes are (i) to amplify the round-off errors and (ii) to require a very great number of points on the free surface, in order to avoid round-off errors, which increase considerably the operation count per time step. Independently of these numerical limitations I think that the mechanism you have mentioned would more attenuate the primary wave and favour the frequency down-shift.

Our main aim was to consider the effects of an irreversible process such as viscous damping and surface tension on the long time evolution of the two sidebands of the Benjamin-Feir instability.

V. Shrira

It seems that one should be very careful while interpreting these results for oceanic waves as 3-dimensionality changes qualitatively the nonlinear interactions, producing, in particular, frequency downshift. The reported results look more suitable for description of waves in long narrow tanks. Influence of the wall friction can be modelled that way.

Author's reply

Our aim was to understand the frequency downshifting phenomenon observed in a tank by Lake et al. (1977). However I think that the mechanism described herein can reveal some analogy with more realistic 3D wave fields where dissipation due to breaking is important.

M.-Y. Su

At the initial condition of $(ak)_o \approx 0.24$ which will incite strong 3-D instability. How is your computer simulation of 2-D side-band instability to yield a physically accurate result on frequency down-shifting phenomenon?

Author's reply

It is well known that for wave steepness $\epsilon > 0.30$ the dominant instabilities are of class II phase locked with the basic wave and three dimensional. We have focused our study on the two-dimensional waves train although our model may be easily extended to three dimensional patterns. As previous authors we have first considered the frequency down-shifting phenomenon in the framework of two-dimensional waves which is today a phenomenon not well understood (for two-dimensional wind waves see Hara and Mei [6/]). Extensions to three-dimensional wave groups will be conducted in order to introduce the three-dimensional instabilities of class II which arise on the steepest crests of the train.

V.E. Zakharov

Modulation of the weakly-nonlinear Stokes waves is described by the Nonlinear Schrödinger equation. In one dimension it is a complete integrable system, having many solutions periodical in time. Did you try to compare your results with the predictions of the NLS theory?

Author's reply

We have not compared our results to the NLS theory but we have found for small wave steepness (ak = 0.13) a good agreement with the results given by the fourth order evolution equations derived from the Zakharov equation on the NLS equation.

The Numerical Computation of Surface Waves.

By V.R.Kogan, V.V.Kuznetsov, E.N.Pelinovsky.
(USSR)

The problems connected with the numerical computations of nonstationary surface waves using the boundary problem method of analytical functions are being discussed in the present report. The given method summarizes the M.S.Longuet-Higgins (1976) approach and consists of the following.

The region of potential flow in a moving coordinate system on each time-stepping transforms into the unit circle by the conformal mapping G(t). The advantage of this method is in the quick computation of the conformal mapping G(t). It takes 0.05 sec on PC-IT 386 and is as much as 80 times faster than the previous one. The results of the theory of singular integral equations were used to construct this method. The variational theory of conformal mapping by M.A.Lavrentyev and the method of quick computation of the singular integrals with Gilbert channel play here the main role. It is necessary to underline that the singular integral equation is solved one time at t=0 to find initial conditions. Then the problem reduces to solving the first-order ordinary differential equations in t on the unit circle. The energy integral and the condition of harmonicity are hovering around 10^{-9}- 10^{-6}. The method was tested on the solution of gravity waves of small amplitude and progressive capillary waves (G.D.Crapper).

The problems about the dynamics of gravity and gravity-capillary waves were investigated. A new mechanism of the birth of capillary ripple on the long gravity wave. The method is generalized in several directions. In particular, it has been used to calculate the waves of finite depths. The field of application of Korteweg-De Vries equations and the

nonlinear shallow-water theory was investigated. The method was applied for viscous water in quasi-potential approximation. Using the representation of non-analytical function as a superposition of potentials of simple and double layers as well as the integral on region flow an efficient computation method of nonpotential flows, described by Navye-Stokes equation, was developed.

The given approach may be treated in the broad sense: first, the connection between the surface wave theory and the transformation of the circle into itself, is being established: secondly,it became possible to use the results of boundary tasks of analytical functions in surface wave study, in particular, their stability.

References.

Longuet-Higgins,M.S. and Cok elet E.D. 1976 The deformation of steep surface waves on water, Proc. R. Soc. Lond. A. 350, 1-26.

Crapper G.D. 1957 An exact solution for progressive capillary waves of arbitrary amplitude. J. Fluid Mech. 2, 4, 532-540.

Kogan V.R. and Kuznetsov V.V. 1989 The method of numerical computation of nonstationary gravity-capillary waves of finite amplitude. v.29, N 6, 844-852.

CANONICAL TRANSFORMATIONS AND REDUCED EQUATIONS IN THE HAMILTONIAN THEORY OF WEAKLY NONLINEAR SURFACE WAVES

Vladimir P. Krasitskii

P.P.Shirshov Institute of Oceanology, Academy of Sciences of the USSR, 23 Krasikova, 117218 Moscow

The main results of this study can be summarized as follows. For weakly nonlinear purely gravity irrotational surface waves the fourth-order Hamilton equation of motion (*cf.* Zakharov 1968)

$$i\frac{\partial a_0}{\partial t} = \frac{\delta H}{\delta a_0^*} = \omega_0 a_0 + \int U^{(1)}_{0,1,2} a_1 a_2 \delta_{0-1-2}\, dk_{12}$$

$$+ 2\int U^{(1)}_{2,1,0} a_1^* a_2 \delta_{0+1-2}\, dk_{12}$$

$$+ \int U^{(2)}_{0,1,2} a_1^* a_2^* \delta_{0+1+2}\, dk_{12}$$

$$+ \int V^{(1)}_{0,1,2,3} a_1 a_2 a_3 \delta_{0-1-2-3}\, dk_{123}$$

$$+ \int V^{(2)}_{0,1,2,3} a_1^* a_2 a_3 \delta_{0+1-2-3}\, dk_{123}$$

$$+ 3\int V^{(1)}_{3,2,1,0} a_1^* a_2^* a_3 \delta_{0+1+2-3}\, dk_{123}$$

$$+ \int V^{(4)}_{0,1,2,3} a_1^* a_2^* a_3^* \delta_{0+1+2+3}\, dk_{123}$$

$$+ \int W^{(1)}_{0,1,2,3,4} a_1 a_2 a_3 a_4 \delta_{0-1-2-3-4}\, dk_{1234}$$

$$+ \int W^{(2)}_{0,1,2,3,4} a_1^* a_2 a_3 a_4 \delta_{0+1-2-3-4}\, dk_{1234}$$

$$+ \frac{3}{2}\int W^{(2)}_{4,3,2,1,0} a_1^* a_2^* a_3 a_4 \delta_{0+1+2-3-4}\, dk_{1234}$$

$$+ 4\int W^{(1)}_{4,3,2,1,0} a_1^* a_2^* a_3^* a_4 \delta_{0+1+2+3-4}\, dk_{1234}$$

$$+ \int W^{(3)}_{0,1,2,3,4} c^*_1 a^*_2 a^*_3 a^*_4 \delta_{0+1+2+3+4} dk_{1234} \qquad (1)$$

with the Hamiltonian (the sum of kinetic and potential energies of the fluid)

$$H = \int \omega_0 a^*_0 a_0 dk_0$$

$$+ \int U^{(1)}_{c,1,2} (a^*_0 a_1 a_2 \delta_{0-1-2} + c.c.) dk_{012}$$

$$+ \tfrac{1}{2} \int U^{(2)}_{c,1,2} (a^*_0 a^*_1 a^*_2 \delta_{0+1+2} + c.c.) dk_{012}$$

$$+ \int V^{(1)}_{c,1,2,3} (a^*_0 a_1 a_2 a_3 \delta_{0-1-2-3} + c.c.) dk_{0123}$$

$$+ \tfrac{1}{2} \int V^{(2)}_{c,1,2,3} a^*_0 a^*_1 a_2 a_3 \delta_{0+1-2-3} \, dk_{0123}$$

$$+ \tfrac{1}{4} \int V^{(4)}_{c,1,2,3} (a^*_0 a^*_1 a^*_2 a^*_3 \delta_{0+1+2+3} + c.c.) dk_{0123}$$

$$+ \int W^{(1)}_{c,1,2,3,4} (a^*_0 a_1 a_2 a_3 a_4 \delta_{0-1-2-3-4} + c.c.) dk_{01234}$$

$$+ \tfrac{1}{2} \int W^{(2)}_{c,1,2,3,4} (a^*_0 a^*_1 a_2 a_3 a_4 \delta_{0+1-2-3-4} + c.c.) dk_{01234}$$

$$+ \tfrac{1}{3} \int W^{(3)}_{c,1,2,3,4} (a^*_0 a^*_1 a^*_2 a^*_3 a^*_4 \delta_{0+1+2+3+4} + c.c.) dk_{01234} \qquad (2)$$

can be transformed to the Hamilton *reduced equation*

$$i \frac{\partial \delta_0}{\partial t} = \frac{\delta \tilde{H}}{\delta \delta^*_0} = \omega_0 \delta_0 + \int \tilde{V}^{(2)}_{0,1,2,3} \delta^*_1 \delta_2 \delta_3 \delta_{0+1-2-3} dk_{123} +$$

$$+ \int \tilde{W}^{(2)}_{0,1,2,3,4} \delta^*_1 \delta_2 \delta_3 \delta_4 \delta_{0+1-2-3-4} dk_{1234}$$

$$+ \tfrac{3}{2} \int \tilde{W}^{(2)}_{4,3,2,1,0} \delta^*_1 \delta^*_2 \delta_3 \delta_4 \delta_{0+1+2-3-4} dk_{1234} \qquad (3)$$

with the *reduced Hamiltonian*

$$\hat{H} = \int \omega_0 \ell_0^* \ell_0 \, dk_0 + \frac{1}{2} \int \tilde{V}^{(2)}_{0,1,2,3} \ell_0^* \ell_1^* \ell_2 \ell_3 \delta_{0+1-2-3} \, dk_{0123}$$

$$+ \frac{1}{2} \int \tilde{W}^{(2)}_{0,1,2,3,4} (\ell_0^* \ell_1^* \ell_2 \ell_3 \ell_4 \delta_{0+1-2-3-4} + \text{c.c.}) dk_{01234} \qquad (4)$$

by suitable choice of the coefficients $A^{(n)}$, $B^{(n)}$, $C^{(n)}$ in the canonical transformation of the form

$$\begin{aligned} c_0 = \ell_0 &+ \int A^{(1)}_{0,1,2} \ell_1 \ell_2 \delta_{0-1-2} \, dk_{12} \\ &+ \int A^{(2)}_{0,1,2} \ell_1^* \ell_2 \delta_{0+1-2} \, dk_{12} \\ &+ \int A^{(3)}_{0,1,2} \ell_1^* \ell_2^* \delta_{0+1+2} \, dk_{12} \\ &+ \int B^{(1)}_{0,1,2,3} \ell_1 \ell_2 \ell_3 \delta_{0-1-2-3} \, dk_{123} \\ &+ \int B^{(2)}_{0,1,2,3} \ell_1^* \ell_2 \ell_3 \delta_{0+1-2-3} \, dk_{123} \\ &+ \int B^{(3)}_{0,1,2,3} \ell_1^* \ell_2^* \ell_3 \delta_{0+1+2-3} \, dk_{123} \\ &+ \int B^{(4)}_{0,1,2,3} \ell_1^* \ell_2^* \ell_3^* \delta_{0+1+2+3} \, dk_{123} \\ &+ \int C^{(1)}_{0,1,2,3,4} \ell_1 \ell_2 \ell_3 \ell_4 \delta_{0-1-2-3-4} \, dk_{1234} \\ &+ \int C^{(2)}_{0,1,2,3,4} \ell_1^* \ell_2 \ell_3 \ell_4 \delta_{0+1-2-3-4} \, dk_{1234} \\ &+ \int C^{(3)}_{0,1,2,3,4} \ell_1^* \ell_2^* \ell_3 \ell_4 \delta_{0+1+2-3-4} \, dk_{1234} \\ &+ \int C^{(4)}_{0,1,2,3,4} \ell_1^* \ell_2^* \ell_3^* \ell_4 \delta_{0+1+2+3-4} \, dk_{1234} \\ &+ \int C^{(5)}_{0,1,2,3,4} \ell_1^* \ell_2^* \ell_3^* \ell_4^* \delta_{0+1+2+3+4} \, dk_{1234} \; . \end{aligned} \qquad (5)$$

In the above equations, we have used the compact notations in which the arguments $\mathbf{k}_j$ (horizontal wave-vectors) in a, δ, ω, $U^{(n)}$, $V^{(n)}$, $W^{(n)}$ and δ-functions are replaced by subscripts j, with the subscript zero assigned to $\mathbf{k}$. Thus, for example, $a_j = a(\mathbf{k}_j,t)$, $\omega_j = \omega(\mathbf{k}_j)$, $U^{(2)}_{0,1,2} = U^{(2)}(\mathbf{k}, \mathbf{k}_1, \mathbf{k}_2)$, $\delta_{0-1-2} = \delta(\mathbf{k} - \mathbf{k}_1 - \mathbf{k}_2)$, *etc.* For differentials we have used the notations $d\mathbf{k}_0 = d\mathbf{k}$, $d\mathbf{k}_{012} = d\mathbf{k}d\mathbf{k}_1 d\mathbf{k}_2$, *etc.*, and the integral signs denote corresponding multiple integrals in the limits from $-\infty$ to $+\infty$. The asterisk and c.c. stand for complex conjugate, and δ for functional derivative.

The vertical displacement of the surface $\zeta(\mathbf{x},t)$ above the point $\mathbf{x} = (x,y)$ is related to the "normal variable" $a(\mathbf{k},t)$ by

$$\zeta(\mathbf{x},t) = \frac{1}{2\pi}\int\left[\frac{\omega(\mathbf{k})}{2g}\right]^{1/2}\left[a(\mathbf{k},t) + a^*(-\mathbf{k},t)\right]\exp(i\mathbf{k}\mathbf{x})d\mathbf{k}$$

where $\omega(\mathbf{k}) = [g|\mathbf{k}|\,\mathrm{th}(|\mathbf{k}|h)]^{1/2}$ is the dispersion relation of linear gravity waves with g as the gravitational acceleration and h as a constant depth of fluid layer in equilibrium state.

The structure of the Hamiltonian expansion implies its reality. The coefficients $U^{(n)}$, $V^{(n)}$, $W^{(n)}$ will not be given in this short contribution. We merely note that these coefficients should satisfy the "natural symmetry conditions" consisting in independency of the integrals in H of redenoting the dummy variables of integration. Note also that the coefficient $V^{(2)}$ should satisfy the following symmetry conditions:

$$V^{(2)}_{0,1,2} = V^{(2)}_{1,0,2} = V^{(2)}_{0,1,2} = V^{(2)}_{2,1,0} \quad . \tag{6}$$

Similar conditions should hold for $\tilde{V}^{(2)}$.

The coefficients $A^{(n)}$, $B^{(n)}$, $C^{(n)}$ in the transformation (5) should also satisfy proper natural symmetry conditions and, moreover, they should satisfy some "canonicity conditions" for the transformation to be canonical one. These conditions can be obtained, for example, through the Poisson brackets:

$$\int \left[\frac{\delta a(k)}{\delta \varepsilon(q)} \frac{\delta a(k')}{\delta \varepsilon^*(q)} - \frac{\delta a(k)}{\delta \varepsilon^*(q)} \frac{\delta a(k')}{\delta \varepsilon(q)} \right] dq = 0 \ ,$$

$$\int \left[\frac{\delta a(k)}{\delta \varepsilon(q)} \frac{\delta a^*(k')}{\delta \varepsilon^*(q)} - \frac{\delta a(k)}{\delta \varepsilon^*(q)} \frac{\delta a^*(k')}{\delta \varepsilon(q)} \right] dq = \delta(k - k') \ .$$

With these canonicity conditions we can derive explicit expressions for the coefficients $A^{(n)}$, $B^{(n)}$, $C^{(n)}$ of the canonical transformation and for the kernels $\tilde{V}^{(2)}$, $\tilde{W}^{(2)}$ of the reduced equation. Details of the calculations for $A^{(n)}$, $B^{(n)}$, $\tilde{V}^{(2)}$ are given in Krasitskii (1990). We note, however, that calculations using the Poisson brackets are related with cumbrous algebra, and it is easier to derive $A^{(n)}$, $B^{(n)}$, $C^{(n)}$ by direct substitution of the transformation (5) into evolution equation (1) and reducing resulted equation to (3).

Here we present only some of the results obtained. The coefficients $A^{(n)}$, $B^{(n)}$, $C^{(n)}$ can be subdivided into the two groups: non-resonant ($A^{(1)}$, $A^{(2)}$, $A^{(3)}$, $B^{(1)}$, $B^{(3)}$, $B^{(4)}$, $C^{(1)}$, $C^{(4)}$, $C^{(5)}$) and resonant ($B^{(2)}$, $C^{(2)}$, $C^{(3)}$) ones. Some explicit and structural expressions are as follows:

$$A^{(1)}_{\zeta,1,2} = - \frac{U^{(1)}_{0,1,2}}{\omega_0 - \omega_1 - \omega_2} \ , \quad A^{(2)}_{\zeta,1,2} = - 2 A^{(1)}_{2,1,0} \ , \quad A^{(3)}_{\zeta,1,2} = - \frac{U^{(3)}_{0,1,2}}{\omega_0 + \omega_1 + \omega_2} \ ,$$

$$B^{(1)}_{\zeta,1,2,3} \propto (\omega_0 - \omega_1 - \omega_2 - \omega_3)^{-1}, \quad B^{(3)}_{\zeta,1,2,3} \propto (\omega_0 + \omega_1 + \omega_2 - \omega_3)^{-1} \ ,$$

$$B^{(4)}_{\zeta,1,2,3} \propto (\omega_0 + \omega_1 + \omega_2 + \omega_3)^{-1}, \quad C^{(1)}_{\zeta,1,2,3,4} \propto (\omega_0 - \omega_1 - \omega_2 - \omega_3 - \omega_4)^{-1},$$

$$C^{(4)}_{\zeta,1,2,3,4} \propto (\omega_0 + \omega_1 + \omega_2 + \omega_3 - \omega_4)^{-1}, \quad C^{(5)}_{\zeta,1,2,3,4} \propto (\omega_0 + \omega_1 + \omega_2 + \omega_3 + \omega_4)^{-1},$$

$$B^{(2)}_{\zeta,1,2,3} = A^{(3)}_{0,1,-0-1} A^{(3)}_{2,3,-2-3} + A^{(1)}_{1,2,1-2} A^{(1)}_{3,0,3-0} + A^{(1)}_{1,3,1-3} A^{(1)}_{2,\zeta,2-0}$$

$$- A^{(1)}_{0+1,0,1} A^{(1)}_{2+3,2,3} - A^{(1)}_{0,2,0-2} A^{(1)}_{3,1,3-1} - A^{(1)}_{\zeta,3,0-3} A^{(1)}_{2,1,2-1} .$$

The expressions for $C^{(2)}$ and $C^{(3)}$ are far more lengthy and will not be given here. Note that the non-resonant coefficients are inversely proportional to the non-resonant frequency differences, and this gives possibility to reduce the Hamiltonian (an attempt to eliminate $\tilde{V}^{(2)}$ and $\tilde{W}^{(2)}$ from $\tilde{H}$ leads to singularities in $B^{(2)}, C^{(2)}, C^{(3)}$ at corresponding resonant frequency differences).

The kernels $\tilde{V}^{(2)}$ and $\tilde{W}^{(2)}$ have the following structure:

$$\tilde{V}^{(2)}_{0,1,2,3} = Z_{0,1,2,3} + (\omega_0 + \omega_1 - \omega_2 - \omega_3)\, B^{(2)}_{0,1,2,3}\,, \tag{7}$$

$$\tilde{W}^{(2)}_{0,1,2,3,4} = X_{0,1,2,3,4} + (\omega_0 + \omega_1 - \omega - \omega_3 - \omega_4)\, C^{(2)}_{0,1,2,3,4} \tag{8}$$

where, for example,

$$Z_{0,1,2,3} = -2\Big[U^{(1)}_{0,2,0-2} A^{(1)}_{3,1,3-1} + U^{(1)}_{2,0,2-0} A^{(1)}_{1,3,1-3} + U^{(1)}_{0,3,0-3} A^{(1)}_{2,1,2-1} + U^{(1)}_{3,0,3-0} A^{(1)}_{1,2,1-2} - U^{(1)}_{0+1,0,1} A^{(1)}_{2+3,2,3} - U^{(3)}_{-0-1,0,1} A^{(3)}_{-2-3,2,3}\Big] + V^{(2)}_{0,1,2,3}\,.$$

The kernels (7) and (8) satisfy all required symmetry conditions. We note that neither of the two addenda in the right-hand sides of (7) and (8) satisfy these symmetry conditions separately - only the entire right-hand sides satisfy these conditions. It should be emphasized that this theory do not impose any constraints on smallness of resonant frequency differences $\omega_0 + \omega_1 - \omega_2 - \omega_3$ and $\omega_0 + \omega_1 - \omega_2 - \omega_3 - \omega_4$, and it essentially distinguishes our approach from those in use.

Neglecting quadratic terms in the reduced equation (3) we obtain

$$i\frac{\partial \delta_0}{\partial t} = \frac{\delta \tilde{H}}{\delta \delta_0^*} = \omega_0 \delta_0 + \int \tilde{V}^{(2)}_{0,1,2,3} \delta_1^* \delta_2 \delta_3 \delta_{0+1-2-3}\, dk_{123} \tag{9}$$

with the reduced Hamiltonian

$$\tilde{H} = \int \omega_0 \delta_0^* \delta_0\, dk_0 + \frac{1}{2} \int \tilde{V}^{(2)}_{0,1,2,3} \delta_0^* \delta_1^* \delta_2 \delta_3 \delta_{0+1-2-3}\, dk_{0123} \tag{10}$$

The equation (9) is often referred to as the Zakharov equation. This equation in its original version (Zakharov 1968) was derived by heuristic considerations and it is not Hamiltonian, as was pointed out by Caponi *et. al.* (1982). As a matter of fact, this original approach corresponds to $\tilde{V}^{(2)}_{0,1,2,3} = Z_{0,1,2,3}$. The kernel $Z_{0,1,2,3}$ does not satisfy all symmetry conditions in (6): it is symmetrical only relatively to permutation of the arguments 2 and 3, but not symmetrical relatively to permutation of 0 and 1 and to permutation of the pairs (0,1) and (2,3). This is the formal cause for non-Hamiltonian structure of the Zakharov equation in its original version. Similar remarks can be attributed to non-Hamiltonian version of the fourth-order reduced equation of the type (3) (Stiassnie & Shemer 1984). Numerical calculations of instability growth rates and long time wave evolution, based on the cubic reduced equation (9), have shown that differences between calculations with Hamiltonian and non-Hamiltonian versions of the kernel $\tilde{V}^{(2)}$ are observed (in the examples considered) for sufficiently large wave steepnesses.

The reduced Hamiltonians (4) and (10) are obvious integrals of motion, *i.e.* the reduced equations (3) and (9) conserve the total energy. In addition, there are integrals of motion of the form

$$I = \int f(\mathbf{k}) a^*(\mathbf{k}) a(\mathbf{k}) d\mathbf{k}$$

The value I is the wave momentum for $f = \mathbf{k}$ and the wave action for $f = 1$. It follows from the reduced equation (3) that I evolves in accordance with the equation

$$\frac{\partial I}{\partial t} = -\frac{i}{2}\int (f_0 + f_1 - f_2 - f_3)\tilde{V}^{(2)}_{0,1,2,3} a^*_0 a^*_1 a_2 a_3 \delta_{0+1-2-3}\, dk_{0123}$$

$$+\left[-\frac{i}{2}\int (f_0 + f_1 - f_2 - f_3 - f_3)\tilde{W}^{(2)}_{0,1,2,3,4} a^*_0 a^*_1 a_2 a_3 a_4 \delta_{0+1-2-3-4}\, dk_{01234} + c.c.\right]$$

It is seen from this equation that reduced equation (3) conserves only the momentum, but equation (9) conserves both the momentum and the action. Thus, five-wave interactions, described be quadratic terms in (3), violate conservation of action.

In the case of capillary-gravity waves, permitting three-wave interactions, the lowest-order reduced equation is the second-order one:

$$i\frac{\partial \delta_o}{\partial t} = \frac{\delta \tilde{H}}{\delta \delta_o^*} = \omega_o \delta_o + \int U^{(1)}_{o,1,2} \delta_1 \delta_2 \delta_{o-1-2} dk_{12} + 2 \int U^{(1)}_{2,1,o} \delta_1^* \delta_2 \delta_{o+1-2} dk_{12}$$

with the reduced Hamiltonian

$$\tilde{H} = \int \omega_o \delta_o^* \delta_o dk_o + \int U^{(1)}_{c,1,2} (\delta_o^* \delta_1 \delta_2 \delta_{o-1-2} + \text{c.c.}) dk_{o12} ,$$

where now the surface tension should be taken into account in $\omega(\mathbf{k})$. This approach corresponds to retaining only linear and quadratic terms in the evolution equation (1) and the canonical transformation (5). The coefficients of this canonical transformation are :

$$A^{(1)}_{c,1,2} = A^{(2)}_{c,1,2} = 0, \quad A^{(3)}_{c,1,2} = - \frac{U^{(3)}_{o,1,2}}{\omega_o + \omega_1 + \omega_2} .$$

This transformation is possible because for capillary-gravity waves the "frequency difference" $\omega_o + \omega_1 + \omega_2$ is non-resonant. In this case the reduced equation conserves only the wave momentum (in addition to $\tilde{H}$) and does not conserves the wave action.

REFERENCES

Caponi E.A., Saffman P.G. & Yuen H.C. 1982 Instability and confined chaos in a nonlinear dispersive wave system. *Phys. Fluids* 25, 2159-2166.

Krasitskii V.P. 1990 Canonical transformation in a theory of weakly nonlinear waves with a nondecay dispersion law. *Sov. Phys. JETP* (Eng. trans.) 71(5), 921-927.

Stiassnie M. & Shemer L. 1984 On modification of the Zakharov equation for surface gravity waves. *J. Fluid Mech.* 143, 47-67.

Zakharov V.E. 1968 Stability of periodic waves of finite amplitude on the surface of deep fluid. *J. Appl. Mech. Tech. Phys.* (Eng. trans.) 2, 190-194.

Discussion of Krasitskii's paper

M.W. Dingemans

In your equations you have contributions from both three- and four-wave interactions. For four waves you consider exact resonance, which is only possible when all four waves are free. However, at a shorter time-scale already bound waves are generated (3-wave interaction, second-order Stokes). The implication is that when $\omega = \Omega(k,a^2)$ and for $\mathbf{k}_1 + \mathbf{k}_2 + \mathbf{k}_3 + \mathbf{k}_4 = 0$ one has $\omega_1 + \omega_2 + \omega_3 + \omega_4 = 0(a^2)$ implying that exact resonance on the resonance manifold is not fulfilled. In fact, the resonant manifold has a certain width. For four-wave interaction near-resonance is obtained.

Author's reply

First of all, I have equations for combined four- and five-wave interactions. For four waves, as well as for five waves, I don't consider exact resonance, and the four waves are not free. Moreover, the resonance frequency differences $\omega_0 + \omega_1 - \omega_2 - \omega_3$ and $\omega_0 + \omega_1 - \omega_2 - \omega_3 - \omega_4$ are non-zero and in my method, are quite *arbitrary* ones (in other words, the resonant manifold has an arbitrary width). I recall that wave instabilities occur when resonance frequency differences are non-zero. The bound waves and Stokes corrections arise as results of solution of the integro-differential equations of Zakharov type.

V.I. Zakharov (comment)

Effects of self-interacting of the gravitational waves are included in the "improved" equations automatically.

Performing of a canonical transformation with non-singular coefficients is normally correct mathematical procedure, not affecting any physical processes, described by the equation.

So, the simplest simplified equation

$$\frac{\partial a_k}{\partial t} + i\omega_k a_k = i \int T(\mathbf{k},\mathbf{k}_1,\mathbf{k}_2,\mathbf{k}_3) a_{k_1}, a_{k_2}, a_{k_3} \, \delta(\mathbf{k} + \mathbf{k}_1 - \mathbf{k}_2 - \mathbf{k}_3) dk_1, dk_2, dk_3$$

has an exact solution

$$a_k = A\,\delta(\mathbf{k}-\mathbf{k}_0) e^{-(\omega_{k_0} - T|A|^2 + \ldots)T} = T(k_0,k_0,k_0,k_0)$$

the expansion

$$\omega \longrightarrow \omega_{k_0} - T|A|^2 + \ldots$$

presents first terms of the function $\omega = \omega(\mathbf{k}_1|A|^2)$, describing an amplitude dependence of a Stokes wave frequency.

Wave breaking and non-uniformities of atmosphere and ocean

V.A.Dulov, V.N.Kudryavtsev

Marine Hydrophysical Institute,Sevastopol,USSR

Wave breaking shows the occurrence of processes of energy and impulse dissipation in wind waves(WW). The parameters of wave breaking are measured comparatively easily and may be estimated even visually (by Beaufort number). It is important, that they effect radiowave emission and scattering. Wave energy input is determined not only by the wind but also by the atmosphere stratification and spatial variations of surface currents.Under real conditions non-uniformities of currents, ocean temperature variations and adapted variations of atmospheric boundary layer exist simultaneously and affect wave breaking integrally.

The relation between the ocean spatial non-uniformities and wave breaking permits to realize diagnosis of the ocean variability from space by the method of radio-sounding (Dulov,Kudryavtsev, Suetin,1990).

1.Theoretical analysis.

At moderate and high wind speed the main energy losses result from surface breaking. Thus,in the equation of WW spectral energy (E) balance breaking is considered as dissipative term S_b:

$$\frac{dE}{dt} = \frac{\partial E}{\partial t} + \frac{\partial \Omega}{\partial k_i}\frac{\partial E}{\partial x_i} = S_{cw} + S_n + S_b \qquad (1)$$

$$S_{cw} = \alpha E + k_i \frac{\partial U_j}{\partial x_j}\frac{\partial E}{\partial k_j} - \frac{1}{2} l_i l_j \frac{\partial U_i}{\partial x_j} E$$

S_n are nonlinear interactions, ω,c are frequency and phase velocity, α is interaction coefficient between wind and waves, $\Omega = \omega + k_i U_i$, $l_i = k_i / k$. The source Scw describes the energy input at interaction of waves with wind and currents.Wave breaking is formed such a spectral interval where $S_n + S_{cw} > 0$. For well developed waves low-frequency boundary of this interval is in vicinity of several wave number of spectral peak (k_p). Moreover,there exist wave number vicinity (k_s), where one dimensional energy flux, due to nonlinear interaction, equals zero: $P(k_s) = 0$. Numerical calculations of integral of nonlinear interactions ground the assumption that $\zeta = k_s/k_p \sim 2$-3. (Hasselmann K. at.al.1973). Then the full rate of dissipation (D) acquires the form

$$D = \int_{k > k_s} S_{cw} \vec{dk} - \int_{k > k_s} dE/dt \; \vec{dk} \qquad (2)$$

Let us assume that undisturbed WW spectrum is developed under the effect of uniform wind and is steady within the dissipation interval ($k > k_s$).Then undisturbed dissipation and its variation have the form:

$$D_o = \int_{k>k_s} \alpha_o E_o \vec{dk}, \qquad \delta D = J_1 + J_2 + J_3 \qquad (3)$$

$$J_1 = -\delta k_s \oint (k\,\alpha_o\,E_o)_{k=k_s} d\Theta; \quad J_2 = \int_{k>k_s} \frac{d}{dt}\delta E\, \vec{dk}; \quad J_3 = \int_{k>k_s} \delta S_{cw} \vec{dk}$$

J_1 is determined by variations of nonlinear interactions. Finally,it brings to redistribution of wind energy input between the dissipation interval and another part of the spectrum. For the undisturbed spectrum proposed by Toba (1973), and the wind-wave interaction coefficient(α) proposed by Plant (1982)

$$E_o = A\,(\Theta - \Theta_w)(u_*/c)\,k^{-4}, \quad \alpha/\omega = m\,(u_*/c)^2 \cos(\Theta - \Theta_w),$$

the integral dissipation will be of the following form (Phillips,1985)

$$D_o = m\,f_1 g^{-1} \ln(k_*/k_s)\,u_*^3, \quad f_1 = \oint A \cos\Theta\, d\Theta, \quad k_* = g/u_*^2, \qquad (4)$$

where u* is the friction velocity of atmosphere,Θ_w is the direction of wind vector ,$A(\Theta - \Theta_w)$ is the energy directional distribution, m=2-4.

We shall characterize wave breaking by a white cap coverage (Q). As Q is closely related to dissipation, we may consider that there is a functional dependency Q = Q(D).Using different empirical expressions for the surface drag coefficient C_D and dependency of white cap coverage on wind we determined that white caps are proportional to dissipation (Dulov, Kudryavtsev,in press) : D ~ Q.

Let us estimate the effect of stratification on wave breaking. The energy of wind-to-wave input depends on the profile of wind speed in the vicinity of coincidence layer (Z_c).In real conditions the height of this layer for $k=k_S$ is sufficiently smaller than the Monin-Obukhov scale(L). Thus dissipation should not depend explicitly on the stratification parameter and is defined by the expression (4). In case meteorological parameters are measured on the fixed horizon(z_m), the relation between white caps coverage in the stratified atmosphere and in the neutral one (D_n) will be of the form:

$$D_o/D_n = \left[\,1 - C_D^{1/2}\,\Psi(z_m/L)/\varkappa\,\right]^{-3} \qquad (5)$$

$\Psi(z_m/L)$ - is empirical function (see Large,1979), $\varkappa$=0.4. For estimate calculations, Ψ may be taken as $\Psi \sim -z/L$. As it follows from this expression wave breaking at unstable stratification is stronger than at neutral one,and at stable stratification it weakens.The influence of stratification upon white caps coverage based on our experiments, is shown on Fig 1-3.The dependency of white caps coverage on wind speed for various types of atmospheric stratification and for neutral one (Q_n) are presented on Fig 1-2. White caps are proportional to wind in power 3.9.The difference of wind power from 3 is caused by dependency of the drag coefficient on wind. The connection of white caps coverage with stratification is shown on Fig 3. The empirical dependency has the form: $Q/Q_n - 1 \approx -2z/L$.As we can see the atmosphere stratification essentially effects wave breaking.

Let us define the time of relaxation of dissipation interval.As stabilization of this interval is performed by nonlinear mechanisms, the time of its relaxation (τ) should not depend on the type of disturbance. We have estimated it having transferred the dissipation

interval from one state to another one under the effect of wind variation:

$$\tau = \int_{k>k_s} \partial E_o/\partial W \, \vec{dk} \left[\int_{k>k_s} \partial S_{cw}/\partial W \, \vec{dk} \right]^{-1} \qquad (6)$$

Further, we'll consider the steady regime of wave evolution, when we may ignore the evolution term Jz as compared to the wind- current source Ja.(see eq.(3)).This regime occurs when the spatial (X) and temporal (T) scales of wind-current source excess the relaxation scale: $T \gg \tau$, $X \gg \tau G$ or $T \gg 170W/g$, $L \gg 40W^2/g$,where G is the group velocity of WW for k=ks.At this condition the dissipation interval evolutionates in the current field in such a way, that the local balance between the energy input and its dissipation is realized:

$$Q \sim D = \int_{k>k_s} S_{cw} \vec{dk} \qquad (7)$$

This expression describes the white caps coverage variation in case the variations of atmospheric parameters and current are present.For the case,when WW travel on non-uniformities of currents the expression (7) may be rewritten as:

$$K = \frac{Q - Q_o}{Q_o} = -\tilde{\beta} \frac{W}{\varepsilon} \left\{ \operatorname{div} \vec{U} + \tilde{\beta}_1 \left[\left(\frac{\partial U_1}{\partial x_2} + \frac{\partial U_2}{\partial x_1} \right) \sin 2\theta_w + \left(\frac{\partial U_1}{\partial x_1} - \frac{\partial U_2}{\partial x_2} \right) \cos 2\theta_w \right] \right\} \qquad (8)$$

$$\tilde{\beta} = \beta(1+\beta_1)/2 \ , \ \tilde{\beta}_1 = (1-\beta_1)/(1+\beta_1) \ , \beta = -2f \left[mC_D \xi^{3/2} \ln(\xi C_D) \right]^{-1} (1 - C_D^{1/2} \Psi/\varkappa)^2$$

$$f = \frac{\oint (1+2\cos^2\theta) A(\theta) d\theta}{3\varkappa_1} \qquad \beta_1 = \frac{\oint (1+2\sin^2\theta) A(\theta) d\theta}{\oint (1+2\cos^2\theta) A(\theta) d\theta}$$

The wave breaking response to the current gradients is determined by the values of coefficient β , which depend on spectral parameters. For plausible values of wave spectrum parameters the range of the model coefficient may be estimated as: β=1000 - 40000 ,β_1=0.4 - 0.7 If the value 10^4 is taken as an estimation of β ,we obtain currents'gradients $5\ 10^{-3}$ inducing two-fold variations of white caps coverage. Equation (8) gives rise to a conclusion that at one and the same value of the current velocity gradient the contrast of wave breaking for divergent current may be by 3-7 times greater than for the current without divergence.

E x p e r i m e n t s

The main volume of field data on effect of currents upon wind wave breaking refers to manifestation of short-period internal waves and frontal zones with scales of an order of 1 km.(Fedorov and Ginzburg, 1986) The surface manifestations of such phenomena are simple enough to be observed and measured. Experiments on study of influence of currents with scale 10 to 100 km are rather difficult due to their spatial extension and natural variability of wind speed. We have chosen the way of experimental investigation of the effect the simplest types of currents upon the wave breaking, and namely:

- purely convergent-divergent currents

- currents of a jet character (the current of Gulf-Stream type)

a) Zones of convergence and divergence.

Large-scale internal waves (IW) with a period of about an hour and more are ideal examples of convergent-divergent currents. At phase speed of 2 m/sec IW with a period of 2 hours has wave length of about 14 km. For IW the divergence of surface current is proportional to the velocity of the vertical thermocline displacement. The experiments were held in 1989 in the north-western region of the Tropical Atlantic. Fig.4 illustrates a typical fragment of registration of wave breaking. White caps coverage are depicted in relative values. The characteristic feature here is the presence of short-period (5-20 min) IW. The observations of short-period IW manifestation are described (Dulov et.al.,1986,Dulov and Kudryavtsev 1988) For the purpose of the given experiment they are considered as "noise". The same Figure depicts low-frequency variation of thermocline with a period of 1 hour. Fig.5-7 shows registrations of thermocline depth (H), wave breaking and wind speed where short-period IW are excluded by low-frequency filter. We have analyzed this data using the model eq.(8).For the neutral stratification and currents of purely convergent-divergent character, the relation between of wave breaking, wind speed and thermocline vertical motions will be of a form:

$$Q_m = aW^3(1+\beta(W/g)Z) \qquad Z = H_o^{-1}(\partial H/\partial t)(\cos\theta_w^2+\beta_1\sin\theta_w^2) \qquad (9)$$

In the regions, where $\partial H/\partial t > 0$ (convergence zone) wave breaking is intensified and in the regions, where $\partial H/\partial t < 0$ (divergence) wave breaking is damped.The calculations of Q_m performed using the expression (9) are depicted at Fig.5-7 (dashed line). Experimental data reveals the reality of the relation between wave breaking and vertical motions of thermocline. The β -order is equal to 10^4 that follows from theoretical analysis.

b) Quasi-geostrophic frontal zone

The frontal Gulf Stream zone is an ideal region for investigation of evolution of wind wave parameters on a jet-like current.Moreover, the ocean surface temperature variability in the quasi-geostrophic frontal zones leads to spatial variation of atmospheric stratification. For the analysis we choose measurements performed in Gulf Stream in August this year. The analysis of experiments was performed using theoretical results. Wave breaking was considered as the function of three parameters: a) wind speed, b) ocean currents shear, c) atmospheric stratification (z/L). Further defined was the functional dependency of white caps measurements and leading parameters one in a form (see equation (8)):

$$Q_m = aW^{3.9}(1+ cz/L + bG) \qquad G = -\frac{1}{2}\cdot 10^4(W/g)\frac{\partial U_l}{\partial n}\sin[2(\theta_v-\phi)] \qquad (10)$$

$\partial U_l/\partial n$- is gradient of velocity across stream, ϕ is direction of current vector. We supposed, that model described experimental data if it satisfied Fisher-criterion. The first experiment was performed on August 21 (Fig.8). During the experiment the wind was blowing from the warm side of the front to the cold one,and had the component directed along the current.Fig.8 illustrates variations of air/water temperature, wind speed and its direction, currents'velocity,

white caps coverage, atmospheric stratification (z/L). This experimental data was exposed by 3-factors analysis.The empirical model has the form:

$$Q_m = 9 \cdot 10^{-5} W^{3.5}(1-3z/L+4G)$$

On Fig.8 are shown the model of white caps coverage variation (FA) caused by atmospheric factors:$FA = a\,W^{3.5}(1 + cz/L)$. This component of the model doesn't describe white caps measurements. This difference may be explain by influence of current shifts upon the wave breaking.Fig 8 presents model calculation of contribution of the measured current shifts to wave breaking variations (FG) and normalized differences of measured white caps from atmospheric model part (KA):

$$FG = Q_m/(aW^{3.5}) - cz/L - 1 \equiv bG$$

$$KA = Q/(aW^{3.5}) - cz/L - 1 \qquad K = Q/(aW^{3.5}) - 1$$

The relation of this calculations is obvious and we can conclude that in this case model is adequate to experimental data. The coefficient of the current shifts transfer to the wave breaking contrast is of order 10^4. Similar results were obtained by analysis of the experiment performed in August 31 in the same region. The reference information is given in the Fig.9. The experiment was conducted under similar conditions. This data was also subjected to three-factor analysis. Corresponding empirical model has the following form:

$$Q_m = 9 \cdot 10^{-5} W^{3.5}(1-5z/L+1.8G)$$

Fig.9. presents the atmospheric model component(FA) and the current shift one(FG). We can see that the model satisfies to experimental data . On the cold side of the Gulf Stream the white caps coverage is greater than it may be expected for the given atmospheric parameters, and on the warm side it is less. It was predicted by theoretical analysis.

Conclusion

Theoretical analysis and experimental results permit to assume, that current non-uniformities with scales of several dozens of kilometers affect the white caps coverage. The most prominent effects may be expected for divergent currents.Jet-like currents affect wave breaking less effectively. At the same current velocity gradient the wave breaking contrast caused by a jet-like current is 4-7 times weaker than that of the divergent one.Jet-like currents, typical of geostrophic frontal zones affect sufficiently the atmospheric boundary layer resulted from spatial surface temperature variations. In this case the complex effect of atmospheric and dynamic factors may be strong.

Manifestations of the ocean synoptical variability on its surface in the form of spatial variations of wave-breaking intensity provides an opportunity to observe large-scale hydrological peculiarities by remote methods. As wave-breaking is one of the main factors forming proper microwave surface radiation, it seems possible to perform such observations from space by means of microwave scanners (Dulov, Kudryavtsev and Suetin, 1990).

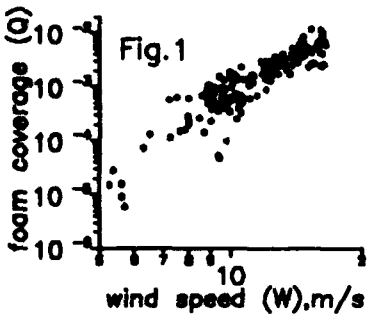
Fig.1
foam coverage (Q)
wind speed (W),m/s

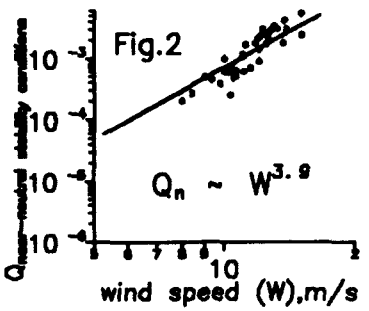
Fig.2
$Q_n \sim W^{3.9}$
wind speed (W),m/s

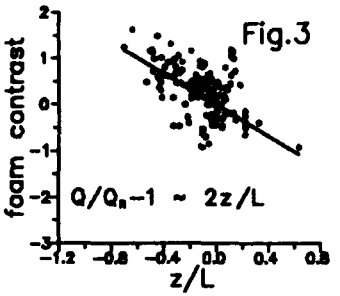
Fig.3
foam contrast
$Q/Q_n - 1 \sim 2z/L$
z/L

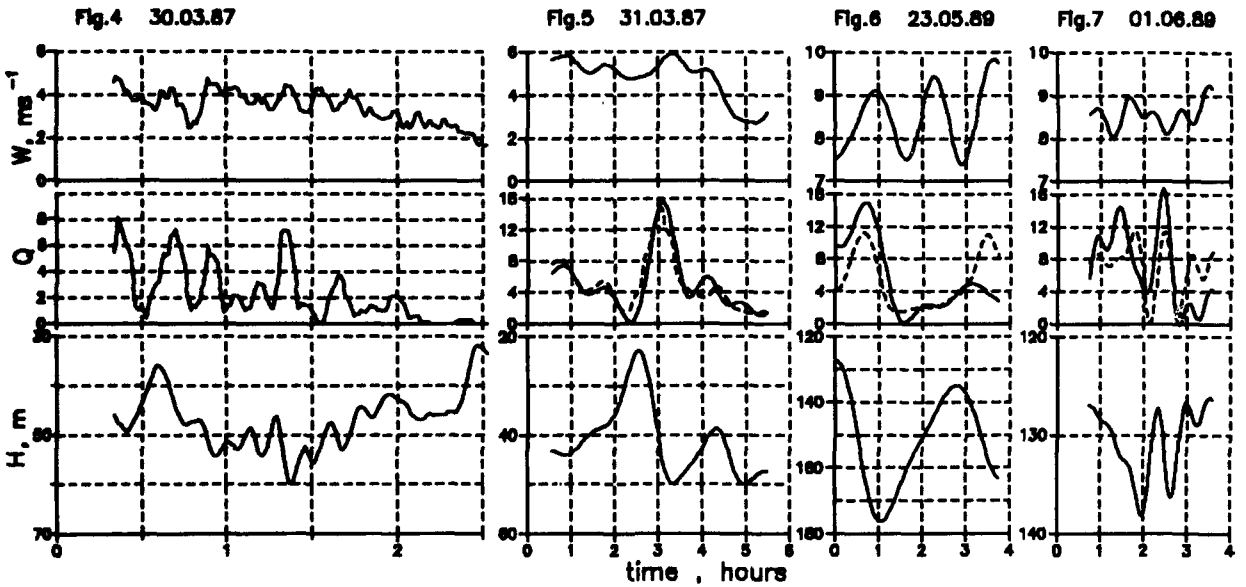
Fig.4 30.03.87
Fig.5 31.03.87
Fig.6 23.05.89
Fig.7 01.06.89
W, ms⁻¹
Q
H, m
time , hours

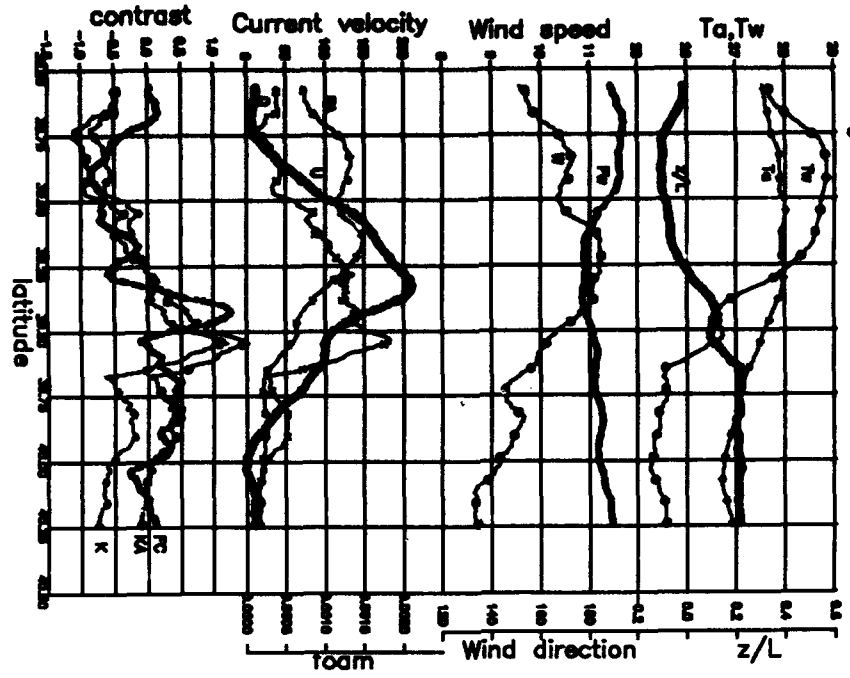

Fig.8 Gulf Stream,21.08.91

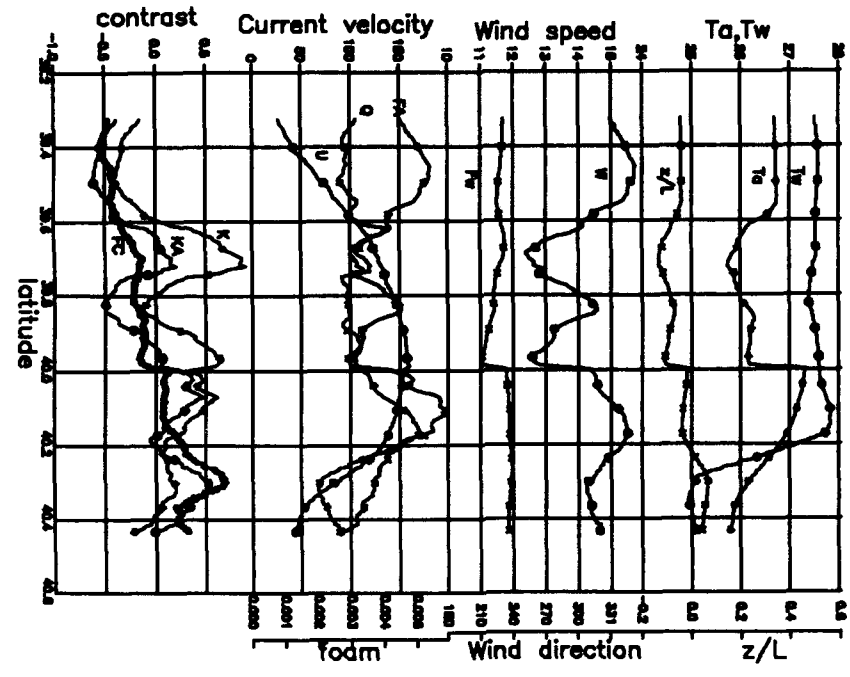

Fig.9 Gulf Stream,31.08.91

References

Dulov,V.A.,S.I.Klyushnikov and V.N.Kudryavtsev, 1986: Effect of internal waves on wind waves breaking. Field observations. Morskoy Gidrofizicheskiy Zhurnal, 6, 14-21 (in Russian).

Dulov,V.A. and V.N.Kudryavtsev,1988: Effect of internal waves on intensity of falling-down wind waves. Theoretical analysis. Morskoy Gidrofizicheskiy Zhurnal, 2, 9-15 (in Russian).

Dulov,V.A., V.N.Kudryavtsev and V.S.Suetin, 1990: Non-uniformities of ocean currents and surface radio-brightness temperature. Issledovaniya Zemli iz Kosmosa, 1, 14-19 (in Russian).

Dulov,V.A. and V.N.Kudryavtsev,(in press): Wave breaking and non-uniformities of atmosphere and ocean. J.Phys.Oceanogr.

Fedorov,K.N. and A.I.Ginzburg, 1986: Phenomena on the ocean surface observed visually. Oceanology, 26, 5-14.

Hasselmann,K. et al., 1973: Measurements of wind-wave growth and swell decay during the Joint North Sea Wave Project (JONSWAP). Ergänz. Deutsch. Hydrogr. Zeitsch., A8, 12, 95p.

Large,G.,1979: The turbulent flux of momentum and sensible heat over the open sea during moderate to strong wind. Thesis, Univ. Columbia, 180p.

Plant,W.J.,1982: A relationship between wind stress and wave slop. J.Geophys.Res., 87, 1961-1967.

Toba,Y., 1973: Local balance in the air-sea boundary processes. III On the spectrum of wind waves. J.Oceanogr.Soc.Japan, 29, 209-220.

Discussion of Kudryavtsev and Dulov's paper

P.A.E. Janssen

You have investigated the effect of atmospheric stability on wave breaking with a model where wave breaking depends on the friction velocity. I object to this because I would expect that white capping is a purely hydrodynamical process related to the water motion. Thus an alternative explanation of your results could be that in unstable cases the wind input is larger because of larger friction velocity giving steeper waves and therefore larger dissipation.

Author's reply

In our model rate of dissipation is proportional to energy input. The energy wind-to-wave input depends on friction velocity in power 3. We have shown, that white caps coverage is proportional to dissipation of energy, then, white caps coverage is proportional to friction velocity in power 3 too. As it follows from this, the white caps at unstable stratification is greater than at neutral one. Your explanation is similar, but is made from another point of view (your point of view is hydrodynamical, but mine is energetical).

A Hamiltonian Formulation for Uniformly Travelling Water Waves

R.S.MacKay
Nonlinear Systems Laboratory, Mathematics Institute,
University of Warwick, Coventry CV4 7AL

Abstract: Numerical work of many people on the bifurcations of spatially periodic solutions suggests that the equations for uniformly travelling water waves (two-dimensional, irrotational gravity waves with no surface tension, on inviscid fluid of infinite depth) have a reversible Hamiltonian formulation, with horizontal position in the wave-frame playing the role of time. Recently, I have found such a formulation [BM]. This explains why the bifurcation diagram for periodic uniformly travelling waves looks so much like that for the area-preserving Hénon map. It also leads to predictions of many other forms of uniformly travelling wave, such as quasiperiodic, homoclinic and chaotic waves. The symplectic form becomes degenerate whenever the horizontal velocity at the surface in the wave frame becomes zero, in particular at Stokes' 120^0 crests. I believe that the analysis of this degeneracy will shed much light on the almost highest waves.

1. Introduction

By uniformly travelling water waves, I shall mean solutions of the following problem:

$$\Delta\varphi = 0 \qquad \text{in } y < \eta(x), \tag{1}$$
$$\nabla\varphi \to -c \qquad \text{as } y \to -\infty, \tag{2}$$
$$\eta + \tfrac{1}{2}|\nabla\varphi|^2 = \tfrac{1}{2}c^2 \qquad \text{on } y = \eta(x), \tag{3}$$
$$\varphi_y - \eta_x\varphi_x = 0 \qquad \text{on } y = \eta(x), \tag{4}$$

where c is a constant (the wave speed). The variables x and y are horizontal and vertical coordinates, respectively, in a frame moving with the wave. The function φ represents the velocity potential in the frame of the wave, and η the surface elevation. The choice of the Bernoulli constant corresponds to a choice of origin for y.

After the flat state ($\eta = 0, \varphi = -cx$), the simplest solutions are those which are periodic in x. Up to horizontal translation, they appear to come in two-parameter families, where suitable parameters are the wavelength λ and some measure of amplitude, for example $a = \frac{1}{2}(\eta_{max} - \eta_{min})$. There is a scaling symmetry: if (η,φ,c) is one solution then so is $(\tilde\eta,\tilde\varphi,\tilde c)$ for any $s \in \mathbb{R}^+$, where

$$\tilde\eta(x) = s\eta(x/s), \tag{5}$$
$$\tilde\varphi(x,y) = s^{3/2}\varphi(x/s,y/s),$$
$$\tilde c = s^{1/2}c\,.$$

So only the scale-invariant combination $A = 2\pi a/\lambda$ is important, and it is enough to look for periodic solutions with a fixed period, say $\lambda = 2\pi$. A basic family of periodic waves, with one trough and crest per wavelength, is known, which connects the infinitesimal sinusoidal waves of linear theory to Stokes' wave with a 120^0 crest [AFT].

Bifurcations of periodic waves, that is, branching in the set of periodic solutions, has been observed by many people, e.g. [CS,LH1,LH2,Zuf,As]. For example, at A = 0.404961 a branch of periodic waves with alternate troughs and crest slightly different is observed to bifurcate from the basic family. Since the wavelength doubles at this bifurcation, we say the bifurcating branch has period 2, the basic wave being assigned period 1. There are many other bifurcations of higher period from the basic family, as sketched in Figure 1, albeit confined to the interval $0.402233 < A < 0.404961$, but apparently dense in this interval. Many of these branches have their own bifurcations. For example, the period 2 branch itself period doubles to a period 4 branch which doubles to a period 8 and so on. Note that the labelling of branches could in principle run into trouble if, for example, a bifurcating branch reconnects later with a different ratio of wavelengths, as has been observed in some other problems (e.g. [KE]), but no ambiguity will be encountered in the current presentation.

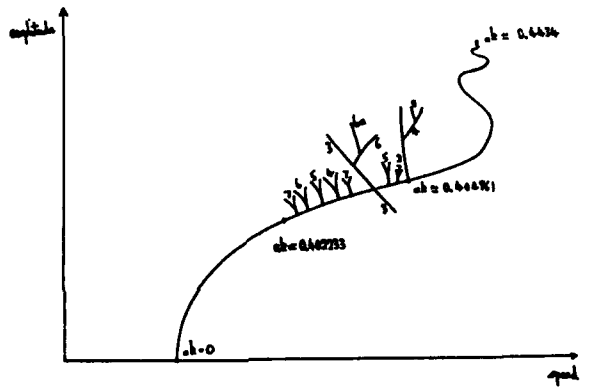

Figure 1: A sketch of some of the bifurcations from the basic family

When Philip Saffman introduced me to these bifurcations, my immediate reaction was that they look just like those for the area-preserving Hénon map [Hen], a one-parameter family of reversible area-preserving mappings f_μ of the plane which it will be convenient to write in the form

$$x' = \mu + 2x - x^2 - y \qquad (6)$$
$$y' = x\,.$$

It is a discrete-time analogue of a two-degree of freedom reversible Hamiltonian system. So I set about looking for a reversible Hamiltonian formulation for uniformly travelling water waves, with horizontal position in the waveframe playing the role of time. Note that Zakharov's Hamiltonian formulation [Zak] answers a different question. He obtained a Hamiltonian formulation to evolve the whole wavefield $\eta(x)$, $\phi(x,y)$ in time. We want to evolve just some information on one vertical line, labelled by its horizontal coordinate x, to all other vertical lines, under the assumption that we are looking at a steady wave in some moving frame.

I also suggested some further numerical tests. In particular, when Saffman mentioned to me that it was an open question whether asymmetric uniformly travelling water waves can occur,

I suggested to look for a symmetry breaking bifurcation in one of the places where I knew the Hénon map has one. The bifurcation route for the Hénon map is to follow one of the period 3 branches until it period doubles, follow its period double, which itself period doubles then restabilises via another period doubling and subsequently loses stability again, this time by symmetry breaking, giving a pair of asymmetric period 6 solutions. Zufiria looked for the analogous features in the water wave problem and found exactly the same route occurs [Zuf], thus adding to the evidence for a reversible Hamiltonian formulation.

In fact, uniformly travelling water waves in finite depth had already been formulated as a reversible system by Kirchgassner [K]. The generic properties and bifurcations of symmetric objects (ones which are their own reflection) in general reversible systems are very similar to those in reversible Hamiltonian systems, but this does not extend to non-symmetric objects. So it is better to find a formulation which is Hamiltonian as well as reversible.

Mielke recently succeeded in doing this for finite depth and non-zero surface tension [Mie]. In fact it is not hard. He starts from the variational formulation, rescales the domain vertically to make it a strip, and then takes the Legendre transform with respect to x. It is straightforward to extend this result to infinite depth, by using a vertical shift rather than a rescaling. Finite depth has the advantage that Mielke was able to prove that all small enough amplitude uniform travelling wave solutions with given speed lie in a finite-dimensional centre manifold for the evolution equations, on which they become a finite-dimensional reversible Hamiltonian system (the same was done by Kirchgassner, except for obtaining the Hamiltonian structure). It is not clear whether this can be done in the case of infinite depth, but it is not necessary for our purposes.

Extension of Mielke's formulation to zero surface tension is not so easy, however. The Legendre condition, permitting the Legendre transform, fails in the limit. But I realised that essentially all that happens is that one degree of freedom is removed and the zero surface tension problem looks like a constrained Hamiltonian system. It is analogous to taking motion of a particle in a potential which becomes very large away from a surface S in the configuration space. In the limit that the potential becomes infinite off S, the perpendicular degree of freedom is eliminated, but the system still has a Hamiltonian formulation: one simply restricts the phase space and the Hamiltonian to the cotangent bundle of S and restricts the symplectic form to its tangent space. In the water wave problem the form of the "constraining potential" is somewhat different, but the same conclusion holds.

2. Hamiltonian formulation

A reversible Hamiltonian system has four ingredients: a manifold M (called the *phase space*), a symplectic form ω on M, a function H on M (called the *Hamiltonian*), and an involution R which preserves H and changes the sign of ω. A *symplectic form* is a closed nondegenerate antisymmetric bilinear form on the tangent bundle of M. That means (treating the concepts in reverse order) that for any pair of infinitesimal displacements ξ and ζ from a point in M (*tangent vectors*) it gives a real number $\omega(\xi,\zeta)$, linear in both ξ and η, $\omega(\zeta,\xi) = -\omega(\xi,\zeta)$, the only ξ for which $\omega(\xi,\zeta) = 0$ for all ζ is $\xi = 0$, and the integral of ω over any contractible 2-sphere is zero. The standard symplectic form on $\mathbb{R}^{2n}$, with coordinates $(q,p) \in \mathbb{R}^n \times \mathbb{R}^n$ is

$$\omega = \sum_{i=1}^{n} dp_i \wedge dq_i \,, \tag{7}$$

which when applied to tangent vectors $\xi = (\xi q, \xi p)$ and $\zeta = (\zeta q, \zeta p)$ (think of these as two choices of $(\delta q, \delta p)$ in the usual notation for an infinitesimal displacement), gives

$$\omega(\xi,\zeta) = \sum_{i=1}^{n} \xi p_i \, \zeta q_i - \zeta p_i \, \xi q_i \,. \tag{8}$$

The evolution is given by the equations $\dot{z} = X(z)$, $z \in M$, where X is the vector field such that

$$\omega(\xi, X) = dH(\xi) \tag{9}$$

for all tangent vectors ξ (it is unique by nondegeneracy of ω). In the case of the standard symplectic form (7) the vector field X has components

$$\begin{aligned} \dot{q}_i &= \partial H/\partial p_i \\ \dot{p}_i &= -\partial H/\partial q_i \,, \end{aligned} \tag{10}$$

which is the standard form for a Hamiltonian system.

I present now a reversible Hamiltonian formulation for uniformly travelling water waves, for the case of infinite depth and zero surface tension. Using the new vertical coordinate

$$Y = y - \eta(x), \tag{11}$$

the quantities F, U and w below will have the following interpretations:

$$\begin{aligned} F(x,Y) &= \varphi(x,y) + cx \\ U(x,Y) &= \varphi_x(x,Y) \\ w(x) &= \int^x \eta(x')\, dx' \,. \end{aligned} \tag{12}$$

The phase space, symplectic form and Hamiltonian each depend on the wave speed c, which we regard as an external parameter. Let M_c be the set of quadruples $Q = (F,U,\eta,w)$, where F and U are smooth functions from $(-\infty,0] \to \mathbb{R}$ with $F(Y), F_Y(Y) \to 0$, $U(Y) \to -c$ as $Y \to -\infty$, and η and w are real numbers. The phase space M_c' is the restriction of M_c to the subset satisfying the constraints:

$$\begin{aligned} w &= -\int_{-\infty}^{0} UF_Y \, dY \\ \eta &+ \tfrac{1}{2}(U^2 + F_Y^2)_0 = \tfrac{1}{2}c^2. \end{aligned} \tag{13}$$

Here and elsewhere, subscript 0 denotes values at $Y = 0$.

The symplectic form is the infinite-dimensional analogue of the standard symplectic form

$$\omega_c = dw \wedge d\eta + \int_{-\infty}^{0} dU \wedge dF \; dY \tag{14}$$

on M_c, restricted to M_c'. The Hamiltonian is Benjamin's flow-force invariant $\bar{S}$ [Ben], whose functional form is

$$H_c(F,U,\eta,w) = -\tfrac{1}{2}\eta^2 + \tfrac{1}{2}\int_{-\infty}^{0} [(U+c)^2 - F_Y^2]\, dY \tag{15}$$

The involution is

$$R(F,U,\eta,w) = (-F,U,\eta,-w)\ , \tag{16}$$

which can be seen to preserve H_c and change the sign of ω_c.

It is now an exercise to check that the resulting equations $Q_x = X_c(Q)$, with X_c defined by (9), correspond to equations (1-4). Incidentally, one can check at the same time that ω_c is non-degenerate on M_c'; this turns out to be true if $U_0 \neq 0$, but fails when $U_0 = 0$, a point to which we shall return at the end of the next section.

3. Consequences

(i) The first consequence of our reversible Hamiltonian formulation is that since it is a one-parameter family of autonomous Hamiltonian systems it decomposes into a two-parameter family of systems, the two natural parameters being the wave speed c and the flow force invariant $\bar{S}$. The former is an external parameter in our formulation, the latter is the value of the Hamiltonian, which is conserved. Hence, for example, we expect periodic solutions to come in two-parameter families (up to horizontal translation), as indeed is observed numerically.

(ii) Secondly, if there is a fold curve in the projection of any family of periodic solutions onto the $(c,\bar{S})$ plane, then generically on crossing the fold curve one obtains not just the two solutions from that family but an infinite bifurcation tree of periodic solutions coming out densely from one of them, in a complicated but well-defined way. This is a standard result for Hamiltonian systems with a saddle-centre periodic solution (e.g. [Mey]). In particular, if μ is an appropriately scaled parameter along a path in the $(c,\bar{S})$ plane, crossing a generic fold transversely at $\mu = 0$, then there will be a period q bifurcation near $\mu = \sin^4 \pi p/q$, for each $0 < p \leq q/2$, coprime with q. In fact, there is a 4D centre manifold with a surface of section on which the return map is a one-parameter family of area-preserving maps (reversible if the original system is), given to lowest order in x,y and μ by our form (6) of the Hénon map. Note that there should even be branches of periodic solutions not attached to the basic tree which can be deduced this way (period 5 and higher).

In Figure 2, Baesens and I [BM] computed the projection of the basic family of waves with wavelength fixed $\simeq 2\pi$ onto the $(c,\bar{S})$ plane, using Longuet-Higgins method [LH]. One can obtain all other solutions in the basic family by the scaling symmetry (5). The track in $(c,\bar{S})$ of any solution under the scaling transformation is a quartic, $\bar{S}$ proportional to c^4. Hence we see that any quartic tangent to our wavelength 2π curve is the projection of a fold curve in the basic family. We found a fold point at $A \simeq 0.40222$. This agrees to 5 decimal places with the beginning of the interval where bifurcations are observed, as we should expect from the above argument.

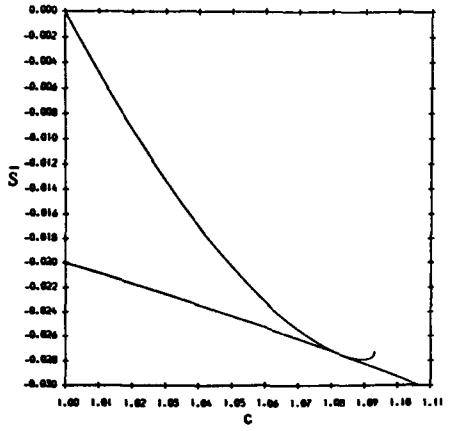

Figure 2: Projection of numerically computed basic waves of wavelength 2π onto $(c,\bar{S})$

(iii) In addition to the *bifurcation tree of periodic solutions* attached to the basic family, we should expect to see other types of uniformly travelling wave, corresponding to other generic features in the unfolding of a saddle-centre of periodic orbits for a reversible Hamiltonian system. These include quasiperiodic solutions, solutions homoclinic to a periodic one, solutions heteroclinic between two periodic ones, and chaotic solutions corresponding to all random choices of doubly infinite sequences of 0s and 1s. This is represented schematically in Figure 3. It is an interesting computational challenge to look for some of these numerically. It will be interesting too to make "surface of section" plots for uniformly travelling waves with fixed $(c,\bar{S})$, for example to plot the pair (η,w) every time that $\eta_x = 0$. This could be done already for periodic solutions, and I expect the familiar island chain picture to emerge. Another interesting challenge is to prove existence of chaotic waves using the idea of the "anti-integrable limit" [AA].

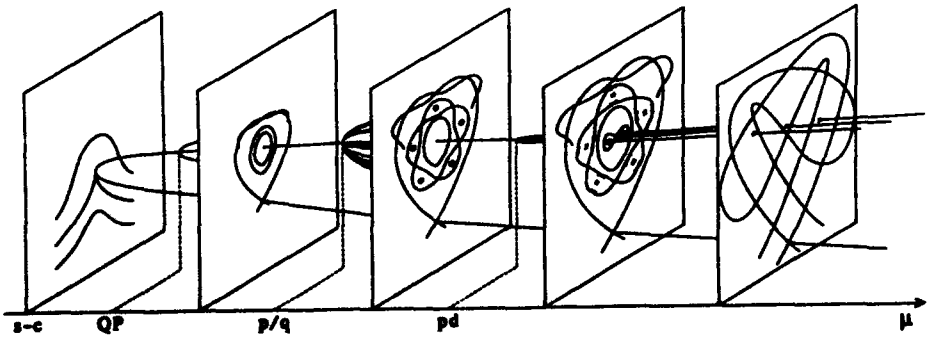

Figure 3: Sketch of some of the bifurcations arising from a saddle-centre periodic solution

(iv) The curve in Figure 2 appears to be forming a spiral. This fits with Longuet-Higgins observations and analysis [LHF]. In this case, there should be an infinite sequence of folds in the basic family, accumulating at the highest wave, as sketched in Figure 4. It follows that on one side of each fold we should expect another bifurcation tree. An open question is which side of the fold has the bifurcations. Is it always the side corresponding to the higher wave, as for the first fold, or does it alternate sides, for example? The answer is determined by the direction in which the relevant pair of Floquet multipliers move round a fold. These are the spatial Floquet multipliers for the linear stability of the periodic wave for our Hamiltonian evolution in x. They come in reciprocal pairs λ,λ^{-1}. At a fold there is a double multiplier +1. Following a typical path round a fold, the "residue" $R = (2-\lambda-\lambda^{-1})/4$ passes smoothly through 0 at non-zero speed. The bifurcations from the periodic solution occur for $0 < R \leq 1$, hence just on the side where $R > 0$. Is the relevant pair of multipliers for the second fold the continuation of the relevant pair for the first fold? In this case, the bifurcations would be on the lower side of the fold, and would proceed in the reverse direction, "eating up" all the solutions created by the first fold. Or is it a new pair, e.g. from $R < 0$? In principle it should be easy to calculate the multipliers of a periodic solution numerically. The equations are essentially just a generalisation of the equations to find a bifurcation point, e.g. [LH]. It would be very interesting to find out how they behave along the basic family. Also the direction in which the residue increases round a fold should be related to the Morse index of the periodic solution (cf. [Mad]) as a critical point of Luke's variational principle (e.g. [Wh]).

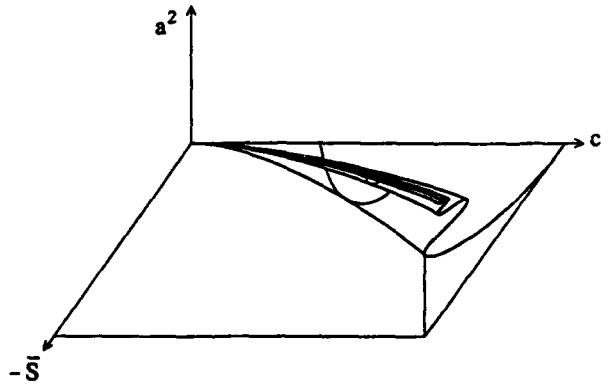

Figure 4: Conjectured picture for the whole of the basic family up to the highest wave

(v) The symplectic form becomes degenerate at 120^0 crests. This suggests that one might be able to understand the almost highest solutions, in particular Longuet-Higgins spiral, by analysing generalised Hamiltonian systems where the symplectic form is allowed to be degenerate on some submanifolds. Unfortunately, the kernel of the symplectic form at a 120^0 crest seems to have dimension 1, according to my calculations, whereas for a finite-dimensional system the kernel always has even dimension. This suggests that the almost highest waves are an essentially infinite-dimensional problem, but maybe one can still pull something out of it.

4. Generalisations

For uniformly travelling water waves with finite depth and/or non-zero surface tension, there is also a reversible Hamiltonian formulation. The Hamiltonian is again the flow-force invariant. There are now additional parameters to the speed and flow-force invariant. If there is a fold in the projection of a family of periodic solutions onto the parameter plane, then typically

one should expect to see the same sort of bifurcation picture as described above.

If one adds viscosity, plus a time-independent energy source to compensate, then uniformly travelling waves should still be describable as evolution of some collection of quantities in x, but the evolution is unlikely to have a Hamiltonian formulation, so one is unlikely to have the same richness of possible solutions. Nonetheless, many interesting things can be deduced for uniformly travelling waves of other problems which do not have a Hamiltonian formulation (e.g. [Bri],[KE]). If the energy source is invariant under reflection in x, then damped water waves will have a reversible formulation, but I have not yet seen a plausible way to realise this case.

References

[AFT] Amick CJ, Fraenkel LE, Toland JF, On Stokes conjecture for the wave of extreme form, Acta Math 148 (1982) 193-214

[As] Aston PJ, Analysis and computation of symmetry-breaking bifurcation and scaling laws using group theoretic methods, preprint

[AA] Aubry S, Abramovici G, Chaotic trajectories in the standard map: the concept of anti-integrability, Physica D 43 (1990) 199-219; and Erratum, in press

[BM] Baesens C, MacKay RS, Uniformly travelling water waves from a dynamical systems viewpoint: some insights into bifurcations from the Stokes family, preprint

[Ben] Benjamin TB, Impulse, flow force and variational principles, IMA J Appl Math 32 (1984) 3-68

[Bri] Bridges T, A dynamical systems approach to boundary layer transition, Warwick preprint, Jan 1991

[CS] Chen B, Saffman PG, Numerical evidence for the existence of new types of gravity waves of permanent form on deep water, Stud Appl Math 62 (1980) 1-21

[Hen] Hénon M, Numerical study of quadratic area-preserving mappings, Q J Appl Math 27 (1969) 291-312

[KE] Kent P, Elgin J, Travelling-wave solutions of the Kuramoto-Sivashinsky Equation, preprint, Imperial College, Sept 1991

[K] Kirchgassner K, Wave solutions of reversible systems and applications, J Diff Eq 45 (1982) 113-127

[LH1] Longuet-Higgins MS, Bifurcation in gravity waves, J Fluid Mech 151 (1985) 457-475

[LH2] Longuet-Higgins MS, Bifurcation and instability in gravity waves, Proc R Soc Lond A 403 (1986) 167-187

[LHF] Longuet-Higgins MS, Fox MJH, Theory of the almost-highest wave. Part 2. Matching and analytic extension, J Fluid Mech 85 (1978) 769-786

[Mad] Maddocks J, talk at CalTech, Dec 90

[Mie] Mielke A, Hamiltonian and Lagrangian flows on center manifolds with applications to elliptic variational problems, preprint

[Wh] Whitham GB, Linear and nonlinear waves (Wiley, 1974)

[Zak] Zakharov VE, Stability of periodic waves of finite amplitude on the surface of a deep fluid, J App Mech Tech Phys 2 (1968) 190-194

[Zu] Zufiria JA, Non-symmetric gravity waves on water of infinite depth, J Fluid Mech 181 (1987) 17-39

Discussion of MacKay's paper (Session F)

P.G. Saffman

Are there any prospects of connecting the infinity of steady periodic solutions with the 'real world'? Do you see any possible selection mechanisms in the mathematical formulation which may allow us to predict results of experiments?

Author's reply

The infinity of steady spatially periodic waves, and indeed of other types of steady wave, may have limited direct relevance to the real world, where to my knowledge steady waves are rare, apart from small amplitude period-1 waves and solitons on finite depth. Probably most of the steady waves are temporarily unstable, and hence unlikely to be directly observable. Furthermore, if one adds dissipation (e.g. viscosity) plus some compensating energy source (e.g. wind), many of these solutions may not continue to exist.

However, just as to Poincaré periodic orbits were the sole breach by which to seek to understand the range of possible behaviours in celestial mechanics, maybe steady waves will provide the key to understanding non-steady water surfaces. Perhaps the general solution can be regarded as bouncing around a matrix of steady wave solutions in some random way (in space and time) (maybe escaping every now and then in the form of a breaking wave), just as classical chaos can be regarded as built around a framework of periodic orbits. Indeed, Eckmann and Procaccia have succeeded in using such a viewpoint in large aspect ratio convection. I believe your own idea of "vortical states" aims to do the same in turbulence.

Regarding the selection of solutions, I believe that dissipation is the key. Hamiltonian models (such as have been found for all inviscid fluid problems) produce an over-abundance of possible solutions. The addition of even a small amount of dissipation shrinks the set of asymptotic solutions to measure zero (at least for bounded finite-dimensional systems). The resulting attractors can still be very numerous and complicated, but there is at least some selection. Associated to each attractor is an invariant measure which describes the average behaviour of most solutions attracted to it. Then the issue becomes to make quantitative statements about these measures. One may still ask which of these attractors is selected. This is in principle a question of initial conditions. Some authors, however, suggest that the times to reach an attractor in real fluid systems may be huge, so that the attractors are irrelevant. Even if not, in practice small noise (e.g. from the molecular level) may cause one to spend considerable time away from the attractors or to hop between them. If the noise is unbounded then it leads to a unique stationary measure, which is the ultimate in selection. Maybe this measure is what we really want.

P.G. Saffman (comment)

The paper by MacKay 'Hamiltonian formulation of uniformly travelling water waves' confirms the belief that there are infinitely many steady forms of uniformly propagating surface waves. Other work, for instance the generation of waves by wind, finds a great sensitivity of results to the assumed form of the wind profile.

We are now faced with the problem of being unable to predict what will happen, not because we can't find solutions, but because we have too many possible solutions and no way to choose between them.

New selection mechanisms, or novel statistical approaches, are required to reduce the classical uncertainty which faces us, and bring order out of the chaos. Progress in the useful practical application of theoretical discoveries is likely to be severely limited until we overcome the abundance of choice and find criteria for selecting a 'most probable solution'.

Nonlinear Interaction of Short and Long Gravity Waves

Chiang C. Mei
Department of Civil Engineering
Massachusetts Institute of Technology
Cambridge, MA 02139 USA

We shall present some recent theoretical results on the nonlinear interaction of short and long surface waves in deep water. Both waves are assumed to be narrow-banded, but their scales are vastly different so that the typical wavelength of the short wave is much shorter than the amplitude of the long wave. Specifically, the wavenumber ratio is $K/k = O(\epsilon^2)$ and the frequency ratio is $\Omega/\omega = O(\epsilon)$, where capital letters are associated with the long wave. In the conventional formulation in Eulerian coordinates the nonlinear kinematic and dynamic conditions pose obstacles which are usually handled by employing curvilinear coordinates embedding the free surface. For finite-amplitude long waves, this calls for a significant effort to compute the long waves. Here we shall discuss the use of Lagrangian coordinates in terms of which the position of the free surface is known *a priori*. The transformation from Lagrangian back to Eulerian coordinates is straightforward.

Two applications of this approach will be discussed. In the first, we assume that both the short and long waves are of mild slopes and slowly varying. It will be shown that the evolution of the short wave envelope can be described by the product of two factors. One factor corresponds to the classical results of linearized short waves, and implies that the short waves steepen at the long-wave crests but flattens at the long-wave troughs. The second factor is governed by a cubic Schrodinger equation with constant coefficients, in the Lagrangian coordinates. Therefore, the short wave can be unstable or stable to sideband disturbances depending on the wave steepness. We have examined the evolution of a stable soliton envelope of short waves as a train of long wave passes. If the long wave is uniform then the crest of the soliton is alternately advanced and reflected as each crest and trough of the long waves passes by. On the average the long waves also carries the short soliton forward by its drift velocity. If a packet of long waves approaches a short wave soliton

envelope from behind, the soliton crest is pushed to and fro by the crests and troughs of the long waves and forward by the Stokes drift for a finite distance.

We then describe the interaction of weakly nonlinear short waves on a uniform train of finite amplitude long waves, $KB = O(1)$. To facilitate the analysis Gerstner's simple and exact solution for a periodic long wave is used. This long wave is not irrotational; the vorticity is the greatest and of the order $O(KB)$ at the free surface; it is counter-clockwise if the waves advance from left to right. The evolution of the short wave is described by a cubic Schrodinger equation. The coefficients now vary periodically with the long waves phase. The side-band instability of the short wave envelope now obeys a Mathieu-type equation with periodic coefficients. Therefore, new regions of instability are now present in addition to the classical bandwidth of Benjamin and Feir. Numerical solution of the cubic Schrodinger equation indicates that for moderately steep long waves, either by increasing the short wave steepness, or by reducing the scale contrast, the evolution of short waves changes from regular to chaotic. In order to analyze the chaos, we approximate the Schrodinger equation by a truncted two-mode system coupling the carrier wave and a pair of unstable sidebands. All their harmonics are excluded. Numerical analysis of the simplified Hamiltonian system shows that progress toward chaos is consistent with the numerical calculation of the full Schrodinger equation.

Three dimensional interaction of obliquely interacting short waves and long waves have also been worked out.

Discussion of Mei's paper

N. Huang

Have you considered dissipation for the short waves in your computation?

Author's reply

Not yet. Dissipation can conceivably change the details of chaotic behaviour.

P.A.E.M. Janssen

You mentioned that one of the disadvantages of the Gerstner wave is that it has vorticity. However, another disadvantage is that a Gerstner wave has no Stokes drift. Does the absence of the Stokes drift of the long wave seriously affect the interaction with the short waves.

Author's reply

Over the time scale of $\sigma t = 0(kA)^{-1}$, the effect must be weak as shown by the good agreement of our Lagrangian theory with the Eulerian theory of Longuet-Higgins. Over the time scale of $\sigma t = 0(kA)^{-2}$ where nonlinear modulations occur, the omission of Stokes drift in the long wave may have some effect. Since our primary result is due to the oscillatory gravity provided by the long wave, a leading order effect, I think the Stokes drift will not change the result significantly. Further check, is needed, however.

D.H. Peregrine

Please comment further on the oblique waves.

Author's reply

Our results to date include linear modulations of short waves intersecting the long wave at a finite angle. For nonlinear modulations we have only considered slightly oblique side-bands. The problem for arbitrary angle of incidence is too messy.

P.G. Saffman

The Lagrangian representation is unsteady. It is possible to imagine a flow in which disturbances to the Lagrangian description grow without bounds while the flow is linearly stable in the Eulerian representation. Can this give rise to difficulties in the formulation of stability criteria for the Lagrangian representation?

Author's reply

I don't think so in our problem. In the limit case of no long waves, the side band instability criteria deduced by the Lagrangian theory are identical to those by the Eulerian theory (for both 2 and 3D). For long-time evolution, both Eulerian and Lagrangian theories must give finite results. Our result can be transformed to the Eulerian coordinates without qualitative change since the coordinates are related one-to-one.

NONLINEAR DYNAMICS OF INTERNAL WAVES IN THE OCEAN

Efim N.Pelinovsky

Academy of Sciences of the USSR
Institute of Applied Physics
46 Uljanov str., Nizhny Novgorod (Gorky), 603600, USSR

Observations of internal waves in the ocean show that many of them are nonlinear ones. Groups of solitons were registered by remote sensing. It was shown that there exists a universal spectrum of internal waves for open - ocean conditions (Garret - Munk spectrum). Review of the author's papers on the development of theoretical methods describing the evolution of a nonlinear internal wave field and corresponding observation data are presented in this paper.

1. The kinetic equation for the description of a quasi - stationary spectrum of internal waves is derived [1]. The spectra of the weak turbulence of the internal wave ensemble which correspond to a constant energy flux are found under the assumption of existing inertial interval [1]. It is shown that theoretical spectra are in a good correspondence with some observed spectra of oceanic turbulence, but can not explain the origin of Garret - Munk spectrum. A kinetic equation for the description of the internal wave transformation in frontal zones and on shallow water is solved in the absence of nonlinear effects [2]. The expressions obtained for the frequency spectra agree relatively well with the observed data in frontal zones.

2. The problem of the prediction of extremely large internal wave heights in the ocean is discussed. The methods of external statistics are used for the calculation of the frequency of internal wave appearance [3,4]. Theoretical results are illustrated by data of the wave observation which were obtained in the Atlantics (1989), the Mediterranean and Black seas (1991). The corresponding data of the frequency of wave appearance for seas are smaller than for the ocean which can be explained by weak tidal effects [2].

3. The description of the impulse perturbation is based on the evolution equations of Korteweg - de Vries and Benjamin - Ono types. Our experimental investigation of internal waves on the shelf of the Okhotsk Sea in 1986 showed good correlation between observed soliton parameters and theoretical ones in the framework of the Korteweg - de Vries equation [5,6]. The sensitivity of the coefficients of this equation to time and space variability of the vertical structure of the Vaisala - Brunt frequency profile and the possibility to employ simplest two - layer model for ocean stratification are estimated from the data of experimental investigation [2,6]. The new result is as follows: non - monotonic dependence of nonlinear coefficient on depth for real oceanic stratification. It leads to the conclusion that nonlinear effects are strongly amplified on the shelf and the wave is typically transformed into an undulated bore on the shelf [7].

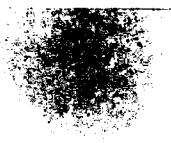

References

1. Pelinovsky E.N., Raevsky M.A. Weak turbulence of ocean internal waves. - Izvestiya,Atmospheric and Oceanic Physics, 1977, v. 13, No. 2, pp. 187 - 193.
2. Report on RV "Professor Kolesnikov", cruise 27, 1991. Technical Report of Marine Hydrophysical Institute. 1991.
3. Ivanov V.A., Pelinovsky E.N., Talipova T.G. The frequency of intense internal wave appearance. - Dokl. Akad. Nauk SSSR 1991, v. 318, No. 6, pp.1101 - 1104 (in Russian).
4. Ivanov V.A., Pelinovsky E.N., Talipova T.G. Long - term prediction of intense internal wave heights in the Atlantics.-. Annales Geophysicae, 1990, Spec. Issue, p. 316.
5. Nagovitsyn A.P., Pelinovsky E.N. Solitary internal wave observation in coastal zone of Okhotsk sea. - Meteorology and Hydrology 1988, No. 4, pp. 124 - 126 (in Russian).
6. Nagovitsyn A.P., Pelinovsky E.N., Stepanjants Yu.A. Observation and analysis of solitary internal waves at the coastal zone of Okhotsk sea. - Morskoi Gidrofiz. Journal 1990, No. 1, pp. 54 - 58 (in Russian).
7. Gorjachkin Yu.N., Ivanov V.A., Pelinovsky E.N. Transformation of tidal internal waves on Guinea shelf. - Morskoi Gidrofiz. Journal 1991, No. 4, pp. 53 - 59 (in Russian).

Discussion of Pelinovsky's paper

A. Voronovich

Are your spectra of weak nonlinear internal waves local?

Author's reply

We investigate locality of spectrum of weak turbulence only in case of small scale internal waves (see Pelinovsky, E.N., Rawsley, M., Weak Turbulence of ocean internal waves, Izvestiya, Atmospheric and Oceanic Physics 1977, vol. **13**, 2). The spectrum $\epsilon_{\vec{k}} = \sqrt{PN}\, k^{-4} F(\omega^{\vec{k}}/N)$ is local if the F increases smaller than ω^{-2} in the limit $\omega \longrightarrow 0$. Here P the energy flux and N Brunt-Vaysala frequency.

A. Voronovich (comment)

I investigated the exact nonlinear solutions of kinetic equation for long-period internal waves and discovered that all of them are non-local and hence senseless physically. This contradicts the statement of Pelinovsky, but I am not sure that I am completely right.

G. Watson

Your theory neglects the terms which describe the effects of the time-averaged velocity in the ocean as a function of depth.

Would the inclusion of these terms have a significant effect on the results?

Author's reply

Because the internal waves have the propagating speed comparable with currents in the ocean the influence of the currents is very significant. Maybe, the existence of Garrett-Munk spectrum is connected with currents, its probably the result of hydrodynamical instability in tides. From the other side, I cannot use Zakharov's approach for waves in the ocean with currents because the nonlinear coefficients of interactions are not homogeneous function of wave number.

Nonlinear effects in water-wave focussing

D.H. Peregrine
Department of Mathematics, Bristol University

Consider the focussing of a steady wave train. For short waves the ray approximation of linear theory indicates where focii occur. They are at cusps of envelopes of the rays. Ray theory fails at the ray-envelopes (i.e. caustics) and at their cusps. However, uniform linear short-wave results can be found by using an Airy function at caustics and Pearcey's (1946) function at cusps. Ray diagrams such as figure 1 show that waves near a focus are travelling in a narrow spread of directions. This means the parabolic wave equation is a good approximation to the full elliptic problem. This approximation is readily extended to weakly nonlinear waves giving a nonlinear Schrödinger (NLS-) equation (Yue and Mei, 1980). This particular NLS equation is the one with stable plane waves and dark-soliton solutions.

Peregrine (1983) describes the qualitative effects of nonlinearity. Through study of conjugate plane-wave solutions and by ignoring certain terms of highest derivative in a real variable version of the necessarily complex NLS- equation, it is deduced that wave jumps rather than ray envelopes are the basic skeleton of nonlinear waves near a caustic. Taking account of the full NLS- equation it becomes clear that the wave jumps are dispersive with an undular structure similar to a sequence of dark solitons. Although many written accounts of NLS- dark-solitons stress a similarity to the solitons of the KdeV equation, there are differences which are crucial to a full interpretation of the wave patterns behind a focus. These are partly described in Peregrine (1985).

Deep-water experiments at Edinburgh show qualitative and quantitative agreement with theory (for a preliminary report see Peregrine, Skyner, Stiassnie and Dodd 1988). In addition for the values of focussing parameters most relevant to coastal applications, it is clear that diffraction can often fully dominate focussing so that no enhancement of amplitude is obtained in the focal region. For example figure 2 shows contours of wave amplitude for waves focussing over an angle of 15° towards the point marked +. The relevant dimensionless parameter for the linear problem is the Fresnel number $N = k f \tan^2\alpha$ where k is the wavenumber, f the focussing distance and α, half the focussing angle. In this case it is 0.9. This is not atypical of coastal refraction.

As in the development of the concept of wave action. Study of nonlinear effects draws attention to linear properties of waves.

References

Pearcey, T. (1946) The structure of an electromagnetic field in the neighbourhood of a cusp of a caustic. The London, Edinburgh and Dublin, *Philosophical Magazine and Jour. of Science.* 7th Series, **37**, 311-317.

Peregrine, D.H. (1983a) Wave jumps and caustics in the propagation of finite-amplitude water waves, *J. Fluid Mech.*, **136**, 435-452.

Peregrine, D.H. (1985) Water waves and their development in space and time, *Proc. Roy. Soc. A*, **400**, 1-18.

Peregrine, D.H., Skyner, D., Stiassnie, M. and Dodd, N. (1988) Nonlinear effects on weakly focussed waves, *Proc. 21st Conf. Coastal Engng. A.S.C.E.*, 1, 732-742.

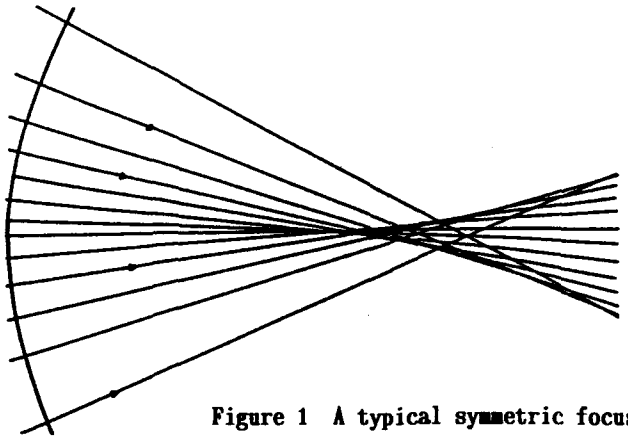

Figure 1 A typical symmetric focus

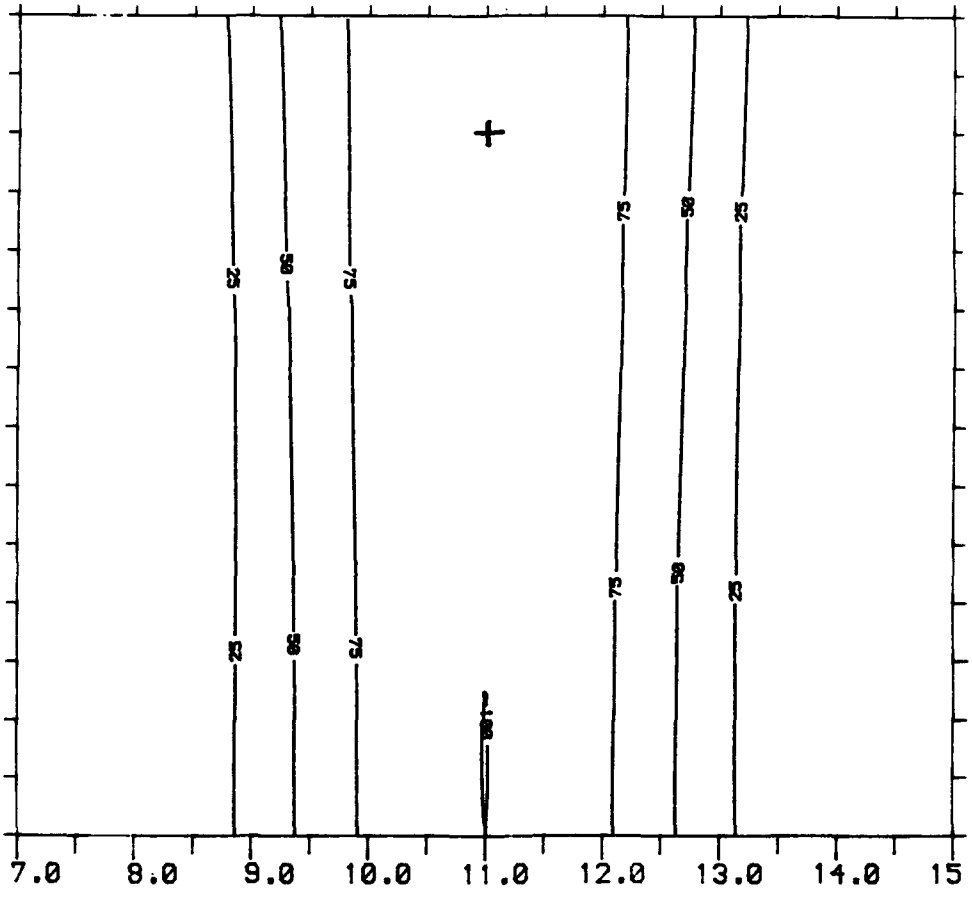

Figure 2 This figure shows the effects of focussing being counteracted by diffraction. It shows contours of wave amplitude computed with the nonlinear Schrodinger equation for waves entering the region from the bottom as a beam focussed on the cross (+).

Singularities in two-dimensional water waves

D.H. Peregrine
Department of Mathematics
Bristol University, BS8 1TW, England

Note: *A talk with this title was originally to be given by S. Tanveer. He flew to England, but then was called back. P.G. Saffman informed us that "His work obtains complex ordinary differential equations for the precise positions and strengths of the singularities, which are in general branch points." Please see Tanveer 1991 "Singularities in water waves and Rayleigh-Taylor instability." Proc.Roy.Soc.London A 435, 137-158.*

Abstract

A number of comments concerning singularities in 2D water wave problems are made.

Singular solutions

Perhaps the simplest singular solution with a free surface is that for stagnation-point flow over a flat bed y = 0. The free surface is at

$$y = -\frac{A}{t} \quad \text{and the velocity potential equals} \quad \frac{A}{2t}(x^2 - y^2).$$

The flow for $t < 0$ approaches a singularity at $t = 0$. By consideration of conservation of mass, or otherwise, it is easily seen that the singularity can only arise in the idealised case where the solutions applied to an infinite domain $-\infty < x < \infty$. Whether, or not, this non-physical restriction to infinite circumstances holds for other singularities is less obvious.

The above solution is one of many exact free surface solutions that have been given by Longuet-Higgins (1976,1980,1982,1983a,1983b) and many of these have singularities which require some nonphysical restriction such as an infinite domain. As he demonstrated (Longuet-Higgins, 1983a) experimental wave motion can generate very violent and sudden motions which may represent a proximity to a singular solution. The violent flip-through motion Cooker and Peregrine (1991) described in this volume may also be of this nature. There is still much work to be done in this area.

Singularities and numerical approximation

Singularities of a velocity potential outside a fluid domain are amongst the earliest examples of fluid motion given in courses on potential flow. Although they are less commonly encountered for water waves the 120° degree corner singularity for the highest steadily propagating wave is well known (Lamb, 1932, p418). Longuet-Higgins and Fox (1977) use a sequence of dipoles to give flow near the crest of the almost highest wave. McIver and Peregrine (1981a,b) in unpublished reports show further that steady and unsteady waves can be very well represented by a small number of singularities in a spatially periodic domain. For the solitary wave the domain must be periodic in the vertical, as consideration of flow in its outskirts shows.

The most successful computational methods for steep unsteady water waves are based on boundary-integrals which are often considered to represent a distribution of singularities along the free surface. However, these do not represent a singularity of the flow. There are difficulties in clarifying whether or not true flow singularities are being computed when a numerical computation breaks down.

The simplest case is when two different parts of a free surface meet, as when the jet of a breaking wave plunges into the water in front of the wave. This is usually clearly resolved if the jet is big enough. However, numerical programs commonly fail because they cannot adequately resolve the fine jet that occurs in most breaking waves. Some people then talk of singularities or cusps on the surface, but in our experience, with some of the most accurate free-surface programs, we cannot support such a view and simply consider that surface curvature continually increases as in some of Longuet-Higgins (1976,1983b) solutions for parabolas and hyperbolas. For example, our own computation with waves of spatial period 2π fail once curvature of the jet tip exceeds 100 to 700 depending on the local discretization point density. In more than 10 years of experience with these flows we only have two examples which might have a local singularity on the surface and both require closer study.

References

Cooker, M.J. and Peregrine, D.H. 1991 Numerical solutions of violent water wave impact against a vertical wall. Proc. Nonlinear Water Wave Workshop, Bristol University, ed. D.H. Peregrine.

Lamb, H. 1932 Hydrodynamics, Cambridge Univ. Press, 6th ed. xv+738pp.

Longuet-Higgins, M.S. 1976 Self-similar, time dependent flows with a free surface. Jour. Fluid Mech. **73**, 603-620.

Longuet-Higgins, M.S. 1980 On the forming of sharp corners at a free surface. Proc.Roy.Soc.Lond.A **371**, 453-478.

Longuet-Higgins, M.S. 1982 Parametric solutions for breaking waves. Jour. Fluid Mech. **121**, 403-424.

Longuet-Higgins, M.S. 1983a Bubbles, breaking waves and hyperbolic jets at a free surface. Jour. Fluid Mech. **127**, 103-121.

Longuet-Higgins, M.S. 1983b Rotating hyperbolic flow: particle trajectories and parametric representation. Quart.J.Mech.Appl.Math. **36**, 247-270.

Longuet-Higgins, M.S. and Fox, M.J.H. 1977 Theory of the almost highest wave: the inner solution. Jour. Fluid Mech. **80**, 721-741.

McIver, P. and Peregrine, D.H. 1981a Motion of a free surface and its representation by singularities. School of Mathematics, Bristol Univ. Report No. AM-81-12.

McIver, P. and Peregrine, D.H. 1981b The computation of unsteady and steady free surface motions using a small number of singularities in the exterior flow field. School of Mathematics, Bristol Univ. Report No. AM-81-13.

OBSERVATIONS OF THE EVOLUTION OF NONLINEAR DEEP-WATER GRAVITY WAVE TRAINS

B. Chapron* and A. Ramamonjiarisoa**

* NASA Goddard Space Flight Center, Wallops Flight Facility,Wallops Island VA 23337 U.S.A.

** Institut de Mécanique Statistique de la Turbulence, Marseilles, FRANCE.

Experiments were conducted in the well-known IMST large wind-wave facility (Coantic and Favre, 1974) in order to better specify the effects of dispersion, nonlinearity, dissipation, wind input, ...on the wave trains evolution.

The respective dimensions (length x width x depth) of the wave and the air flows test sections of the facility are : 40 x 3 x 1m and 40 x 3 x 1.50m.

The facility is equipped with an electrohydraulic wavemarker which served to generate wave trains with various characteristics parameters : i) frequency : N_0 = 2Hz (period T_0 = 0.5s), ii) duration : 14 T_0, iii) initial steepness (in absence of wind) : 12%, 15%, 19% and 22%.

The effect of wind flow of small (3m/s) or moderate (5m/s) velocity was considered.

The basic experimental data consisted of records of the water deflection level at respective fetchs : 7, 14, 17, 21, 25 and 31 meters.

The experimental arrangement is quite similar to those used by others authors (Lake et al, 1977; Mollo-Christensen and Ramamonjiarisoa, 1982; Hatori and Toba, 1982, Su, 1982). The novelty of the investigation results mostly from an extensive use of time-frequency representation.

A "time-frequency (or scale)" representation of a time (t)-dependent signal x(t) is known to proceed from formal expression :

$$C_x(\tau,\sigma) = \int x(t)\, f_{\tau,\sigma}(t)\, dt \qquad (1)$$

where f(t) is the analyzing signal and the representation is given in terms of the coefficients $C_x(\tau,\sigma)$ associated with the time parameter τ and the frequency or scale parameter σ. A musical score is the most common example of time-frequency representation of a time-dependent acoustic signal.

---

* Present adress : Departement d'Oceanographie Spatiale
IFREMER, Centre de Brest. B.P. 70. 29280 Plouzane-FRANCE.

During this work, three types of representations were used namely, the Short-Time Fourier Transform (STFT) or windowed Fourier transform, the Pisarenko Spectral Decomposition (PSD) and the wavelets Transform (WT).

In STFT, $f_{\tau,\sigma}$ has the form :

$$f(t) = g(\tau-\sigma)\exp 2i\pi\sigma t \qquad (2)$$

where g(t) is the window function and σ is a frequency.

The STFT is nothing but a spectral decomposition applied to a short sample of $x(t)$ centred around the time value τ. The time frequency representation of x(t) is obtained by sliding the window with a suitably chosen time translation step.

In PSD, the windowed signal is represented as a sum of sinusoïds and a noise b(t). Then, for data discretized with time increment Δt :

$$x(n) = \sum_j a_j \exp i\,(2\pi\sigma_j n\,\Delta t + \varphi_j + b(n)) \qquad (3)$$

Unlike STFT, PSD is a parametric model in which a_j et σ_j are the unknowns parameters. Expression (3) leads to the fact that x(t) has the structure of an Autoregressive-Moving Average (ARMA) random process (Kay and Marple, 1981). Then, after determining the ARMA coefficients $\underline{A} = \{a_j\}$ through the matrix equation :

$$R_{xx}\,\underline{A} = \sigma_b^2\,\underline{A} \qquad (4)$$

where R_{xx} is the data autocorrelation matrix and σ_b^2 the noise variance, the frequencies σ_j are determined from the roots Z_i of unit modules of the polynomial :

$$Z^{2p} + a_1 Z^{2p-1} + \ldots + a_{2p-1} Z + a_{2p} = 0 \qquad (5)$$

formed from the coefficients a_i

$$\left.\begin{aligned} Z_j &= \exp(i2\pi\sigma_j\Delta t) \qquad (a)\\ \sigma_j &= [\tan^{-1} I(Z_n)/R_e(Z_n)]/2\pi\Delta t \qquad (b)\end{aligned}\right\} \qquad (6)$$

The time-frequency representation of x(t) is obtained, like in STFT by sliding the window. The determination of the amplitude associated with the σ_j requires one more calculation step (Kay and Marple, 1981)

In WT, $f_{\tau,\sigma}(t)$ has the form:

$$f_{\tau,\sigma} = \frac{1}{\sqrt{\sigma}}\,O\left(\frac{\tau-t}{\sigma}\right) \qquad (7)$$

where O(t) is the "analyzing wavelet". Unlike in STFT where the window function g(t) is of fixed length, in WT, O(t) is of short variable length depending on σ. Then, this parameter can be adjusted to the scales of interest in x(t) so that WT constitutes a potential basic tool for multiscales analysis.

A critical review of various methods in spectral decomposition was made by Kay and Marple (1981) while wavelet transformation is still the topic of intensive basic work (see e.g. Daubechies, 19). Various "wavelets" with their own intrinsic properties were introduced

beside the commonly used Morlet wavelet. Note that there exists this time no unique method which satisfies simultaneously all the requirements for time, scale and amplitude resolution. The decision for using a method or combination of different methods would result from preliminary physical consideration (see e.g Szu, 1991). Of major interest is the fact that the original date x(t) can be reconstructed from the coefficients $C_x(\tau,\sigma)$. In WT_x instead of recording x(t), it may be more convenient to record directly the coefficients.

The results corresponding to three different observational conditions are reported and briefly discussed.

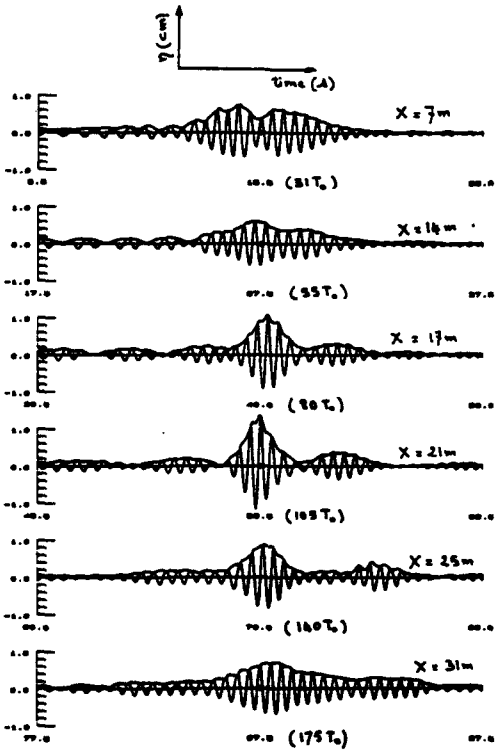

Figs.1.

The first results correspond to an initial wave group steepness of order 12% without wind action. The water deflection level records at increasing fetches (fig. 1), reveal already some basic features of the evolution, namely : i) the development of modulational instability leading, after about 100 T_0 *, to the formation of many groups of short lengths. The amplitude modulation reaches value close to 100% ii) the amplification of the main group between 80 T_0 and 105 T_0 followed by breaking, between 105 T_0 and 140 T_0 at the highest crests iii) the splitting of the main group leading to a final continuous waveform at small amplitude. The Spectral analysis of the signals reveals a highly peaked spectrum at 2Hz for the initial waveform, the development of side bands modes at the intermediate stages and a return to a highly peaked spectrum at 2Hz at the final stage.

Some features of the time-frequency representation using the Pisarenko Spectral Decomposition are shown on figures 2.

After 30 T_0, the modulational instability is already visible but the signal contains uniformly in time components at 2Hz and 4Hz. At 105 T_0, when the maximum amplitude modulation rate is reached, the time-frequency representation exhibits two close and parallel frequency lines as natural signature of the modulation. Dispersion clearly operated so that the group ahead of the main and highest group is at frequency slightly smaller that 2Hz while the group being is at frequency slightly higher. This agrees at least-qualitatively with the

* Zero time corresponds to the starting of the wavemaker

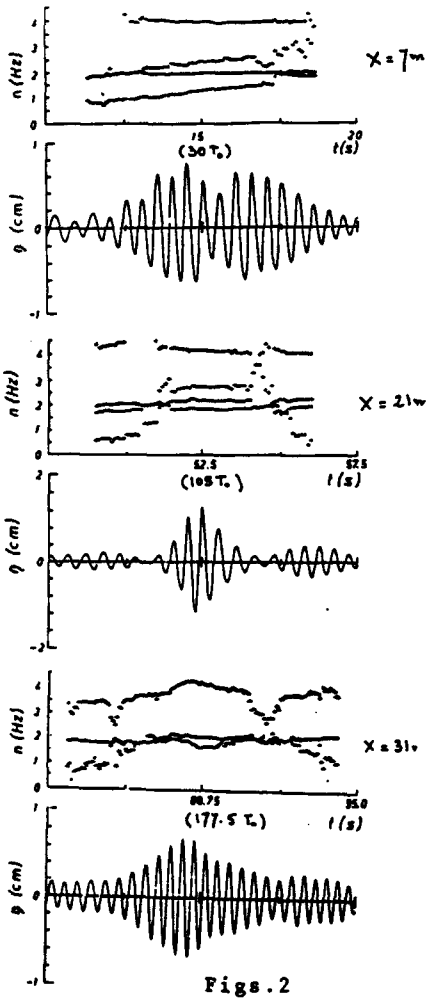

Figs . 2

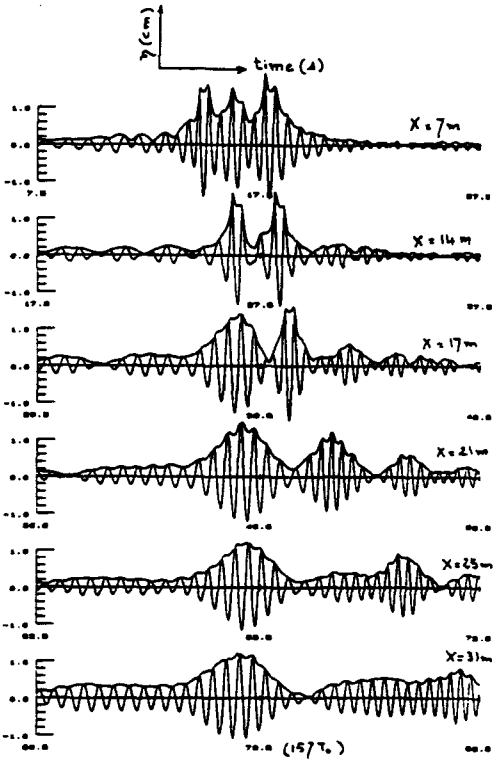

Figs.3

computational result of Lo and Mei (1985). The final stage (iii) mentioned previously is characterized by a quasi-linear time variation of the frequency along the waveform. Clearly, there is no evidence of possible return to the initial state contrarily to the suggestion from standard spectral density analysis. The possibility of total separation of the groups suggested by the previous authors and the experimental results of Su (1982) is not confirmed.

The obeervations at order 19% initial wave group steepness show (fig. 3) no striking new feature of the evolution with respect to that described above. A noticeable fact is that, in agreement with the computational result of Dold and Peregrine (1986), for waves which grow to breaking, the number of waves in one modulation depends upon the wave steepness. The observed numbers (at a fixed points) are about 7-8 at 12% steepness and about 4 at 19% steepness. Those values are about twice the computed values for spatial modulation. This is expected from linear deep-water gravity wave dispersion relation the previous authors foundto be a fairly good approximation except for a fraction of a wave period before breaking.

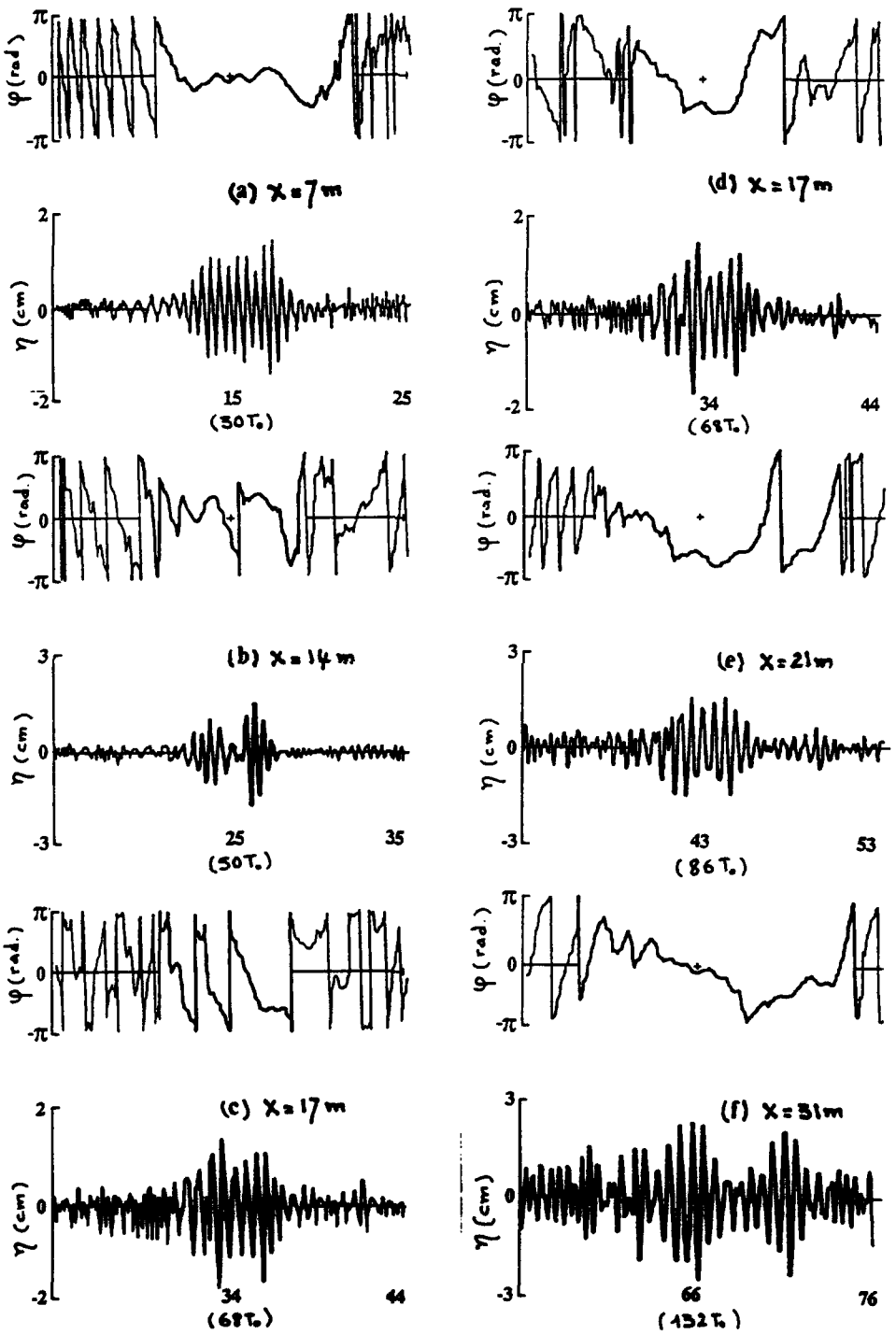
(a) X=7m
(d) X=17m
(b) X=14m
(e) X=21m
(c) X=17m
(f) X=31m
φ (rad.)
η (cm)
π
0
-π
2
-2
3
-3
15
25
(30T₀)
34
44
(68T₀)
25
35
(50T₀)
43
53
(86T₀)
34
44
(68T₀)
66
76
(132T₀)

Figs.4

Figure 4 illustrates the results when a group of about 12% initial steepness suffered the effect of a wind flow at 5 m/s. A "phase-time" representation was obtained using a Short-Time-Fourier Transform. This technique provides of course, also the group amplitude which is not displayed.

At 7m fetch (after $30T_o$), the steepness is of order 19% because of the group simplification by the wind. It is seen (fig. 4a) that, in the main part of the group, the phase, referred to frequency 2Hz, is almost constant. There exists a low frequency precursor ahead of the main group and a high frequency tail behind. At $50T_o$, an almost 100% amplitude modulation is reached and the picture is similar with that found at $77T_o$ in the no wind case and 19% initial steepness (fig. 3).

Fig. 4c shows the striking feature associated with the wind effect, namely, the two groups instead of moving away from another have collided to produce a new group at frequency smaller than 2Hz (negative slope of the phase function). The phase estimate referred to frequency 1.5Hz shows (fig.4d) this is new center frequency. Again there is lower frequency ahead of the group and higher frequency at the back.

Between $68T_o$ and $132T_o$, the longest time available two facts are noticeable : i) an amplification combined with a splitting of the new group, ii) the development of modulation. At $132T_o$, the frequency still varies from low to high values with respect to the time. The development of modulation may suggest the possibility of new collision.

Detailed aspects of this work, concerning especially the time frequency representation, can be found in Chapron (1988). The observed physical mechanism of interest here is the collision of two successive group, leading to a rapid subharmonic transition. The collision appears to be a specific feature due to the wind action. Without wind the groups move away from another in agreement with previous observational and computational results. The subharmonic transition needs much shorter time or space in comparison with what is found in theoretical models. This type of collision may be an alternative to explain the so-called frequency downshift in laboratory wind-wave fields.

References

CHAPRON B. (1988) - Une étude de la propagation et des instabilités des trains d'ondes de gravité en profondeur infinie.
Thèse de Doctorat N°20 6 88 36. Université d'Aix-Marseille II.

COANTIC M. and A. FAVRE (1974) - Activities in and preliminary results of air-sea interactions research at I.M.S.T.
Advan. Geophys., 18A, 391-405.

DAUBECHIES I. (19) - The wavelet transform, time-frequency localization and signal analysis.
ATxT Bell Laboratories. 600 Mountain Avenue. Murray Hill, NJ 07974 U.S.A.

DOLD J.W. and D.H. PEREGRINE (1986) - Water-wave modulation.
20th Int. Conf. on Coastal Engineering. American Society of Civil Engineers, Taipe, R.O.C. 10-14 Nov.

HATORI M. and Y. TOBA (1982) - Transition of mechanically generated regular waves to wind waves under action of wind.
Submitted to J. Fluid Mech.

KAY S.M. and S.L. MARPLE Jr (1981) - Spectrum Analysis. A modern Perspective. Proceed.
IEEE, **69**, 1380-1419.

LAKE B.M., YUEN H.C., RUNGALDIER H. and W.E. FERFUSON (1977) - Nonlinear deep water waves : theory and experiment. 2. Evolution of a continuous wave train.
J. Fluid Mech., **83**, 49-74.

LO E. and C.C. MEI (1985) - A numerical study of water wave modulation based on a higher-order nonlinear Schrödinger equation.
J. Fluid Mech., **150**, 395-416.

MOLLO-CHRISTENSEN E. and A. RAMAMONJIARISOA (1982) - Subharmonic transition and group formation in a wind wave field.
J. Geophys. Res., **87**, 5699-5717.

SU M.Y. (1982) - Evolution of group of gravity waves with moderate to high steepness.
Phys. Fluids, **25**, 2167-2174.

SZU H.H. (1991) - Elucidation of ocean waves by nonlinear soliton wavelet dynamics.
Nonlinear Water Waves Workshop 1991. University of Bristol, England, 22-25 Oct.

Discussion of Ramamonjiarisoa's paper

C.C. Mei (comment)

To the experiments reported by Dr Ramamonjiarisoa our recent theory (Hara & Mei 1991, J. Fluid Mech. Sept.) appears relevant. There we studied the instability of sinusoidally modulated Stokes waves under the influence of wind. Waves are weakly nonlinear. Wind is weak and frequency downshift is found.

D.H. Peregrine (comment)

In the context of the effect of wave steepness on wave train evolution the nonlinear evolution from the Benjamin-Feir instability was computed by Dold and Peregrine using a full irrotational flow (for a preliminary report see Dold and Peregrine, 1986, Proc. 20th Coastal Engng. Conf.). Except for the shortest modulations wave trains with amplitude $ak > 0.1$ evolved to breaking in times of 0(100 periods). Insofar as this is relevant to ocean waves, we might expect the surface wave energy density to exceed that corresponding to a wave train of $ak = 0.11$ only under active wave generation by wind.

Further to a question in an earlier session by Zakharov, we have made comparison with the nonlinear Schrödinger (NLS) solution. One example is summarised in figures 1 and 2. Figure 1 is a view of the envelope of a wavetrain which is modelled by a periodic spatial domain containing four waves. The growth, decay and recurrence of modulation is shown for 840 periods. The effect of linear group velocity is nullified. The figure needs careful study because of the motion of wave groups through the spatial period due to a nonlinear contribution to the group velocity (a higher-order effect which occurs in the Dysthe equation). This does not occur in figure 2 which is the corresponding NLS solution. Similarly the initial growth rate is less in the full solution than in the NLS solution, again consistent with the Dysthe equation. However there is qualitative agreement in both the time scales of modulation evolution and in the range of wave amplitude.

One detail not clear from these figures concerns the zeros of the envelope of wave amplitude. For NLS solutions there are two simultaneous zeros each side of a maximum. For the full potential flow similar near-zero values of the envelope occur but staggered by about 10 periods in time. For these 10 periods there is one less wave crest.

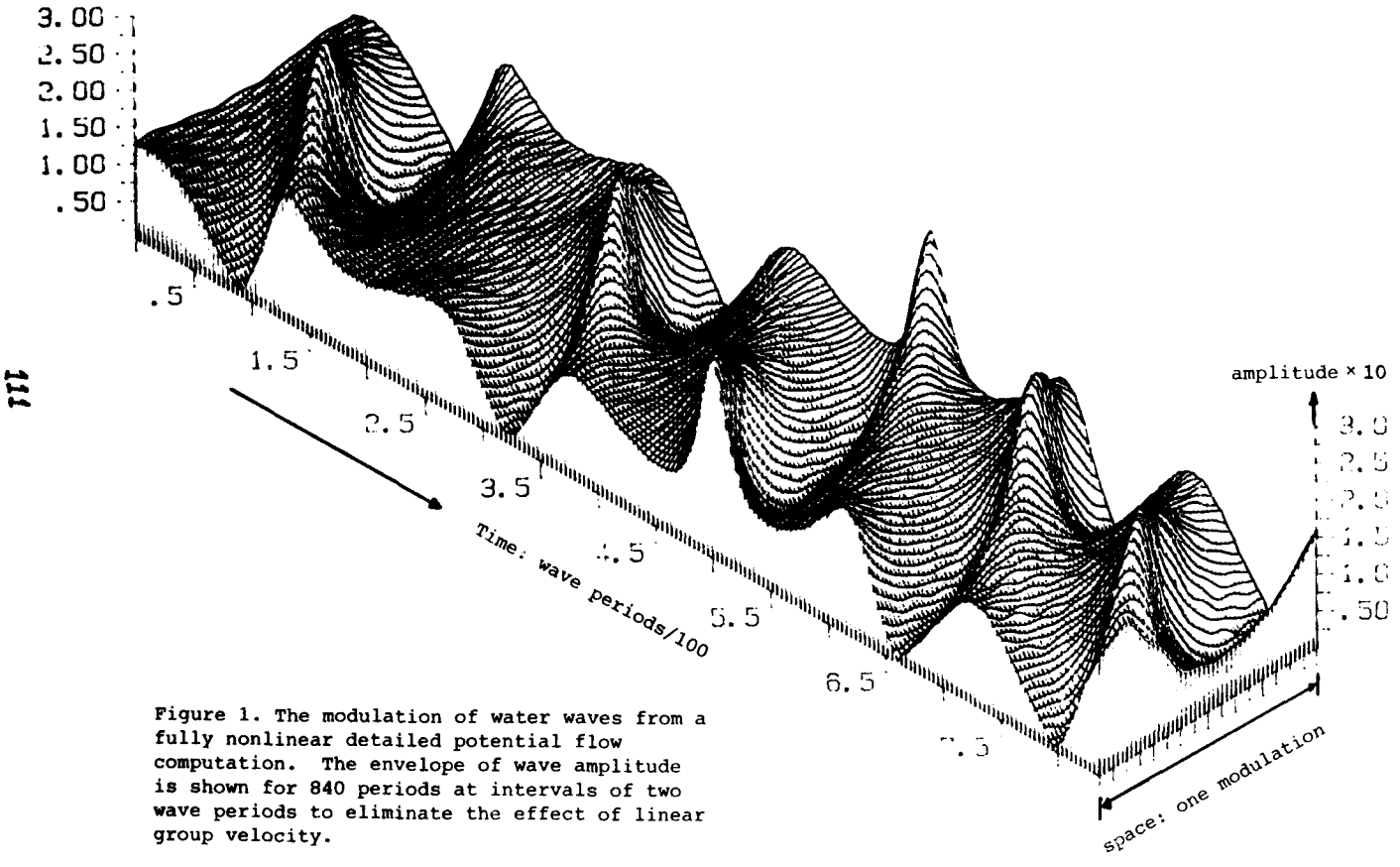

Figure 1. The modulation of water waves from a fully nonlinear detailed potential flow computation. The envelope of wave amplitude is shown for 840 periods at intervals of two wave periods to eliminate the effect of linear group velocity.

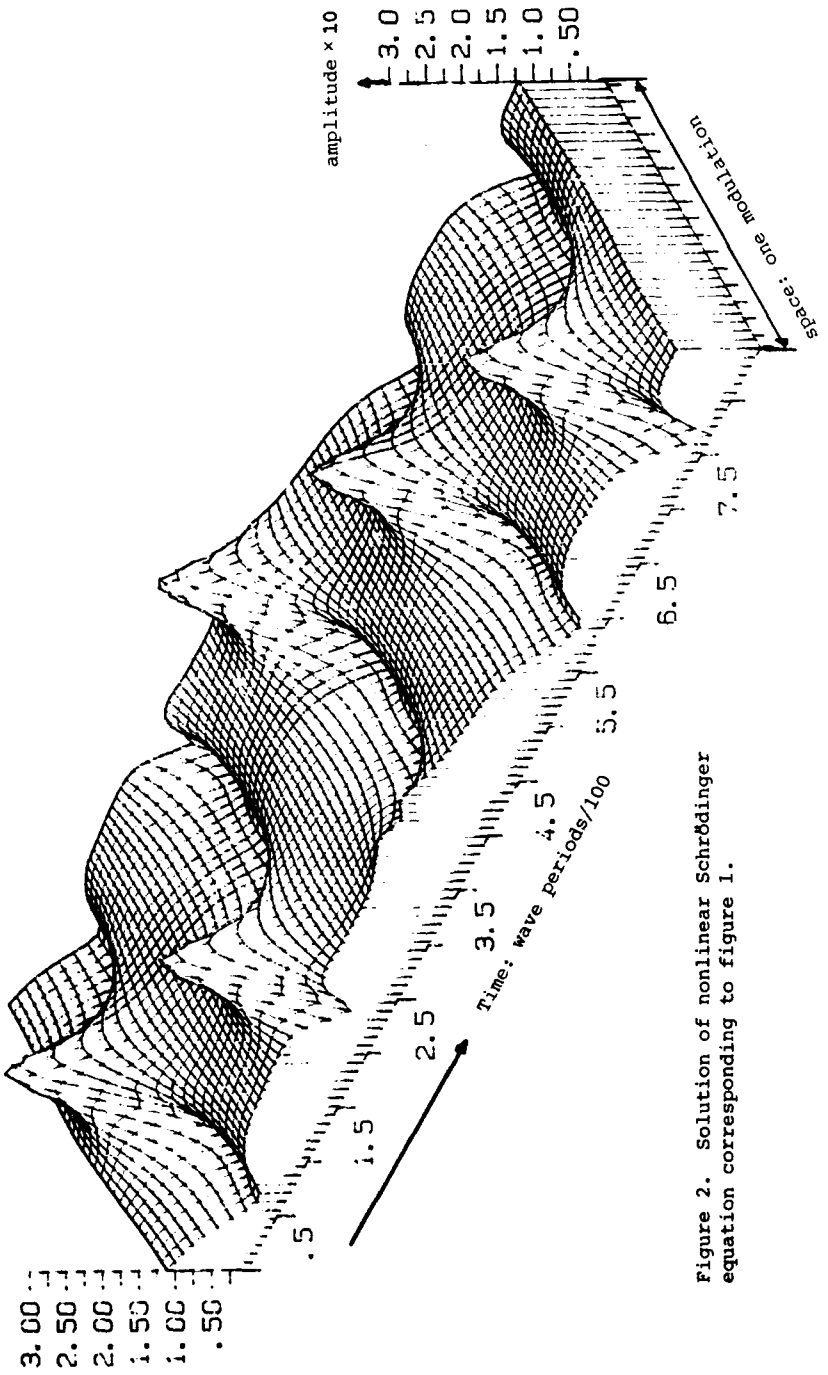

Figure 2. Solution of nonlinear Schrödinger equation corresponding to figure 1.

ON THE CONSTRUCTION OF NORMAL VARIABLES FOR WAVES IN UNSTABLE n-LAYERED SHEAR FLOW

N.N.ROMANOVA

Institute of Atmospheric Physics USSR Academy of Sciences

Pyzhevsky 3, Moscow 109017 USSR

Surface and internal gravity waves are studied in the model of multi-layered stably stratified fluid. The unperturbed density and vorticity are assumed to be constant in each layer and discontinuous at the interface between layers. The upper part of the fluid moves horizontally, while the lower layer of infinite depth is at rest. The upper surface is free. We investigate the irrotational disturbances such that the interfaces are displaced to $z_j=h_j+\eta_j(x,t)$, where t is time, x,z are the horisontal and vertical coordinates, and h_j is the height of the j-th unperturbed layer. The velocity perturbations have the form $u_{jx}= \partial\Psi_j/\partial x$, $u_{jz}= \partial\Psi/\partial z$, where Ψ_j is a velocity potential satisfying Laplace's equation in either layer. The disturbances are assumed to decay to zero as $z \to -\infty$. At interfaces have the standart kinematic and dynamical boundary conditions are assumed. We provide the Hamiltonian description for the waves collinear with the flow. The following functions are introduced as dependent variables: $\eta_j(x,t)$ and $\Phi_j(x,t) = (\Psi_j - \Psi_{j+1})|_{z=h_j+\eta_j}$. It can be shown that in the Boussinesq approximation the boundary conditions can be rewritten in terms of η_j,ϕ_j. in the following form [1]:

$$\frac{\partial}{\partial x}\dot{\Phi}_j = -\frac{\partial}{\partial x}\frac{\delta\mathcal{H}}{\delta\eta_j} + \nu_j\frac{\delta\mathcal{H}}{\delta\Phi_j}, \qquad \dot{\eta}_j = \frac{\delta\mathcal{H}}{\delta\Phi_j}, \qquad (1)$$

where ν_j is the vorticity jump at the j-th interface, $\mathcal{H}$ is the total energy, and $\delta/\delta\Phi_j$, $\delta/\delta\eta_j$ denote variational derivatives. In the horisontal wavenumber space the system (1) becomes

$$\mathcal{A}\,\dot{\mathbb{D}}(k) = i\,\frac{\delta\mathcal{H}}{\delta\mathbb{D}^*(k)}, \qquad (2)$$

where $\mathbb{D}(k) = (\Phi_1(k),\ldots,\Phi_n(k),\ \eta_1(k),\ldots,\eta_n(k))$, $\mathcal{A}$ is the Hermite matrix of order $2n$:

$$\mathcal{A} = \begin{vmatrix} 0 & \begin{matrix} t & & \\ & \ddots & \\ & & t \end{matrix} \\ \begin{matrix} -t & & \\ & \ddots & \\ & & -t \end{matrix} & \begin{matrix} -\nu_1/k & & \\ & \ddots & \\ & & -\nu_n/k \end{matrix} \end{vmatrix}$$

For sufficiently small surface displacement the total energy $\mathcal{H}$ may be expanded by a series. The quadratic part of $\mathcal{H}$ in the new variables has the form:

$$\mathcal{H}_2 = 1/2\int_{-\infty}^{\infty}(\mathbb{D}^*(k),\tilde{h}_2\mathbb{D}(k))dk,$$

where $\tilde{h}_2$ is the $2n$-order Hermite matrix of the form:

$$\tilde{h}_2 = \begin{vmatrix} a_{jm} & -ikV(h_1) & \cdots & -ikV(h_n) \\ ikV(h_1) & g\lambda_1 + v_1 V(h_1) & & \\ \vdots & & \ddots & \\ ikV(h_n) & & & g\lambda_n + v_n V(h_n) \end{vmatrix},$$

where $a_{jm} = \begin{cases} |k|\exp(|k|(h_j - h_n))ch(|k|(h_m - h_n)), & m > j. \\ |k|\exp(|k|(h_m - h_n))ch(|k|(h_j - h_n)), & m < j. \end{cases}$ $\lambda_j = \frac{\rho_j - \rho_{j+1}}{\rho_j}$.

We construct the following transformation of dependent variables $\mathbb{D}(k,t)$ to the normal variables $\mathbb{A}(k,t) = (a_1, \ldots, a_{2n})$:

$$\mathbb{D}(k,t) = Z(k)\mathbb{A}(k,t).$$

The j-th column of the matrix $Z(k)$ is the eigenvector corresponding to the j-th eigenvalue of linearized problem:

$$|\tilde{h}_2 + \omega_j \mathcal{A}|\vec{z}_j = 0.$$

In the area of stability, when the eigenvalues ω_j are real and different, this transformation diagonalizes the matrices $\mathcal{A}$ and $\tilde{h}_2$, and the normalisation condition $(\vec{z}_j^*, \mathcal{A}\vec{z}_j) = -1$ leads us to the following system:

$$\dot{\mathbb{A}}(k) = -i \frac{\delta \mathcal{H}}{\delta \mathbb{A}^*(k)},$$

where (a_j, ia_j^*) is a pair of canonical variables.

The density energy of the j-th mode is equal to $E_j(k) = \omega_j |a_j|^2$.

In the case of linear instability, when a pair of complex

roots ω_j, $\omega_m=\omega_j^*$ appears in the spectrum of eigenvalues, the dynamical equation for the corresponding normal variables a_j, a_m have the form

$$\dot{a}_j=\delta\mathcal{H}/\delta a_m^*, \qquad \dot{a}_m=-\delta\mathcal{H}/\delta a_j^*.$$

A pair of canonical variables is a_j, a_m^*, and the density energy corresponding to them is $E(k)= 1/2\omega_j a_j a_m^*+c.c.$.

At the marginally unstable point k_0, when the two roots of the linear dispersion equation become equal, the structure of canonical equations is different, and the pair of canonical variables that corresponds to one multiple eigenvalue ω_0 is (a_0, ia_1^*). The equations for them are

$$\dot{a}_0=-i\delta\mathcal{H}/\delta a_1^*, \quad \dot{a}_1=-i\delta\mathcal{H}/\delta a_0^*.$$

The density energy that corresponds to marginally unstable mode is equal to $E(k_0)=1/2\omega_0(a_1^*a_0+a_0^*a_1+a_0a_0^*)$.
In contrast to the stable case, when the eigenvector of linear problem corresponding to the eigenvalue ω_o is normalized by the factor $\sqrt{|\omega\partial L/\partial\omega||_{\omega=\omega_0}}$, in the marginally stable case the normalizing factor for the eigenvector is $\sqrt{1/2\omega^2|\partial^2 L/\partial\omega^2||_{\omega=\omega_0}}$, where $L(\omega,k)$ is the right-hand side of dispersion equation in the special form. The introduction of canonical variables in the unstable area of wavenumbers essentially facilitates the description of nonlinear wave interaction in unstable and nonequilibrium media. For short waves, when increments due to linear instability are small, nonlinear interactions between different modes markedly change the stability picture of the linear theory.

References:

1.V.P.Goncharov. Nonlinear waves in flows that are vorticity-homogeneous in a layerwise manner.Izv.Akad.Nauk SSSR. Fiz. atmos. i okeana, 22, N 5, 1986.

2.N.N.Romanova. Construction of normal variables for waves in two-layer medium with linear velocity profile.Izv.Akad.Nauk SSSR. Fiz. atmos. i okeana, 25, N 12, 1989.

3.N.N.Romanova. Normal variables for waves in unstable n-layer moving media. Izv. Akad. Nauk SSSR, Fiz.atmos. i okeana, in print.

Discussion of Romanova's paper

V.I. Shrira (comment)

I would like to attract attention to the importance of the results derived by Dr Romanova. She has developed an approach which enables one to extend the Hamiltonian technique for the wide class of unstable media. The particular example considered, just illustrates the flexibility and power of this approach.

Effect of shear layer profiles on wind wave generation

P.G. Saffman†
Applied Mathematics 217-50
Caltech, Pasadena, CA 91125

The results of calculations of the effect of changes in wind profile on the instability of air blowing over water will be described. Viscosity is neglected and the Rayleigh equation for infinitesimal disturbances is solved numerically to find the growth rate of unstable waves. Howard's semi-circle theorem is still valid and is used to explain some of the features of the results. Agreement of growth rates with those predicted by Miles's (1957) quasi-steady analysis of wave growth is found to be poor, but there is high sensitivity to changes in the wind profile. The computations retrieve the Kelvin-Helmholtz instability in the limit of a highly sheared profile.

Also, a simple model of wind-water shear layers, which employs linear wind and water profiles, is studied to find the effect of water shear on the wind instability. Water shear is found to be stabilizing or destabilizing, depending upon the mode, and windows of stability are predicted to occur.

References.

E.A. Caponi, H.C. Yuen, F.A. Milinazzo & P.G. Saffman 1991 Water wave instability induced by a drift layer. J. Fluid Mech. **222**, 207–213.

E.A. Caponi, M.Z. Caponi, P.G. Saffman & H.C. Yuen 1991 A simple model for the effect of water shear on the generation of waves by wind. Proc. Roy. Soc. (submitted).

J.W. Miles 1957 On the generation of surface waves by shear flows. J. Fluid Mech. **3**, 185–204.

F.A. Milinazzo & P.G. Saffman 1990 Effects of a surface shear layer on gravity and gravity-capillary waves of permanent form. J. Fluid Mech. **216**, 93–112.

L.C. Morland & P.G. Saffman 1991 Effect of wind profile on the instability of wind blowing over water. J. Fluid Mech. (submitted).

L.C. Morland, P.G. Saffman & H.C. Yuen 1991 Waves generated by shear layer instabilities. Proc. Roy. Soc. **A433**, 441–450.

† Work done with E.A. Caponi, M.Z. Caponi, F.A. Milinazzo, L.C. Morland & H.C. Yuen.

Discussion of Saffman's paper

J.A. Battjes (comment)

Just for the historical record: the conclusion that vorticity in the same sense of rotation as the particle orbits advances onset of breaking, compared to the irrotational case (and the opposite as well, of course) was reached as early as 1944 by Miche.
Reference R. Miche, "Mouvements ondulatories de la mer en eau profondeur constante ou décroissante", Annales des Ponts et Chaussées, 1944, pp.25,131,270,369.

P.A.E.M. Janssen

What kind of numerical method did you use. E.g. did you use Frobenies series around the critical layer and employed analytical continuation. Also, did you compare analytical results with the exponential.

Author's reply

For the stable waves the phase speed (c_r) is fixed outside the range of the undisturbed velocity profile. For the unstable waves, a fixed value of c_i is taken. In either case, the system of equations and the eigenvalue problem is non-singular and standard iterative methods can be employed. A critical layer analysis is not required. For the stable waves, a Newton iteration gives wavenumber k in terms of c_r, and when unstable the iteration determines k and c_r for each c_i. The exact solution for the exponential profile is for the exchange of stability case c = 0, and does not overlap the range for which our numerical method applies.

C.C. Mei (comment)

Since different steady drift-current models give very different growth rates, would it be more urgent to avoid all steady drift models and to turn our attention to *deducing* the current by a transient analysis (cf. Kanwai (198?) for capillary gravity waves?)

A. Ramamonjiarisoa

The first results shown seem to contradict those of Valenzuela and others who found an increase of the amplification rate with respect to Miles' result when the water drift layer is taken into account.

Author's reply

There is a problem of interpretation here. The simple model actually agrees with Valenzuela in predicting a stabilization of long (Miles type) disturbances and an enhanced instability of the short wave (generalized Kelvin-Helmholtz) disturbances. The advantage of the model is that this comes simply from solution of a quartic, instead of having to solve a complicated Orr-Sommerfeld problem. Disagreement in detail between a simple and complicated model is to be expected, but resolution of such conflicts often leads to increased understanding.

M.-Y. Su (comment)

This is a further expansion of Prof. Saffman's comments. There is a real need to establish connection between theoretical computation and experimentally realizable waves. With ak > 0.25, 2D wave trains/packets are unstable leading to 3-D bifurcation, for example. What is then the use of studying the infinite other possibilities of bifurcations for ak = 0.402 to 0.404, or even to the Stokes limit of ak = 0.443?

D.H. Peregrine (comment)

Even in the simpler case of solitary waves it appears to be extremely difficult to generate a solitary wave with amplitude more than 0.6 of the depth. On the other hand in a slowly-varying environment, such as a *very* gently sloping beach we can expect the higher solutions, and the Tanaka instability to be relevant.

Applications of Genus 2 Solutions of the Kadomtsev-Petviashvili Equation

By

Norman Scheffner[1], Joe Hammack[2], and Harvey Segur[3]

The Kadomtsev-Petviashvili (KP) equation (1970) is a nonlinear partial differential equation of the form

$$(f_t + 6ff_x + f_{xxx})_x + 3f_{yy} = 0 \tag{1}$$

which describes the propagation of surface gravity waves on water of uniform depth. The equation evolves from the assumptions that the waves are

1) weakly dispersive,
   i.e., long, shallow water waves: $(k_X D)^2 << 1$
2) weakly nonlinear,
   i.e., moderate amplitude: $(F_{max}/D) << 1$
3) weakly two-dimensional,
   i.e., X-direction predominance: $(k_Y/k_X)^2 << 1$

where the dimensional variables k_X, k_Y are wave numbers in the X,Y directions, F_{max} is the maximum surface elevation above mean water level, and D is depth. All three effects are considered to be of comparable influence. The scaled variables in (1) are related to dimensional variables according to

$$x = (X - (gD)^{\frac{1}{2}}T)/D, \quad y = Y/D \tag{2}$$

$$t = (gD)^{\frac{1}{2}}T/(6D), \quad f = 3F/(2D) \tag{3}$$

[1]Coastal Engineering Research Center, US Army Engineer Waterways Experiment Station, Vicksburg, MS, USA.
[2]Departments of Geosciences and Mathematics, The Pennsylvania State University, University Park, PA, USA.
[3]Program in Applied Mathematics, University of Colorado, Boulder, CO, USA.

The KP equation admits an infinite family of exact periodic solutions of the form

$$f(x,y,t) = 2\,\partial^2_x \ln \theta_N \qquad (4)$$

in which θ_N is a Riemann Theta Function of genus N where the genus number indicates the number of underlying spatial and temporal periodicities. These solutions were discovered by Krichever (1977) and made computational for low genera by Dubrovin (1981) and Segur and Finkel (1985). Genus 1 solutions are exactly equivalent to the single period and wavelength cnoidal wave solutions of the Korteweg-deVries equation (1895). Genus 2 solutions describe waves that have two spatial and two temporal periodicities and propagate with permanent form with respect to a translating coordinate system. The surface pattern of the genus 2 solutions can be visualized as a tiling of hexagonal-shaped features, varying in size according to the underlying spatial and temporal periods. This paper summarizes the verification effort undertaken to determine if genus 2 KP solutions provide an accurate description of genuine two-dimensional, nonlinear waves in shallow water. An initial task of this study was therefore to generate appropriate wave fields in the laboratory against which genus 2 solutions could be compared. These waves were generated in the directional-spectral wave generation facility located at the U.S. Army Engineer Waterways Experiment Station's Coastal Engineering Research Center, located in Vicksburg, Mississippi, USA shown in Figure 1.

Figure 1 Directional-Spectral wave generator

The wave generator measures 27.7 m wide and contains 60 programmable wave paddles, each 0.46 m in width. The wave basin contains a region of uniform depth of 20.0 cm which extends 12.55 m from the face of the generator to the toe of a 1:30 sloped beach. Experimental wave fields are produced by simultaneously generating two intersecting cnoidal wave trains. When the underlying waves are of equal wavelength and crest elevation, a symmetric hexagonal wave pattern results. Verification that Genus 2 solutions adequately model these symmetric cases was reported by Hammack, Scheffner, and Segur (1989). More recently, a series of experiments was undertaken to test the Genus 2 KP solutions as a model of asymmetric wave patterns, generated by varying the underlying period, wavelength, and angle of intersection of each of the constituent cnoidal waves. In this manner, a wide range of wave patterns was generated for use in extending the verification of the genus 2 theory to asymmetric nonlinear waves.

An array of capacitance-type wave gages were used to measure the spatial and temporal variation of the water surface. In addition, the instantaneous surface pattern was obtained by using overhead photographs of the wave field, synchronized with strobe lights located on the beach. An example wave pattern is shown in Figure 2, which resulted from the intersection of two cnoidal waves, one with a wavelength of 2 m and the other with a wavelength of 3 m. Each has a maximum crest elevation of 3 cm above mean water level and is generated at an angle of approximately +/- 30 deg from a plane perpendicular to the axis of the generator. In Figure 2, the generator is located at the top of the photograph such that the wave is propagating toward the bottom of the page. The bright areas represent the illuminated crest regions while the

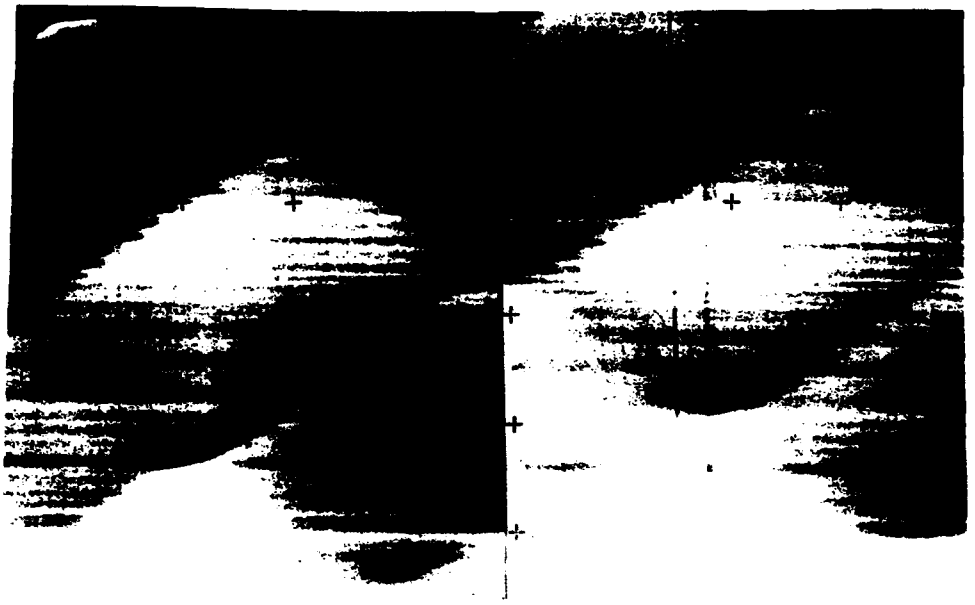

Figure 2 Laboratory generated wave

darker portions of the photograph represent trough regions behind the crests. The locations of sharp contrast represent areas of interaction where the two cnoidal waves intersect. The remnants of the original cnoidal wave crests can be seen as saddle regions connecting the interaction crests. The nonlinearity of the interaction of the two cnoidal waves is evidenced as a phase shift in the saddle alignment before and after the interaction.

In order to test genus 2 solutions as a model for laboratory generated waves, dimensionalized solutions must be compared to the temporal and spatial distribution of measured wave parameters. This comparison begins with the construction of a genus 2 Riemann Theta Function, written in the form of a double Fourier series

$$\theta_2(\phi_1,\phi_2;B) = \sum_{m_1=-\infty}^{\infty}\sum_{m_2=-\infty}^{\infty} \exp\left[\frac{1}{2}(m_1^2 b + 2m_1 m_2 b\lambda + m_2^2(b\lambda/\chi)) + i(m_1\phi_1 + m_2\phi_2)\right] \quad (5)$$

The phase variables ϕ_1 and ϕ_2 are defined as

$$\phi_1 = \mu_1 x + \nu_1 y + \omega_1 t + \phi_{10} \quad (6)$$

$$\phi_2 = \mu_2 x + \nu_2 y + \omega_2 t + \phi_{20} \quad (7)$$

where the scaled parameters μ_1, μ_2, ν_1, and ν_2 represent spatial wave numbers; ω_1 and ω_2 are angular frequencies; and ϕ_{10} and ϕ_{20} are arbitrary phase constants. The Riemann matrix B is defined as a real-valued, symmetric, negative definite matrix which can be written according to

$$B = \begin{bmatrix} b & b\lambda \\ b\lambda & b\lambda/\chi \end{bmatrix} \quad (8)$$

where b is negative and represents a measure of wave height and λ and χ represent measures of two-dimensionality of the wave field.

Genus 2 solutions require the specification of the 11 solution parameters contained in the phase arguments and the Riemann matrix. The parameters ϕ_{10} and ϕ_{20} represent a constant phase shift in the solution, however, the remaining 9 parameters are termed dynamical, their specification determines the spatial and temporal structure of the solution. Furthermore, these parameters are not independent, free parameters, but are constrained by three algebraic criteria resulting from the requirement that the solution be unique and nontrivial. Thus, 6 free dynamical parameters are required to define a unique biperiodic KP solution.

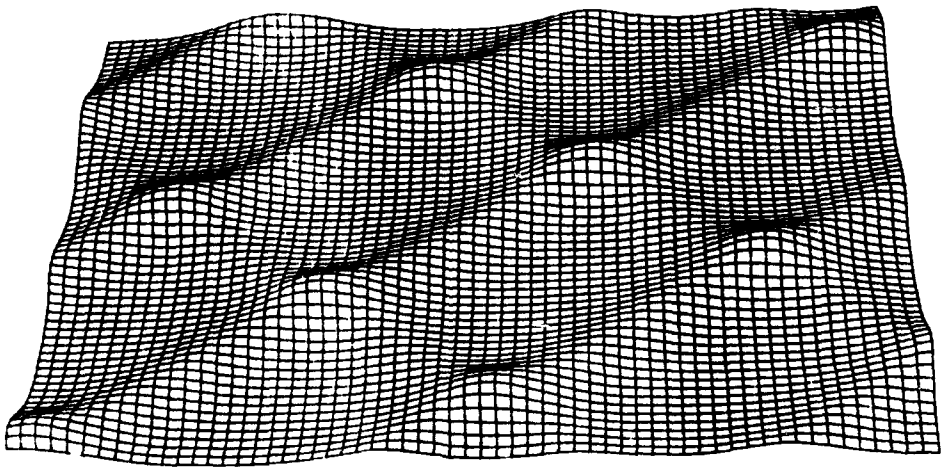

Figure 3 Perspective view of computed wave field

Verification of genus 2 solutions as a viable model for the laboratory waves requires the development of a procedure for selecting scaled solution parameters which generate dimensional solutions which best match the measured characteristics of the generated wave fields. Quantification of model solution to laboratory measurement is made by comparing computed solution time traces of the water surface to measured time series taken at the 9 gage locations within the wave tank. In this paper, we report the approach used to develop this correspondence. As an example, the computed wave field corresponding to Figure 2 is shown in Figure 3. A comparison overlay of the measured wave traces (_____) and the computed traces (.....) is shown in Figure 4. Conclusions of this paper demonstrate that Genus 2 solutions of the KP equation accurately describe the nonlinear features of a large family of laboratory generated wave fields.

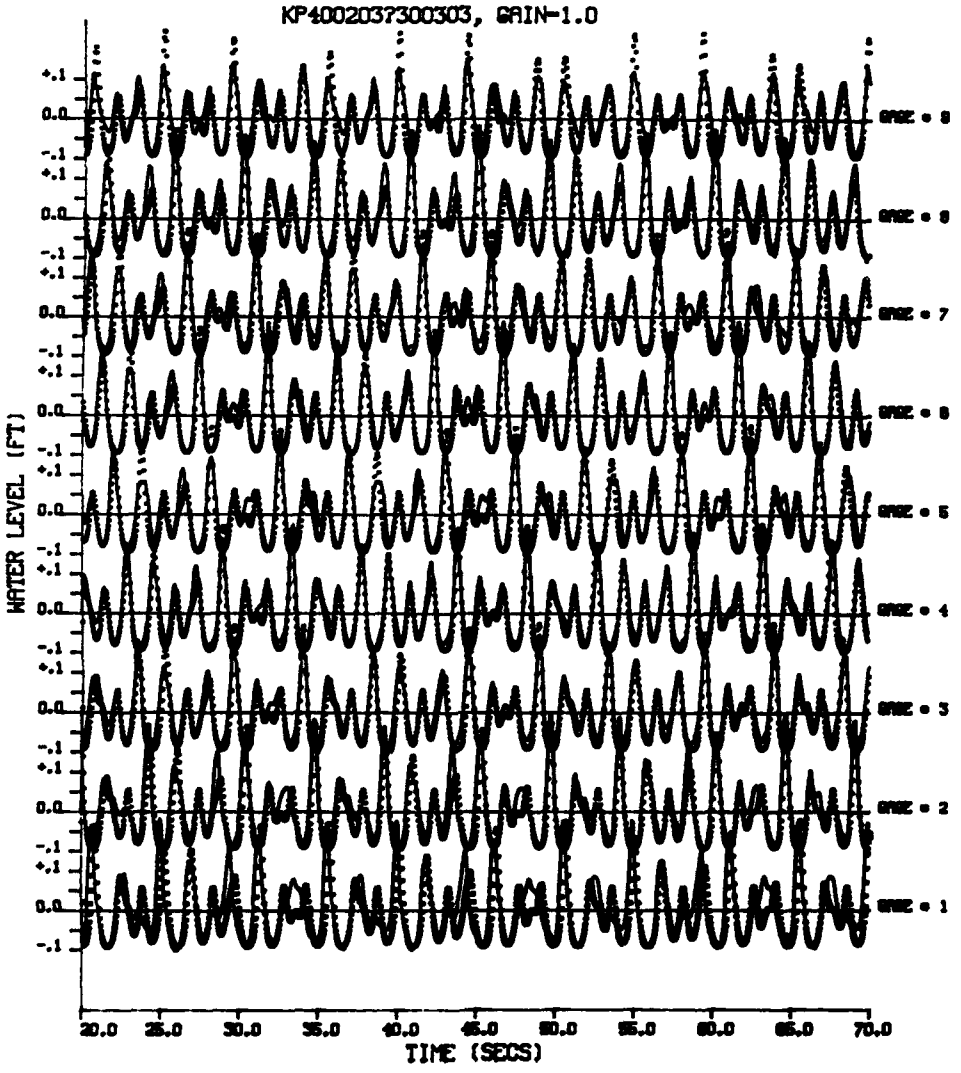

Figure 4. Comparison of measured waves to genus 2 solutions

ACKNOWLEDGMENTS

The authors acknowledge support of the Coastal Engineering Research Center, U.S. Army Engineer Waterways Experiment Station, Vicksburg, MS for making these experiments possible, and for partial financial support by National Science Foundation Grant No. DMS-9096165 at the University of Colorado and Army Research Office Contract No. DAAL03-89-K-150 at the University of Florida. The authors also acknowledge the Office, Chief of Engineers, U.S. Army Corps of Engineers, for authorizing publication of this paper.

REFERENCES

Dubrovin, B.A., 1981, "Theta Functions and Non-Linear Equations," Russ. Math. Surv. 36, 11-92.

Hammack, J., Scheffner, N., and Segur, H., 1989, "Two-Dimensional Periodic Waves in Shallow Water," J. Fluid Mech., 209, 567-589.

Kadomtsev, B.B. and Petviashvili, V.I., 1970, "On the Stability of Solitary Waves in Weakly Dispersing Media," Sov. Phys. Dokl. 15, 539-541.

Korteweg, D.J. and deVries, G., 1895, "On the Change of Form of Long Waves Advancing in a Rectangular Channel, and on a New Type of Long Stationary Wave," Phil. Mag. 39, 422-443.

Krichever, I.M., 1977, "Methods of Algebraic Geometry in the Theory of Non-Linear Equations," Russ. Math. Surv. 32, 185-313.

Segur, H and Finkel A., 1985, "An Analytical Model of Periodic Waves in Shallow Water," Studies in Applied Math., 73, 183-220.2

Discussion of Scheffner, Hammack and Segur's paper (Session C)

M.W. Dingemans (comment)

I have a question about the predictability and practical use of the genus-2 solutions of the KP equation. For cnoidal waves (genus-1) it is clear that wave height and wave period gives after some iteration the elliptic parameter. For genus-2 solution it seems to be not clear how to choose the six parameters, when, e.g., wave height, wave period and wave direction are given.

Author's reply

A guide is given in H. Segur & A. Finkel, 1985, An analytical model of periodic waves in shallow water, Studies in Appl. Math. 73, 183-220.

WATER WAVE NONLINEAR INTERACTIONS OWING TO DRIFT CURRENT. DIRECTIONAL SPECTRA FORMATION

Victor I.Shrira

P.P.Shirshov Institute of Oceanology USSR Academy of Sciences, Krasikova 23, Moscow 117218, USSR

1.Introduction

It is well known that wind blowing above free water surface generates simultaneously both water waves and a subsurface shear current commonly called the drift current. Thus, strictly speaking, studying nonlinear evolution of the wave field, one should consider simultaneous evolution of the waves and the current. There is a number of linear and nonlinear mechanisms of interaction between waves and shear current, of which some were briefly reviewed in [1]. Here we focus our attention on the mechanism of weakly nonlinear resonant interaction between water waves and and a vortical mode, which exists owing to the shear current. Adopting the term common for other branches of physics, we shall refer to it as induced scattering (IS), which in this context means the transformation of the wave field due to resonant absorbtion (or generation) of difference harmonics of the field in the critical layers in the drift current.

Strong motivation to distinguish IS among other mechanisms of wave-current interaction comes from its role in one of the key problems in wind wave theory, the formation of directional spectrum of wind waves. The most fundamental questions, such as, *"Why the angular distribution is so narrow for the energy carrying waves"* and *"Why anyway do wind waves propagate windward ?"*, which were open for a long time, can be explained very naturally on the basis of IS mechanism. (The main content of the present lecture as well as the history of the problem in brief are given in [2-4].)

2.Statement of the problem

We consider the evolution of an ensemble of free (i.e. not interacting with the wind) gravity waves on the surface of an ideal deep fluid propagating upon a drift shear current. There is a natural separation of scales which allows us to assume the drift current to be given and steady, horizontally uniform and directed windward. We also do not take into account all wind-wave

interactions, the wind enters the problem only indirectly through the magnitude of the drift flow and the wave action flux to large scales.

We assume that initially an ensemble of gravity waves is given by the spatial spectrum of wave action $N_{\vec{k}}$. The problem is to derive an equation describing the evolution of the wave spectrum (the kinetic equation), taking into account the induced scattering of surface waves by the drift current perturbations, and to study its implications for the wave spectrum dynamics.

The geophysical problem contains a number of natural small parameters exploited in our investigation. The nonlinearity parameter of surface waves, ε, characterizes the smallness of the horizontal velocity of the particles in the wave as compared to the phase velocity C of the surface wave. The small parameter μ characterizes the smallness of the drift current compared to the same phase velocity.

3.Kinetic equation

Let us first elaborate the crucial point. Each pair of surface wave harmonics with wave vectors, say, $\vec{k}_1$ and $\vec{k}_2$, and frequencies ω_1 and ω_2, generates "difference harmonics" due to nonlinearity of the Euler equations and the boundary conditions at the free surface , i.e. perturbations of the medium with a space-time structure of the form

$$exp\ \{i[(\vec{k}_1 - \vec{k}_2)\vec{x} - (\omega_1 - \omega_2)t]\}. \qquad (\omega_1 = \omega(\vec{k}_1))$$

For the difference harmonics with a phase-velocity component c directed along the current,

$$c = (\omega_1 - \omega_2)/(k_{1x} - k_{2x}),$$

less than the maximal current velocity U_{max} there occurs a critical layer at the depth $z = z_c$ (i.e., a layer where the phase velocity c matches the current velocity: $c = U(z_c)$). The resonant interaction of the difference harmonics with the flow is the mechanism of wave-field transformation under consideration.

To derive the kinetic equation we first solve the purely dynamic problem of calculating the difference harmonics, or in other words, of the induced low-frequency motions. At the second stage, upon calculation of the total effect of the energy exchange

between the waves and the flow due to the mentioned critical layers, we obtain the desired equation for the evolution of the wave field

$$\partial_t N_{\vec{k}} = I_1[N_{\vec{k}}] + N_{\vec{k}} \int G_{\vec{k}\vec{k}_1} N_{\vec{k}_1} \, \delta(\omega - \omega_1 - U(z_c)\,(k-k_1))\, d\vec{k}_1 = I_1 + I_2$$

Here I_1 is the collision integral responsible for the standard quadruple resonant interaction derived by Hasselmann, while I_2 describes the induced scattering. The kernel $G_{\vec{k}\vec{k}_1}$ is an antisymmetric function of $\vec{k}$, $\vec{k}_1$ given in [2,3]. I_2 is proportional besides ε^4 to the small parameter μ, and a certain *large* parameter M, which appears owing to low-wave-number cut-off of the induced motions and remains unspecified at the present stage of this theory. Nevertheless we can conclude that for the range of parameters relevant for the ocean I_2 greatly exceeds I_1, which is $O(\varepsilon^3)$. The fact that their ratio $\mu M / \varepsilon^2 \gg 1$ means that *induced scattering is the most effective generic mechanism of wind wave nonlinear interactions.* (We note that even if we assume the unspecified *large* parameter M to be $O(1)$ the IS remains at least as effective as the standard four-wave interactions).

Neglecting for a while I_2 we consider wave field evolution caused by IS. This interaction occurs on the resonant surface prescribed by the δ-function in the collision integral. Assuming for simplicity the wave angular spectrum to be narrow and expanding the dispersion relation $\omega_1 \approx (gk_1)^{1/2}$ near k and designating the difference $\vec{k}_1 - \vec{k}_2$ as $\vec{\kappa}$ we obtain

$$\omega_1 - \omega_2 = \vec{U}(z_c)\vec{\kappa} \approx C(k)/2\,[\kappa_x + 1/2k\,(k_{1y}^2 - k_{2y}^2)\,]$$

or in the explicit form

$$\kappa_x = {}^1/_{2k}\,\frac{(k_{1y}^2 - k_{2y}^2)}{1 - 2U_c/C} \approx {}^1/_{2k}\,(k_{1y}^2 - k_{2y}^2)$$

It is easy to see that:i) this resonance surface $\vec{k}_1(\vec{k}_2)$ is very close to the circle $k = const$, i.e. *IS transforms only angular distribution, not affecting directly the frequency spectrum.*

ii) the small difference in the frequencies of a pair interacting components has the same sign as κ_x. This means that if the $G_{\vec{k}\vec{k}_1}$ *sign* κ_x is positive the wave with the lower frequency will

transfer action to the wave with higher frequency, i.e. from the wave with larger transverse wavenumber to the wave with smaller transverse wavenumber.

It is found that for the water waves propagating *along* the current $G_{\vec{k}\vec{k}_1} sign\ \kappa_x$ is always positive and therefore *IS narrows the angular distribution;* for the waves oriented *against* the current *the spectrum broadens.* Thus for the wind waves IS is the mechanism providing formation of the observed narrow angular distribution. Under certain acceptable assumptions the integral kinetic equation reduces to the differential one, and the explicit solutions describing angular spectrum evolution for arbitrary initial distribution can be found [2,3].

Conclusions

i) Nonlinear evolution of the wind wave field is a *two-scale* process: IS causes rapid angular redistribution, not affecting directly the frequency spectrum; while the standard four-wave interactions provide much more slow dynamics of the frequency distribution.

ii) For the water waves propagating downstream IS always narrows the angular distribution; for the waves oriented against the current the spectrum broadens. Thus, for the wind waves IS is the mechanism providing formation of the observed narrow angular distribution. The preferred direction of the wind wave propagation is given not by the wind directly, but via the direction of the drift current.

References

1.V.I. Shrira, *The mechanisms of water wave transformation on shear flows /* Proceedings of the IUTAM Symposium 'Breaking Waves', Sydney, 1991 (in press)

2. V.I.Shrira and V.E.Zakharov, *Water wave nonlinear interactions owing to drift current.Part* 1. *formation of the angular spectrum of wind waves* (J. Fluid Mech., submitted)

2. V.E.Zakharov and V.I.Shrira, *Formation of the angular spectrum of wind waves /*Sov. Phys. JETP 71(6), 1990, 1091-1100.

3 V.B.Fridlender and V.I.Shrira *Kinetics of the wind waves with arbitrary spectrum upon the drift current//* Izvestia USSR Academy of Sci., Atmospheric and Oceanic Physics, 1992, v.28, (in press).

Discussion of Shrira's paper

P. Janssen (comment)

In 1984 Konen, Hasselmann and Hasselmann found from numerical integration of the kinetic equation a directional spectrum which was in good agreement with existing data on directionality. They used the full Boltzmann integral for nonlinear interaction, Snyder et al. wind input and isotropic source function for white capping. This gives sufficient anisotropy to produce a narrow spectrum. By the way, it should be realised that in these numerical experiments the directional resolution was quite coarse. More recent results with higher resolution gave even narrower spectrum.

C.C. Mei (comment)

Since wind fluerates both waves and the drift current, would wind be more important than the drift current in influencing the angular spectrum? $\rho_{air} < c\rho_{water}$, but this contrast affects both waves and current!

D.H. Peregrine

Please give the relation between this work and theories of Langmuir circulation.

Author's reply

The mechanism of induced scattering on the drift current is based on the interaction of the two surface wave harmonics and the vortical mode in the shear current. The latter can be identified as Langmuir circulation. The existing theories of Langmuir circulation focus their attention on the circulation itself, while we are interested in the feedback of these vortical structures on the wave field evolution, and therefore our purposes a rather rough description of the circulation is sufficient.

L. Tsimring (comment)

I would like to mention my paper in Izvestiya, Atmos. Ocean Physics, 1989, Vol. 25, 4, where I've considered the induced scattering of waves by wind and this effect also leads to the narrowing of the spectrum.

V. Zakharov (comment)

The top question is - why the wave spectrum becomes more narrow in the process of wave drifting from a high frequency to a low frequency region? It looks more likely that this spectrum must become more isotropic in this process. A very narrow spectrum becomes immediately wide (V.E. Zakharov, A.V. Smilga,1981). We studied also stability of the isotropic Kolmogorov spectrum and found its stability. We believe that this problem could be solved by taking into consideration new degrees of freedom - "low frequency "waves. Good candidate for these waves are vorticity on a shear flow. This is why we studied interaction with these perturbations.

P. Saffman

Further to Professor Mei's question:

Why does the wind acting by itself produce a narrow spectrum? Is it obvious that the Miles mechanism alone does not produce a narrow spectrum when acting upon a not isotropic field of initial disturbances?

Author's reply

The wind acting by itself produces an anisotropic, but not very narrow spectrum. The resulting spectrum depends strongly on initial conditions, if we assume Miles' mechanism is the governing one. However, in case we consider the Caushy problem for Miles-Phillips' mechanism, we shall not get narrow spectrum, as the Phillips' mechanism generates the oblique systems of waves.

We can also lay aside theoretical consideration and just refer to experimentally established facts: at early stages of the wind wave development, the "young" waves have rather wide angular distributions, which become more and more narrow, as the waves become older. Certainly, in all the experiments we cannot separate the effects of wind itself and wind induced current.

The principal question I tried to clarify in my talk was in fact, not "why the spectrum of wind waves is so narrow", but what makes the waves spectrum become more and more narrow in the process of its nonlinear evolution in the spectral range, where wind does not practically interact with waves.

FIELD OBSERVATION OF NONLINEAR EFFECTS AND DIRECTIONAL SPECTRA OF WIND WAVES

Yu.P.Soloviev

Marine Hydrophysical Institute Ukr Acad.of Science
Sevastopol, USSR

In recent years the experimental study of nonlinear effects, the angular distribution of the wave energy and the group structure of wind waves was performed in the Black Sea. The measurements were made with an array of resistance-type wave gauges fixed on the stable offshore platform at 30 m depth. For the most cases the deep water condition was valid, the wind velocity and the drift current were observed. The frequency-wavenumber spectra $F(\omega,k,\theta)$ were calculated by using the maximum likelihood method without any assumption about the relation between ω and k. It allowed to determine the dispersion relation directly from the data. It is shown that for typical cases of developed wind waves ($V/C_m \sim 1$, V is the wind velocity, C_m is the phase velocity of the spectral peak component) the free waves dominate in the region $\omega \leqslant 2.5\,\omega_m$. In the vicinity of the spectral maximum they satisfy the linear dispersion relation. The significant part of the deviation from the linear theory, for example, the excess of the phase velocity, is due to the drift current. The residual is explained quantitatively by the weak nonlinear interactions between spectral components. The nonzero dispersion of the wave energy outside the nonlinear dispersion region in (ω, k) space can be attributed to the bound components.

The new parametrization was proposed for the angular distribu-

tion of the wave energy from V/C_m and ω/ω_m, which is independent on specific form of approximating function. It is shown that the width of angular spectra is more depended on ω/ω_m than on V/C_m. The angular spread is found to be more narrow as compared to the known results, in particular for the high frequencies.

The results of long-term measurements of the wave amplitude variations under steady wind conditions are presented. If the sea surface displacement is assumed as a random Gaussian process, then the main properties of the wave envelope are determind by the envelop of the temporal correlation function, which can be defined via the spectrum width. The experimental spectra and other characteristics of the wave envelope are in good agreement with the modelling estimates based on this approach to typical wind wave realizations. While the wave envelope may be described by the linear theory, the low frequency variations of the sea level, which were reveled only in a case of steep high wind waves, are apparently the nonlinear effect. It is found that the predominant changes in sea level have periods within 10 - 100 s and their r.m.s. amplitude is about 5% of the mean wave amplitude. The high coherence with the wave envelope allows to treat this long waves as forced by wave groups (Longuet-Higgins, Stewart, 1962). The experimental results are compared with the theory.

MODULATION OF SHORT SURFACE WIND WAVES BY INTERNAL WAVES

B.B.Krivinsky and Yu.P.Soloviev

Marine Hydrophysical Institute UKR Acad. of Science
Sevastopol, USSR

This paper is concerned with the perturbation of the higf-frequency range of developed wind waves ($f/f_m \sim 5$-10, $V/C_m \sim 1$, f_m and C_m are the frequency and the phase velocity of the spectral peak component, V is the wind velocity) relative to the undisturbed level, produced by internal wave current variations. The theoretical analysis was made on the base of the balance of wave action spectral density $N(\mathbf{k}) = (g/k)^{1/2} F(\mathbf{k})$, where $F(\mathbf{k}) = B(\mathbf{k})\, k^{-4}$ is the wavenumber spectrum and $B(\mathbf{k})$ is the dimensionless function, determining the spectrum level for a large k (beyond the spectrum peak). The corresponding equation for a fixed wavenumber vector $\mathbf{k}$ and stationary nonuniform current field has been obtained and investigated by Phillips (1984), including the forms of source functions (input from the wind, nonlinear transfer and dissipation).

In the frame of references, moving with the phase velocity of internal wave C_i, under steady conditions and one-directional current $U = U_o\, f(x')$, this equation may be written in the following form

$$\left[\frac{C}{2}\cos\theta + U_o f(x') - C_i\right]\frac{\partial b}{\partial x'} + \frac{9}{2}\cos^2\theta\, U_o \frac{\partial f}{\partial x'}\, b -$$

$$- k\cos\theta \frac{\partial f}{\partial x'}\frac{\partial b}{\partial (k\cos\theta)} = L\, m\omega (u_*/C)^2 (b - b^n), \qquad (1)$$

where U_o is the magnitude of current variations, $f(x') = \sin(2\pi \frac{x}{L})$, L is the internal wavelength, ω is the circular frequency, u_* is the friction velocity, θ is the angle between the current and k,

$m = 0.04\cos(\theta_k - \theta_v)$ is the wind input coefficient, suggested by Plant (1982), $b = B/B_0$ is the local degree of spectrum relative to its undisturbed level. Under open sea conditions the wide angular distribution of the wave energy is expected to be $\sim \cos^{1/2}(\theta_k - \theta_v)$ (Babanin, Soloviev, 1987), therefore the third term on the left (1) will be neglected. Then (1) can be written in dimensionless form:

$$\left[P_2 + \frac{f(x')}{\cos^2\theta}\right]\frac{\partial b}{\partial x'} + \frac{9}{2}\frac{\partial f}{\partial x'}\, b = P_1 (b - b^n), \qquad (2)$$

where

$$P_1 = \frac{L\, m\, \omega}{U_o \cos^2\theta}(u_*/C)^2, \qquad P_2 = \frac{(C/2)\cos\theta - C_i}{U_o \cos^2\theta}.$$

These two parameters describe the possible variety of the dynamical interaction internal waves, surface waves and the wind. For the most open sea conditions the parameter $P_2 < 0$, whereas the short surface waves propagate slower or in the opposite direction to the internal waves.

The equation (2) was integrated numerically for various values of $0 < P_1 < 5000$ and $-32 < P_2 < -1$ beyond the resonance point. The value of the index n, which describes the balance between the wind input and the rate of dissipation, was taken as 2. Values of the mean contrast $K_1 = (b_{max} - b_{min})/(b_{max} + b_{min})$, the asymmetry of the contrast $K_2 = (b_{max} - 1)/(1 - b_{min})$, the phase of the internal wave with location b_{max} and their analytical approximation were calculated. For the low wind speed and the same direction of surface and internal waves the contrast maximum occurs close to the maximum of current at the trough of internal wave. The contrast decreases in case of the opposite direction surface and internal waves and with growth of the wind speed. For strong winds the phase

tends to the maximum of the current gradient on the back slope of internal wave.

This model was verified by the comparison with field data. The surface displacement for the frequency range $f_o \geq 0.75$ Hz, characteristics of internal waves, the wind velocity, the drift of the ship and other parameters were measured in the Atlantic ocean, north-east of the coast of Brazil. The method of measurements was described by Soloviev et.al.(1983). Since the ship was moved by the internal wave current, the truthful frequency spectra S(f) were estimated by a Doppler correction of frequency-shifted spectra using the mean speed of the drift, the form of the angular distribution and the linear dispersion relation. Here we consider only the surface wave variance $m_o = \int S(f)df$ for $f \geq f_o$. The run of internal waves can be approximated by 30 dispersionless harmonics. It seems also appropriate to define the internal wave current as a sum of different components. The comparison between the model and experimental results showed that the main features are in good agreement, if the index n was taken as 1.5. It should be noted, that the variations in b depend on n within $1.3 < n < 1.7$ rather weakly.

REFRENCES

Phillips,O.M., 1984: On the response of short ocean wave components at a fixed wavenumber to ocean current variations. J.Phys. Oceanogr., 14, 1425-1433.

Plant,W.J., 1982: A relationship between wind stress and wave slope. J.Geophys.Res., 87, 1961-1967.

Babanin,A.V., Soloviev,Yu.P., 1987: Parametrization of the width of angular distribution of wind waves energy at limited fetches. Izv. Ac.Sc.USSR, Phys.Atm. and Ocean, 23, 868-876.

Soloviev,Yu.P.,B.B.Krivinsky, A.K.Kuklin, V.G.Proschenko, 1983:Changes in short wind waves characteristics under the influence of internal waves in the ocean. Izv.Ac.Sc.USSR, Phys.Atm. and Ocean, 19, 1180-1187.

Discussion of Soloviev's paper

G. Watson

What is the source of the internal waves in that region?

Author's reply

The original source is the internal tidal wave, reflected from the shoreline. On the non-uniform current this wave generates high-frequency internal waves.

THE MULTIFRACTAL STRUCTURE OF THE OCEAN SURFACE

by

MICHAEL STIASSNIE*

The wavenumber spectrum of the ocean surface elevation contains detailed information regarding the large-scale structure of that surface. The high wavenumber behaviour of this spectrum contains some global information regarding small-scale structures and the singularities of the ocean surface. A more complete picture of these singularities is provided by the multifractal spectrum f (α).

The singularities of the surface are classified by their strength which is given by their Lipschitz-Holder exponent α. Each collection of singular points with a common $\alpha > 0$ forms a fractal set with dimension $f \leq 2$, embedded in the horizontal plane. A typical multifractal spectrum of a rough surface is shown in the figure.

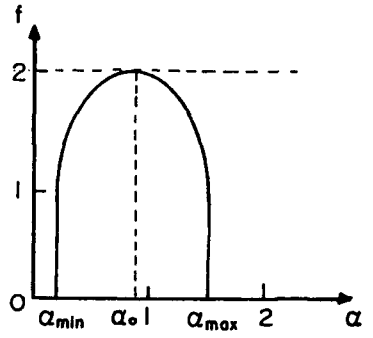

The f (α) curve provides detailed information about the singular structure of the surface. For example, the fractal (box counting) dimension of the surface D, and the exponent β of the power-law decaying wavenumber spectrum (assuming small scale isotropy), expressed in terms of the f (α) curve properties are give by:

$$D = 1 - \alpha_1 + f(\alpha_1), \text{ where } \frac{df}{d\alpha}\Big|_{\alpha=\alpha_1} = 1 \tag{1}$$

$$\beta = 4 + 2\alpha_2 - f(\alpha_2), \text{ where } \frac{df}{d\alpha}\Big|_{\alpha=\alpha_2} = 2 \tag{2}$$

The derivation of (1) and (2) is given in the Appendix A.

Short gravity waves are probably isotropic, and it is well established that $\beta = 7/2$.

In order to obtain an approximate expression for the multifractal spectrum curve, we assume: i) that the ocean surface is regular almost everywhere, i.e. that $\alpha_0 = 1$, (see figure); and ii) that the f (α) curve (at least its more interesting left part) is not far off from a quarter of an ellipse.

---

*Coastal and Marine Engineering Research Institute, Department of Civil Engineering, Technion, Israel Institute of Technology, Haifa 32000, Israel

Equation (2) with $\beta = 7/2$ and the above assumptions yield

$$\left(\frac{f}{2}\right)^2 + \left(\frac{\alpha - 1}{0.75}\right)^2 = 1 \qquad (3)$$

The fractal dimension of the surface calculated from (1) and (3) is found to be $D = 2.13$.
This is different from the D=2.25 which was obtained under the assumption of a monofractal surface (see Stiassnie, Agnon and Shemer, 1991).

Most of the small-scale energy is concentrated in singularites with Lipschitz-Holder exponent $\alpha_2 = 0.55$, and is spread over a fractal set with dimension $f_2 = 1.6$.

I suggest that the physical interpretation of the above result is that most of the deep ocean wave breaking process (whitecaps formation) is concentrated on a fractal set with dimension of about 1.6; a fact which could be checked by analyzing aerial photos of a stormy ocean surface. Note that f_2 is probably independent of the sea-state. The sea-state should be related to an appropriate measure of this set.

Note that for a case of a free water surface which is fractal the spatial derivatives do not exist, and the quadratic terms in the kinematic boundary condition become meaningless. To overcome this difficulty I propose, in Appendix B, a weak formulation of the water wave problem, which is derived from Hamilton's principle.

Appendix A: Multifractal Analysis of Rough Surfaces

1. *Definitions:*

Let z (x,y) be a continuous, bounded single-valued function in the unit square $0 \le x,y \le 1$. In the sequel we divide the unit square into a large number $N^2(\delta) = \delta^{-2}$ of indentical small squares with side δ. We also use discretized coordinate values $x_i = i\delta$, $y_j = j\delta$, i, j = 0,1,2,..., N.

The "range" of z (x,y) in a $\delta x \delta$ square is defined as

$$\Delta(x_i, y_j, \delta) = \sup z(x,y) - \inf z(x,y) \qquad (A.1)$$

where $x_i \le x \le x_i + \delta$ and $y_j \le y \le y_j + \delta$.

The box counting dimension of the surface z (x,y) is the value D for which the measure M has a finite (not zero and not infinite) value

$$M = \lim_{\delta \to 0} \delta^{D-1} \sum_{i,j=0}^{N-1} \Delta(x_i, y_j, \delta) \qquad (A.2)$$

The local behaviour of the function z (x,y) is represented by α - the Lipschitz-Holder (L-H) exponent defined by

$$\Delta (x_i, y_j, \delta) = g (x, y)\, \delta^{\alpha} \tag{A.3}$$

where g (x, y) is a good function (non-singular) of $x_i \le x \le x_i + \delta$ and of $y_i \le y \le y_i + \delta$.
The L-H exponent is always positive but may vary in a rather general manner. More specific, we denote by $f(\alpha) \le 2$, the box-counting dimension of the set of points in the unit square which have a common α.

The number of δ x δ squares which is needed to cover the sets in the unit square for which z has L-H exponent in the range $(\alpha, \alpha + d\alpha)$ is

$$n (\alpha) = \rho_1 (\alpha)\, \delta^{-f(\alpha)}\, d\alpha \tag{A.4}$$

where ρ_1 is a good function. We also introduce the good function $\rho_2 (\alpha)$, as the average of g (x, y) in (A.3), taken over all points (x_i, y_j) for which the surface z (x, y) has L-H exponent α. The function f (α) is called the *Multifractal Spectrum*.

2. *Derivation of the f (α) Curve*

We start from a q - Measure

$$M_q = \lim_{\delta \to 0} \delta^{\tau (q)} \sum_{i,j=0}^{N-1} \mu_{ij}^{q} \tag{A.5}$$

where the relative weight of the i, j square is

$$\mu_{ij} (\delta) = \Delta (x_i, y_j, \delta) \Big/ \sum_{i,j=0}^{N-1} \Delta (x_i, y_j, \delta) \tag{A.6}$$

From (A.6), (A.3) and (A.2), for points (x_i, y_j) with L-H exponent α, we have

$$\mu (\alpha, \delta) = g (x, y)\, \delta^{\alpha} / M\, \delta^{1-D} \tag{A.6a}$$

The sigma (Σ) term on the r.h.s. of (A.5) is recalculated with the aid of (A.4) and (A.6a),

$$\sum_{i,j=1}^{N-1} \mu_{ij}^{q} = \int_0^{\infty} \rho_1 (\alpha)\, \delta^{-f(\alpha)} \left(\frac{\rho_2}{M}\right)^{q} \delta^{(D + \alpha - 1)\, q}\, d\alpha \tag{A.7}$$

Using the method of steepest descent to extract the dominant term from (A.7) in the limit of small δ

$$\lim_{\delta \to 0} \sum_{i,j=1}^{N-1} \mu_{ij}^{q} = \rho_1 (\alpha_q) \left(\frac{\rho_2 (\alpha_q)}{M}\right)^{q} \left(\frac{2\pi}{f'' (\alpha_q)\, \ell n\, \delta}\right)^{1/2} \cdot \delta^{-f(\alpha_q) + q (D + \alpha_q - 1)} \tag{A.8}$$

where $f'(\alpha_q) = q$ and $f''(\alpha_q) < 0$ (A.8a)

Substituting (A.8) into (A.5), we get

$$\tau = f(\alpha) - q(D + \alpha - 1) \tag{A.9}$$

Taking the derivative with respect to q of (A.9) and applying (A.8a), we find

$$\frac{d\tau}{dq} = 1 - \alpha - D \tag{A.10}$$

Equations (A.9) and (A.10) enable to calculate $f(\alpha)$, once $\tau(q)$ is known.

3. *Fractal Dimension and Spectral Exponent*

From (A.2), (A.3) and (A.4)

$$M = \lim_{\delta \to 0} \delta^{D-1} \int_0^\infty \rho_1 \delta^{-f(\alpha)} \rho_2 \delta^{\alpha} \, d\alpha \tag{A.11}$$

Using the method of steepest descent and the fact that M is finite, gives

$$D = 1 - \alpha_1 + f(\alpha_1); \qquad \left.\frac{df}{d\alpha}\right|_{\alpha = \alpha_1} = 1 \tag{A.12}$$

In order to obtain the spectral exponent, we start by calculating an approximation to the mean-square increment assuming small-scale isotropy of the surface z

$$\left\langle [f(x + \delta\cos\theta, y + \delta\sin\theta) - f(x, y)]^2 \right\rangle \propto \int_0^\infty \frac{\delta^{-f(\alpha)}}{\delta^{-2}} \cdot (\delta^{\alpha})^2 \, d\alpha \underset{\delta \to 0}{\propto} \delta^{-f(\alpha_2) + 2 + 2\alpha_2} \tag{A.13}$$

where $\left.\frac{df}{d\alpha}\right|_{\alpha = \alpha_2} = 2$

The high wavenumber limit of the spectrum is written as

$$\Psi(\underline{k}) \underset{k \to \infty}{\propto} k^{-\beta} \tag{A.14}$$

The Wiener-Khintchine relations enable us to compare the small increment limit ($\delta \to 0$) of the two-dimensional Fourier-transform of (A.14) with (A.13) which yields

$$\beta = 4 + 2\alpha_2 - f(\alpha_2) \tag{A.15}$$

Appendix B: Weak Formulation of the Water-Wave Problem

Hamilton's principle asserts that the motion of a dynamical system from one configuration to another renders stationary the integral

$$\iiint_R L \, dxdydt \tag{B.1}$$

where the appropriate Lagrangian L, as shown by Luke (1967), is given by the principle of stationary pressure

$$L = -\rho \int_{-\infty}^{\eta(x,t)} [\phi_t + 1/2(\nabla\phi)^2 + gz] dz, \tag{B.2}$$

R is an arbitrary region in the $(\underline{x},t)$ space, ρ is the density of the water. η is the free surface elevation and φ is the flow potential. Using standard procedure of calculus of variations and integrating by parts gives

$$-\hat{\delta}\iiint_R \frac{L}{\rho} dxdydt =$$

$$= \iiint_R \{(1/2(\nabla\phi)^2 + \phi_t + gz)_{z=\eta} \hat{\delta}\eta + \int_{-\infty}^{\eta} (\nabla\phi \bullet \nabla(\hat{\delta}\phi) + (\delta\phi)_t) dz\} dxdydt =$$

$$= \iiint_R \{ (\phi_t + 1/2(\nabla\phi)^2 + gz)_{z=\eta} \hat{\delta}\eta + [\frac{\partial}{\partial t}\int_{-\infty}^{\eta} \hat{\delta}\phi dz + \frac{\partial}{\partial x}\int_{-\infty}^{\eta} \phi_x \hat{\delta}\phi dz + \frac{\partial}{\partial y}\int_{-\infty}^{\eta} \phi_y \hat{\delta}\phi dz] -$$

$$- \int_{-\infty}^{\eta} (\phi_{xx} + \phi_{yy} + \phi_{zz}) \hat{\delta}\phi dz - ((\eta_t - \phi_z + \eta_x\phi_x + \eta_y\phi_y) \hat{\delta}\phi)_{z=\eta} \} dxdydt = 0 \tag{B.3}$$

Here $\hat{\delta}(*)$ represents the variation of the quantity *. The term in square brackets integrates out to the boundaries of the domain R, and is equal to zero, since $\hat{\delta}\phi$ is assumed to vanish there. Setting $\hat{\delta}\eta = 0$ and $\hat{\delta}\phi = 0$ at $z = \eta$ yields

$$\iiint_R \int_{-\infty}^{\eta} (\phi_{xx} + \phi_{yy} + \phi_{zz}) \hat{\delta}\phi dxdydzdt = 0 \tag{B.4}$$

for any appropriate $\hat{\delta}\phi$.

Since $\hat{\delta}\eta$ and $\hat{\delta}\phi$ at $z = \eta$ can take 'arbitrary' values, one obtains

$$\iiint_R [\phi_t + 1/2(\nabla\phi)^2 + gz]_{z=\eta} \hat{\delta}\eta \, dxdydt = 0, \tag{B.5}$$

$$\iiint_R [\eta_t + \eta_x\phi_x + \eta_y\phi_y - \phi_z)\hat{\delta}\phi]_{z=\eta} dxdydt = 0 \tag{B.6}$$

Replacing $\hat{\delta}\eta$ and all $\hat{\delta}\phi$ by Dirac's Delta function in (B.4) to (B.6) yields the classical Euler equations for water-waves. But, if one has fractal (weak) solutions in mind, one must be somewhat 'more careful'. Having in mind solutions with fractal properties, one could insert Dirac's delta function in (B.4) and (B.5); but not in (B.6) where $\hat{\delta}\phi$ is taken as a product of Dirac's delta function in time and an *appropriate spatial variation* denoted by $\hat{\delta}\tilde{\phi}$ (x,y)

$$\phi_{xx} + \phi_{yy} + \phi_{zz} = 0, \qquad z < \eta, \tag{B.4'}$$

$$\phi_t + 1/2(\nabla\phi)^2 + g\eta = 0, \qquad z = \eta, \tag{B.5'}$$

$$\iint_{-\infty}^{\infty} (\eta_t + \eta_x\phi_x + \eta_y\phi_y - \phi_z)_{z=\eta} \hat{\delta}\tilde{\phi} \, dxdy = 0, \tag{B.6'}$$

Again, for classical differentiable solutions one usually takes the following two-dimensional Dirac's Delta function

$\hat{\delta}\tilde{\phi} = \delta\left(\sqrt{(X-x)^2+(Y-y)^2}\right)/2\pi\sqrt{(X-x)^2+(Y-y)^2}$, (see Courant and Hilbert 1962, p. 791).

The *Riesz Fractional Integral* in two dimensions of h(x,y) and of order v, as defined by Riesz (1949) can serve as a generalization of Dirac's Delta function:

$$-\infty I^{\nu}_{\infty}(f) = \frac{\Gamma(1 - \frac{\nu}{2})}{\pi 2^{\nu}\Gamma(\frac{\nu}{2})} \iint_{-\infty}^{\infty} h(x,y)[(X-x)^2+(Y-y)^2]^{\frac{\nu}{2}-1} dxdy, \tag{B.8}$$

According to Lighthill (1959) p. 28, $\lim_{\varepsilon \to 0} (\Gamma(\varepsilon))^{-1}|x|^{\varepsilon-1} \to 2\delta(x) = \delta(|x|)$,

thus

$$-\infty I^{0}_{\infty}(f) = h(X,Y) \tag{B.9}$$

I suggest that equation (B.10), which was obtained from (B.7) with

$h = (\eta_t + \eta_x\phi_x + \eta_y\phi_y - \phi_z)\,|_{z=\eta}$, and $v = 1 - \alpha_{min}$ (α_{min} is showen in the figure) should be taken as a replacement to the so-called kinematic condition:

$$\int\int_{-\infty}^{\infty} \{\eta_t + \eta_x\phi_x + \eta_y\phi_y - \phi_z\}|_{z=\eta(x,y,t)} [(X-x)^2+(Y-y)^2]^{(1+\alpha_{min})/2}\, dxdy = 0, \qquad (B.10)$$

This completes the weak formulation and makes clear my opinion regarding the nature of the *appropriate* $\hat{\delta}\tilde{\phi}$

$$\hat{\delta}\tilde{\phi} = \frac{\Gamma(1-\frac{v}{2})}{\pi 2^v \Gamma(\frac{v}{2})} [(X-x)^2+(Y-y)^2]^{\frac{v}{2}-1} \qquad (B.11)$$

Note that one can show that although $\frac{dW}{dx}$ where W(x) is the univariate Weierstrass function of dimension 1+v, does not exist, its fractional integral ${}_{-\infty}I^{v}_{\infty}\left(\frac{dW}{dx}\right)$ exists and is finite. The extension of this result to two dimensions guided me in the above formulation.

References

1. Courant, R. & Hilbert, D., 1962. Methods of Mathematical Physics, Vol. 2, John Wiley, 830p.
2. Lighthill, M.J., 1959. Introduction to Fourier Analysis and Generalized Functions, Cambridge University Press, 79p.
3. Luke, J.C. 1967. A variational principle for a fluid with a free surface, J. Fluid Mech., 27, 395-397.
4. Riesz, M., 1949.L'integrale Riemann-Liouville et le probleme de Cauchy, Acta Mathematica, 81, 1-223.
5. Stiassnie, M., Agnon, Y., & Shemer, L. 1991. Fractal dimensions of random water surfaces, Physica D. 47, 341-352.

Acknowledgements

This study is supported by the U.S. Office of Naval Research under Grant No. N00014-91-J-1449.

Discussion of Stiassnie's paper

M.A. Donelan (comment)

The idea that short gravity waves are isotropically distributed arises from a misinterpretation of wavenumber spectra deduced from stereo photographs. The wavenumber spectra are only capable of resolving one half of the wavenumber plane.

M. Tulin

You have derived a dimension for "breaking". In clarification, was this based on some definition of breaking, for example, a limiting steepness?

Author's reply

I have provided what I hope is a plausible argument, which suggests that most of the ocean-wave breaking process is located on a fractal set (embedded in the horizontal plume) with dimension 1.6, and that the singularity of the water surface at the points which belong to this set is related to a Lipschitz-Holder exponent value of 0.55.

The above conclusion is not based on the limiting steepness concept. At present I am trying to work out the link between these quantities.

Some Recent Laboratory and Field Measurements of Surface Breaking Waves

Ming-Yang Su

Naval Oceanographic and Atmospheric Research Laboratory
Stennis Space Center, Mississippi 39529-5004

Abstract

During the past two years, we have conducted several series of experiments on breaking of surface gravity waves and its subsequent air entrainment, which forms plumes of bubbles. These experiments were conducted both in the laboratory and in the open sea employing various sensors based on both electromagnetic and acoustic principles. The laboratory experiments were performed in a very large tank, in both fresh and salt water, and were used to quantify the significant effects of salinity on the production and evolution of bubbles due to wave breaking.

From the open sea experiments, extensive measurements of near-surface void fraction under moderate to high sea states yield some remarkable new statistics of occurrence of breaking waves as well as the significant effect of wave age on such statistics.

From both the laboratory and open ocean measurements, a universal size distribution of bubbles with radius ranging from 34 to 1200 microns due to surface gravity wave breaking has been observed.

A summary of these extensive laboratory experimental and at-sea measurement results along with comparisons with variously published results shall be presented with this paper.

Introduction

One of the most obvious and characteristic features of wave breaking in the open sea is the entrainment of air by the plunging of, and/or creeping near, the crest of a steep wave, which generates in turn, a series of bubble plumes beneath and behind the breaking wave. Our interest in this investigation is concerned equally with the frequency of occurrence of breaking waves and the amount of air entrained due to such wave breaking in the moderate to high sea states. To accomplish simultaneously these dual, but related, objectives of our research interest, we decided to detect the presence of breaking waves by direct measurement of near surface void fraction,

which is expressed as percentage of air content in the water, by means of a floating vertical array tethered to a R/V, on which several void fraction meters are installed at various depths. A very brief summary of the results of this field measurement on both the void fraction statistics and breaking wave frequency statistics under moderate to strong wind are presented here.

The instrumentation for void fraction and bubble density measurement is depicted in Figure 1. This system consists of three sensor arrays on a line 150 meters long tethered to a ship; (a) the horizontal void fraction array which is used for obtaining breaking wave statistics and breaking wave motion; (b) the vertical void fraction array which is used for obtaining depth profiles of void fraction ranging from 0.5% to 60%; and (c) the vertical acoustic resonator arrays which is used for obtaining bubble size density profile with bubble radius ranging from 34 to 1200 microns. The void fraction meter is based on a theory developed by James Maxwell (1891), while the acoustic resonator is originally developed by Breitz and Medwin (1989).

Results and Comparison

A. Breaking Wave Statistics

The cumulative average in percentages for four cases, A-D, during SWADE are plotted in Figure 2 along with the five ranges of void fraction denoted by letters *a*, *b*, *c*, *d*, and *e*, respectively, and with the mean wind speeds of 10 and 15 m/s.

Each "void fraction event" may be interpreted as one "breaking wave event", if we define a breaking wave to be a wave which entrains air into the water that becomes a plume of bubbles with a measurable void fraction to a depth of 12" below the surface. This definition will preclude all the micro-breaking by capillary waves and gravity-capillary waves with wave lengths less than about 2 m. We shall next compare our field measurements with several published field measurements on breaking wave statistics by various investigators employing different techniques and definitions on what constitutes a "breaking wave".

In the paper by Holthuijsen and Herbers (1986), the observed occurrence percentage (fraction) of breaking waves from five different field measurements as a function of wind speed (U_{10}) are compared. Their Figure 7 is reproduced here in Figure 2 for comparison with our results.

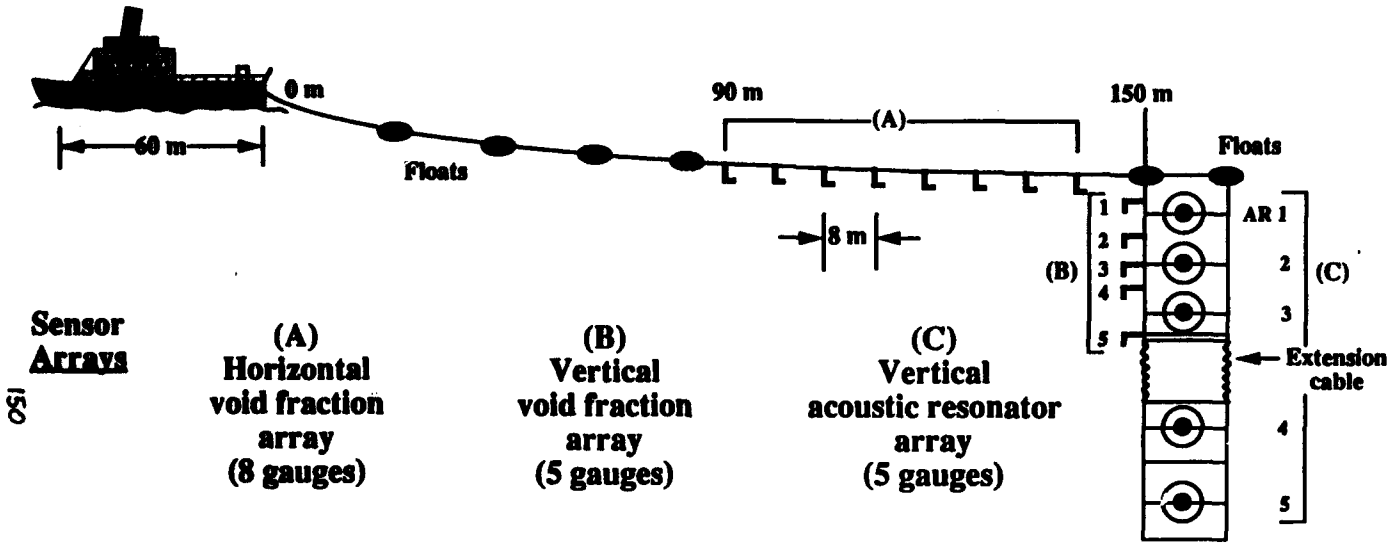

Figure 1. The NOARL Bubble Measurement System.

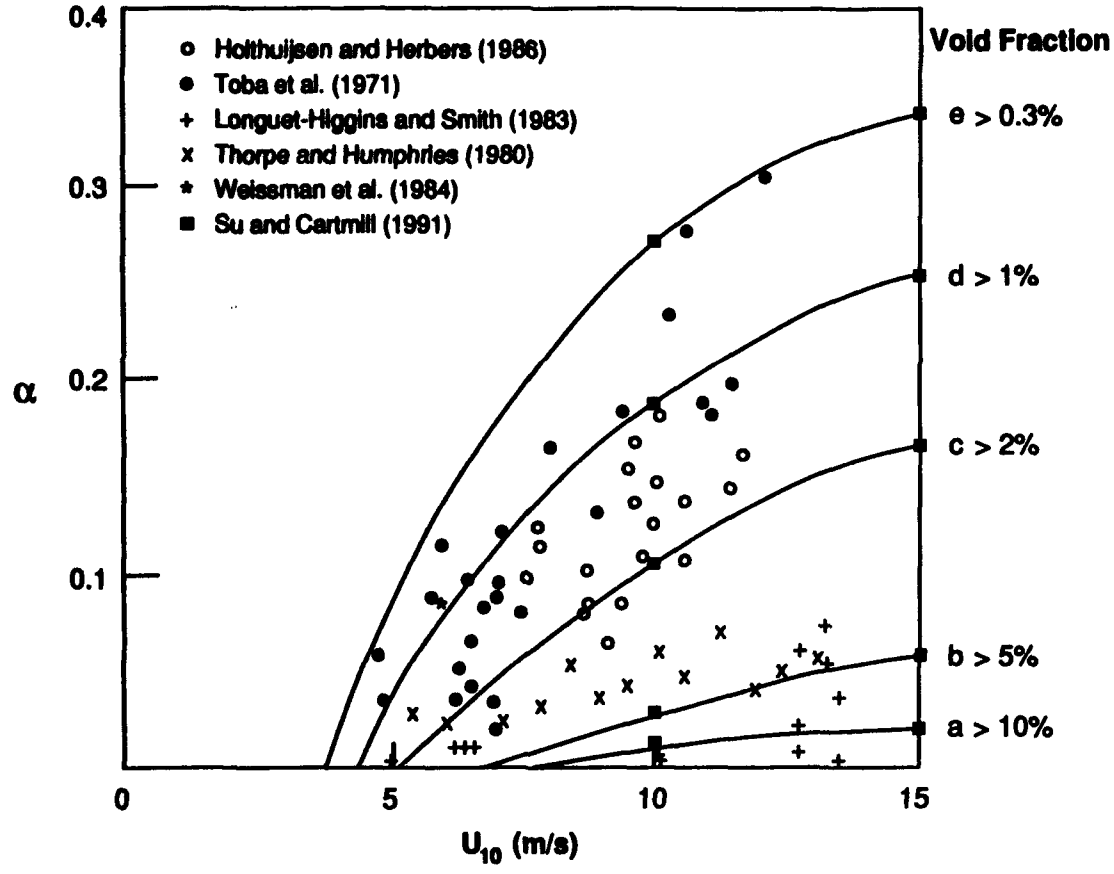

Figure 2. Breaking Wave Statistics – The Probability Occurence (α) in Terms of Void Fraction with Comparison with Previous Field Measurements.

Toba et al. (1971) and Holthuijsen and Herbers (1986) use the similar technique of coupling visual identification of white capping with wave height measurement. Even though this method might be the most positive way to say a wave is in the process of breaking, some degree of subjective judgement is still involved, particularly when the breaking area is small. Thorpe and Humphries (1980) use telephotography in place of direct visual observation. This method could miss counting smaller breaking waves in contrast to the former method. As such, the observed number of breaking waves should be less in the latter case, as exhibited in Figure 2. Weissman et al. (1984) employed the method of detecting the presence of high frequency components (5-50 Hz) in the waves as the definition of breaking waves. Their measurement at a low wind speed of about 6 m/s involved only very small breaking waves, which should agree better with those by direct visual observation (such as Toba, et al.). Longuet-Higgins and Smith (1983) employed a "jump meter" to measure the slope of large and/or dominant waves near a North Sea tower. Waves with the steep slope beyond some chosen threshold values are then considered to be breaking waves. Since the "jump meter" technique is designed for detecting larger waves, many small breaking waves are ignored. It is reasonable to suggest that small breaking waves occur more often than large breaking waves. Hence, Longuet-Higgins and Smith's count would be much lower than all of the other methods described earlier.

It is very interesting to note that curves *a* and *e* encompass all the earlier data points, and curves *b*, *c*, and *d* provide some dividing boundaries to data points from different techniques. The fact that *e* and *c* with 1% > VF > 0.30% agrees more with Toba et al. (1971) might imply that Toba and his colleagues have been more careful than the others to pick up many more smaller breaking waves. The observed data by Holthuijsen and Herbers (1986) are bounded nicely by curves *d* and *c* with 2% > VF > 1%. The data obtained by Thorpe and Humphries (1980) fall more into the bounds defined by curves *b* and *c* with 5% > VF 2%. The data presented by Longuet-Higgins and Smith (1983) seem to lie more below curve *b* with VF > 5% and above curve *a* with VF > 10%.

The surprisingly good overall match between the void fraction event statistics, interpreted as the equivalent breaking wave statistics, from the five previous field measurements may strongly suggest that the quantitative measure of void fraction is physically better than other techniques for detecting breaking waves and their relative scale and intensity in the open ocean.

B. Near Surface Bubble Density

We have conducted three series of laboratory experiments on bubble density distribution under mechanically or wind-generated breaking waves and also participated in two SWADE cruises in 1991 for bubble density measurements under moderate and strong wind conditions.

Detailed analyses and results from these laboratory and field experiments can not be presented in the limited given space available in the proceedings here, but the overall characteristics of the bubble density with radius ranging from about 10 to 1200 microns can be seen from Figure 3. The bubble density model is derived based on these SWADE results as well as NOREX 85 experiment from the NORDSEE Tower in the North Sea in 1985 (Su, et al., 1988). The latter experiment has provided the bubble size density from 10 to 34 microns range.

Further accounts of the results on both breaking wave statistics and bubble density in both laboratory and field experiments shall be reported in journals in the near future.

References

1. Breitz, N. and H. Medwin. 1989. Instrumentation for in situ Acoustical Measurements of Bubble Spectra Under Breaking Waves. JASA 86(2). pp. 739-743.
2. Farmer, D.M. and S. Vagle. 1989. Wave Guide Propagation of Ambient Sound in the Open Surface Bubble Layer. JASA 86(5). pp. 1987-1908.
3. Holthuijsen, L.H. and T.H.C. Herbers. 1986. Statistics of Breaking Waves Observed as Whitecaps in the Open Sea. J. Phys. Oceano. 16. pp. 290-297.
4. Longuet-Higgins, M.S. and N.D. Smith. 1983. Measurement of Breaking Waves by a Surface Jump Meter. J. Geophys. Res. 88-C14. pp. 9823-9831.
5. Maxwell, J.C. 1891. A Treatise on Electricity and Magnetism. Dover 1945.
6. Su, M.Y., S.C. Ling and J. Cartmill. 1988. Optical Microbubble Measurement in the North Sea in Sea Surface Sound, ed. by B.R. Kerman. pp. 211-224.
7. Thorpe, S.A. and P.N. Humphries. 1980. Bubbles and Breaking Waves. Nature 283. pp. 643-665.

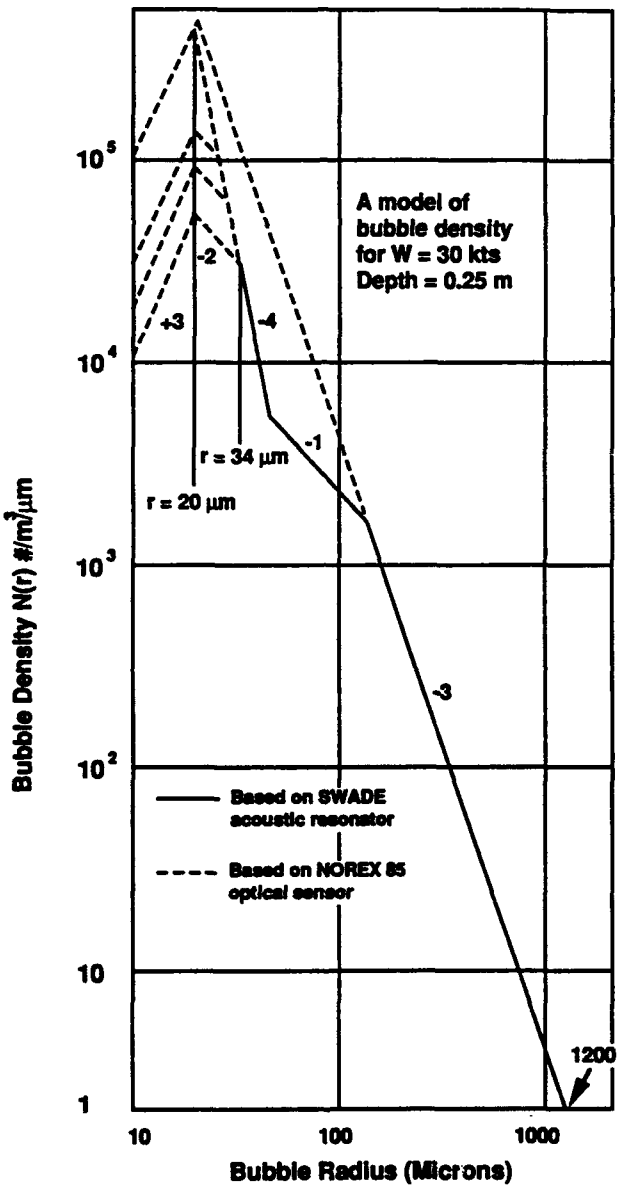

Figure 3. A Model of Bubble Density Based On Laboratory and Field Measurements.

8. Toba, Y., H. Kunishi, K. Hishi, S. Kawai, Y. Shimada and N. Shibota. 1971. Study on Air-Sea Boundary Processes at the Shirahama Oceanographic Tower Station. Disaster Prevention Research Institute. Kyoto University Annals. 148. pp. 519-531. (In Japanese with English abstract).

9. Weissman, M.A., S.S. Atakturk and K.B. Katsaros. 1984. Detection of Breaking Events in a Wind-Generated Wave Field. J. Phys. Oceano. 14. pp. 1608-1619.

10. Weller, R.A., M.A. Donelan, M.G. Briscoe and N.E. Husug. 1991. Riding the Crest - A Tale of Two Wave Experiments. Bulletin Am. Met. Soc. 72(2). pp. 163-183.

Discussion of Su's paper

Comment

Parallel work to your own is going on at the Polytechnic of the South West, Plymouth, England, under Dr Peter Hewson. Also the differences between salt and fresh water bubble size has been very carefully experimented upon by J.R. Scott (1975) (Applied Ocean Research ?).

R. Glazman

I am not sure that the five measurement attempts employed in your plot are really the best available experimental data sets on the wind-speed dependence of the breaking wave rates. These data cover too diverse experimental conditions: wind fetches from a few kilometers to a hundred or so, fresh water basins and sea water, etc. Also different authors here used very different, sometimes quite questionable, methods to detect breaking wave events. For instance, Longuet-Higgins and Smith didn't measure breaking waves, they measured events of rapid local sea level variations, etc. On the other hand, there exist more reliable data on breaking wave rates such as the whitecap photographic observations by Monahan, Bondur and Sharkov, and others - more relevant to ocean conditions. Why not use those?

Author's reply

The statistical distribution of breaking waves as given by Monahan et al. is percentage of white capping which does not distinguish difference size of breaking waves. As such his measurement cannot be compared with our measured statistics without introducing other assumptions. I fully understand the fact that various techniques and ocean conditions are involved in these five previous breaking waves statistics I cited for comparison. Using void fraction measurement, the intensity (and therefore possibly indicating size of breaking waves) can be more definitively measured than the purely surface exhibition of white capping on aerial photographs.

V.I. Zakharov (comment)

I use the opportunity to underline again how well the theoretical estimate for the velocity of wave-breaking onset

$$V \simeq \left[\frac{Sw}{\rho_{air}}\right]^{\frac{1}{2}} (\Gamma g)^{\frac{1}{4}} \simeq 5\ 60\ 6\ \text{m/sec}$$

fits to the experimental results. And I would like to underline that existence of two-phase flow in breaking waves is a challenge for theoretical physicists.

N. Huang

The bubble size distribution measured with an optical device showed a -5 to -6 power law spectrum for the larger bubbles, which are t' small bubbles measured with acoustical device. But the acoustica device showed a -4 power law spectrum. Are they inconsistent?

Author's reply

The bubble size distribution measured with the optical device was obtained within 20m of the North Sea tower (1985) and was strongly affected by the presence of the tower. As such the distribution is not typical as would be expected in open ocean. Those bubble distributions measured by the acoustic resonators were done in open ocean. Therefore, these two distributions *should not be the same. Unfortunately, Dave* Farmer has adopted the atypical distribution shape for inverting his acoustical measurement of bubbles.

Elucidation of Ocean Waves by Nonlinear Soliton Wavelet Dynamics

BY HAROLD H. SZU, Ph.D.
Information Science Group Leader
Information & Mathematical Sciences Branch, R44

Abstract: Using the techniques of nonlinear soliton dynamics to understand systematically and comprehensively the nonlinear dynamic mechanism that underlies the observed phase transition phenomena, from the low sea state, i.e., the first order phase transition for the wind-surface wave generation, to the high sea state, i.e., from the wave breaking to the second order phase transition towards a fully developed turbulence. Thereupon, a better unmasking scheme of the surface waves is anticipated and becomes possible for the detection of quieter transient signatures in a noisy high sea state.

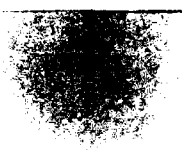

LOW FREQUENCY NEARSHORE MOTIONS INDUCED BY WIND WAVES

Edward F. Thompson and Michael J. Briggs
U.S. Army Engineer Waterways Experiment Station
Vicksburg, Mississippi, U.S.A.

INTRODUCTION

Nonlinear behavior in ocean waves increases as water depth decreases. Thus, wind waves (with periods between 1 and 30 seconds) which propagate into shallow nearshore waters can be strongly modified by nonlinear processes. These processes are only partially understood. Laboratory and field data provide essential documentation and insights on nonlinear processes. Major advances in laboratory and field wave data collection and analysis over the last decade have greatly enhanced the value of these tools for investigating second order nonlinear phenomena.

One consequence of nonlinearities during wind wave shoaling is the emergence of significant low frequency motions (with periods between 30 sec and several minutes) in and around the surf zone. Recent laboratory experiments are used in this study to provide data on the evolution of low frequency motions under controlled incident wave conditions. Theoretical predictions of low frequency motions are compared to laboratory results. Only the two-dimensional on-offshore motions, often referred to as surf beat, are considered.

THEORY

The process by which short (wind) waves create long waves can be explained theoretically by two mechanisms. First, radiation stress forces a depression of local mean water level under high short waves and an elevation under low short waves. Thus a low frequency component of sea surface motion is induced. The second mechanism is the relatively slow variation in time of the point of nearshore wave breaking as groups of high short waves alternate with groups of low short waves. This mechanism is a function of nearshore bottom slope as well as incident short wave characteristics.

The theory used to interpret measurements in this study was developed by Sand (1982a, 1982b). It is based on consideration of radiation stress. Assumptions inherent in the theory include no breaking, constant local water depth, and no directional spread. The theory can be used to predict both the long wave time series and spectrum based on the Fourier "a" and "b" coefficients of the short wave spectrum.

LABORATORY EXPERIMENTS

Experiments were conducted as part of the Generalized Beach Model (GBM) series in the U.S. Army Engineer Waterways Experiment Station's (WES) directional basin (Briggs and Smith, 1990). The 28-m by 40-m basin contained a fixed, mortar bottom which was flat within 4.5 m of the wavemaker and then formed a 1:30 slope (Fig. 1). Water depth at the wavemaker was 50 cm. Absorber material lined the basin back and sides. The sides had no solid walls but were open to adjacent basins to help minimize reflections. The model scale was approximately 1 to 25. Twenty surface wave gages were arranged in one cross-shore array and two longshore arrays.

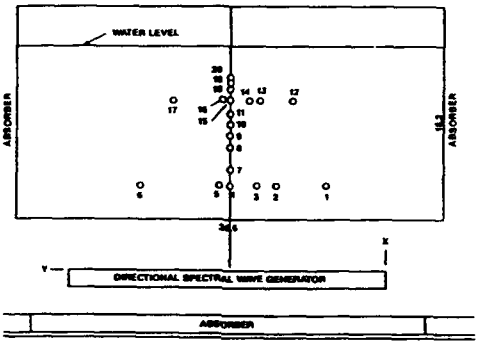

Figure 1. Basin and gage layout.

Wave conditions were generated with the TMA spectral form using a gamma value of 3.3. The cases are characterized by peak period as swell (2.5 sec) and sea (1.25 sec). They are further characterized by directional spread as "directional" (broad directional spread typical of sea) or "unidirectional" (no directional spread). Wave data were collected at the sampling rate of 10 Hz to give a usable record length of 500 sec for swell and 250 sec for sea.

Laboratory time series were subjected to spectral analysis using a Fast Fourier Transform routine with no windowing and 24 degrees of freedom. Significant wave height, H_{mo}, was calculated for both the short and long wave parts of the spectrum. Frequencies less than half the peak frequency were considered as part of the long wave spectrum. This cutoff is arbitrary, but it includes most long wave energy without significant contamination from the low frequency tail of the wind wave spectrum.

Long wave significant height, H_{moLW}, increases as depth decreases (Figs. 2 and 3). Also H_{moLW} is consistently higher for unidirectional waves than for directionally-spread waves. Both of these characteristics are expected from theory. Some evidence of possible low frequency basin oscillation was observed in long wave

spectra at the shallower gages (Thompson and Briggs, 1991). Predictions of $H_{mo,u}$ from unidirectional theory, shown in the figures, should be compared to the unidirectional laboratory results. Predictions are only shown at points seaward of the surf zone. Predictions and measurements are the same order of magnitude. However the details are not consistent; predictions exceed measurements for swell but the reverse is true for sea. Possible explanations for the differences are described in the discussion accompanying this abstract.

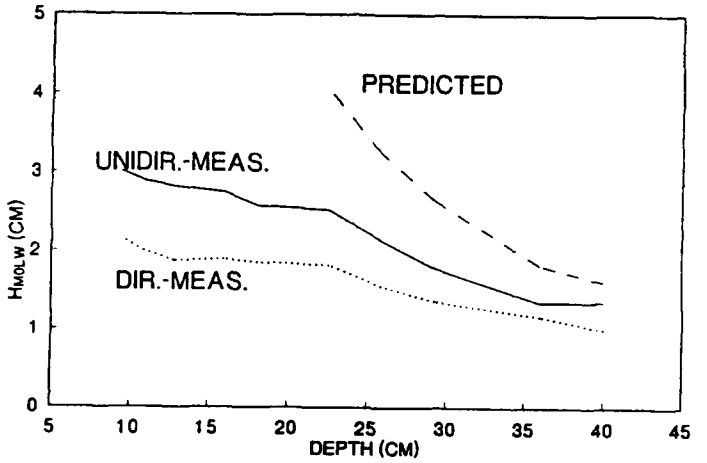

Figure 2. Long wave significant height for swell.

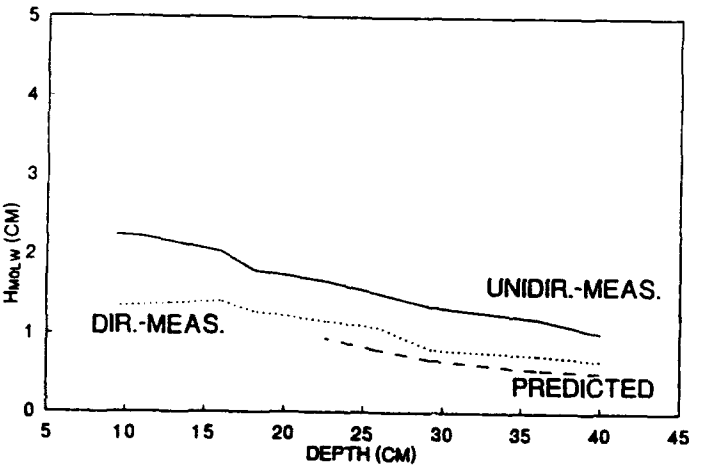

Figure 3. Long wave significant height for sea.

Interesting nonlinearities emerge in the short as well as the long wave spectrum during shoaling. The importance of these nonlinearities in predicting nearshore field spectra was recently demonstrated by Freilich et al. (1990). Selected GBM laboratory tests were run with incident spectra scaled from field measurements at Torrey Pines Beach. These experiments validated the accuracy of laboratory simulation of nonlinear processes in shoaling short wave spectra (Elgar et al., 1992).

ACKNOWLEDGEMENTS

The authors wish to acknowledge the Office, Chief of Engineers, U.S. Army Corps of Engineers, for authorizing publication of this paper. It was prepared under the In-House Laboratory Independent Research Program of the U.S. Army Engineer Waterways Experiment Station.

REFERENCES

Briggs, M.J., and Smith, J.M. 1990. "The Effect of Wave Directionality on Nearshore Waves," Proc., ICCE, Delft, The Netherlands.

Elgar, S., Guza, R.T., Freilich, M.H., and Briggs, M.J. 1992. "Laboratory Simulations of Directionally Spread Shoaling Waves," J. Waterway, Port, Coastal and Ocean Engrg., ASCE (in publication).

Freilich, M.H., Guza, R.T., and Elgar, S.E. 1990. "Observations of Nonlinear Effects in Directional Spectra of Shoaling Gravity Waves," JGR, 95(C6), June, 9645-9656.

Sand, S.E. 1982a. "Long Wave Problems in Laboratory Models," J. Waterway, Port, Coastal and Ocean Engrg., ASCE, 108(WW4), 492-503.

Sand, S.E. 1982b. "Wave Grouping Described by Bounded Long Waves," Ocean Engrg., 9(6), 567-580.

Thompson, E.F., and Briggs, M.J. 1991. "Long Waves in Laboratory Wave Basin Shoaling Tests," Proc. 24th IAHR Cong., Madrid, Spain.

Discussion of Thompson's paper

J.A. Battjes

Concerning your statements concerning the bound and the free long waves propagating towards the beach:

1) Have you separated the long-wave signals into the bound and the free component, using the gauge array and assuming the appropriate propagation speeds?

2) Can you explain why the presence of free long waves in addition to the bound ones (due to the manner of wave generation) would lead to overprediction in the case of swell and underprediction in the case of sea?

Author's reply

1) We have not separated the bound and free long wave components, but I agree that this would be a useful exercise.

2) The wavemaker control signal was empirically adjusted to give very low long wave energy at the wavemaker. However the irregular wavetrain being generated requires a bound long wave component. This component was not explicitly generated by the wavemaker. To satisfy the condition of no net long wave energy at the wavemaker boundary, a free long wave must also appear. The free and bound long waves are opposite in phase at the wavemaker. The free long wave travels at the group velocity appropriate to its frequency. The bound long wave travels at the group velocity of the short waves. In the case of our swell tests, the two group velocities are nearly the same, appropriately equal to the depth-limited velocity. Thus the phase differences between free and bound long wave components persist as the waves propagate away from the wavemaker up onto the slope. Because the free and bound waves continue to counter-balance each other, the net measured long wave energy is less than the bound wave energy. The theory predicts only bound long wave energy. Hence the overpredictions relative to the swell measurements is not surprising. For our sea tests, the group velocities of the free and bound waves differ significantly. By the time the waves propagated from the wavemaker to the most seaward gauges, phase differences between free and bound long waves are no longer preserved. The net measured long wave energy is greater than the bound long wave energy alone. The underprediction of theory relative to measurements in this case is not surprising.

M.A. Dingemans

The explanation of your conclusion that in the 1D-case more long-wave energy is generated than in the directionally-spread case is the following. In the 1D-situation the wave components travel together for a relatively long time and therefore interaction between them can be effective. In the directionally-spread situation the various components are almost immediately out of phase and therefore the interaction between them cannot lead to significant contribution for most cases.

Author's reply I agree.

G. Watson

To what do you attribute the observation that there was little long wave energy propagating away from the beach? Why were the incoming waves not reflected?

Author's reply

The side boundaries of the basin consisted of absorber material but no solid walls. Long wave energy could pass easily through the absorber, but, rather than being reflected back into the basin, it propagated into large, open areas of a wider basin. The open side boundaries are believed to be a major factor in reducing long wave reflections. Subsequent tests with solid side boundaries helped confirm this conclusion.

THE GENERATION OF SURFACE WAVES BY A FREE VORTEX

R.P. Tong and D.H. Peregrine
School of Mathematics, University of Bristol,
University Walk, Bristol BS8 1TW, England.

Introduction

Observations of fluid motions provide many instances where concentrated filaments of vorticity occur in flows which are otherwise largely irrotational. Experiments involving the passage of surface waves over a submerged vertical plate (Skyner(1989)) reveal a variety of behaviours, depending on the wave input, as vortex filaments are shed and meet the surface. The work reported here examines this later stage of the interaction of vortex and free surface by means of an efficient numerical algorithm developed from the boundary-integral method of Dold and Peregrine(1986). In the case of weak vortices, a connection is shown between the analytic solutions of Tyvand(1991) for an impulsively started vortex (valid for small times) and Novikov(1981) for a steady state.

Mathematical Formulation

A semi-infinite fluid domain Ω is defined in two-dimensions, bounded above by a free-surface $\partial\Omega_F$ and below by a horizontal flat bed $\partial\Omega_B$. Cartesian coordinates are chosen with the x-axis in the undisturbed free surface and with the y-axis vertically upwards so that the bed is at y = -h. We consider the motion of an incompressible, inviscid fluid without surface tension, which is irrotational except at the location $\mathbf{x}_v(t) = (x_v(t), y_v(t))$ of a point vortex with fixed counter-clockwise circulation. Under these assumptions the flow field is defined by a scalar velocity potential $\Phi(x,y,t)$ which satisfies the following equations.

$$\nabla^2\Phi = 0 \qquad \text{in } \Omega - \{\mathbf{x}_v\} \qquad (1)$$

$$\frac{D\mathbf{x}}{Dt} = \nabla\Phi \qquad \text{on } \partial\Omega_F, \quad \mathbf{x} = (x,y) \qquad (2)$$

$$\frac{D\Phi}{Dt} = \tfrac{1}{2}|\nabla\Phi|^2 - \frac{y}{Fr^2} \qquad \text{on } \partial\Omega_F \qquad (3)$$

$$\frac{\partial\Phi}{\partial y} = 0 \qquad \text{on } \partial\Omega_B \qquad (4)$$

$$\lim_{|x-x_v|\to\infty} \nabla\Phi = 0 \qquad \mathbf{x} \in \Omega \qquad (5)$$

where $\frac{D}{Dt}$ denotes the material derivative. Lengths are scaled by the

initial depth D of the vortex, velocities by $\frac{\Gamma}{D}$ where Γ is the magnitude of the circulation and time by $\frac{D^2}{\Gamma}$. Results are described in terms of a Froude number F as defined by Tyvand(1991) with $F = \frac{Fr}{2\pi}$, $Fr = \frac{\Gamma}{(gD^3)^{1/2}}$.

The motion of the vortex location is given by Helmholtz' Theorem as

$$\frac{d}{dt}\mathbf{x}_v = \lim_{x \to x_v} \nabla\Phi \qquad (6)$$

The problem specification is completed by an initial condition,

$$y(t=0) = \eta(x) \qquad \text{on } \partial\Omega_F \qquad (7)$$

$$\Phi(x,y,0) = f(x,y) \qquad \text{on } \partial\Omega_F \qquad (8)$$

These equations are solved numerically using a modified form of the boundary-integral algorithm for semi-infinite domain as described by Tanaka et al(1987). The surface position is defined in terms of a real parameter ℓ as $\mathbf{x}(\ell,t) = (x(\ell,t),y(\ell,t))$ and is discretized by choosing integer values of this parameter. The free surface and its associated potential values along with the vortex location can then be integrated forward in time by means of a 5th-order Taylor method giving,

$$u_{n+1} = u_n + \delta t\, T_5(u_n)$$

$$T_5(u) = \frac{Du}{Dt} + \frac{\delta t}{2!}\frac{D^2u}{Dt^2} + \ldots + \frac{\delta t^4}{5!}\frac{D^5u}{Dt^5}$$

where $u = (x(\ell,t),y(\ell,t),\Phi(\ell,t),x_v(t),y_v(t))$, $\ell = 1(1)N$. Equations (2) and (3) enable the components of the Taylor polynomials to be expressed in terms of $\nabla\Phi$ and its time derivatives, since

$$\frac{D\Phi}{Dt} = \tfrac{1}{2}\left|\frac{D\mathbf{x}}{Dt}\right|^2 + \mathbf{x}.\mathbf{j}, \qquad \frac{D^2\Phi}{Dt^2} = \frac{D\mathbf{x}}{Dt}.\left(\frac{D^2\mathbf{x}}{Dt^2} + \mathbf{j}\right),$$

$$\frac{D\mathbf{x}}{Dt} = \nabla\Phi, \qquad \frac{D}{Dt^2}\mathbf{x} = \nabla\Phi_t + \nabla\tfrac{1}{2}|\nabla\Phi|^2,$$

etc.

Using the principle of superposition for the Laplace equation at any particular instant in time, the velocity potential can be defined as

$$\Phi(x,y,t) = \phi^r(x,y,t) + \phi^s(x,y,t)$$

where ϕ^r is regular in the whole of Ω, while ϕ^s has a logarithmic singularity at $\mathbf{x}_v$ which accounts for the point vortex. The terms in the Taylor polynomials can then be computed by the following procedure when the surface position and its associated potential values are known.

(1) A suitable function ϕ^s is chosen which determines ϕ^r on the surface. The derivatives of ϕ^r tangential to the surface are then approximated by polynomial interpolation.

(2) The Cauchy formula is applied in the complex plane to obtain a system of equations for the normal derivatives of ϕ^r, where the contour of integration consists of the discretized interval of the free surface and its reflection in the flat bed. (The extent of the computational domain is chosen so that the contribution from the end segments

necessary to complete the contour can be neglected.) Thus,

$$q(z_p) = \phi^r{}_x|_p - i\,\phi^r{}_y|_p = (\frac{dz_p}{ds})^*(\phi^r{}_s|_p - i\,\phi^r{}_n|_p)$$
$$= \frac{1}{i\pi} PV\int_{\partial\Omega} \frac{q(z_p)}{z - z_p} dz \qquad p = 1(1)N$$

for $z_p \in \partial\Omega$ with s and n denoting tangential and normal derivatives respectively. The surface velocities can then be obtained as

$$\nabla\Phi = \nabla\phi^r + \nabla\phi^s$$

(3) The vortex velocity is given by

$$\frac{d}{dt} x_v = \nabla\phi^r|_{x_v} + \nabla\phi^{s2}|_{x_v}$$

where

$$\phi^{s2} = \phi^s - \frac{\Gamma}{2\pi}\arctan\{\frac{y - y_v}{x - x_v}\}$$

and $\nabla\phi^r|_{x_v}$ is computed by the Cauchy formula.

(4) Steps (1)-(3) are repeated for Φ_t and Φ_{tt} while backward differencing is used for the higher order time derivatives.

The form of ϕ^s has an important effect on the efficiency of the algorithm. If the fluid domain is regarded as being contained within a channel of width 2h, then the singularity of the vortex produces an infinite series of images which leads to the choice,

$$\phi^s(x,y,t) = \phi_1(x,y,t) + \phi_2(x,y,t)$$
$$\phi_1 = \frac{1}{2\pi}\arctan(\coth[s(x - x_v)]\tan[s(y - y_v)])$$
$$\phi_2 = -\frac{1}{2\pi}\arctan(\coth[s(x - x_v)]\tan[s(y + y_v + \frac{2h}{D})])$$
$$s = \frac{\pi D}{4h}$$

This decays exponentially as $|x| \to \infty$ and hence leads to a reduction in the extent of the computational domain when compared with the definition of ϕ^s as the vortex potential plus a single image in the flat bed. Thus, for an impulsively started vortex with $\eta(x) = 0$, $\Phi(x,\eta,0) = 0$, the error resulting from the truncation of the domain at $|x| = 100$ is bounded by 2.6×10^{-6} for the infinite image series at $t = 0$, but by 1.5×10^{-3} for the single image form of ϕ^s.

Results

The motion of an impulsively started vortex with $\frac{h}{D} = 20$ is examined. This can be viewed as an approximation to the infinite depth case since the differences in surface and vortex velocities at $t = 0$ are $O(10^{-4})$. The vortex has an initial velocity $(\dot{x}_v,\dot{y}_v) = (\frac{D}{4h}\mathrm{cosec}(\frac{\pi D}{h}),0)$ and thus moves in a direction opposite to that of a surface wave with the same direction of particle motion (i.e. counter-clockwise). Taking $F = 0.1$ as typical of weak vortices where gravity effects are dominant,

a wave is generated as the motion develops which moves ahead of the vortex. The resulting pressure gradient causes a slowing of the vortex motion until it reverses its horizontal direction. There is close agreement up to this time between the numerical result and the third order analytic solution of Tyvand(1991) for the vortex location (see Fig 1). After turning the vortex produces a second wave moving ahead of it in the opposite direction to the first crest. This process is repeated so that further waves are generated with successive crests travelling in alternate directions, but decreasing in elevation as the vortex approaches a steady state of the type described by Novikov(1981) (Fig 2). The generation of waves is related to the oscillation of the vortex velocity about a steady value which is approximated by replacing the free surface with a rigid wall (Fig 3).

As the Froude number is increased beyond 0.12 the progress towards a steady state is interrupted by surface breaking during the formation of the second crest. For $F > 0.6$ the velocity field of the vortex dominates with the surface being drawn strongly downwards behind it and the computation breaks down due to the increasing surface curvature and accelerations in this region. When $F = 1.5$ the vortex does not slow down but acquires a positive acceleration for the duration of the computation.

The initial condition,

$$\eta(x) = 0, \qquad \Phi^{st} = \phi_1(x,0,0) + \phi_2(x,0,0), \quad s = \frac{\pi D}{2h}$$

which gives the motion of a vortex near a rigid wall, can be regarded as a perturbation of the steady state. The vortex then moves with a velocity that oscillates about a mean value which is close to its initial velocity. For $F < 0.12$, waves are generated in a similar manner to the impulsive start case, but on a smaller scale. For larger Froude numbers surface breaking halts the computation and this takes the form of an overturning wave for values near 0.5 (Fig 4). Such breaking is observed in experiments as well as in corresponding numerical simulations of vortex pairs by Telste(1989), Yu and Tryggvason(1990) and Ohring and Lugt(1991).

Financial support from the Science and Engineering Research Council under grant GR/E65128 is gratefully acknowledged.

REFERENCES

Dold, J.W. and Peregrine, D.H.(1986) An efficient surface-integral algorithm applied to unsteady gravity waves, In: Morton, K.W. and Baines, M.J.(eds) *Numerical Methods for Fluid Dynamics II*, 671-679 Oxford University Press.

Novikov, Y.A.(1981) Generation of surface waves by discrete vortices, *Izv. Atmos. Ocean. Phys.* 17, 709-714.

Ohring, S. and Lugt, H.J.(1991) Interaction of a viscous vortex pair with a free surface, *J. Fluid Mech.* 227, 47-70.

Skyner, D.(1989) private communication.

Tanaka, M., Dold, J.W., Lewy, M. and Peregrine D.H.(1987) Instability and breaking of a solitary wave, *J. Fluid Mech.* 185, 235-248.

Telste, J.G.(1989) Potential flow about two counter-rotating vortices approaching a free surface, *J. Fluid Mech.* 201, 259-278.

Tyvand, P.A.(1991) Motion of a vortex near a free surface, *J. Fluid Mech.* 225, 673-686.

Yu, D. and Tryggvason, G.(1990) The free-surface signature of unsteady, two-dimensional vortex flows, *J. Fluid Mech.* 218, 547-572.

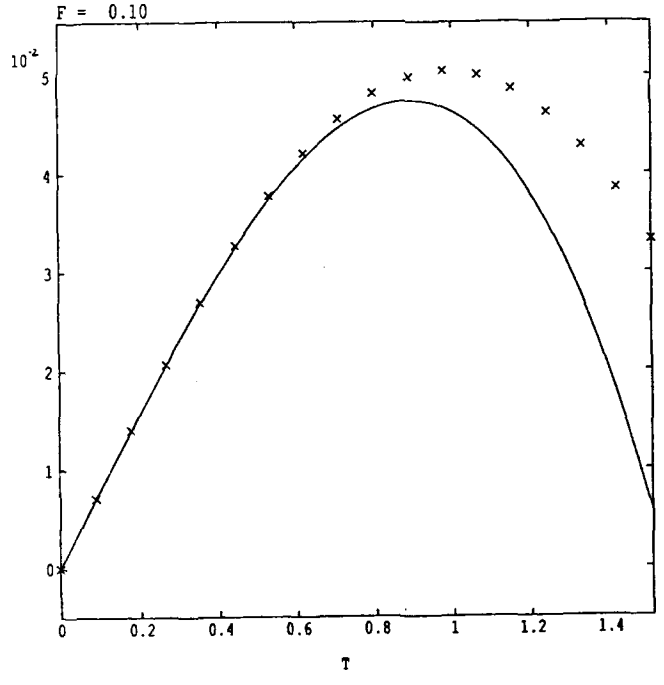

Fig 1 Horizontal displacement of vortex for F = 0.1, $\frac{h}{D}$ = 20 (impulsive start); ——, Tyvand's solution $X(t) = 0.07958t - 0.03326t^3$; × , computed solution.

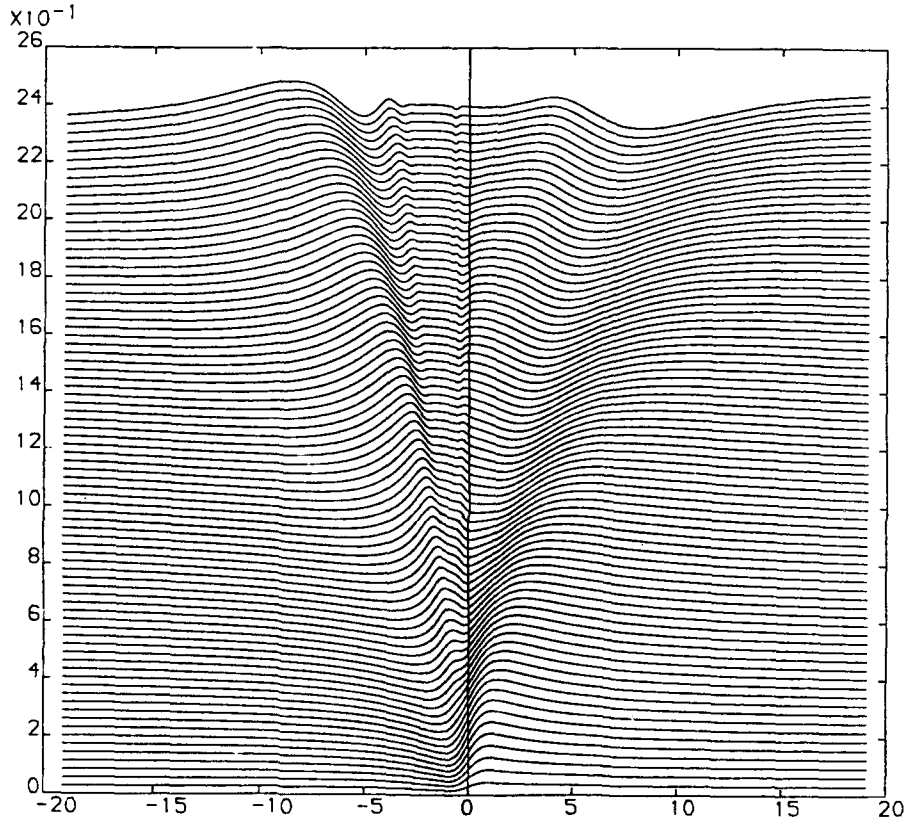

Fig 2 F = 0.1. $\frac{h}{D}$ = 20 (impulsive start); surface profiles for t = 0(0.098)7.11, with vertical exaggeration (length scales on both axes).

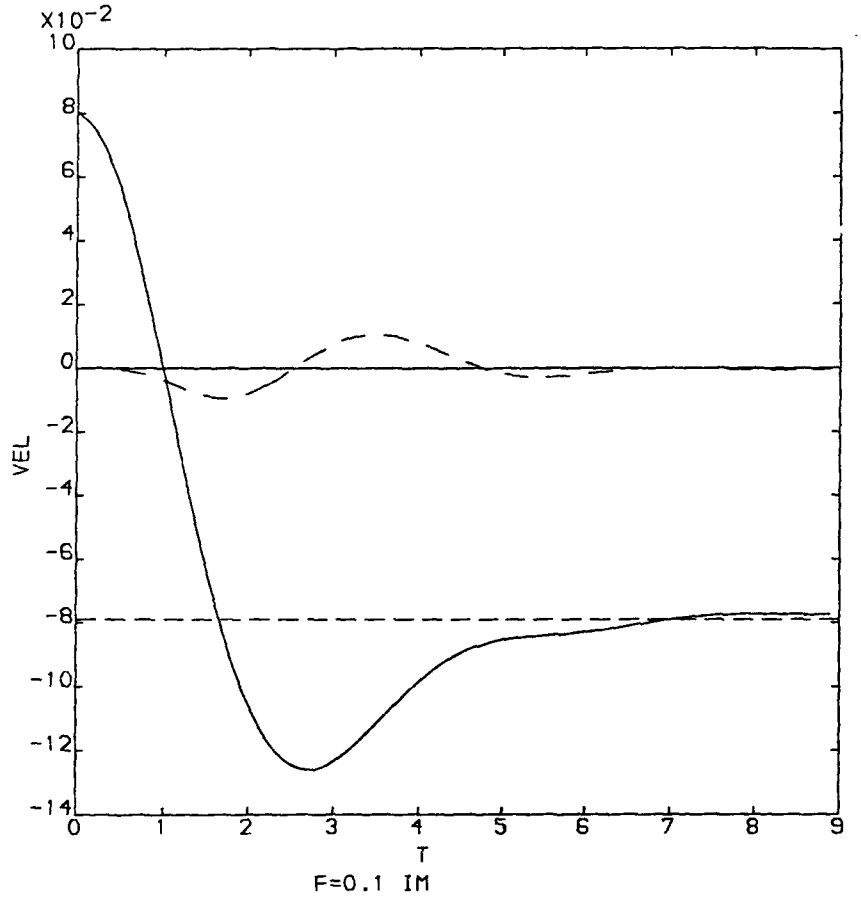

Fig 3 F = 0.1, $\frac{h}{D}$ = 20 (impulsive start); vortex velocity as a function of time; ——, $\dot{x}_v$; — —, $\dot{y}_v$. Rigid wall velocity is (-0.0798,0).

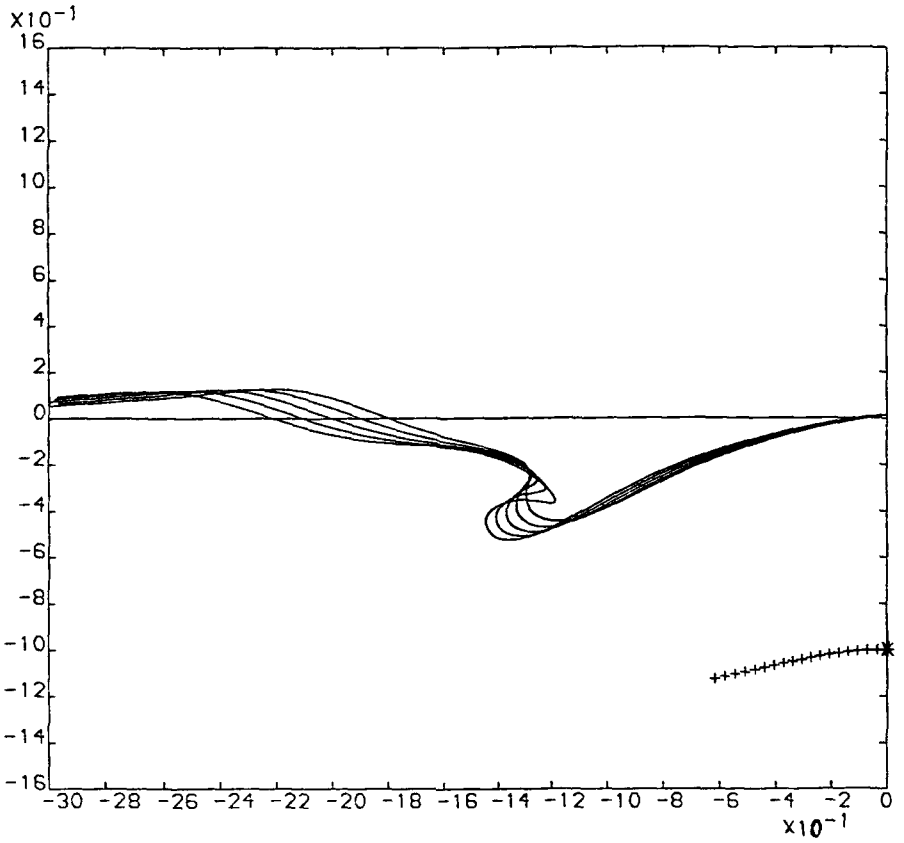

Fig 4 F = 0.5, $\frac{h}{D}$ = 20, initial condition: η = 0, $\Phi = \Phi^{st}$; surface profiles for t = 6.22(0.44)8.0, with vortex trajectory (+) from t = 0 (*).

Discussion of Tong and Peregrine's paper

C.C. Mei (comment)

In a recent doctoral thesis by T.W. Tsai (under Dick Yue), a related numerical theory has been completed. The physical problem is the interaction of the free surface with the vortex sheet generated at the submerged tip of a vertical plate translating at a constant speed parallel to the free surface. Wave breaking is found ahead and behind the plate.

WAVE GENERATION BY GUSTY WIND: A KINETIC THEORY

L.Tsimring, Yu.Troitskaya
Institute of Applied Physics, USSR Academy of Sciences
46 Uljanov str., 603600 N.Novgorod, USSR

Surface wave generation by gusty wind is studied using a kinetic equation for the one-point velocity distribution function in the air $f(\mathbf{r}, \mathbf{v}, \mathbf{t})$ (Lundgren, 1967):

$$\frac{\partial f}{\partial t} + \frac{\partial f}{\partial \mathbf{r}} - \frac{\partial \langle p \rangle}{\partial \mathbf{r}} \frac{\partial f}{\partial \mathbf{v}} = St[f, f_2] \tag{1}$$

where $\langle p \rangle$ is the pressure at the point $\mathbf{r}$ and time t averaged over fluctuations, $St[f, f_2]$ is the "collision" term due to viscosity and pressure fluctuations, and f_2 is a two-point velocity distribution function. The right-hand side of (1) can be estimated as f/τ, where τ is the characterisic time scale of turbulence. If the time scale of external process T (the surface wave period in the present case) is much less than τ, "collisionless" approach can be employed neglecting $St[f, f_2]$. Starting from a homogeneous version of (1), an analog of the Rayleigh equation for the wavy disturbances of vertical velocity in the air w is obtained (Nikolayeva & Tsimring, 1986):

$$a(z)\frac{d}{dz}\left(\frac{1}{b(z)}\frac{d}{dz}\left(\frac{a(z)}{b(z)}w\right)\right) - k^2 w = 0, \tag{2}$$

where

$$a(z) = \int_L \frac{F du}{u - c}, \quad b(z) = \int_L \frac{\partial F/\partial u}{u - c} du,$$

F is an undisturbed velocity distribution function, k and c stand for the wavenumber and phase velocity of the wave component, and L is the real axis u combined with the semicircle of small radius passing under the pole $u = c$.

Using (2) instead of the standard Rayleigh equation one can find a growth rate of surface waves following Miles' (1957) theory. The solution of the boundary value problem for (2) was carried out numerically. It turned out that taking into account large-scale fluctuations of wind velocity allows one to explain the experimentally observed excess of the growth rate of rather long surface waves over values predicted by Miles' theory.

REFERENCES

1. Lundgren,T.S. 1967. Distribution function in the statistical theory of turbulence. Phys.Fluids, v.10, n.5, 969.

2. Miles,J.W. 1957. On the generation of surface waves by shear flows. J.Fluid Mech., v.2, n.5, 185.

3. Nikolayeva,Yu.I. and Tsimring,L.Sh. 1986. Kinetic model of the water wave generation by a turbulent wind. Izvestiya, Atmos.Ocean.Phys., v.22, n.2, 102.

Discussion of Nikolayeva and Tsimring's paper

V.P. Krasitskii

In what sense do you understand a small correction of distribution function? What is the normalization condition of this correction?

Author's reply

The distribution function f is split into two parts: f_0 and f_1. The integration of f and f_0 over u and v are unities, so the normalisation of f_1 is always $\iint_{-\infty}^{\infty} f_1 du dw = 0$.

N. Huang (comment)

I would like to present some experimental results that may offer some comparisons with the two papers (Saffman and Tsimring) on wind wave generation. I have measured wave generation by sudden turn-on of the fan in my tank. The waves generated are in the Kelvin-Helmholtz instability range according to Saffman. The measured phase velocity, however, are that of the free waves plus the Doppler shift. The growth rates of the waves are much higher than predicted by Miles, but they are not uniform. There seems to be several distinct stages: first the saturation of slope, then the growth of elevation and saturation. Can these discrepancies be the results of 1) unsteadiness of the wind and the shear current, 2) sensitivity of the theoretical calculation to the current profile used? and 3) turbulence in the wind?

Three-Dimensional Side-Band Wave Systems And Their Associated Evolution Problems

Marshall P. Tulin and Jiyue J. Li
Ocean Engineering Laboratory
University of California, Santa Barbara

1. Summary

We are interested here in the non-linear evolution for all time of the three-wave resonant system χ, χ^+, χ^-, and other non-linear properties of the wave system. Our major results are: finding the coupled non-linear equations defining the 3 wave side-band system; showing the existence and defining special non-interactive systems; finding 3-d waves of permanent form isolated from the Stokes wave; showing the non-existence of 1-d soliton wave groups; defining initial instability in analytic form; finding recurrent solutions in closed form, dependent on a single parameter; showing the existence of recurrent solutions where the side-bands acquire all of the energy in the original basic wave; finding phase plane solutions and diagrams, which elucidate the system dynamics.

2. Resonant and Near-Resonant Three-Dimensional Wave Systems

Consider a basic wave on deep water with complex amplitude A, wave number k, frequency ω, phase $\chi = kx - \omega t$, where $\omega^2 = gk$. It is perturbed by a pair of 3-d side-bands,

$$\chi^+ = k(1+p)\,x + kq\,z - \Omega^+ t, \quad \chi^- = k(1-p)\,x - kq\,z - \Omega^- t, \tag{2.1}$$

where
$$\Omega^{+2} = \omega^2\,[(1+p)^2 + q^2]^{1/2}, \quad \Omega^{-2} = \omega^2\,[(1-p)^2 + q^2]^{1/2} \tag{2.2}$$

The dimensionless perturbation wave numbers (p, q) need not necessarily be small. The side bands are resonant or near resonant with the second-harmonics of the basic wave since

$$\chi^+ + \chi^- = 2\chi + \Delta\omega\, t \tag{2.3}$$

where $\Delta\omega = 2\omega - (\Omega^+ + \Omega^-)$ is of $O(ak)^2$. It is given by,

$$\Delta\omega = \{2 - [(1+p)^2 + q^2]^{1/4} - [(1-p)^2 + q^2]^{1/4}\}\,\omega \tag{2.4}$$

It is called the detuning parameter and accounts both for corrections to the dispersion relation of $O(ak)^2$ and for slightly off-resonant systems. We shall later emphasize small (p, q) for which $\Delta\omega/\omega \equiv p^2/4 - q^2/2$. The exact resonance ($\Delta\omega = 0$) corresponds to Phillips'(1960) figure 8 in the (p, q) plane.

The side bands defined here were shown (first) by Benjamin-Feir (1967) to lead to the initial instability of the basic wave. The consideration above can be easily generalized to the case of resonance with higher harmonics of the basic (Stokes) wave, leading to the generalized Class I and II instabilities of McLean et al (1981). However, the side-band system resonant

with the second harmonic is the most rapidly growing for low wave steepness such as exists in the ocean, and is thus of particular interest.

3. Evolution Equations for Near-Resonant Three-Wave Systems

The free surface condition of constant pressure (surface tension neglected) and the kinematic condition are expressed to third order in the small parameter, $\varepsilon = (ak)$, leading to differential relations for ϕ and η to be satisfied upon the surface $y = 0$, where ϕ is a harmonic wave function (invicid flow) and η the wave train. Utilizing multi-scale perturbation analysis the resulting solutions for η and ϕ, to the second order, ε^2, are found to be

$$\eta = \frac{1}{2} A_j e^{i\chi_j} + i \frac{1}{2\omega_j} \frac{\partial A_j}{\partial t} e^{i\chi_j} + \frac{1}{4} \Gamma_{ij} \sqrt{K_i K_j}\, A_i A_j e^{i(\chi_i+\chi_j)} + \frac{1}{8} \tilde{\Gamma}_{ij} \sqrt{K_i K_j}\, A_i \overline{A_j} e^{i(\chi_i-\chi_j)} + c.c. \tag{3.1}$$

$$\phi = \frac{1}{2} \phi_{10} - i \frac{\omega_j}{2K_j} A_j e^{i\chi_j + K_j y} + i \frac{1}{4} G_{ij} \sqrt{\omega_i \omega_j}\, A_i A_j e^{i(\chi_i+\chi_j)+\sqrt{(K_1^m+K_2^m)^2+(K_1^z+K_2^z)^2}\, y}$$
$$+ \frac{1}{2} \phi_{20} + y \frac{\partial A_j}{\partial t} e^{i\chi_j + K_j y} + i \frac{1}{8} \tilde{G}_{ij} \sqrt{\omega_i \omega_j}\, A_i \overline{A_j} e^{i(\chi_i-\chi_j)+\sqrt{(K_1^m-K_2^m)^2+(K_1^z-K_2^z)^2}\, y} + c.c. \tag{3.2}$$

where index (i, j) takes the values 0, 1, 2 and represents the wave modes; and index (m, n) takes the values 1, 2 and represents the two directions (x, z). The complex wave amplitudes $A_0=A$, $A_1=B^+$, $A_2=B^-$, for the basic wave (A) and two side bands (B^+, B^-), and the potential (and harmonic) flow ϕ_{10} are slowly varying functions of x_1, z_1, t_1, and the harmonic flow ϕ_{20} is a slowly varying function of x_2, z_2, t_2. These slowly varying flows are introduced into the analysis for the sake of generality, and we retain them for the same reason. They need satisfy boundary conditions at $y = 0$: $(\phi_{10})_y = 0$; $g\varepsilon(\phi_{20})_y + (\phi_{10})_{tt} = 0$. The flow (ϕ_{10}) represents the effect of a slowly varying current at the surface, such as might be generated by an internal wave. This flow can generate doppler frequency changes and energy exchange due to interactions between the current and the waves. We include ϕ_{10} in (3.3) but not thereafter.

The analysis to order ε^3 yields a compatibility condition consisting of three coupled non-linear PDE's of parabolic type, yielding A, B^+, B^-,

$$\frac{\partial A_r}{\partial t} + \alpha^r_m \frac{\partial A_r}{\partial x_m} = i \frac{\beta^r_{mn}}{2} \frac{\partial^2 A_r}{\partial x_m \partial x_n} - i\, A_r \nabla(\phi_{10}) \cdot K_r - i\, \omega_r K_r^2 [C^r_j A_r |A_j|^2 + D^r_{jk} e^{i\alpha_r \Delta\omega t} \overline{A_j} A_j A_k] \tag{3.3}$$

where summation is not intended over index r = 0, 1, 2. The group velocity vectors α^r_m and the dispersion tensors β^r_{mn} are defined in terms of the linear dispersion relations for deep water,

$$\alpha^r_m = \partial\omega_r/\partial K_m; \quad \beta^r_{mn} = \partial^2 \omega_r/\partial K_m \partial K_n; \quad K_0 = k\,[1, 0]; \quad K_1 = k\,[1+p, q]; \quad K_2 = k\,[1-p, -q].$$

The coefficients Γ_{ij}, G_{ij}, C^r_j, D^r_{ijk} and α_r in (3.1) - (3.3) are functions of p, q and of order one; the coefficients with tildes in (3.1) - (3.2) have zero diagonals.

These three parabolic equations govern the temporal and spatial modulation of the amplitudes and phases of the interacting basic wave and its three-dimensional side bands for near resonant systems. Coupled equations of this general type were first derived for general dispersive systems by Benny & Newell (1967), but have not been applied to side band resonant systems. The evolution equation, (3.3), reduces to the usual NLS equation on deep water for a single wave train (Benny & Newell (1967), Zakharov (1968), Davey & Stewartson (1974)) when the side band amplitudes disappear. See the review, Yuen & Lake (1982).

4. Non-Interactive Finite Waves

The evolution equations possess isolated stable equilibrium points which correspond to non-interactive side band systems in the physical space. If

$$A = a\, e^{i\theta}, \quad B^+ = b^+ e^{i\theta^+}, \quad B^- = b^- e^{i\theta^-}, \quad \text{and} \quad \gamma = 2\theta - \theta^+ - \theta^- - \Delta\omega t \tag{4.1}$$

then for the existence of these non - interactive systems, a_0, b_0^+, $b_0^- \approx$ constant, (3.3) requires,

$$\gamma_0 \equiv \theta_0^+ + \theta_0^- - 2\theta_0 = n\pi, \quad n = 0, 1, 2, \cdots$$

$$[C_0^{b^+} + C_0^{b^-} - 1]\,(ka)^2 - [2C_1^{a} - \frac{1}{2} - C_1^{b^+}]\,(kb^+)^2 - [2C_2^{a} - C_2^{b^+} - \frac{1}{2}]\,(kb^-)^2$$
$$+ (-1)^n [C_3^{b^+} \frac{b^-}{b^+} + C_3^{b^-} \frac{b^+}{b^-} - 2C_3^{a} \frac{b^+ b^-}{a^2}]\,(ka)^2 = \frac{\Delta\omega}{\omega} \tag{4.2}$$

The Stokes wave is recovered when the side band amplitudes disappear, where (4.2) simply represents the order ε^2 correction to the the dispersion relation. With side bands, the two sets of non-interactive solutions ($\gamma = 0, \pi$) represent special wave combinations, both 2 and 3-d, each component separately propagating without change of form, and of which the Stokes wave is a degenerate example. For each set (n = 0, 1) solutions exist dependent continuously on (p, q), (ka_0), and b_0^+/b_0^-. For each independent solution, each component follows a nonlinear dispersion relation coupled to the other two modes:

$$\omega_n = \omega\,[1 + \frac{1}{2}(ka)^2 + C_1^{a}(kb^+)^2 + C_2^{a}(kb^-)^2 + (-1)^n C_3^{a}(kb^+)(kb^-)]$$
$$\Omega_n^+ = \Omega^+\,[1 + C_0^{b^+}(ka)^2 + \frac{1}{2}K^{+2}b^{+2} + C_2^{b^+}(kb^-)^2 + (-1)^n C_3^{b^+}(ka)^2 \frac{b^-}{b^+}]$$
$$\Omega_n^- = \Omega^-\,[1 + C_0^{b^-}(ka)^2 + C_1^{b^-}(kb^+)^2 + \frac{1}{2}K^{-2}b^{-2} + (-1)^n C_3^{b^-}(ka)^2 \frac{b^+}{b^-}] \tag{4.3}$$

It can be shown with the aid of the temporal evolution equations that these non-interactive wave systems are stable. In the examples illustrated in Fig 1. these systems correspond to the limit points P_0, P_π. They are surrounded by closed orbits and can not be reached through the evolution of other resonant systems growing from the infinitesimal side bands.

The waves corresponding to (4.2) do not posses symmetry with respect to the x direction (i.e. they are skewed). Symmetrical 3-d wave forms of non-interactive nature can probably

also be generated in the same way by adding two more resonant side bands to (2.2), corresponding to $K_3/k = [1+p, -q]$ and $K_4/k = [1-p, +q]$, respectively.

5. Finite 3-d Waves of Permanent Form

The bifurcation of finite Stokes waves into three-dimensional permanent forms involving side-bands was discovered by Saffman & Yuen (1980). They have shown that these bifurcations exist only for sufficiently large (critical) steepness of the basic wave. In contrast, here we find 3-d waves of permanent form without a critical value of the basic wave steepness, but which require that one of the side bands be larger than the amplitude of the basic wave. These solutions can not therefore be reached through bifurcation of the Stokes wave. The analysis here is restricted to small values of (p, q).

In the special case where the phase speeds of the non-interactive components are identical, the resulting skew wave is of permanent form. This requires ($C = C^+ = C^-$),

$$\omega_n/k = \Omega_n^+/k(1+p) = \Omega_n^-/k(1-p) \tag{5.1}$$

To order (p^2, q^2) and using (4.3), this leads to, $b^+b^- = -a^2\cos\gamma$, so that waves of permanent form can only exist for $\gamma = \pi$ (n = 1). Then, (5.1) becomes (and (4.2) is also satisfied):

$$2(b^+/a)^2 = (3 - 2\Delta) +/- \sqrt{(3-2\Delta)^2 - 4}, \quad 2(b^-/a)^2 = (3 - 2\Delta) -/+ \sqrt{(3-2\Delta)^2 - 4}, \tag{5.2}$$

where $\Delta = \dfrac{\Delta\omega/\omega}{2(ak)^2} \cong [p^2/4 - q^2/2] / 2(ka)^2$ (5.3)

In order for (5.2) to be satisfied, $\Delta \le 1/2$. (5.4)

In view of inequality (5.4), one of the two side bands must always be large than the basic wave, b (larger) > a, so that these permanent wave solutions are isolated from the 2-d Stokes waves. As in the case of all non-interactive systems they are stable, and are equilibria of center type in the phase diagram.

6. The Non-Existence of Soliton Wave Groups

If wave group behavior is approximated by a simple NLS equation, then a solution exists of the form, $A = a\, e^{i\omega t}\,\mathrm{sech}\,(\beta X)$. Do similar soliton solutions exist for the coupled system described by (2.3)? The equations (3.3) do permit soliton solutions propagating in the direction, $X = (n_1, n_2)\cdot(x_1, x_2)$, with the speed, c^*, of the form, $A_j = r_j e^{i\omega_j t}\,\mathrm{sech}\,[\beta(X - c^* t)]$, dependent on the condition:

$$(1 \pm p) - (\Omega^*/\omega)^3]\, n_1 \pm q\, n_2 = 0 \tag{6.1}$$

It can be shown, however, that for small (p, q) no non-trivial solutions of (6.1) exist. Therefore, in contrast to the single degree of freedom of calculation, the coupled side-band equations do not permit soliton solutions of one-dimensional form. This leaves open the question as to whether two-dimensional solitons exist.

7. Initial Instabilities of the Basic Wave

The initial instability of a basic wave to infinitesimal resonant side-band disturbances has been previously investigated by Benjamin & Feir (1967) [small (a_0k); 2-d]; Longuet-Higgins (1978) [large (a_0k), 2-d]; Crawford, et al (1981) and McLean, et al (1981) [small and large (a_0k), 2 and 3-d]. The latter three investigators utilized numerical computations based on eigenvalue analysis, or the Zakharov equation (Crawford, et al). Here we confirm and extend their work, utilizing analytical formulae based on the specialization of (3.3) to the spatially uniform case. The resulting governing equations are of simple form,

$$a_t = - C_3^a \omega k^2 a b^+ b^- \sin\gamma, \quad b_t^+ = C_3^{b^+} \omega k^2 a^2 b^- \sin\gamma, \quad b_t^- = C_3^{b^-} \omega k^2 a^2 b^+ \sin\gamma, \tag{7.1}$$

$$\gamma_t = \omega \left[- \frac{\Delta\omega}{\omega} + (C_0^{b^+} + C_0^{b^-} - 1)(ka)^2 + \left(\frac{1}{2} \frac{\Omega^+}{\omega} \frac{K^{+2}}{k^2} + C_1^{b^-} - 2C_1^a \right)(kb^+)^2 \right.$$
$$\left. + \left(C_2^{b^+} + \frac{1}{2} \frac{\Omega^-}{\omega} \frac{K^{-2}}{k^2} - 2C_2^a\right)(kb^-)^2 \right] + \omega \left[\left(C_3^{b^+} \frac{b^-}{b^+} + C_3^{b^-} \frac{b^+}{b^-}\right)(ka)^2 - 2C_3^a (kb^+)(kb^-) \right] \cos\gamma \tag{7.2}$$

The side band growth rate, $\rho = \sqrt{C_3^{b^+} C_3^{b^-}}\,(ak)^2 \sin\gamma$, resulting from linearized (7.1) - (7.2), is positive all cases, providing $\sin\gamma_0 > 0$, indicating initial instability. However, rapid changes in γ (demodulation), leading to a reversal of initial growth can occur, and it then prevents substantial net growth of the side band disturbances. There exists a region, though, in which the initial rate of change of γ can be zero, and in this region we later verify that small side-band disturbances grow and achieve amplifications comparable to the basic wave. That region follows from (7.2) when $(\gamma_t)_0 = 0$,

$$\left| \frac{(\Delta\omega/\omega)}{(ka)^2} - (C_0^{b^+} + C_0^{b^-} - 1) \right| < 2\sqrt{C_3^{b^+} C_3^{b^-}} \qquad 0 < \Delta < \left[1 - \frac{p^2}{\sqrt{p^2+q^2}}\right] \tag{7.3}$$

where the left column is exact, and the right is correct to O(p,q); and Δ is defined by (5.3). Within this region there is a locus corresponding to the condition of maximum growth rate, i.e. $\sin\gamma = 1$. This region locus is determined from (7.2) for $(\gamma_t)_0 = \cos\gamma_0 = 0$,

$$\frac{\Delta\omega}{\omega} = (C_0^{b^+} + C_0^{b^-} - 1)(ka)^2 \qquad \Delta = \frac{1}{2}\left[1 - \frac{p^2}{\sqrt{p^2+q^2}}\right] \tag{7.4}$$

The maximum growth rate on the locus (7.4) is, for small (p, q), simply,

$$\rho = \frac{1}{2}\left[1 - \frac{p^2}{\sqrt{p^2+q^2}}\right](ak)^2 \tag{7.5}$$

These relations (7.4) - (7.5) show that for small wave steepness (ak), the side band instability (corresponding to class I resonance) is likely initially 2-d in nature.

The analytical results presented, (7.3) - (7.5), are in excellent agreement with the numerical results of Longuet-Higgins (1978) and McLean (1982) for small (ak) and suitably small (p,q).

8. Temporal Long-Time Evolution of Small Side-Band Disturbances

The equations (7.1) - (7.2) admit three first integrals (the first on the left is energy),

$$s^2 + (s_1)^2 + (s_2)^2 = E,\ (s_2)^2 - (s_1)^2 = F,\ s^2 s_1 s_2 \cos\gamma + \Delta s^2 - \frac{1}{2} h_0 s^4 - h_1 s_1^4 - h_2 s_2^4 = G \qquad (8.1)$$

where $s_j = a_j/a_0$; $\Delta = [\Delta\omega/\omega]/[2(ka_0)^2]$; $h_0 = 1/2$, $h_1 = h_2 = 1/4$; correct to O(p, q). How do those initially small sidebands vary over very large times? The answer lies in the solution of the following temporal evolution equation for s, (8.2), which is based on the reduction of (7.1) utilizing (8.1); small (p, q) and $(s_{1,2})_0 << 1$ are assumed,

$$(dQ/d\tau)^2 = (7/64)\,[Q - Q_1]\,[Q - Q_2]\,[Q - Q_3]\,[Q - Q_4] \qquad (8.2)$$

where $Q = 1 - s^2$, $\tau = 2\,(ka_0)^2\,\omega t$; $Q_1 = (8/7)(1-\Delta)+d_1$, $Q_2 = 8\Delta+d_2$, $Q_3 = d_3$, $Q_4 = d_4$, and where d_j are functions of $(s_1)_0$, $(s_2)_0$ and are $O[(s_{1,2})_0]^2 << 1$.

The solutions of (8.2) were found exactly in terms of Jacobian elliptic functions of first kind, dependent on the numerical value of Δ. The behaviors of the solution Q with time, τ, varies in different ranges of Δ,

range of Δ:	$\Delta < 0$;	$0 < \Delta < 1/8$;	$1/8 < \Delta < 1$;	$\Delta > 1$.
variation of Q:	$0 \Leftrightarrow Q_3$;	$0 \Leftrightarrow Q_2$;	$0 \Leftrightarrow Q_1$;	$0 \Leftrightarrow Q_3$.

As a result, the variation of Q is small except in the middle ranges $0 < \Delta < 1$, and it reaches a maximum, approximately Q = 1, for $\Delta = 1/8$. It is interesting that the latter condition for maximum side-band growth does not correspond to the condition, $\Delta = 1/2$, for maximum initial rate of growth. Recurrent (periodic) solutions are found, with the maximum amplitude reached by the side bands, (b_{max}/a_0), and the recurrence time, T, dependent on Δ. Examples from the solutions are (equal sideband disturbances; $\gamma_0 = \pi/2$),

Δ	b_{max}/a_0	$(ka_0)\,\omega T$
1/2	0.53	$4 \ln [2/\sqrt{3}(s_1)_0]$
1/8	0.707	$(8/\sqrt{7}) \ln [(7/8)^3 / (3(s_1)_0^3)^2]$

The recurrence times can be very large, and vary inversely with the log of the initial side-band amplitudes. The results obtained here are in general agreement with the earlier research of Bryant (1979) and Stiassnie & Kroszynski (1982).

9. Global Evolution in the Phase Plane

In the case of equal side bands, solution loci for arbitrary initial conditions may be readily determined in the phase plane (ξ, ζ), where

$$\xi = \frac{s}{\sqrt{E}} \cos\frac{\gamma}{2} \qquad \zeta = \frac{s}{\sqrt{E}} \sin\frac{\gamma}{2} \qquad (9.1)$$

Utilizing the energy integral, (8.1), the temporal equations (7.1) - (7.2) may be combined to produce coupled equations for ξ, ζ, denoting $\Delta^* = \Delta/E$,

$$\frac{d\xi}{d\tau} = -\frac{E}{8}\zeta(1 - 4\Delta^* + 3\xi^2 - \zeta^2); \quad \frac{d\zeta}{d\tau} = -\frac{E}{8}\xi(3 + 4\Delta^* - 7\xi^2 - 3\zeta^2) \tag{9.2}$$

This system is similar to that of Rabinovich & Fabrikant (1979) describing the modulation decay of a pair of quanta in a non-equilibrium state. Since the problem here involves only a conservative system with two dimensionality, the possibility for chaotic motion is excluded. As they showed, however, when dissipation or forcing effects are taken into account in the side band systems, some dramatic changes can occur in their qualitative behavior, such as the existence of non-elementary attractors.

System (9.2) has 4 sets of equilibrium points and a closed orbit, {C}, depending on Δ^*:

$$O = (0, 0), \qquad \{C\}: \ \xi^2 + \zeta^2 = 1, \tag{9.3}$$

The first above (origin), corresponds to disappearance of the basic wave, and the second (the unit circle) corresponds to vanishing side bands.

$$P_0 = (\pm\sqrt{(3+4\Delta^*)/7}, 0), \qquad P_\pi = (0, \pm\sqrt{1 - 4\Delta^*}), \tag{9.4}$$

These (9.4) correspond to non-interactive solutions, for $\gamma = 0, \pi$ $(n = 0, 1)$, respectively.

$$P_s = (\pm\sqrt{\Delta^*}, \pm\sqrt{1 - \Delta^*}) \tag{9.5}$$

These saddle points, (9.5), determine the location of the important loci, Γ, which divides the phase plane and penetrates through P_s into the interior.

A qualitative picture of phase trajectories is shown in Figure 1.

In the case of vanishing small initial side-band disturbances, $E = 1 + 2\,s_{1_0}^2 \equiv 1$, these solutions must begin just inside the unit circle. It can then be seen that large excursions from the boundary require the existence of the loci Γ, and this is possible for $0 < \Delta < 1$, consistent with the conclusions of linear stability theory, eqn (7.3). The excursions are seen to increase as $\Delta \to 1/8$ where infinitesimal side bands may grow and reach the neighborhood of the origin, and thus acquire almost all of the energy in the basic wave.

In the case of side-bands of a given substantial energy ($E > 1$), the solution can begin anywhere on an circle lying substantially within {C}. It is easy to see, then, that closed orbit solutions around the equilibrium points P_0 and P_π may take place. For particular values of initial sideband energy and phase ($\gamma = 0$ or π), non-interactive solutions exist at the points P_0 ($-3/4 < \Delta^* < 1$) or P_π ($0 < \Delta^* < 1/4$).

For suitably small or large value: $\Delta^* < -3/4$, or $\Delta^* > 1$, no large interactions may be expected beginning from any initial conditions ($b^+ = b^-$). However, there does exist an intermediate region, $-3/4 < \Delta^* < 0$, within which suitably large initial disturbances can undergo large exchanges.

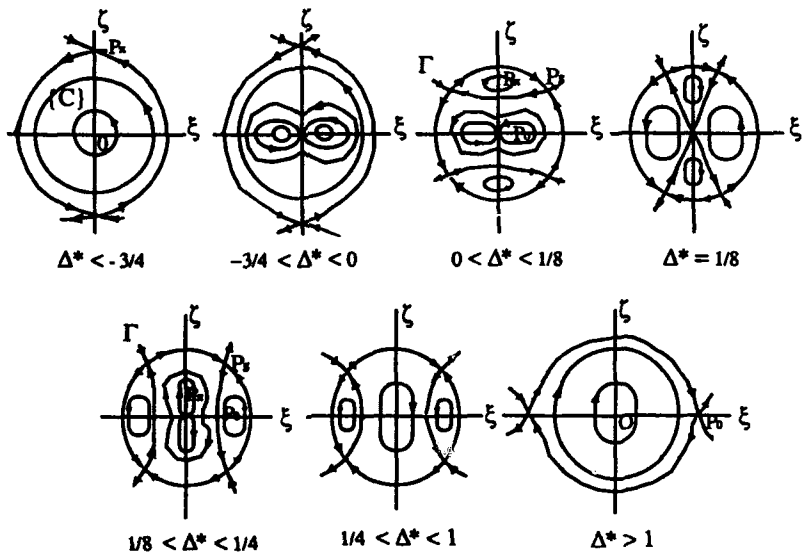

Figure 1. Qualitative phase trajectories for the side-band systems

References

Benjamin, T.B.; Feir, J.E. 1967. The disintegration of wavetrains on deep water. Part 1. Theory. J. Fluid Mech., 27: 417-430.

Benney, D.J.; Newell, A.C. 1967. The propagation of nonlinear wave envelopes. J. Math. Phys. 46: 133-139.

Bryant, P.J. 1979. Nonlinear wave groups in deep water. Stud. Appl. Math. 61: 1-30.

Crawford, D.R. et al. 1981. Stability of weakly nonlinear deep-water waves in two and three dimensions. J. Fluid Mech. 105: 177-192.

Davey, A.; Stewartson, K. 1974. On three-dimensional packets of surface waves. Proc. R. Soc. Lond. A338: 101-110.

Longuet-Higgins, M.S. 1978. The instabilities of gravity waves of finite amplitude in deep water. I.Super-harmonics; II.Sub-harmonics. Proc. R. Soc. Lond. A360: 471-505.

McLean, J.W. et al. 1981. Three dimensional instability of finite amplitude water waves. Phys. Rev. Letters, 46: 817-820.

McLean, J.W. 1982. Instabilities of finite-amplitude water waves. J. Fluid Mech. 114: 315-330.

Phillips, O.M. 1960. On the dynamics of unsteady gravity waves of finite amplitude. Part 1. The elementary interactions. J. Fluid Mech. 9: 193-217.

Rabinovich, M.I.; Fabrikant, A.L. (1979). Stochastic self-modulation of waves in nonequilibrium media. Sov. Phys. JETP 50(2): 311-317.

Saffman, P.G.; Yuen, H.C. 1980. A new type of three-dimensional deep-water wave of permanent form. J. Fluid Mech. 101: 797-808.

Stiassnie, M.; Kroszynski, U.I. 1982. Long-time evolution of an unstable water-wave train. J. Fluid Mech. 116: 207-225.

Yuen, H.C.; Lake, B.M. 1982. Nonlinear dynamics of deep-water gravity waves. Advances in Applied Mechanics, 22: 67-229.

Zakharov, V.E. 1968. Stability of periodic waves of finite amplitude on the surface of a deep fluid. PMTF. 9(2): 86-94. / J. Appl. Mech. Tech. Phys. 9(2): 190-194.

Discussion of Tulin and Jiyue's paper

M. Stiassnie

I suggest to combine the ideas presented by Dr. Kartashova (which discussed the possibility for nonlinear-interactions between discretised spectral modes on a rectangular grid) with Prof. Tulin's results for the evolution of "wave packets" (centred at those grid-points) to improve the study of the evolution of broad spectra.

Author's reply

This is a very interesting idea, which would require working out appropriate evolution equations for the boundary conditions being considered.

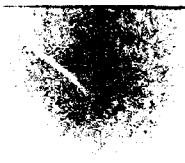

The effect of short ening of waves on random currents

A.G.Voronovich

P.P.Shirshov Institute of Oceanology,
Krasikova 23,Moscow, 117218, USSR

When wavetrain propagates on variable in space and time currents its parameters change. If linear and time scales of currents exceed significantly the period and wave length of the wavetrain this process can be described in geometrical optics approximation. In this paper the evolution of the wavenumber of the train is considered for the case of random currents.

Suppose that in the media at rest the dispersion relation is $\omega = \omega_0(k)$. Then for moving media it takes the form

$$\omega - \underline{k}\underline{U} = \omega_0(k) \tag{1}$$

where $\underline{U}$ is current's velocity. Geometrical optics description means introduction of the phase S with frequency and wave-vector given by the relations $\omega = -\partial S/\partial t$, $\underline{k} = \underline{\nabla} S$. As a result (1) gives the following equation (Hamilton-Jacoby's):

$$\frac{\partial S}{\partial t} + U_i(\underline{x},t)\frac{\partial S}{\partial x_i} + \omega_0(|\nabla S|) = 0 \tag{2}$$

The evolution of coordinates and wavevector of the train is governed by the corresponding Hamilton's equations

$$\frac{dx_i}{dt} = \frac{\partial H}{\partial k_i} = U_i(\underline{x},t) + \omega_0'(k)\frac{k_i}{k}$$

$$\frac{dk_i}{dt} = -\frac{\partial H}{\partial x_i} = -k_\alpha \frac{\partial U_\alpha}{\partial x_i} \tag{3}$$

(summing up over repeating indexes is supposed throughout the paper).

Suppose that $\underline{U}(\underline{x},t)$ is a gaussian random field and τ_0 is ty-

pical correlation time. Assume that during this time interval the parameters of the wavetrain undergo only small changes. Then one can apply for stochastic equations (3) the approximations of the δ-correlated process. In this case the equation for probability density function arises. For arbitrary set of equations

$$\frac{d\xi_i}{dt} = v_i(\underline{\xi},t) + f_i(\underline{\xi},t)$$

with v_i - deterministic and f_i - stochastic functions ($\bar{f}_i = 0$) this equation has the form [1] :

$$\frac{\partial}{\partial t} P(y,t) + \frac{\partial}{\partial y_k} ([v_k(\underline{y},t) + A_k(\underline{y},t)]P) = \frac{\partial^2}{\partial y_k \partial y_l} [F_{kl}(\underline{y},\underline{y},t)P] \quad (4)$$

Here

$$F_{kl}(\underline{y},\underline{y}',t) = \frac{1}{2}\int_{-\infty}^{+\infty} dt' \; \overline{f_k(y,t)\, f_l(y',t')}$$

and

$$A_k = \frac{\partial}{\partial y_l} F_{kl}(y,y',t)\Big|_{y'=y}$$

We have in our case $\underline{\xi} = \underline{y} = (\underline{x},\underline{k})$. Assume space homogeneity and mirror symmetry of the statistics of the currents. If only probabilistic distribution with respect to wavenumbers is of interest one can integrate (4) over x - coordinates. As a result in our case for probability density

$$P(\underline{k},t) = \int P(\underline{x},\underline{k},t)\, d\underline{x}$$

the following equation arises:

$$\frac{\partial P}{\partial t} + \frac{\partial}{\partial k_i} (c_{\alpha i,\beta\alpha}\, k_\beta P) = \frac{\partial^2}{\partial k_i \partial k_j} (c_{\alpha i,\beta j} k_\alpha k_\beta P) \quad (5)$$

with constants $c_{\alpha i,\beta j}$ given by the formula

$$c_{\alpha i,\beta j} = \frac{1}{2}\int_{-\infty}^{+\infty} \overline{\frac{\partial v_\alpha(\underline{x},t)}{\partial x_i} \; \frac{\partial v_\beta(\underline{x},t')}{\partial x_j}}\, dt'$$

Mention that (5) doesn't depend upon dispersion low $\omega = \omega_0(k)$.

Consider now potential currents: $\underline{U} = \nabla\varphi$. Representing the random field φ as

$$\varphi(\underline{x},t) = \int [\hat{\varphi}(\underline{k},\omega)\, e^{i\underline{k}\underline{x}-i\omega t} + \hat{\varphi}^*(\underline{k},\omega)\, e^{-i\underline{k}\underline{x}+i\omega t}]\, d\underline{k}d\omega$$

with

$$\overline{\hat{\varphi}(\underline{k},\omega)\,\hat{\varphi}^*(k',\omega')} = \frac{1}{2\pi}\Phi(\underline{k},\omega)\delta(\underline{k}-\underline{k}')\,\delta(\omega-\omega')$$

we obtain

$$c_{i\alpha,j\beta} = \int \Phi(\underline{k},0)\, k_i k_\alpha k_j k_\beta d\underline{k}$$

Multiplying (5) by k_m and integrating over $\underline{k}$ one comes to the following equation for the first moments of wavenumber $\bar{k}_m$:

$$\bar{k}_m = \int P(\underline{k},t)\, k_m d\underline{k} \qquad \frac{\partial \bar{k}_m}{\partial t} - c_{\alpha m,\beta\alpha}\,\bar{k}_\beta = 0$$

It can be easily seen that the matrix of this linear set is positively determined, as for arbitrary real numbers q_m we have

$$c_{\alpha m,\beta\alpha}\, q_m\, q_\beta = \int (q_m k_m)^2 k^2 \Phi(\underline{k},0)\, d\underline{k} > 0$$

Consequently all $\bar{k}_m$ exponentially grow with time.

Assume now additionally isotropy of the random field φ and consider 2D case. Then (5) transforms to the following equation for one-dimensional distribution function $\tilde{P}(k,t) = 2\pi k P(k,t)$:

$$\frac{1}{\Omega_0}\frac{\partial \tilde{P}}{\partial t} = \left(k^2\frac{\partial^2}{\partial k^2} + \frac{7}{3}k\frac{\partial}{\partial k} + \frac{1}{3}\right)\tilde{P}$$

with

$$\Omega_0 = \frac{3\pi}{4}\int_0^\infty \Phi(k,0)\, k^5 dk$$

The solution of this equation with the initial condition $\tilde{P}(k,0) = \delta(k-k_0)$ is

$$\tilde{P}(\underline{k},t) = \frac{1}{2k_0}\,(\pi\Omega_0 t)^{-1/2}\,\exp\left(\frac{\Omega_0 t}{3} - \frac{(\ln(k/k_0)+4\Omega_0 t/3)^2}{4\Omega_0 t}\right) \qquad (7)$$

or in the other form

$$\tilde{P}(k,t) = \frac{1}{2k_0}\,(\pi\Omega_0 t)^{-1/2}\exp\left(-\frac{\Omega_0 t}{9} - \frac{1}{4\Omega_0 t}\left(\ln\frac{k}{k_0}\right)^2\right)\left(\frac{k}{k_0}\right)^{-2/3} \qquad (8)$$

The expression for the n-th moment of wavenumber

$$\bar{k}^n = \int_0^\infty \tilde{P}(k,t)\,k^n dk$$

follows immediately from (7):

$$\bar{k}^n = k_0^n \exp\,[n(n + 2/3)\,\Omega_0 t]$$

Thus for all integer n $\bar{k}^n$ exponentially grows with time.

One can conclude from (8) that for large t distribution function $\tilde{P}$ tends to $\tilde{P}\sim k^{-2/3}$ for intermediate values of k: $\exp(-\sqrt{\Omega_0 t})<k/k_0<\exp(\sqrt{\Omega_0 t})$ and area of this values expands with time rather fast. The maximum of the distribution $\tilde{P}$ tends to small k when $t \to \infty$.

As a result one can state that the wavetrain propagating on the random currents has a tendency to shorten its wavelength (with exponential speed) as the significant part of the probability density function transfers with time to large k.

It should be stressed that this statement was obtained in the approximation of gaussian δ - correlated process and for potential currents.

1. V.I. Kyatskin Stochastic equations and waves in random media. M., 1980

Discussion of Voronovich's paper

M. Cooker

Please could you provide us with any more references to your work on propagation in non-uniform medium. We are interested in acoustic problems in 3-dimensions when the medium has strongly-varying sound speed with position.

Author's reply

Unfortunately, this abstract is the only thing I have published in English: there are some papers published in Russian, but these works deal with geophysical waves and not acoustical ones. I'll be glad to send references.

M. Dingemans

I have a question about the applicability of your model for a general hydrodynamic field; a splitting in waves and currents is obtained by averaging over the short time scale (the scale of the waves). Such an averaging gives mean motion in which much of the randomness is averaged out. This means that the current field is less random than the wave field and therefore in wave propagation problems we usually have random waves propagating in a non-random medium.

Author's reply

This depends on scales. You can eliminate short-period waves but the waves which remain can still provide statistical ensemble. In fact you can't attribute to the long water waves any fixed structure; they are inevitably random. Moreover, to include the randomness of wavetrains could be a second step.

N. Huang

In your model, you assumed the current field to be a potential flow but random. How realistic is that? Can your model be generalized to any irrotational current field?

Author's reply

The equation which was derived can be immediately applied to the vortex current field as well (you only need to specify coefficients which are determined by the statistics of arbitrary large-scale motion). Nevertheless, surface waves are both potential and random.

E. Pelinovsky

For a one-dimensional situation it is clear that a wave must conserve all quantities after transmission through a layer with random current; in the geometric optics approximation. As a result a wave can change wavenumber only in a layer, but the mean value of k is not changed significantly.

Author's reply

This is not true, because current depends upon t and frequency of the wave-train is not conserved.

L. Tsimring

I don't understand whether your results are valid in the case of time-independent random velocity field, because in that case large wavenumbers can be produced only by large velocities?

Author's reply

No, the large-scale motion should be time dependent (and in a rather strong manner to produce δ-correlation in time).

M.P. Tulin

This is very interesting work. My question concerns the assumptions and limitations of the theory. For example, is it assumed that the currents are small in comparison to the group velocity of the waves. Does the theory include effects such as resonance due to convection of the current patterns?

Author's reply

Generally currents need not be small with respect to group velocity - in some sense we consider "strong nonlinear" effects. But further to proceed to δ-correlated approximation we should assume that the current is weak, but in some other sense the changes of the parameters of the wavetrain should be small within the time interval which is equal to the correlation time.

LOW FREQUENCY WAVES IN THE SURF ZONE

Gary Watson and D. Howell Peregrine
Department of Mathematics, Bristol University,
Bristol BS8 1TW, England.

Abstract

The surf zone on a beach is modelled with a new numerical approximation to the shallow-water equations. The swash zone can show substantial low-frequency elements in the wave motion even when seaward input consists entirely of high frequency waves.

Introduction

Low-frequency waves (LFW) or 'infragravity' waves with periods greater than 30 seconds are important because they can significantly influence coastal sediment transport, and drive harbour oscillations. They can gain amplitudes comparable to those of the higher-frequency wind and swell waves, particularly in storm conditions. This paper presents some results of ongoing attempts to understand the physical mechanisms by which such waves are generated.

It is generally considered that LFW gain energy by non-linear transfer from *modulated* high-frequency waves (short waves). This can occur by a number of mechanisms, as follows:

(a) The varying radiation stress in groups of short waves forces bound LFW which are released when the short waves propagate over depth changes or lose their energy by breaking on a beach.
(b) Modulated short waves break in different depths and the time-varying gradient of radiation stress due to a "moving breaker line" generates LFW.
(c) Fluctuations in wave set-up at the shoreline generate LFW.

All these generating mechanisms are essentially nonlinear. The most strongly nonlinear part of a coastal zone is the surf zone on beaches. In addition the vertical surface excursions due to LFW are at their maximum at the shoreline. These considerations together with a few sample computations showing strong LFW responses in surf zone modelling (Packwood, 1980) have led to the present numerical study of the response of the surf-zone to differing types of forcing at its seaward boundary.

Our long-term objectives are to understand the generation of LFW on real beaches of arbitrary topography, with realistic two-dimensional wave spectra, and also to build up a good numerical model which will be useful for morphodynamic studies.

This paper concerns a much reduced set of initial objectives, which are (a) to study LFW generation using the simplest possible mathematical model, (b) to understand thoroughly the physical processes occurring in such a model, and (c) to optimise the numerical method.

Mathematical and numerical models

The wave field on a real beach is three-dimensional, with significant processes such as longshore currents and edge wave propagation occurring. To model such a wave field comprehensively would be a substantial task. However, since processes (a)-(c) can all occur in a two-dimensional motion, and also occur in shallow water, it is much simpler to study these aspects of LFW generation using a one-dimensional shallow-water model in which the velocity is averaged over depth.

The shallow-water equations for water depth, $(h+\zeta)$, and mean velocity parallel to the bed, u, are

$$\zeta_t + [(h+\zeta)u]_x = 0, \qquad (1)$$

$$u_t + uu_x + g\cos\alpha\ \zeta_x = 0 \qquad (2)$$

where $h = h(x)$ is the depth to the bed from a horizontal reference level, $\zeta = \zeta(x,t)$ is height to the surface from the same reference level, and $\alpha = h'(x)$ is the bottom slope. The equations assume the water depth to be shallow compared with the horizontal scale of the waves - an assumption which does not hold for steep breaking waves, but which is made nevertheless.

A friction term could be included in the momentum equation (2). The inviscid equations are used in this particular study since we aim to elucidate basic mechanisms of surf zone response. In addition, Packwood (1980) found in comparisons with laboratory experiments that frictional terms only made a significant difference to very thin flows in the swash zone. A further advantage of the inviscid equations is that for a beach of constant slope, the angle α can be scaled out of the equations, and the only parameters in the problem are those determined by input conditions.

For surf zone modelling the shallow-water equations need to be augmented by the inclusion of bores, modelled as mathematical discontinuities in water depth and velocity at which both mass and momentum are conserved. The effective numerical modelling of such bores dominates numerical schemes for solving the shallow-water equations. The Lax-Wendroff scheme has been successfully used for many years, e.g. Hibberd and Peregrine (1979), but more efficient schemes are now available.

A new numerical scheme, the weighed average flux method (WAF) (Toro, 1989, 1990) has been adopted for the solution of these equations. The WAF method is a development of currently favoured methods such as Godunov's and Roe's. It is 'shock-capturing', i.e. discontinuities are automatically treated correctly without the need for a special tracking algorithm which would slow the computation down. The method is a development of methods currently favoured for compressible air flow. It has been found to be more efficient and robust than previously used methods. Bores are followed very well and for a given accuracy less discretization points are required than with most methods.

In this method the equations are solved in conservation form

$$\frac{\partial}{\partial t}\begin{bmatrix} d \\ ud \end{bmatrix} + \frac{\partial}{\partial x}\begin{bmatrix} ud \\ u^2 d + \frac{1}{2}gd^2 \end{bmatrix} = \begin{bmatrix} 0 \\ gd\alpha \end{bmatrix} \qquad (3)$$

$$\text{or } \underline{U}_t + \underline{F}_x = \underline{S} \qquad (4)$$

where $d = h + \zeta$ is the total depth, $\underline{U}$ represents the conserved quantities mass and momentum, $\underline{F}$ represents the flux of these quantities and $\underline{S}$ is a source term due to the bottom slope, which has been assumed small. The solution is computed on a staggered grid in which $\underline{F}$ is evaluated at points half-way between the $\underline{U}$-points in both x and t. This enables a straightforward centered-difference formula to be used

$$\underline{U}_i^{n+1} = \underline{U}_i^n + \frac{\Delta t}{\Delta x}(\underline{F}_{i-\frac{1}{2}} - \underline{F}_{i+\frac{1}{2}}) + \underline{S}_i \Delta t. \qquad (5)$$

The intermediate fluxes $\underline{F}_{i+\frac{1}{2}}$ are estimated using the initial value Riemann problem with piecewise constant data $\underline{U}_i^n$, $\underline{U}_{i+1}^n$ with a step at the midpoint of the cell. The flux in this solution is then averaged over the width of the cell at $t = \frac{1}{2}\Delta t$ and this value is used for $\underline{F}_{i+\frac{1}{2}}$, hence the name 'Weighted Average Flux'. A Total Variation Diminishing adjustment is then made to the flux average by means of upwinding, in order to eliminate spurious oscillations near bores.

The source term $\underline{S}$, which is proportional to the bottom slope α, often causes difficulties in similar systems such as the Euler equations. *To avoid such difficulties, the problem is transformed* into a reference frame with horizontal acceleration $g\alpha$. This yields Eqs (3) and (4) with the right-hand sides equal to zero. After solving this problem at each time step, the solution in the desired reference frame is obtained by the reverse transformation. This technique may prove to be of value in other contexts.

Boundary conditions at the two ends of the computational domain are markedly different. At the shoreline the water depth, $h + \zeta$, is zero and its position $x_s(t)$ is such that it has the same velocity as the water. This condition is only approximately satisfied in the model. A depth cut-off of $0.1\alpha\Delta x$ was used to define the shoreline, and the boundary condition satisfied approximately by using the dry-bed Riemann problem, in which one of the initial states is dry, at the shoreline point.

At the seaward boundary we need to prescribe the incoming wave and yet permit outgoing waves to escape without reflection. This is made possible (Hibberd and Peregrine, 1979) by using the Riemann invariants. Expressing equations (1) and (2) in characteristic form using the change of variable $c = [g(h+\zeta)]^{\frac{1}{2}}$ yields

$$\left[\frac{\partial}{\partial t} + (u+c)\frac{\partial}{\partial x}\right](u - 2c + g\alpha t) = 0 \qquad (6)$$

$$\left[\frac{\partial}{\partial t} + (u-c)\frac{\partial}{\partial x}\right](u - 2c + g\alpha t) = 0 \qquad (7)$$

These show that $u+2c+g\alpha t = R_+$ is constant on characteristics propagating at speed $u+c$ (primarily in the +x direction) and $u-2c+g\alpha t = R_-$ is constant on characteristics propagating at speed $u-c$ (primarily in the -x direction). Hence, since t is known, $2c\pm u$ gives the "signal" propagating in the $\pm x$ direction respectively. Thus if the seaward boundary is on the -x side of the domain of integration, $2c+u$ is specified as the incoming wave, and the value of $2c-u$ needed to complete the boundary condition at each time step is found from the previous time step by retracing the appropriate characteristic. The values of $2c-u$ give the reflected wave from a beach in this case.

Results

Before proceeding with more complicated cases, the model was tested against an analytic solution for non-breaking shallow-water motion on a beach. The solution used was that of Carrier & Greenspan (1958). The result for the surface elevation close to the shoreline at ten time values is shown in Fig 1. The numerical solution is very accurate further away from the shoreline. This figure demonstrates that, although acceptable, the solution contains a small error which originates at the shoreline point and propagates offshore. Various schemes are being investigated to eliminate or reduce this error.

A bore of a certain height incident on a beach creates a swash of water up and down the beach which lasts a certain time T_s, depending on beach slope and bore amplitude. When a uniform train of bores separated by a period $T > T_s$ is incident, a periodic motion ensues. However, for $T < T_s$ each bore interacts with the swash of the previous bore and the solution is more complicated, as Fig 2 shows. The seaward input $R_+(t)$ is shown as the dotted line in Figure 2(a) and has been defined as a periodic sawtooth. After the start-up effect has died out, the motion of the shoreline $x_s(t)$ in Figure 2(b) is seen to be irregular, although dominated by motions with period T_s rather than T ($T \approx \frac{1}{3}T_s$ in this case). The trajectories of bores are also shown in this figure. There is almost no outgoing reflected signal $R_-(t)$, the solid line in Fig 2(a) - all the short wave energy is dissipated as the bores propagate up the beach.

To obtain a significant LFW signal, the incident waves must be modulated, as illustrated in Figure 3. The input $R_+(t)$ is a combination of two sine waves of large amplitude giving a strongly modulated wave envelope. Note that there is no LFW component in $R_+(t)$. However, $R_-(t)$ shows a substantial LFW component at the beat frequency, as does the shoreline motion $x_s(t)$, in which large excursions are evident. Note that a sinusoidal input was used merely to illustrate the fact of wave generation at a frequency which was not present in the input signal. In a realistic simulation the seaward boundary should be located shoreward of the break point, where the incoming waves will approximate to bores.

Note that α and g have been scaled out of the problem so that depth is initially 1 at the seaward boundary. If this is rescaled to a slope of 1:30 and an intial depth of 1 metre at the seaward boundary the wave period is approximately 5 seconds, with the LFW period being 50 seconds. The incident wave heights correspond to

a maximum depth ratio (bore height ÷ depth in front of bore) of just over 0.8 as the bores form.

A preliminary investigation into the relationship between incident wave amplitude A_{in} and reflected LFW amplitude A_{out} was made by multiplying the input in Fig 3 by various factors. The result is shown in Fig 4. In 4(a), A_{out}/A_{in} is plotted against A_{in}. The presence of a peak in this curve illustrates the distinctly non-linear response. An arrow on the x-axis shows the range of values of A_{in} which is considered physically realistic. In 4(b), A_{out} is plotted against A_{in} on logarithmic axes. In the realistic range there is a straight line with gradient 1.6, indicating that $A_{out} \propto A_{in}^{1.6}$. Further investigation of this result is under way, to establish how general it is.

Conclusions and future plans

A shallow water equation model of waves in the inner surf zone was found to show a strong LFW response to modulated incident waves. There was also a weak response to regular, unmodulated waves if the wave period was less than the swash period. Preliminary results using a pair of sine waves indicated a LFW amplitude proportional to $A_{in}^{1.6}$ for realistic A_{in}, where A_{in} is the incident wave amplitude.

It is planned to investigate a variety of parameters using this model, including a range of incoming wave spectra, and different beach profiles. Various diagnostics will be used to elucidate the generation mechanism. Comparisons are also to be made with experiments in a tank at Hydraulics Research Ltd. Wallingford, and also with appropriate data from field experiments.

Acknowledgements

Grateful thanks are extended to Dr E.F. Toro of Cranfield Institute of Technology, who has developed the WAF method. He provided core elements of the code used in the model. This work was supported by the Commission of the European Communities under contract MAST 0035-C.

References

G.F. Carrier and H.P. Greenspan, Water waves of finite amplitude on a sloping beach. J.Fluid Mech., 4, 97-109,1958.

S. Hibberd and D.H. Peregrine, Surf and run-up on a beach: a uniform bore, J. Fluid Mech. 95, 323-345, 1979.

A.R. Packwood, Surf and Run-up on Beaches, Ph.D. Thesis, University of Bristol, 1980.

E.F. Toro, A weighted average flux method for hyperbolic conservation laws, Proc. R. Soc. Lond. A 423, 401-418, 1989.

E.F. Toro, Riemann Problems and the WAF Method for the Two-Dimensional Shallow Water Equations, Univ. Trento Report UTM 314, 1990.

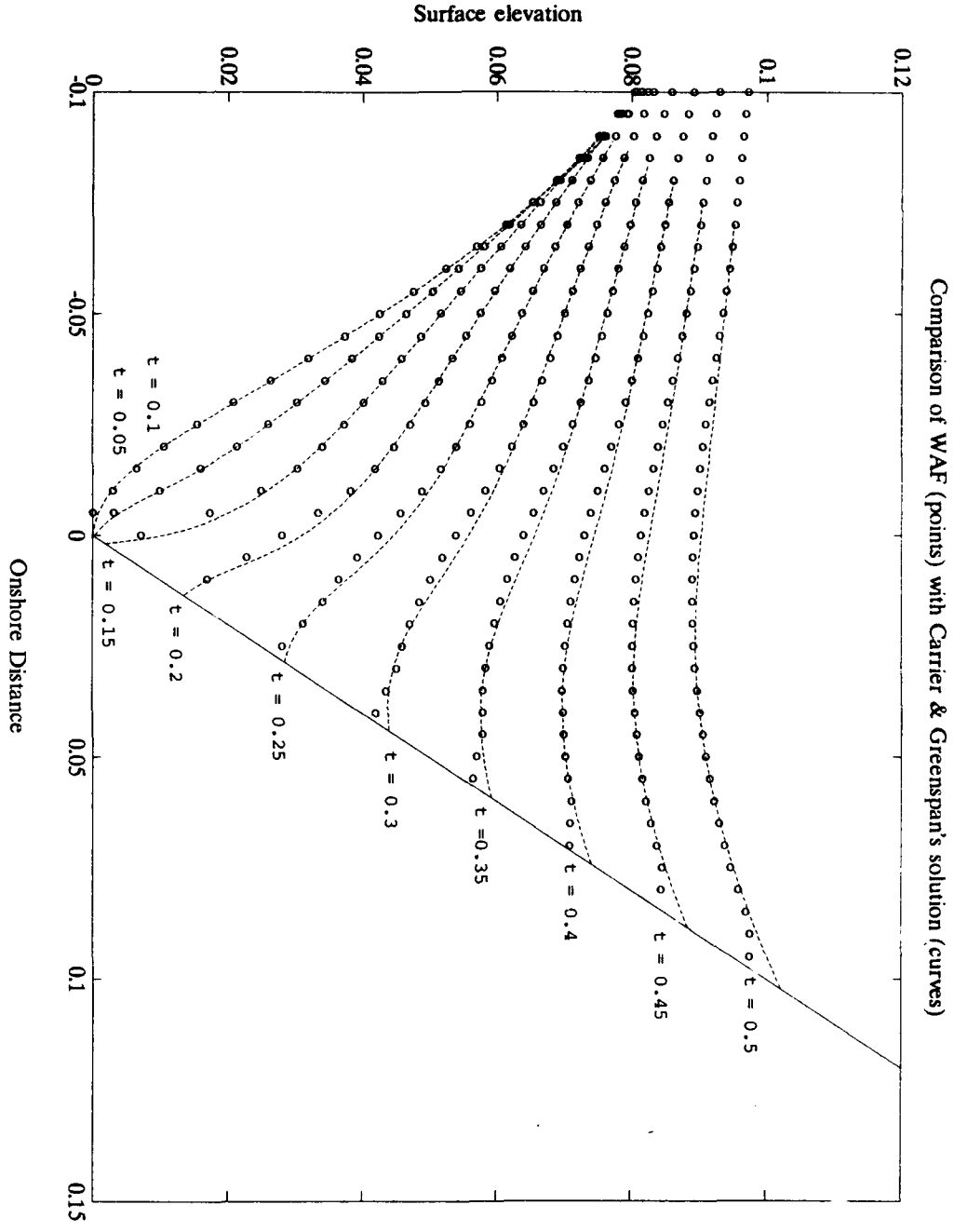

Watson & Peregrine, Fig.1
Comparison of numerical solution with analytic solution

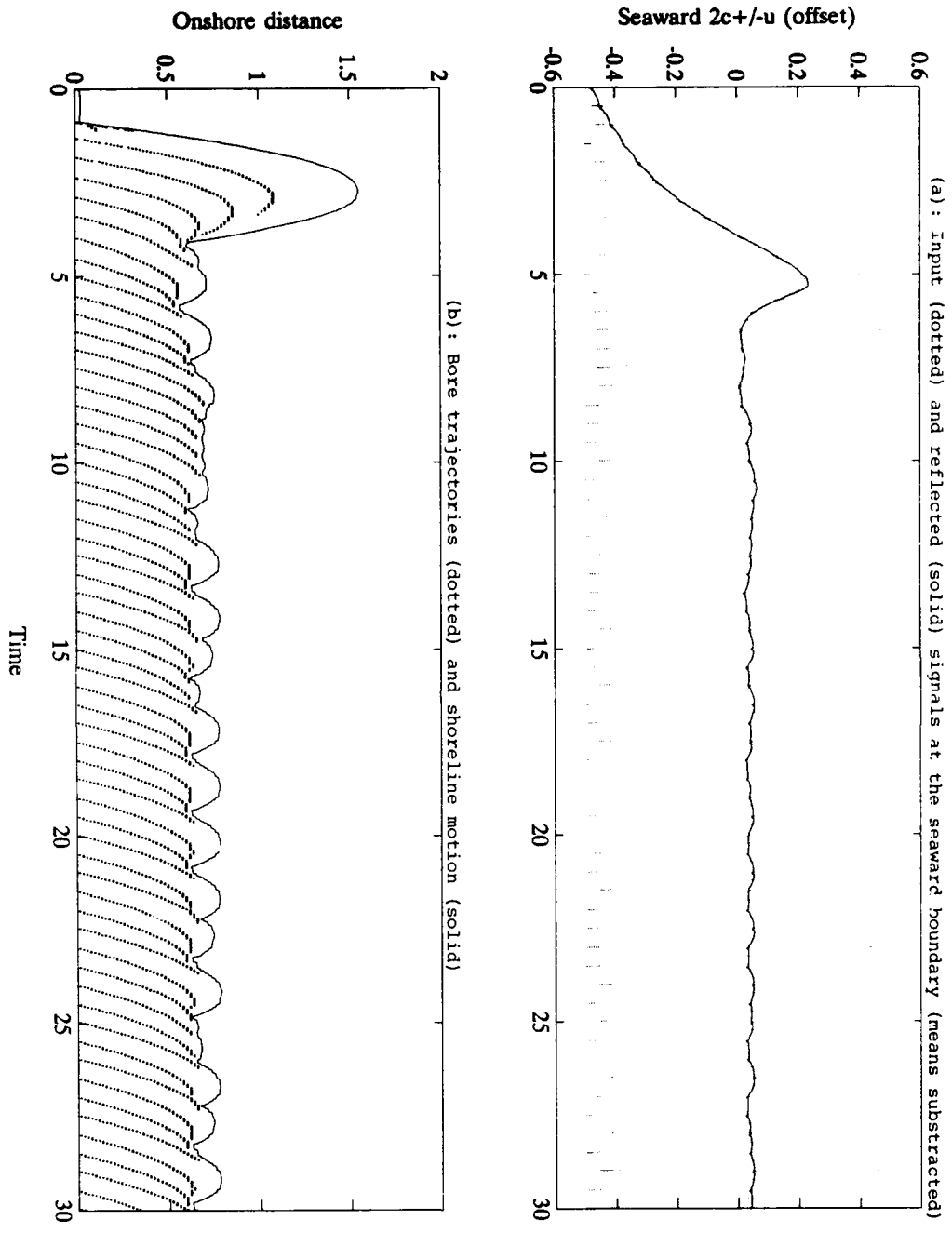

Watson & Peregrine, Fig.2
Model results for regular bores, $T \approx \frac{1}{3}T_s$

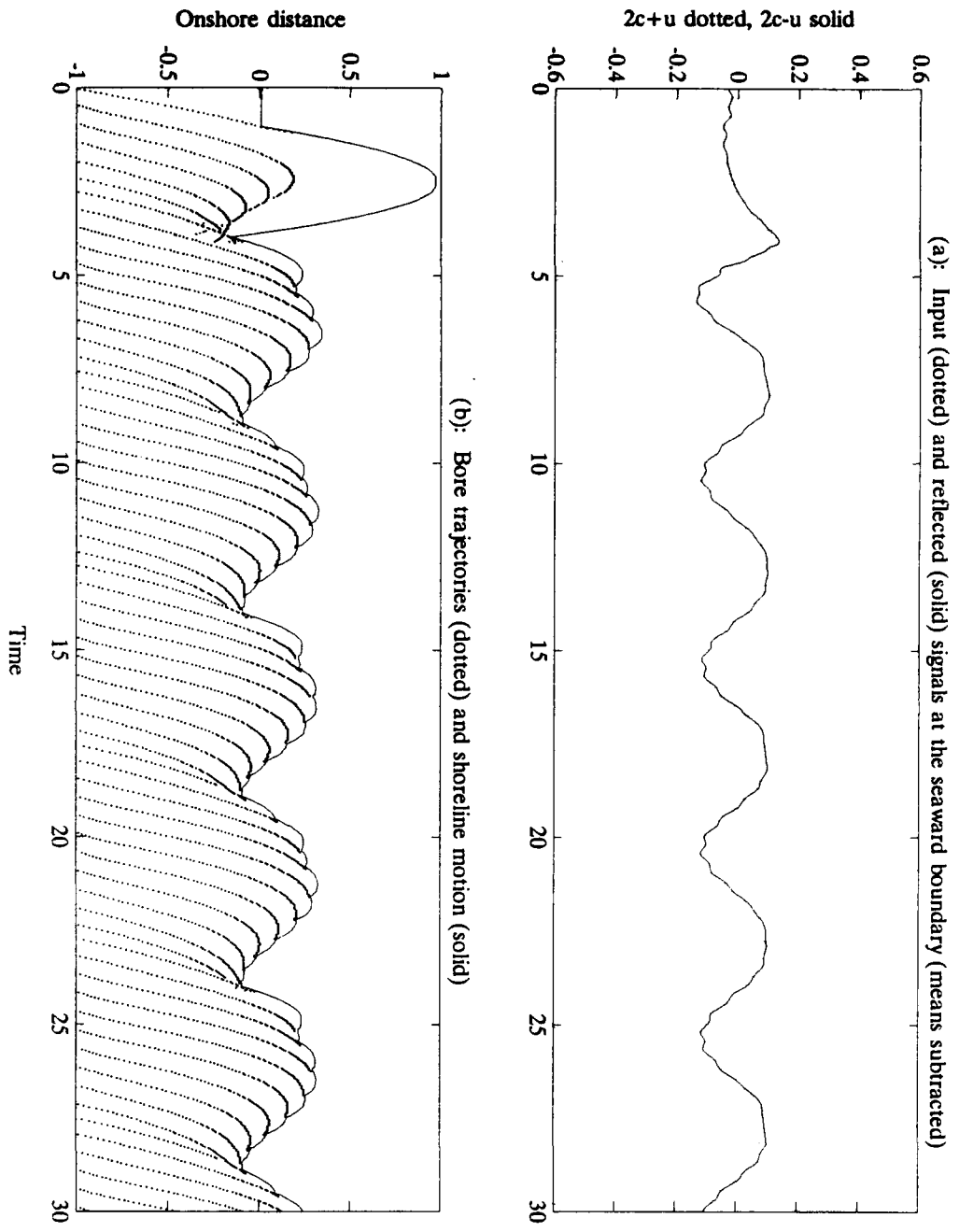

Watson & Peregrine, Fig.3
Model results for two harmonic components, with f/Δf = 10

(a) Reflected LFW signal amplitude (Ao) / Incident amplitude (Ai)

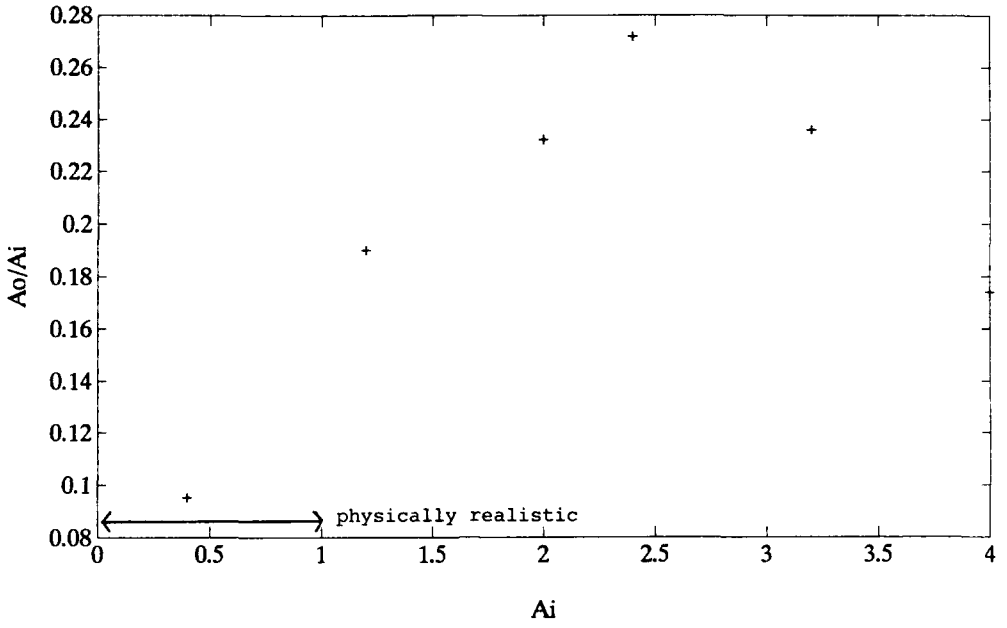

Log plot of reflected LFW v. incident signal amplitude

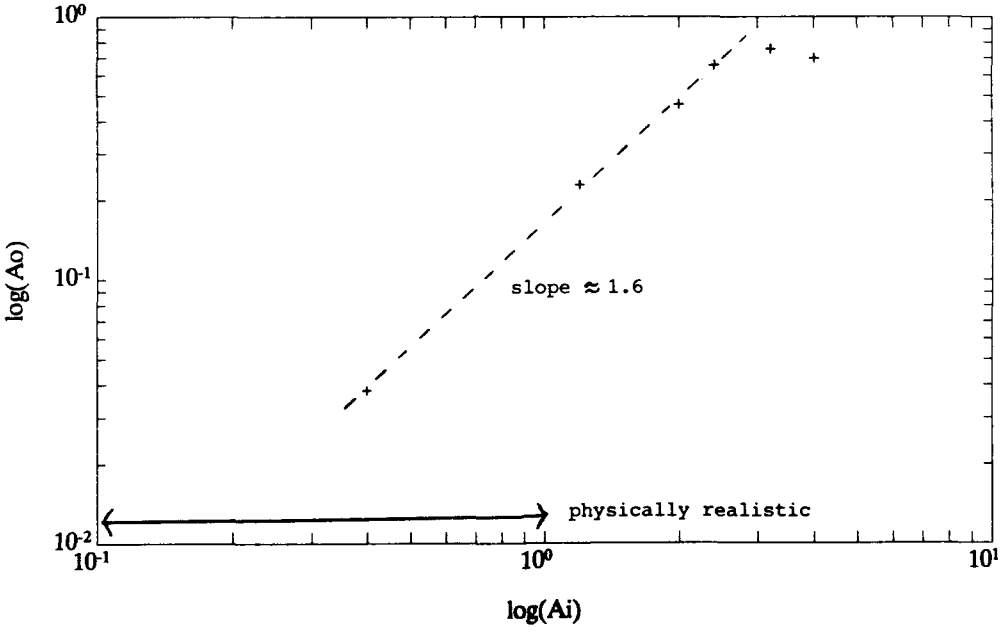

Watson & Peregrine, Fig.4

Effect of incident wave amplitude on outgoing low-frequency wave amplitude

Discussion of Watson's paper

J.A. Battjes

Your results show amplitudes of outgoing (seaward) low-frequency waves roughly proportional to the 1.6 power of the amplitude of the incident high-frequency waves. I would like to point to numerous publications (Munk, Tucker, Guza and Thornton, ...) reporting a very nearly linear relation between these amplitudes.

Author's reply

We have also seen some data measured by Hydraulics Research Limited, indicating a stronger than linear dependence (e.g. Bowers & J. Welsby "Analysis of wave data collected at Port Talbot", Report No. IT 242, March 1983).

V.R. Kogan

1. What boundary conditions have been used?

2. Did you try to solve this problem by other methods, for example by the singular integral method?

3. Is it a time-periodic problem?

Author's reply

1. At the seaward boundary, the Riemann invariant $u + 2c + t$ was specified as a function of time and the equations in characteristic form were used to compute the other invariant, $u - 2c + t$.

2. We have only tried various finite difference methods so far.

3. The forcing at the seaward boundary is periodic in time. The response is normally dominated by components at the forcing frequencies of their sums and differences, but non-periodic components are also present.

C.C. Mei

Airy's equations cannot be used to calculate the first line of breaking. Did you use this scheme to calculate the first line of breaking which would be oscillatory? If not, how do you know what to put in as the seaward boundary condition? (Is the numerical seaward boundary inside the surf zone?)

Author's reply

These shallow-water equations are inappropriate to modelling the neighbourhood of breaking. However, if the breaking region in (x,t) for a single wave is small enough compared with the length and time scales of interest discrepancies in that region will not be important. Earlier work by Packwood (Ph.D. 1980) which included comparison with experiment showed good agreement despite waves breaking within the region being modelled. The numerical seaward boundary would ideally be just inside the surf zone. However in any realistic model the breaking zone is wide and breaking within the model occurs.

E. Pelinovsky

You consider only one kind of generation mechanism of LFW. There is another mechanism due to the nonlinear friction: the term $u|\hat{u}|$ in shallow-water theory. What do you think about it? It's necessary to have robust estimations.

Author's reply

The non-linear friction term will indeed be another mechanism for LFW generation. However, some previous work by Packwood (Ph.D. Thesis, 1980) found that inclusion of friction had only a weak effect in many cases. Friction will be more important on very gentle beach slopes and also perhaps in the backwash. One reason for neglecting it here is to make it easier to understand the other mechanisms due to wave breaking.

H. Szu

Does the amplification of the incoming wave amplitude depend on the ocean bottom slope?

Author's reply

In this work the constant beach slope α was scaled out of the equations by a suitable non-dimensionalisation. Our empirical result was $a_{out} = \kappa a_{in}^{i\,6}$, where a_{in} is the incident short wave amplitude and a_{out} the outgoing low frequency wave amplitude and both are non-dimensionalised against the same reference depth. When the result is written in dimensional form, the power law remains the same, although the constant of proportionality depends on the reference depth. Note that this empirical result is preliminary and has not been investigated using a variety of wave spectra.

STATIONARY WAVES ON THE SURFACE OF A HEAVY LIQUID

E.I.Yakubovich

Institute of Applied Physics, USSR Academy of Sciences

46 Uljanov Str., 603600 Nizhny Novgorod, USSR

A stationary potential two-dimensional flow of an ideal incompressible infinitely deep liquid is considered.

Using the boundary conditions on the surface we have derived a second-order nonlinear ordinary differential equation for complex velocity, that is valid throughout the entire region of the liquid flow.

A solution determining the velocity field of the fluid has been obtained for this equation.

Investigations show that, except a Stokes wave, there always exist singularities in the flow region.

The singularities of the Stokes wave are at the wave peaks of the flow surface.

Thus we have proved that there exist no stationary two-dimensional waves (except a Stokes wave) of an ideal incompressible infinitely deep liquid, that are potential everywhere throughout the flow.

Discussion of Yakubovich's paper

D.H. Peregrine

Author discusses limiting wave, but does not appear to note that $V = 0$ is not a simple zero, there is a singularity at the zero (crest). Longuet-Higgins has shown acceleration is $\frac{1}{2}g$.

Author's reply

There are two forces acting on a particle floating on the water surface: gravity and the gradient of pressure which is perpendicular to the surface. My guess is that the latter force is proportional to the velocity with a constant coefficient B. If so, then at a crest $V = 0$, the acceleration tends to $\vec{g}$, and the particle may move only in vertical direction there.

P.G. Saffman

There is a contradiction with the proofs, starting with Nekrasov and Levi-Civita and extended by subsequent workers, that Stokes waves exist for all heights up to the maximum.

Author's reply

Nekrasov and Levi-Civita searched the solution of the integral equation in the form of series and the convergency of them still has not been proved.

V.E.Zakharov

Direct and Inverse Cascade in the Theory of Water Wave Turbulence

Since the K.Hasselmann's paper of 1962, a kinetic equation for waves is a standard tool in the theory of water wave turbulence. It is used mostly for computer simulation of this process. But it is very important also to understand the basic physical phenomena described by this equation. The kinetic equation has the form

$$\partial n_k/\partial t = St(n,n,n) + f_p + f_d \qquad (1).$$

Here $n_k = \varepsilon_k/\omega_k$, $\omega_k = \sqrt{gk}$, k i a 'wave number', (ε_k is a space spectrum), f_p is a pumping due to interaction with the wind, f_d -damping due to viscosity and breaking processes, $St(n,n,n)$ - is a 'collision term' - a complicated nonlinear operator. Justification of employing the kinetic (weak turbulent) approach to the surface wave turbulence is a result of existence of a natural small parameter

$$\varepsilon = \rho_{air}/\rho_{water} \sim 0.001$$

A pumping term $f_p \sim -\varepsilon\beta(k,\theta)n(k)$ is concentrated in a frequency range $\omega_0 < \omega < 4\text{-}5\omega_0$ $\omega_0 \sim g/U$, U is wind velocity ($\beta(k,\theta) \sim k\cos\theta$ at $k \gg g/U^2$ is a certain structural function). A strongly nonlinear damping term f_d is concentrated at $\omega_d \gg \omega_0$. There are two 'windows of transparency' in k-space.

'The left window'

$$\omega < \omega_0 \qquad (2)$$

and the right window

$$4\text{-}5\,\omega_0 < \omega < \omega_d \qquad (3)$$

where a stationary kinetic equation reduces up to the form

$$St(n,n,n)= 0 \qquad (4)$$

The equation (4) has a big family of solutions that must be found numerically and used for comparison with experiments.

Two the simplest isotropic solutions could be found analytically

$$n_k^{(1)} = \alpha_1 \rho^{1/3}/k^4 \quad ; \quad \varepsilon_k^{(1)} = \alpha_1 \rho^{1/3} / \omega^4 \qquad (5)$$

$$n_k^{(2)} = \alpha_2 \ Q^{1/2} /k^4; \quad \varepsilon_k^{(2)} = \alpha_2 \ Q^{1/3}, \ \omega^{11/3} \qquad (6)$$

These exact solutions are connected with two basic integrals of motion: energy (actually it is only 'formal integral')

$$E=\int \omega_k \ n_k \ dk \qquad (7)$$

and wave action

$$N = \int n_k \ dk \qquad (8)$$

in (5),(6) $\rho \sim \varepsilon_k^{3/2} n^3$ is flux of energy and $Q \sim \varepsilon_k^{3/2} \ U^4 /g$ - flux of wave action from wind to waves. Spectra (5),(6) are Kolmogorov type distributions. The fluxes ρ and Q must have an opposite sign. Energy flux ρ is directed to the high ω region, as far as wave action flux Q is directed to low ω domain. In the case of isotropic pumping $\beta=\beta(\omega)$ the spectrum (5) is realized in the right window of transparency (3) and describes direct cascade of energy, as far as the spectrum (6) is realized in the left window (6), describing an inverse cascade of energy. Divergence of wave action on the distribution (6) means that a 'leading' frequency ω_1 goes to zero infinitely according the law $\omega_o \sim t^{-3/11}$. Experimentally it means 'infinite aging' of the energy carrying waves. This is the most fundamental prediction of the developed theory. It holds in a real situation where a pumping is far from isotropy and is confirmed by remote sensing measurements in the

open ocean.

In reality, low-frequency spectra are strongly anysotropic. It is astonishing that they are still satisfactory described by the formula (6). The formula (5) fits for description of the high-frequency window (3) pretty well also.

Discussion of Zakharov's paper

R. Glazman

Referring to the 2-D turbulence as an analogue of the surface gravity waves in the 4-wave approximation, you make a parallel between the inverse and direct cascades in the spectra of the 2-D turbulence (due to conservation of energy and enstrophy) and the inverse and direct cascades in the spectra of surface gravity waves. However, if we recall that there is an infinite number of conserved integrals in the 2-D motion, your analogy appears to be very incomplete, doesn't it?

Author's reply

There is some uncertainty in the 2-dimensional hydrodynamics. It is not clear, what integral from a set $\int(2?v)^n d\vec{z}$ should be chosen to get a Kolmogorov spectrum for $k \to \infty$. Usual choice $n = 2$ is not founded enough. There is only one additional integral in the surface wave theory, so this difficulty is absent.

N. Huang

In your formulation of the problem, $\kappa\eta$ is used as the small perturbation parameter, which can be uniformly small only for a narrow band wave field. Could you comment on the range of wave number that the spectral functions you derived are still valid?

Author's reply

Validity of the weakly nonlinear theory is in general case non-uniform in κ-space. In the absence of surface tension in a large wave number (small scale) region nonlinearity is always strong. It is so strong that at $\kappa > \frac{g}{\sqrt{?}} \frac{\delta water}{\delta air}$ there is a fractal two-phase behaviour of a fluid. So, a nonlinear theory is valid only for

$$\kappa << \frac{g}{\sqrt{?}} \frac{\delta wat}{\delta ar} .$$

If the surface tension is strong enough, a weakly nonlinear theory is good for all κ-space.

P. Janssen

In the seventies, it was I believe David Webb (?) who showed that (in the framework of 4-wave interactions) the creation of large scales gives rise to a decrease of entropy while the high-wave number range becomes more chaotic producing a higher entropy. The net effect is an increase of entropy, as it should be. Thus, there is no contradiction, actually this is a rather nice example of the production of order out of chaos.

M. Stiassnie

To obtain interesting results we do two important steps.

1) switch from a to b, losing the exact Hamiltonian

2) change from a deterministic model to a stochastic model.

Are these steps absolutely necessary in order to get the interesting results? (i.e. stationary solutions).

Author's reply

1) Hamiltonian property of the approximate equation could be easily restored by a mild changing of the interaction coefficient $T(\mathbf{k},\mathbf{k}_1,\mathbf{k}_2\mathbf{k}_3)$ outside the resonant manifold $\omega_k + \omega_{k_1} = \omega_{k_2} + \omega_{k_3}$.

2) Derivation of a statistical behaviour (including kinetic equation) is based on using formal expansions in powers of a random external noise. So a stochasticity is included in consideration "implicitly".

V.E.Zakharov

On the Formation of Singularities on the Free Surface of Ideal Fluid.

The problem of wave breaking in the physical oceanography arises as a question about formation of singularities on the free surface of ideal fluid, that could be formulated in a following way.

Let us study a potential flow of ideal fluid with a free surface without any external field and surface tension. Does this surface remain smooth in the process of this evolution?

On our opinion the answer is negative. We formulate the following conjecture. The evolution of initially smooth surface leads in a generic case to formation of a 'wedge' type singularity with the creation of very thin and unstable sprays afterwards.

The singularity is described by the self-similiar solution

$$\eta = (L - t)\, F(x/(L - t)) \qquad (1)$$

$$x/(L - t) = \xi$$

$$F(\xi) \to \alpha|\xi| \quad \text{at } \xi \to \infty$$

here $\eta(x,t)$ is a form of free surface. We have arguments in favour that $\alpha = 1/\sqrt{3}$,so a wedge has 120^0 angle. The formulated conjecture is well confirmed by our numerical experiments (together with V.Kogan and V.Kuznetzov).

This result explains the origin of wave breaking and allows us to formulate a paradoxal question - why sea surface is smooth (and not a fractal) at relatively weak wind?

The paradox is resolved by taking into account the surface tension. In the presence of surface tension wave breaking occurs

only if a characteristic wave length is large enough, that takes place in a real situation only if wind velocity exceeds some critical value V_{cr} . The detailed consideration gives for V_{cr} (T is a coefficient of surface tension)

$$V_{cr} \sim \sqrt{\rho_{air}/\rho_{water}}\ (gT) \sim 6 \text{ m/sec}$$

in a good accordance with observations.

E. Pelinovsky

Why have you an explosive crest, but not an explosive trough? I don't see a distinction between positive and negative direction of vertical coordinate.

Author's reply

Theoretically speaking, an explosive through is as good as an explosive crest. But the total picture is not symmetric with respect of change of direction of Z (inside or outside the fluid). Only argument in favour of a crest is the numerical experiment.